UNIVERSITAT POLITÈCNICA DE CATALUNYA BARCELONATECH

Hydraulic fills liquefaction effect on quay stability

Dani Tarragó Munté

UNIVERSITAT POLITÈCNICA DE CATALUNYA
BARCELONATECH
Department of Civil and Environmental Engineering
Division of Geotechnical Engineering and Geosciences

DOCTORAL THESIS

HYDRAULIC FILLS LIQUEFACTION EFFECT ON QUAY STABILITY

Author:

Dani Tarragó Munté

Supervisors:

Prof. Antonio Gens i Solé

Prof. Eduardo E. Alonso Perez de Agreda

Barcelona, 2021

ABSTRACT

The starting point of this thesis is the failure of part of a quay wall under construction. The quay was divided in two phases, failure affected Phase 1 only. The failure and all the relevant associated information on quay design, construction and monitoring records are described in detail together with the results of a site investigation campaign carried out after the failure. Flow liquefaction of the hydraulic fill emplaced behind the quay wall was the main cause of the failure. The state of the hydraulic fill in the quay area is assessed in the light of the current understanding of the phenomenon and of a number of flow liquefaction criteria. In addition, an elastoplastic constitutive law is described that is capable to simulate the undrained brittleness behaviour that underlies the phenomenon of flow liquefaction. It is a critical-state model that incorporates the concept of state parameter. Subsequent finite element analyses are able to reproduce satisfactorily the behaviour of the quay during construction and the features and circumstances of the failure. Two possible triggering mechanisms are identified that can explain the failure: spontaneous liquefaction, or liquefaction of a limited zone caused by the concurrent construction of an embankment. A parametric study verifies the robustness of the simulation and the dependence of stability on the degree of brittleness of the hydraulic fill. The same type of analysis of quay Phase 2, not involved in the failure, revealed that the margin of safety was small if the hydraulic fill liquefied. Soil improvement measures were implemented and an extensive monitoring system was installed. Construction of quay Phase 2 was completed applying the observational method that involved a continuous check of the monitoring data and its comparison with numerical simulation results. An additional site investigation confirmed that the soil improvement measures had succeeded in removing both the flow and the cyclic liquefaction potential of the hydraulic fill, according to currently accepted criteria. The Phase 1 quay involved in the failure was reconstructed with mainly terrestrial fill with no flow potential liquefaction, as confirmed by the corresponding site investigation.

Based on the experience gathered in the case and on the research carried out, an operational scheme dealing with quays constructed with hydraulic fills susceptible to flow liquefaction is proposed. It consists of a protocol to evaluate liquefaction potential of hydraulic fills, the use of a constitutive law capable of simulating flow liquefaction, the implementation of soil improvement measures to reduce flow liquefaction potential and the employment of a monitoring system to control the quay wall behaviour during construction and to provide data for comparison with numerical analyses results.

RESUMEN

El punto de partida de esta tesis es la rotura de parte de un muelle en construcción. El muelle estaba dividido en dos fases, la rotura solo afectó a la Fase 1. La rotura y toda la información relevante sobre el diseño, construcción y resultados de la auscultación se describen en detalle junto con los resultados de la campaña de reconocimiento efectuada después de la rotura. La licuefacción estática del relleno hidráulico colocado en el trasdós del muro del muelle fue la causa principal de la rotura. El estado del relleno hidráulico se estudia en el marco del conocimiento actual del fenómeno y de una serie de criterios de licuefacción existentes. Además, se describe un modelo constitutivo elasto-plástico capaz de simular el comportamiento frágil no drenado que subyace al fenómeno de licuefacción estática. Es un modelo de estado crítico que incorpora el concepto de parámetro de estado. Los consiguientes análisis de elementos finitos reproducen satisfactoriamente el comportamiento del muelle durante la construcción, así como las características y circunstancias de la rotura. Se identifican dos posibles mecanismos desencadenantes que explican la rotura: licuefacción espontánea o licuefacción de una zona limitada del relleno hidráulico debido a la simultánea construcción de una mota. Un estudio paramétrico verifica la solidez de las simulaciones y la dependencia que presenta la estabilidad del grado de fragilidad del relleno hidráulico. Análisis similares de la Fase 2, no involucrada en la rotura, revelaron que el margen de estabilidad era reducido en caso de que el relleno hidráulico sufriera licuefacción. Se implementaron diversas medidas de mejora del terreno y se instaló un extenso sistema de monitorización. La construcción de la Fase 2 se completó usando el método observacional que implicaba una observación continua de los datos de instrumentación y su comparación con los resultados de las simulaciones numéricas. Un reconocimiento del terreno adicional confirmó que las medidas de mejora del terreno habían conseguido eliminar el potencial de licuefacción, tanto estática como cíclica, del relleno hidráulico. La Fase 1 del muelle involucrada en la rotura se reconstruyó con relleno terrestre sin potencial de licuefacción de acuerdo con los datos del reconocimiento del terreno efectuado.

En base a la experiencia y trabajos realizados en este caso, se propone un esquema de actuación para casos de muelles construidos con relleno hidráulico potencialmente licuefactable. Este esquema consta de un protocolo para evaluar el potencial de licuefacción de rellenos hidráulicos, el uso de una ley constitutiva capaz de simular apropiadamente la licuefacción estática, la implementación de un conjunto de medidas de mejora del terreno para eliminar el potencial de licuefacción estática y la instalación de un sistema de auscultación para controlar el comportamiento del muelle durante la construcción y proporcionar datos para comparar con los resultados de los análisis numéricos.

AGRAÏMENTS

Agrair a totes les persones els que d'alguna manera han estat relacionats o han contribuït a la realització d'aquesta tesi doctoral.

Una menció especial al Prof. Antonio Gens, a qui dono les gràcies per assessorar-me i ajudar-me durant la tesi amb coherència i rigor. Aprecio infinitament l'entusiasme, pensament crític, experiència, que m'han transmès en cada moment.També vull donar les gràcies pel suport del Prof. Eduardo Alonso en tot moment.

M'agradaria també reconèixer l'oportunitat que el Prof. Eduardo Alonso i el Prof. Antonio Gens va donar-me per treballar amb ells en l'assessoria de les obres d'Ampliació del Port de Barcelona. Ells m'han ajudat a créixer com a enginyer, treballant en aquest i amb molts altres projectes de gran rellevància.

A Ricardo Madrid i Amadeu Deu del Departament que varen col·laborar de manera directa als treballs desenvolupats després de la ruptura del Moll Prat. Especialment al Ricardo qui va ser el meu mentor durant els primers anys.

Reconèixer el treball dels membres del Comitè d'Experts creat després de la ruptura: Prof. A. Soriano, Dr. J. González, J.I. Grau, G. Gómez i Prof. D. W. Hight; i del equip de tècnics de la Autoritat Portuària de Barcelona: J. Uzcanga, Dr. J.L. Estrada, R. Griell, M.A. Pindado i J. Quintana.

A la Autoritat Portuària de Barcelona per finançar tota la investigació que es presenta en aquesta tesi.

A la Dr. Nubia Gonzalez pel seu traspàs de coneixement envers el model constitutiu utilitzat.

Als professors del Departament de Enginyeria del Terreny que han contribuït en la meva formació acadèmica. En particular al Prof. Toni Lloret, qui va col·laborar activament a la realització d'assaigs de laboratori del reblert hidràulic estudiat a la tesi.

A tots els companys i companyes del Departament amb els qui he compartit "els moments" durant aquests anys, als amics que he fet, i especialment al grup de la comida.

A la meva família i amigues pel seu suport, en especial als meus pares i germana. A la Helena per sempre estar, estimar i comprendrem, i finalment al petit Marcel.

Table of contents

List of figures

List of tables

Chapter 1. Introduction

1.1. Background

Hydraulic fills are soils deposited by a flowing stream of water (van't Hoff & van der Kolff, 2012). They are used to fill enclosures in a variety of engineering projects -such as quays and embankment dams-, or to create land reclamation -new islands, airports, harbours, industrial areas and roads-, as Palm Island Project in Dubai or Maasvlakte 2 in Rotterdam Europoort, The Netherlands.

Hydraulic fills are often created by pumping dredged materials to the construction area. The mixture of water and soil are sprayed through the air into the enclosure, a technique frequently called rainbowing, see Figure 1.1. The hydraulic fills obtained in this way are similar to mining tailings in terms of soil structure, both are generally deposited in a loose state.

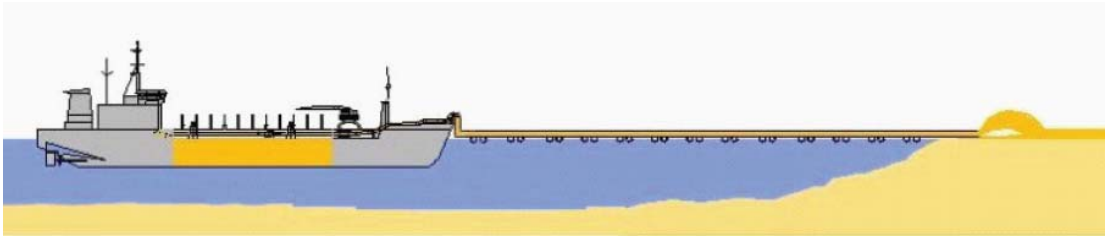

Figure 1.1. The rainbowing technique. Royal Boskalis Westminster nv (2009).

In recent decades, the volume of land reclamation has increased sharply due to the need of cities and facilities to grow towards the sea (Figure 1.2). Because of the difficulty of securing enough volumes of soils for reclamation, dredged materials deposited by hydraulic means is often the preferred option.

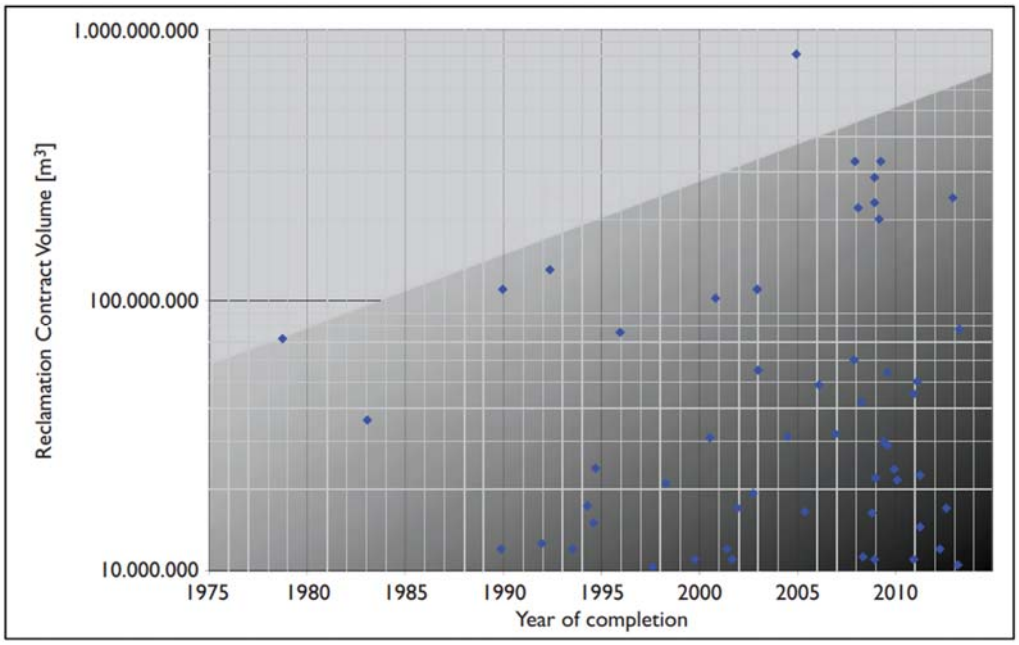

Figure 1.2. Reclamation contract volumes evolution, van't Hoff & van der Kolff (2012).

For instance, the Prat quay -part of the Barcelona Port enlargement-, was constructed using a volume of hydraulic fill close to 70M m^3, it would have been probably impossible to obtain such volume from land soils. Figure 1.3 and Figure 1.4, shows the magnitude and importance of those type of works.

Figure 1.3. Satellite image showing the future emplacement of Prat quay in 2001, source Google Earth.

Figure 1.4. Satellite image showing Prat quay in 2020, originally designed with hydraulic fill, source Google Earth.

A drawback of the use of hydraulic fills is that very often they are susceptible to flow liquefaction. Soil liquefaction is most common in young soils, which do not have undergone a long stress history. These soils are likely to be composed by recently sedimented layers, which are not older than Holocene age deposits. In this context, the youth of soil layers is accentuated in hydraulic fill. Mostly, this type of fill is deposited as part of backfill operations in a very short time, usually a few months.

Different catastrophic failures of different structures due to soil liquefaction have been reported or reviewed in the past by Bishop et al. (1969) and Bishop (1973), Olson and Stark (2002), Yamamuro and Lade (1999), Fourie (2003), Jefferies and Benn (2006), and Alonso and Gens (2006). For some time, there was a degree of confusion in the understanding of this phenomenon and about the correct terms to use. This confusion sometimes spilled over the wider public sphere. In the case of the Prat quay failure, a comic strip linked two mankind's mysteries: soil liquefaction and the blood of San Gennaro (Figure 1.5).

Figure 1.5. Mankind's mysteries, Transporte XXI (2007).

The failure of Prat quay and subsequent related activities were the launching event for this PhD thesis. From 2001 to 2020, quay construction, partial failure of the quay wall, sites investigations, design changes and the final quay reconstruction have taken place.

The present PhD thesis is the result of the research work performed within the Doctoral Programme in Geotechnical Engineering of Universitat Politècnica de Catalunya (UPC), which was mainly focused on the development of an assessment framework for hydraulic fill liquefaction, with special reference to flow liquefaction. This development is based on the simulations, tests and observations carried out after the failure of Prat quay, a landmark case of flow liquefaction. It takes advantage of the large scale site investigations, intense laboratory testing and extensive programme of numerical analyses that were carried out as a consequence of the failure.

1.2. Motivation and objectives

Soil liquefaction problems have been reported since Hazen (1918) who described a liquefaction event that caused failure in 1918. Many other catastrophic failures triggered by soil liquefaction have been reported afterwards. Soil liquefaction has often serious financial and public safety implications (Jefferies and Been, 2006).

Casagrande (1936) defined the concept of critical void ratio and Terzaghi and Peck (1948) described spontaneous liquefaction two basic terms for soil liquefaction understanding. Afterwards, Schofield and Wroth (1968) postulated the critical state framework and models. Another important development was put forward by Been and Jefferies (1985) introducing the concept of state parameter. Those advances have allowed the formulation of constitutive models for soil liquefaction. At the same time, a number of tests were advocated to evaluate soil liquefaction by other pioneers such as Seed, Idriss and Robertson. From those studies, a number of soil liquefaction criteria have been defined. All those advances provide an adequate background for geotechnical engineering works involving hydraulic fills.

In this context, the main aim of the thesis have the development of an operational scheme for actions in the presence of quays constructed with hydraulic fills susceptible to flow liquefaction. It would be based on the following items:

i) Evaluation of the hydraulic fill in Prat quay using specific soil liquefaction criteria
ii) Development of a suitable constitutive model to simulate flow liquefaction for hydraulic fills.
iii) Demonstrating that the soil improvement procedures performed on the Prat quay hydraulic fill were successful in reducing its flow liquefaction potential.
iv) Proposal of a protocol to assess and reduce flow liquefaction for hydraulic fills.

1.3. Thesis layout

This Thesis is organized in six Chapters and six Appendices. Each Chapter contains its own introduction, summary and a list with cited references. The main contents of each Chapter are as follows:

Chapter 2 presents the Phase 1 Prat quay failure. This includes the description of the construction of Phase 1 and Phase 2, the records of quay wall movements before the failure in both phases, the description of the failure itself, the subsequent site investigation, the properties and parameters obtained for each material with particular emphasis on soil strength, and, finally, evidences of flow liquefaction in the Prat quay failure.

In Chapter 3, the phenomenon of hydraulic fill flow liquefaction is reviewed in the context of critical state and state parameter, undrained softening, critical/steady state, peak strength and different triggering mechanisms. Based on the test results obtained from the site investigation, the liquefied strength is estimated and the criteria for flow liquefaction are applied. Finally, a constitutive model for flow liquefaction is presented to simulate the behaviour of hydraulic fill.

In Chapter 4, an account of the finite element (FE) analysis of the Prat quay failure is provided. The description of the analyses include the definition of a suitable constitutive model for each material, the geometry and the material distribution, the boundary conditions and the construction stages. Two different triggering mechanisms are considered; both result in a failure. A parametric study of selected material parameters is performed to check their effect on the prediction of quay failure. Finally, the results of the analyses are compared with field failure observations.

Chapter 5 presents the designed construction of Prat quay -Phase 2 and Phase 1-, after the failure. In this sense, Phase 2 has to be improved and Phase 1 must be reconstructed. Two main analysis of Phase 2 are presented in this Chapter, a FE analysis before soil improvement and a FE analysis during and after soil improvements. Then, criteria evaluation for flow liquefaction before and after soil improvement are compared for the hydraulic fill of Phase 2. This is followed by a brief description of Phase 1 reconstruction. Lastly, a protocol to evaluate liquefaction potential for hydraulic fills is presented.

Finally, Chapter 6 provides the conclusions reached, and gives recommendations for further research.

Appendix A contains the methodology to compute the factor of safety for the FE analyses. Appendix B provides the results of the FE analysis of Prat quay Phase 1 according to initial hypothesis of total hydraulic fill liquefaction. Appendix C describes the results of the simulation of (i) Phase 2 up to the failure of Phase 1 and (ii) once Phase 2 quay was improved, both simulations were analysed in accordance with the initial hypothesis of hydraulic fill liquefaction. Barcelona seismic conditions are presented in Appendix D. Appendix E shows the results of the cyclic liquefaction criteria before and after soil improvement. Finally, the result of a settling column, using hydraulic fill from Prat quay is presented in Appendix F.

1.4. References

Alonso, E. E., Gens, A. 2006. Aznalcóllar dam failure. Part 1: Field observations and material properties. Géotechnique 56, No. 3, 165–183.

Been, K., Jefferies, M. G. 1985. A state parameter for sands. Géotechnique 35, 99–112.

Bishop, A.W., Hutchinson, J.N., Penman, A.D.M., and Evans, H.E. 1969. Geotechnical investigation into the causes and circumstances of the disaster of 21st October 1966. A selection of Technical Reports submitted to Aberfan Tribunal, Welsh Office, Her Majesty's Stationery Office (HMSO), London.

Bishop, A. W. 1973. The stability of tips and spoil heaps, Quaterly Journal of Engineering Geology 6, 335–376.

Casagrande, A. 1936. Characteristics of cohesionless soils affecting the stability of earth fills. J. Boston Society of Civil Engineers 23, 257–276.

Fourie, A.B., Blight, G.E., Papageorgiou, G. 2001. Static liquefaction as a possible explanation for the Merriespruit tailings dam failure. Canadian Geotechnical Journal 38, 707–719.

Hazen, A. 1918. A study of the slip in the Calaveras Dam. Engineering News-Record, 81(26): 1158-1164.

Jefferies, M. & Been, K. 2006. Soil Liquefaction. A critical state approach. Taylor & Francis Book.

Olson, S. M., & Stark, T. D. 2002. Liquefied strength ratio from liquefaction flow failure case histories. Canadian Geotechnical Journal 39, 629–647.

Royal Boskalis Westminster nv (2009). "Trailing Suction Hopper Dredger – technique". Source: http://www.boskalis.com.

Schofield, A. N., Wroth, C. P. 1968. Critical state soil mechanics, McGraw-Hill, London.

Terzaghi, K., Peck, R. B. 1948. Soil mechanics in engineering practice. 2nd ed. Chichester: Wiley, pp 108.

Transporte XXI 2007. Comic strip, El periódico del Transporte y la Logística en español, 15/7/07, Barcelona (2007).

van't Hoff, J. & van der Kolff, A. N. (eds) 2012. Hydraulic fill manual for dredging and reclamation works. Boca Raton, FL, USA: CRC Press/Balkema (Taylor and Francis Group).

Yamamuro, J.A., and Lade, P.V. 1999. Experiments and modelling of silty sands susceptible to static liquefaction. Mechanics of Cohesive-Frictional Materials, 4(6): 545–564.

Chapter 2. Prat quay failure. Description and site investigation

2.1. Introduction

On the first of January 2007, the Prat quay failed catastrophically with significant consequences for the development plans of Barcelona Port. The failure led to economic losses of €75 million, and delayed the start of Prat terminal operations by two years, La Vanguardia (2009). The quay was part of the enlargement of the Barcelona Harbour towards the South that required the lengthening of the East breakwater and the construction of the South breakwater. To accommodate the enlargement, it was also necessary to change the final course of the Llobregat river. Figure 2.1 shows the location of the quay in relation with the new breakwaters and the old and new river mouths.

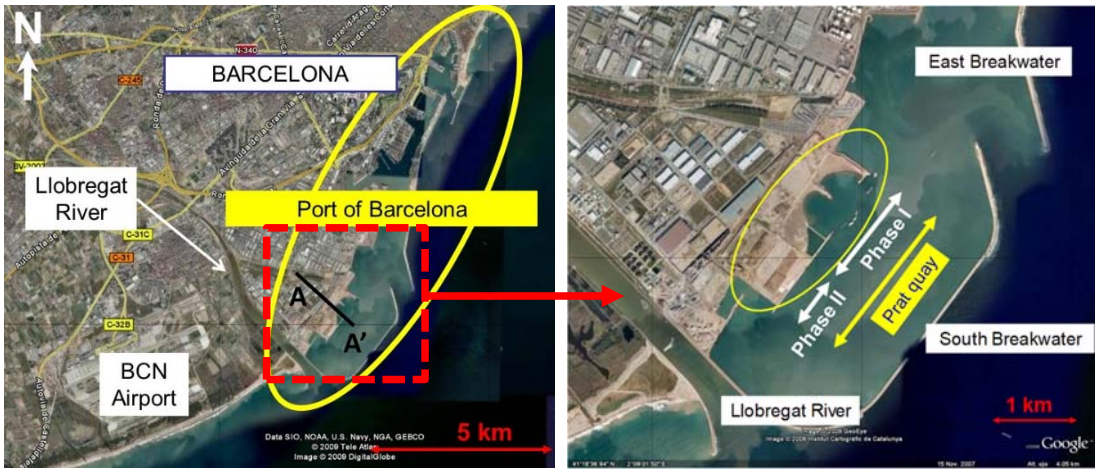

(a) (b)

Figure 2.1. (a) Satellite image showing the location of the Barcelona Port. (b) Satellite image showing the Prat quay, the new breakwaters and the original and new Llobregat river mouth, source Google Maps.

The new quay was intended to provide a working and storage area 1.58 km long 0.6 km wide extending from the quay to the original shoreline. The total length of the quay was divided in two parts: Phase 1, 1000 m long and Phase 2, 580 m long (Figure 2.1b). The quay comprised a concrete caisson wall founded on a rubble mound placed in a dredged trench. The ensemble was founded on soft deltaic deposits; dredged material provided the required fill. Construction started in July 2005 and continued without interruptions until failure occurred.

2.2. Geological and geotechnical profile of the site

The Prat quay was founded on the Holocene deposits of the Llobregat pro-delta. The Llobregat delta is an important sedimentary formation that has been intensely studied. According to Marquès (1974), Bayó (1985), Ventayol (2003) and Lafuerza et al. (2005) the general architecture of the delta consists of six lithological units, which from bottom to top, are: (A) a lower unit of Pliocene blue clays (bedrock); (B) Pleistocene fluvial gravels; (C) delta front and delta plain gravels, sands and some silts, (D) transgressive sands; (E) Holocene pro-delta deposits made up of low permeability clayey silts and silty clays; and (F) a flood plain unit, Figure 2.2.

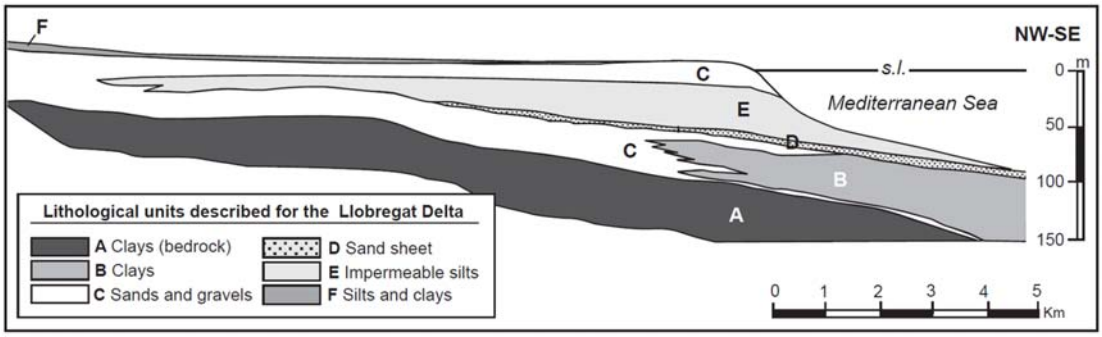

Figure 2.2. General geological profile of the Llobregat delta (modified from Lafuerza et al., 2005).

A more recent detailed stratigraphic study (Gamez, 2007 and Gamez et al., 2009) has identified four depositional sequences bounded by a minimum of three erosional surfaces corresponding to major glacial/interglacial sea-level fluctuations. They result in erosion of previous deposits and their redeposition during sea level fall followed by erosion and resedimentation during sea level rise. The interglacial periods were also characterized by prodelta and delta front facies during highstand sea levels. The study produced a series of detailed geological profiles across the whole delta; Figure 2.3 shows the cross section corresponding to the Prat quay location.

A close-up of the geological profile in the specific area of the Prat quay is shown in Figure 2.4 in which the different materials are identified by their geotechnical terms. The most superficial unit is a sandy alluvial deposit that was in fact partially removed by the dredging of a trench in the first stage of construction. Consequently, the quay wall was founded on a thick deposit of soft silty clay corresponding to the Prodelta geological unit. It can be observed that this unit extends down to a depth of about 70 m where it is underlain by a permeable sand and gravel layer. Presence of biogenic gas in the soft silty clay layer, derived from organic matter, has been reported by Alonso et al. (1995),

Liquete et al. (2008) and Urgeles et al. (2007 and 2011). The presence of gas has also been detected by in situ tests performed during site investigations in the area (Tarragó and Gens 2018).

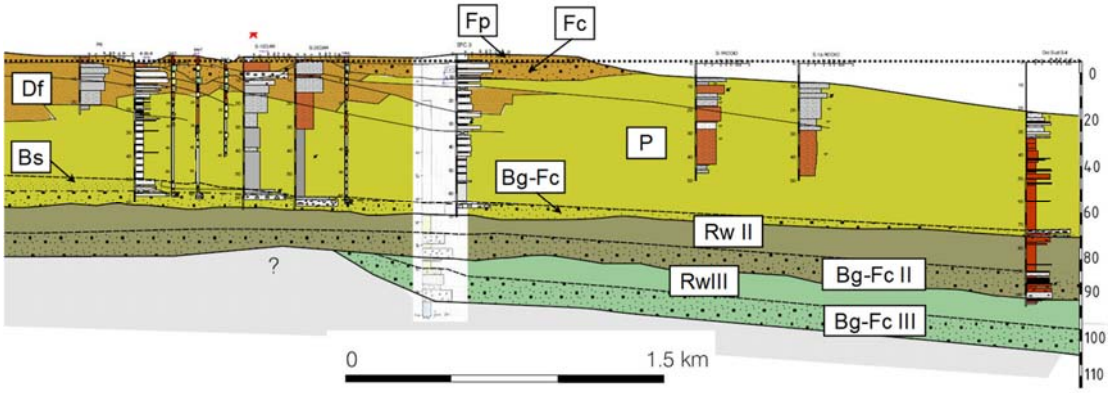

Figure 2.3. Geological profile of the Llobregat delta. Depositional sequence I, Fp: flood plain, Fc: alluvial deposits, Df: delta front, P: Prodelta, Bs: sand beaches, Bg-Fc: gravel facies and alluvial deposits. Depositional sequence II, RW II: fine sediments, Bg-FC II: beach gravels and alluvial deposits. Depositional sequence III, RW III: fine sediments, Bg-FC III: beach gravels and alluvial deposits (modified from Gámez 2007).

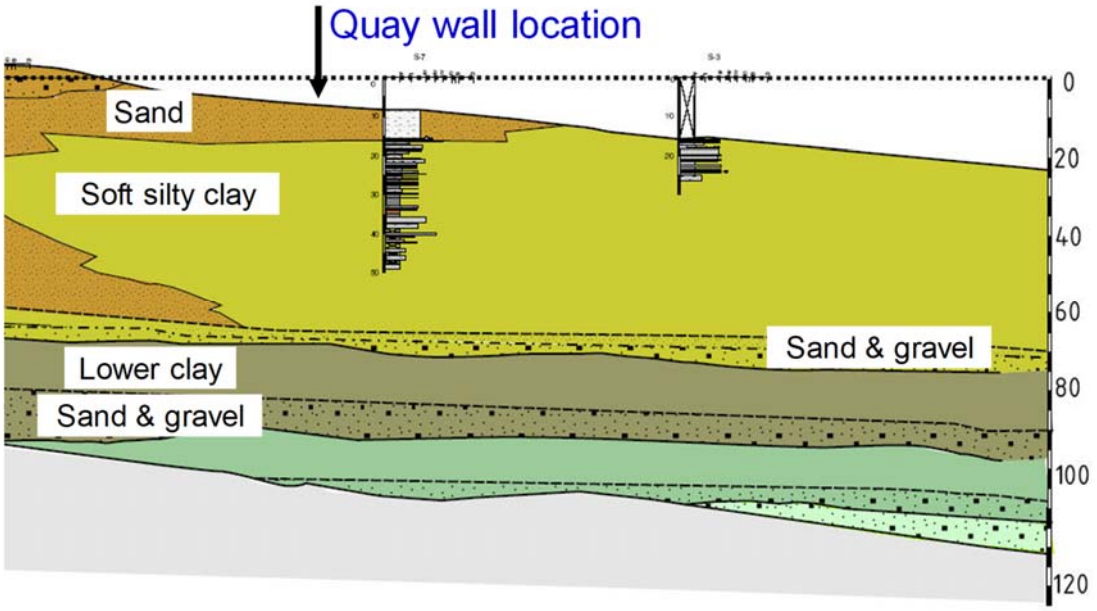

Figure 2.4. Soil profile at the Prat quay area indicating the quay location (modified from Gámez 2007).

2.3. *Construction*

The construction of the Prat quay was carried out in two Phases. The cross-section of Phase 1, the northern sector, is presented in Figure 2.5 and the cross section of Phase 2, the southern sector, is shown in Figure 2.6. Failure involved Phase 1 of the quay only.

The quay wall was constructed with concrete caissons sitting on a rubble mound that was protected by a rip-rap layer on the seaward side. The building sequence for the quay was as follows:

1. Dredging of the natural soil from the initial elevation of -8 m down to -25 m for Phase 1 and -24.50 m for Phase 2 (elevations are referred to mean sea level).
2. Construction of the rubble mound using quarry run material to elevation -16.0 m. The rubble mound material was dumped from barges.
3. Emplacement of the caissons on top of the levelled rubble mound.
4. Filling of the caissons with sand
5. Emplacement of hydraulic fill in the area behind the caissons.

In addition, a rock fill wedge was placed against the back of the caisson in Phase 2 but not in Phase 1. The caissons were 41 m long and 17.5 m high. The caissons of Phase 1 were 18.5 m wide whereas the caissons of Phase 2 were 11.5 m wide. The larger width of the caissons of Phase 1 was due to the fact that the South breakwater was under construction when the caissons were emplaced, so they were designed to withstand possible storms until the protection breakwater was completed. 25 caissons were used for Phase 1 and 15 for Phase 2. For the hydraulic fill, the material dredged in the vicinity of the quay was used. It was mainly fine-grained corresponding to the silty clay Prodelta layer. It was deposited by a flowing stream of water using the rainbowing (or pumping ashore) technique (Figure 2.7). The material was sprayed into enclosures bounded by the quay and lateral embankments built for this purpose, as required by the progress of the works. The fill was variable in grading because of variations at source and because of the segregation that occurred as a result of the method of placement.

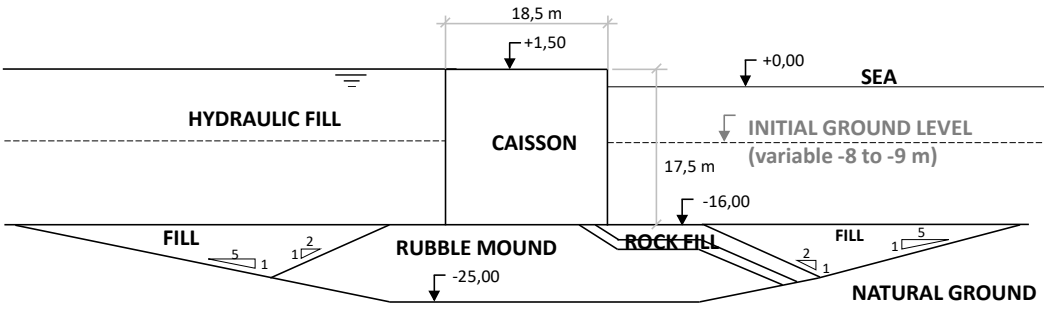

Figure 2.5. Design cross section, Phase 1.

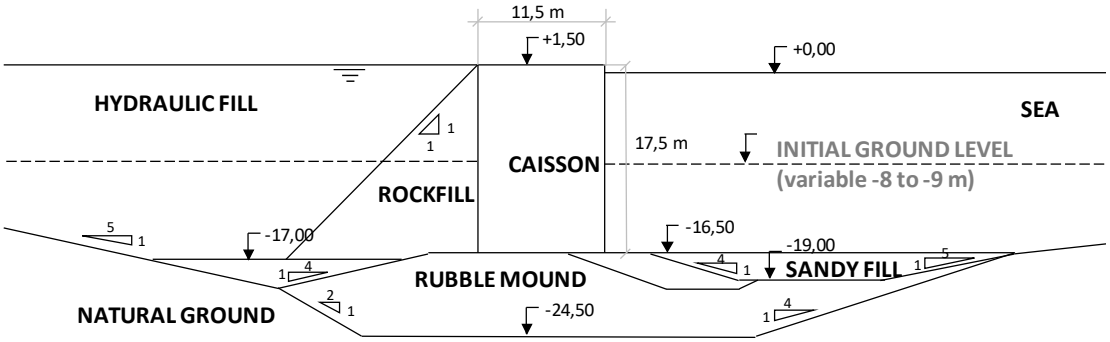

Figure 2.6. Design cross section, Phase 2.

Figure 2.7. Rainbowing technique during construction, Prat quay.

The time-history of Phase 1 construction is presented in Figure 2.8 that shows the increase of fill elevation with time. It can be noted that the fill emplacement spanned a period of approximately 8 months. There was a short pause of about one month when the fill reached an elevation of +0 m. At that point, an earth bund was constructed on top of the caisson to elevation +4 m (Figure 2.9). In this way, the hydraulic fill could be deposited to an elevation higher than that of the top of the caisson (+1.5 m). The aim was to speed up the process of consolidation of fill and foundation ground.

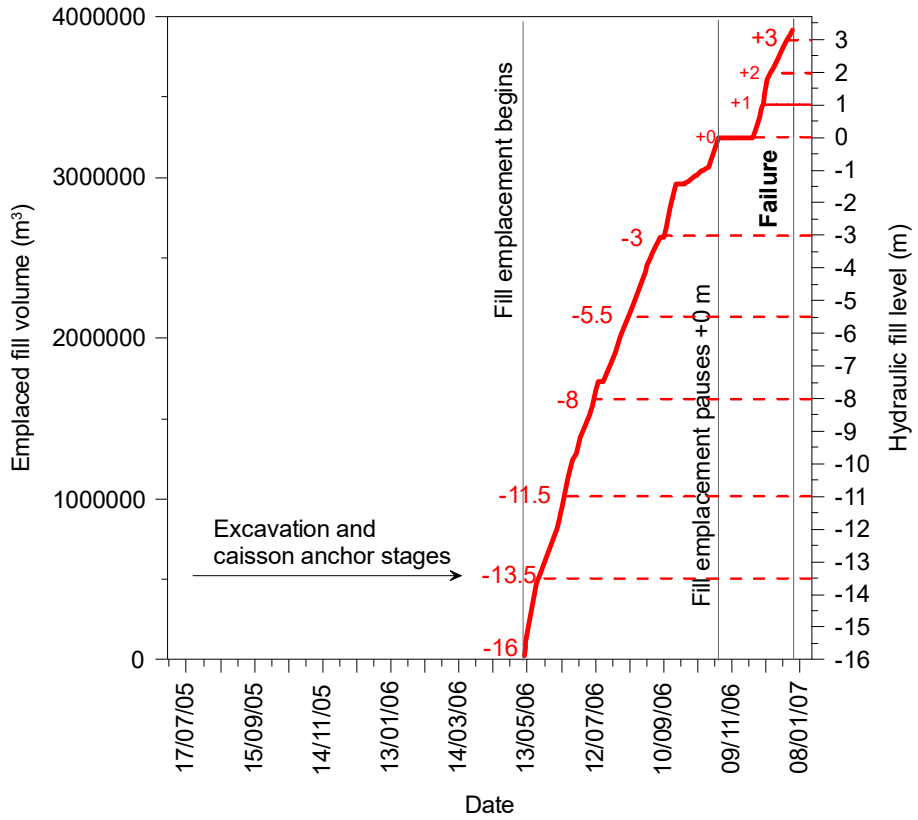

Figure 2.8. Evolution of the hydraulic fill level and deposited volume with time, Phase 1.

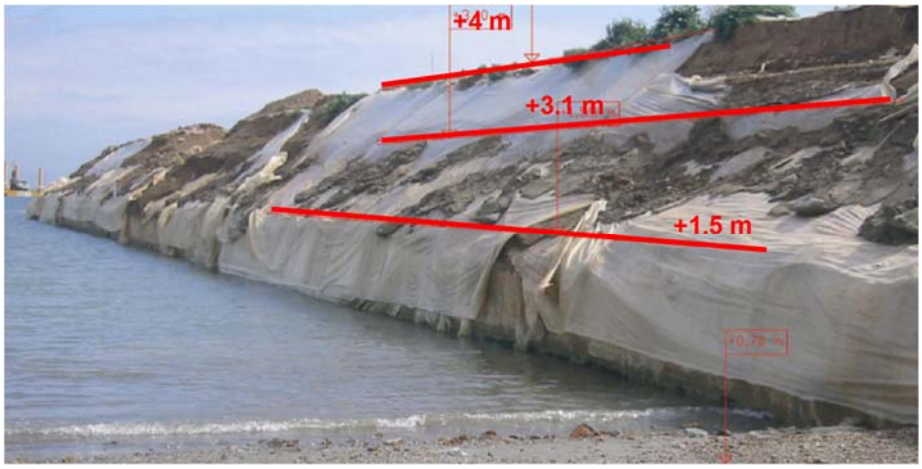

Figure 2.9. Earth bund constructed on top of the caissons (picture taken after the failure).

Settlements and horizontal displacements of the caissons were monitored by surveying; the observations for Phase 1 caissons are plotted in Figure 2.10 and Figure 2.11. Caisson are numbered from South to North; caissons 10 to 24 were involved in the failure. As Figure 2.10 shows, most of the settlements occurred during the emplacement and filling of the caissons and immediate consolidation. Settlements reactivated when hydraulic filling started. In contrast, horizontal movements (Figure 2.11) were small during emplacement and filling of the caissons -when the loading is basically vertical-, and increased significantly as fill elevation increased. The distribution of vertical and horizontal movements just before failure in the different caissons of Phase 1 are shown in Figure 2.12 and Figure 2.13. Settlements are largely uniformly distributed whereas the horizontal displacements of the caisson involved in the failure (10 to 24) were larger. It is possible that the larger horizontal movements were associated with a poorer quality of the fill material. It should be noted that the survey markers were placed at the top corners of the caisson; therefore, observed horizontal movements contain an unquantified caisson rotation effect.

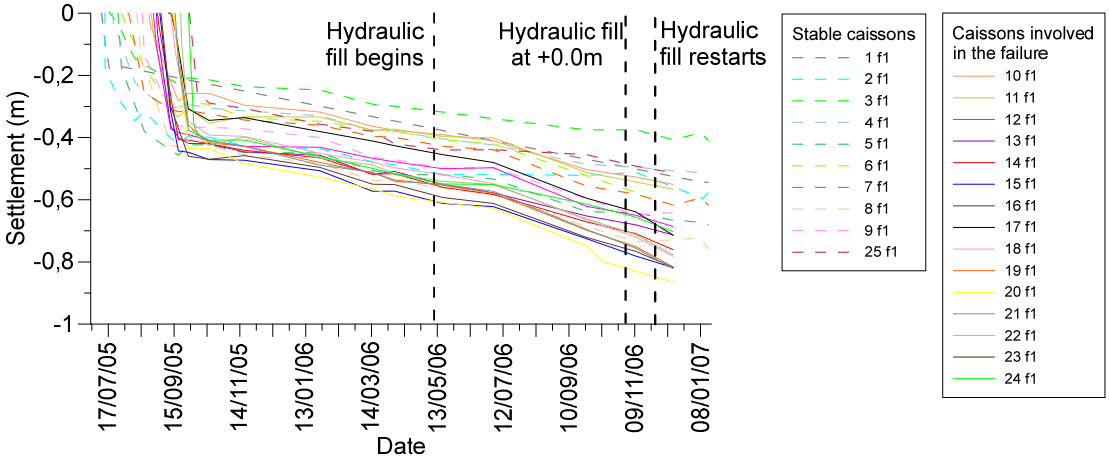

Figure 2.10. Vertical displacement of Phase 1 caissons during construction.

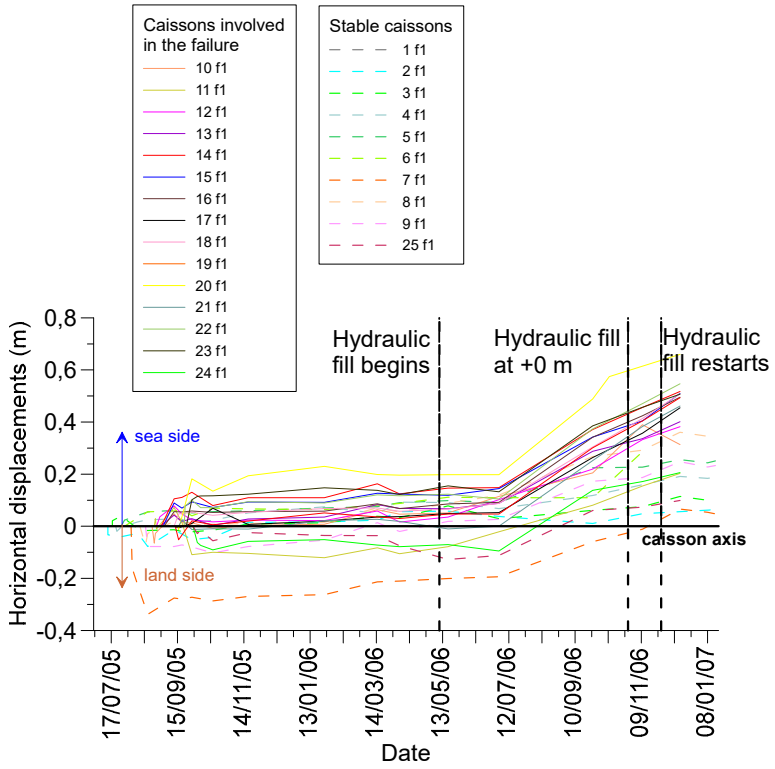

Figure 2.11. Horizontal displacements of Phase 1 caissons during construction.

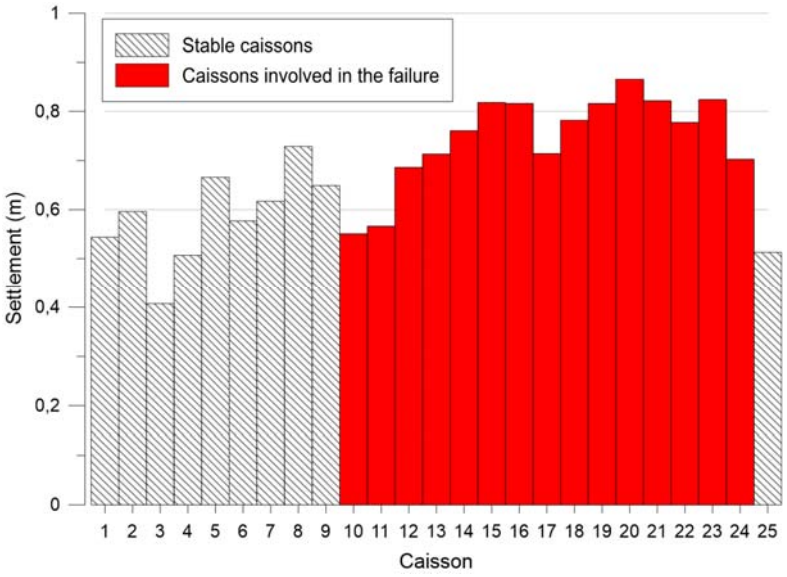

Figure 2.12. Settlements of Phase 1 caissons just before failure. Caissons 10 to 24 were involved in the failure.

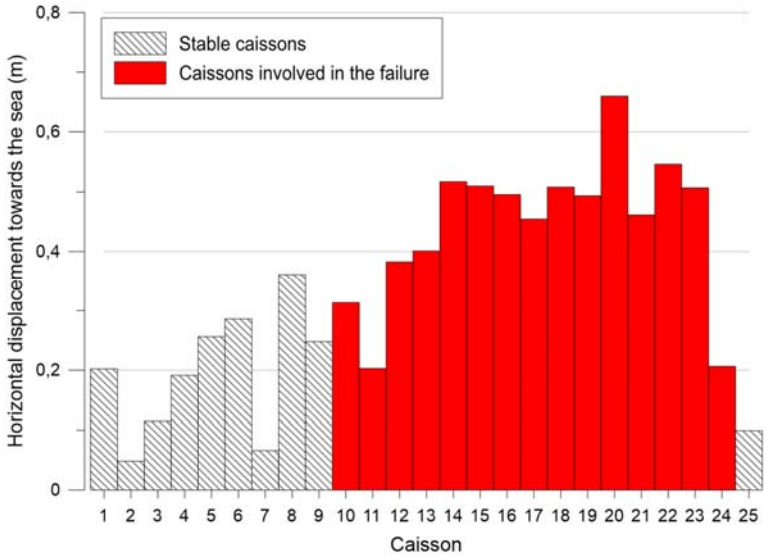

Figure 2.13. Horizontal displacements of Phase 1 caissons just before failure. Caissons 10 to 24 were involved in the failure.

2.4. *The failure*

Immediately before failure, the construction of Phases 1 and 2 had reached the stage reflected in the cross sections of Figure 2.14 and Figure 2.15 were the presence of the earth bund on top of the caissons can be noted. Hydraulic fill elevation in Phase 1 was +3.00 m, higher than that of the top of the caisson. It was also higher than in Phase 2 because completion of Phase 1 was prioritised. There was water on top of the fill reaching a +3.50 m elevation in Phase 1.

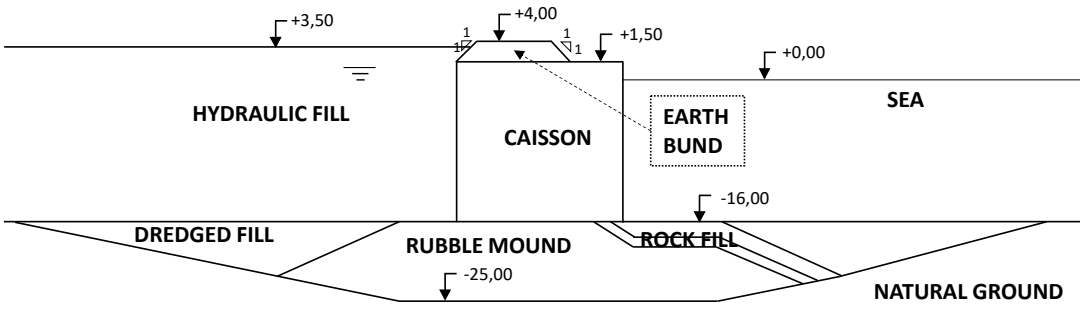

Figure 2.14. Cross section of Phase 1 just before failure.

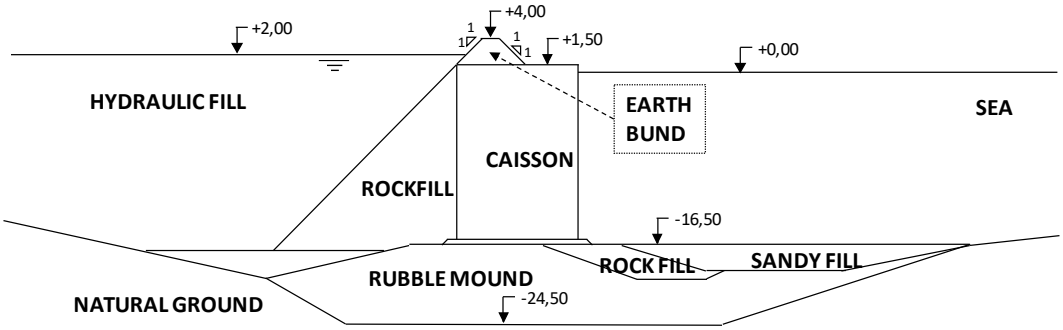

Figure 2.15. Cross section of Phase 2 just before failure.

On January 1st 2007, there was only a person on the quay controlling the hydraulic filing that was taking place from discharge points located in the quay stretch between caissons 14 to 20 approximately. The eyewitness reported that around 10 a.m. he saw five or six discharges of gas and sprayed water into the air next to the quay wall -he described them as "geysers"-, before any movement of the caissons were observed. Immediately afterwards failure took place along a length of 600 m involving caissons 10 to 24. The hydraulic fill liquefied and was able to drag the very heavy caissons for long distances, up to 90 m. The eyewitness had fled the area after observing the gas/water discharges and there was no direct observation of the failure itself. Figure 2.16 and Figure 2.17 show aerial photos where the geometry of the failure can be clearly seen. The back of the failure (Figure 2.18) displays the typical shape of a flow slide. Figure 2.19 depicts the sea level variation recorded in the vicinity. A large sea level variation occurred just after 10 a.m., the oscillations slowly dampening out over a period of one hour.

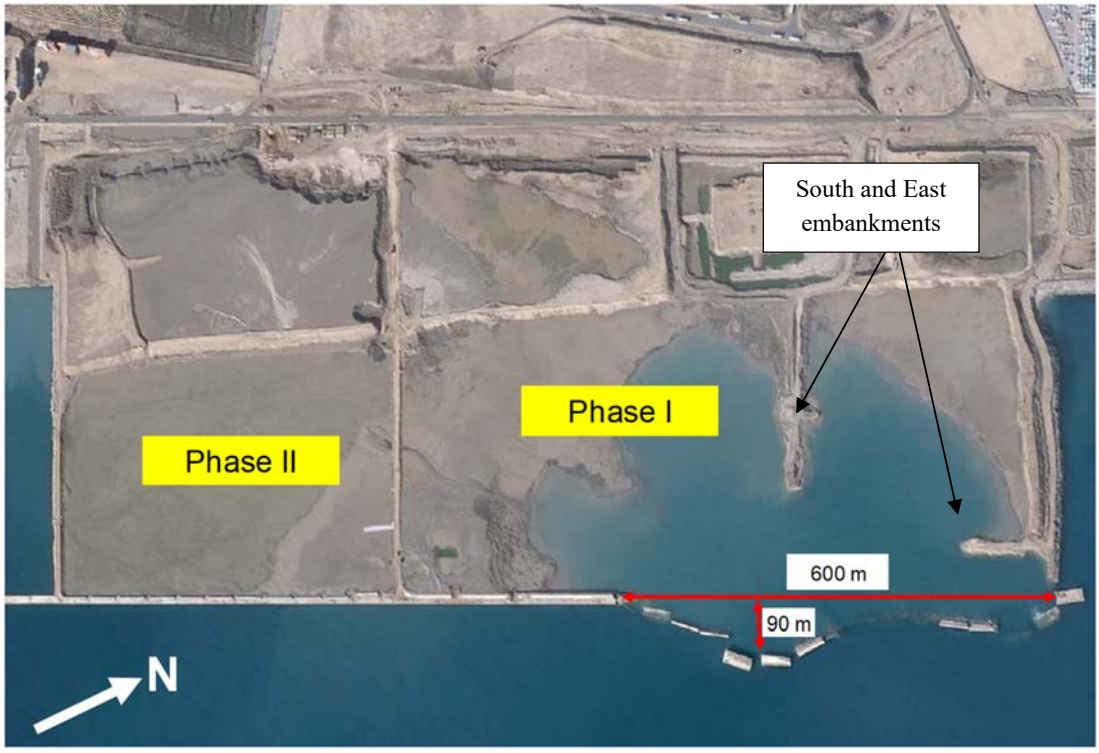

Figure 2.16. Aerial photo of failure showing its length and the maximum distance travelled by the caissons. The locations of the South and East embankments are also shown, (Courtesy of Barcelona Port Authority).

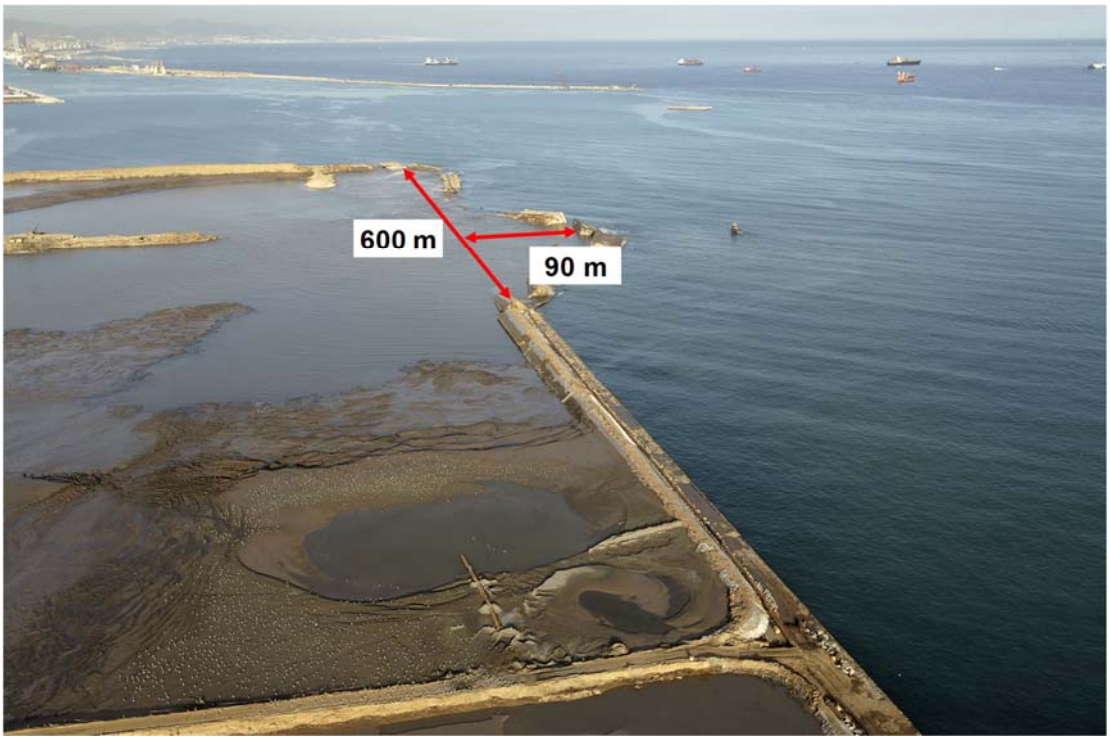

Figure 2.17. Aerial photo of Phase 1 of the failure (Courtesy of Barcelona Port Authority).

Figure 2.18. Aerial photo of Phase 1 of the failure (Courtesy of Barcelona Port Authority).

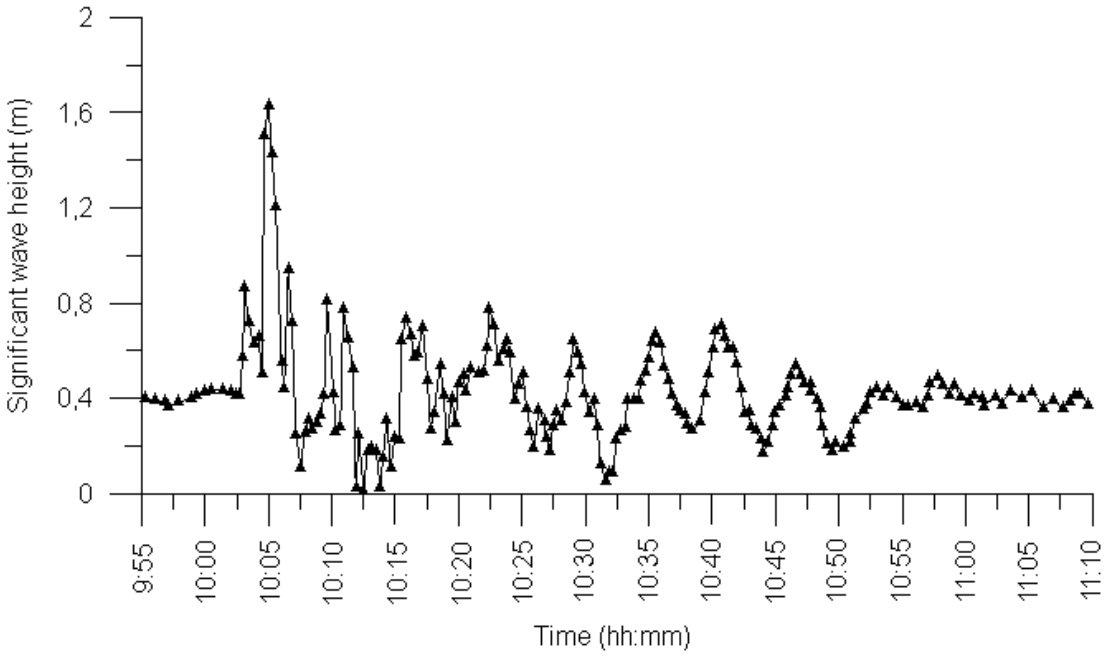

Figure 2.19. Sea level variation recorded in the Barcelona Port on January 1st 2007 from 9:55 a.m. to 11:10 a.m.

Figure 2.20 presents the distribution of horizontal displacements undergone by the different caissons. The maximum movements involved caissons 14 and 15 and three was a second displacement peak corresponding to caisson 23.

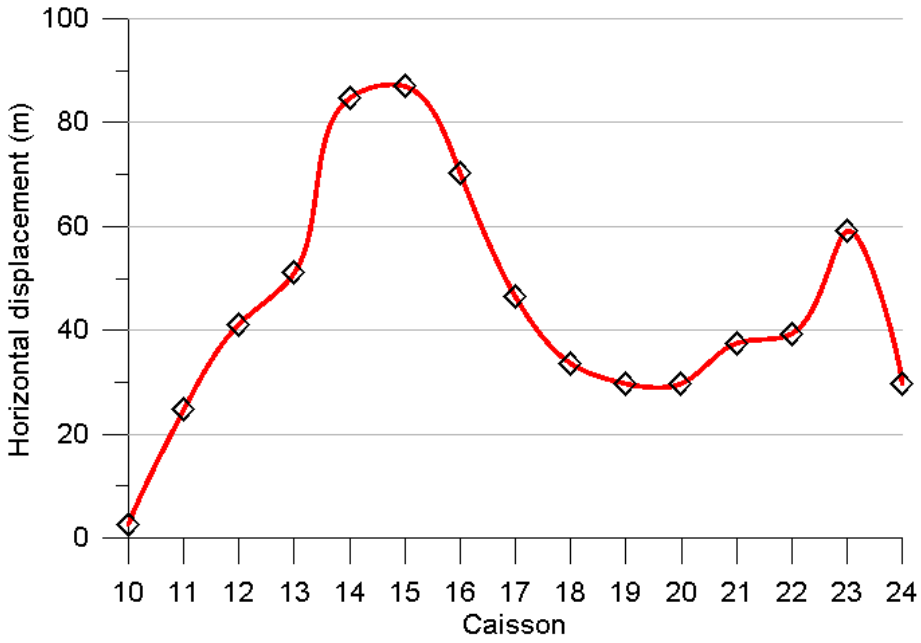

Figure 2.20. Horizontal failure movements of caissons.

Figure 2.16 also shows the location of two embankments, South and East that were being built when the fill reached elevation +2.5 m. Their purpose was to bound an enclosure for preloading fill and foundation. Embankment South used sand fill and embankment East used rock rubble. Embankment South was constructed from the shore towards the quay; at the time of failure its leading edge was at

a distance of about 90 m from the quay wall in front of caisson 14 and 15. Embankment East was constructed from the northern end at a distance of about 60 m from the quay wall and had reached a length of 130 m at the time of failure. It should be noted that parts of the embankments -about 60 m in the case of the South embankment-, disappeared as a consequence of the failure and are not visible in Figure 2.16. The method of construction consisted in dumping the embankment material and displacing the weak fill although not to full depth; thus, the embankments were at limiting equilibrium throughout. It is likely that the gas/water release in front of leading edge of the South embankment triggered its failure; the resulting disturbance caused the fill to liquefy providing the necessary unbalanced force to move the caissons over long distances. Supporting evidence for this mechanism se presented in Chapter 4 that contains the relevant analyses of the failure.

At the time, there was uncertainty about the specific mode of failure immediately after the failure. Preliminary analyses showed that the factors of safety corresponding to a deep-seated failure involving the natural ground and a caisson sliding failure were very similar. However, subsequent investigations found that the rubble mounds were largely intact (Figure 2.21), only a small part of the seaside edge was missing in a few sections. Therefore, it was unambiguously established that the mode of failure was that of the caissons sliding on the foundation rubble mound.

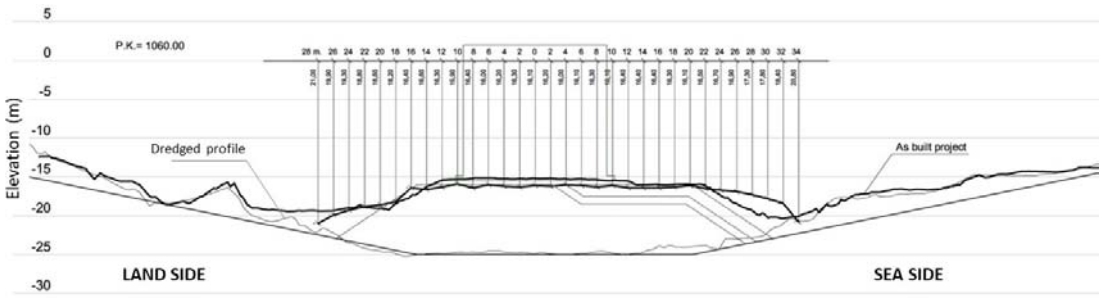

Figure 2.21. Shape of the rubble mound after the failure compared with the as-built profile. Caissons 14-15.

2.5. Site investigation

2.5.1. General

A large-scale site investigation was launched after the failure. It involved drilling of boreholes, including SPT tests and sample extraction, Cone Penetrometer tests (CPTu), VAT permeameter tests and Flat Marchetti Dilatometer (DMT) tests. Laboratory testing on retrieved samples was also performed. The site investigation embraced the failed section, the rest of Phase1 quay and Phase 2 quay. The overall layout of the site investigation is shown in Figure 2.22. There were five cross sections in the Phase 1 zone and two in the Phase 2 area. Only selected results of the site investigation are presented here.

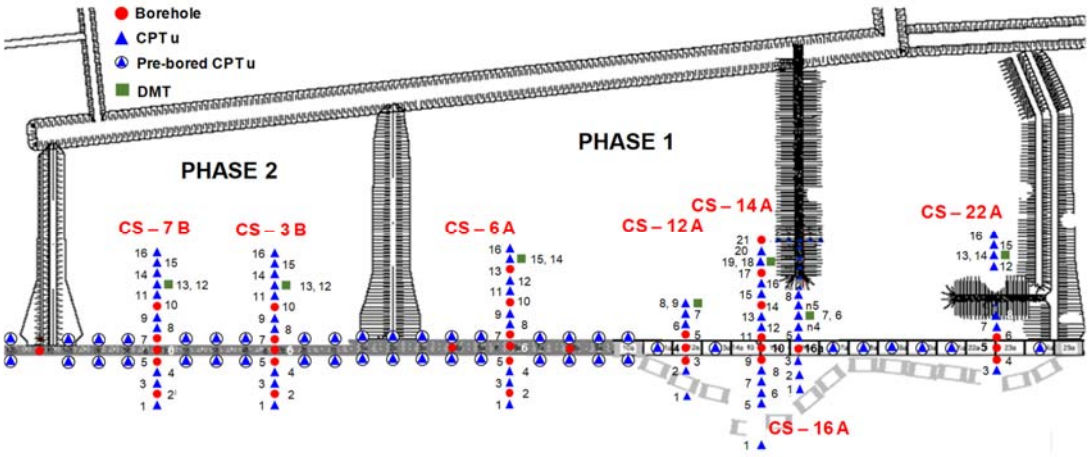

Figure 2.22. Layout of the site investigation after the failure.

Observations of the post-failure bathymetric survey, the borehole logs and the SPT and CPTu tests have been combined in the cross-sections depicted in Figure 2.23, Figure 2.24, Figure 2.25 and Figure 2.26. Figure 2.23 shows Cross-section 14A that corresponds to the failed zone in the region of maximum caissons displacements where it can be observed that some of the material of the rubble mound was removed by the failure or by events after the failure. However, all the boreholes performed found the rubble mound material indicating that no deep-seated failure affecting the natural round had occurred. Similar observations were made in boreholes drilled at the original locations of displaced caissons. Naturally, the hydraulic fill has largely disappeared from this cross-section.

Cross-section CS-6A (Figure 2.24) is an important one because it corresponds to a non-failed section of Phase 1 and it probably provides the most reliable information of the hydraulic fill before failure. Natural ground and hydraulic fill can be easily distinguished in the results of CPTu test and in the borehole logs. For comparison, cross- sections of Phase 2 (CS-3B and CS-7B) are presented in Figure 2.25 and Figure 2.26.

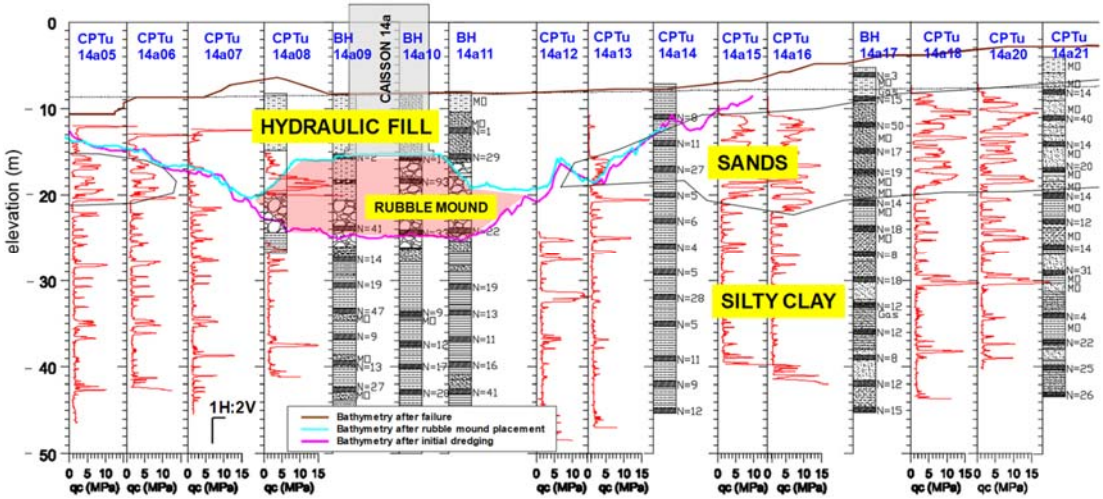

Figure 2.23. Cross section 14A according to borehole records, CPTu and SPT tests results, Phase 1 affected by the failure.

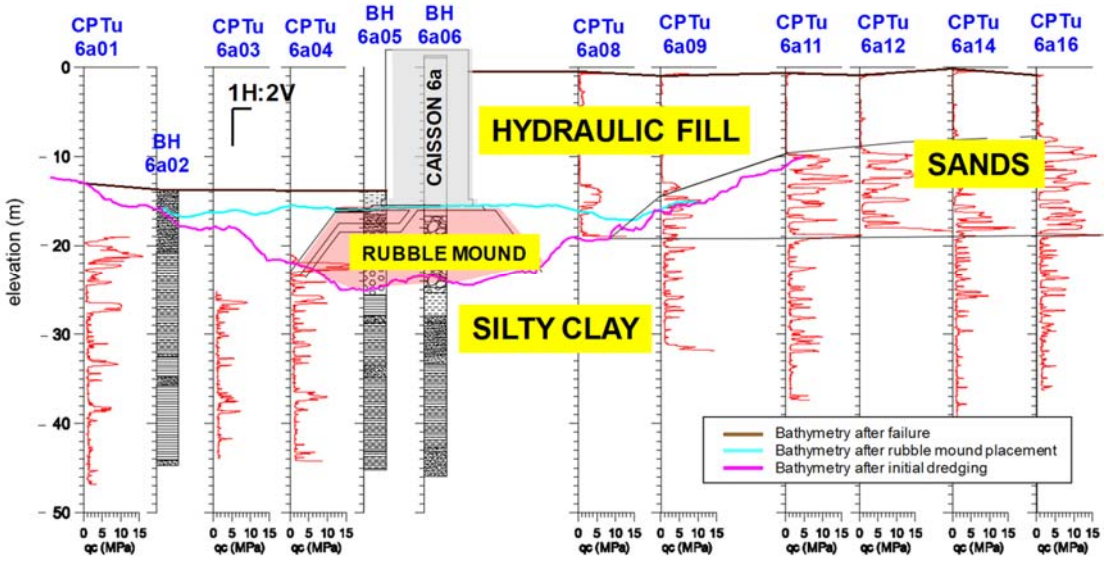

Figure 2.24. Cross section 6A according to borehole records, CPTu and SPT tests results, Phase 1 affected by the failure.

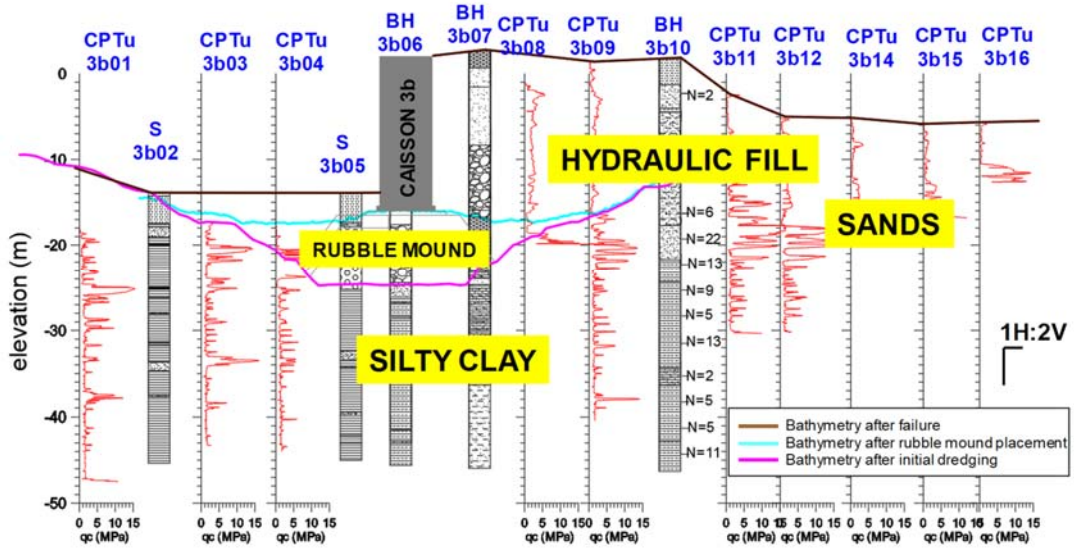

Figure 2.25. Cross section 3B according to borehole records, CPTu and SPT tests results, Phase 2.

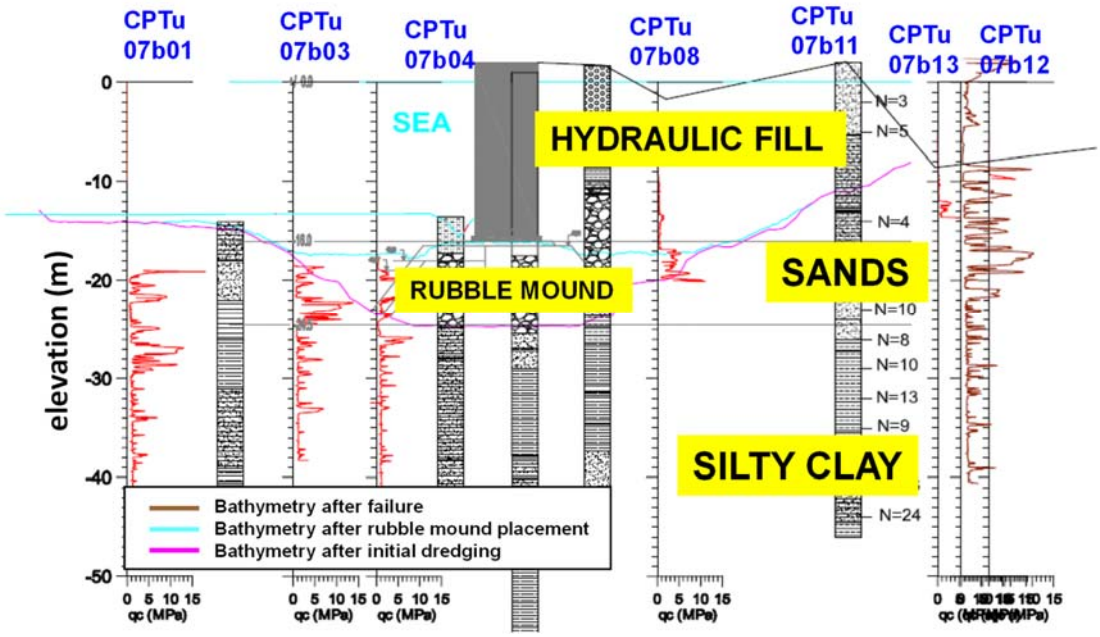

Figure 2.26. Cross section 7B according to borehole records, CPTu and SPT tests results, Phase 2.

During borehole drilling several gas escapes were recorded, mainly from natural ground. To clarify this issue, VAT permeameter tests were carried out at different depths from fill and natural ground. No trapped gas could be detected in the hydraulic fill for both Phase 1 and Phase 2 but biogenic gas identified in the silty clay layer of the natural ground, a specific article about this issue was presented in Tarrago and Gens (2018).

2.5.2. In-situ testing

2.5.2.1. CPTu tests

Cone resistance, pore pressure and sleeve friction measured in the CPTu tests performed in the land area of Cross-section 6A are represented in Figure 2.27, Figure 2.28 and Figure 2.29. It is apparent that cone resistances (Figure 2.27) are very low in the hydraulic fill, the transition to the natural ground is clearly visible. Some excess pore water pressures were generated by cone penetration in the backfill areas of lower q_c, as shown in Figure 2.28. A noticeable behaviour difference between hydraulic fill and in-situ ground is also apparent in the sleeve friction, small values of f_s in the fill were measured, Figure 2.29.

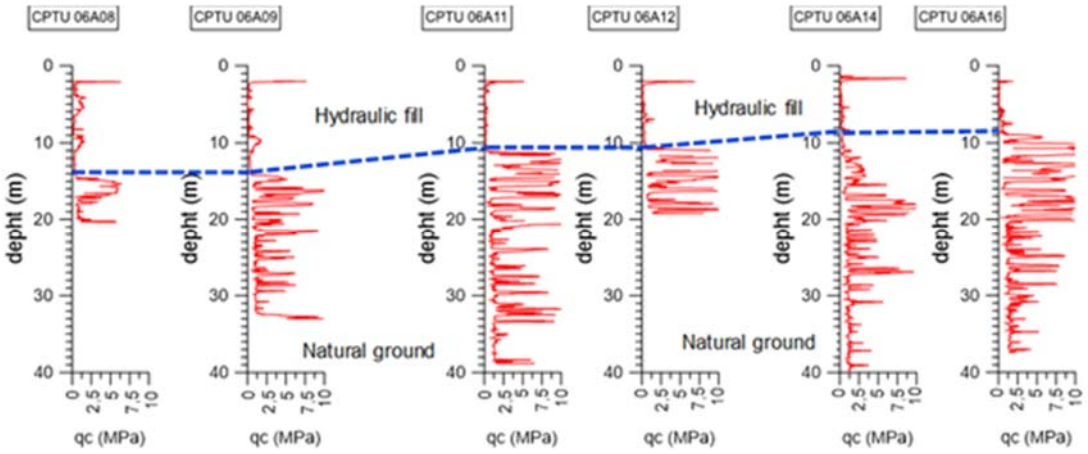

Figure 2.27. Cone resistances in a non-failed section CS-6A of Phase 1.

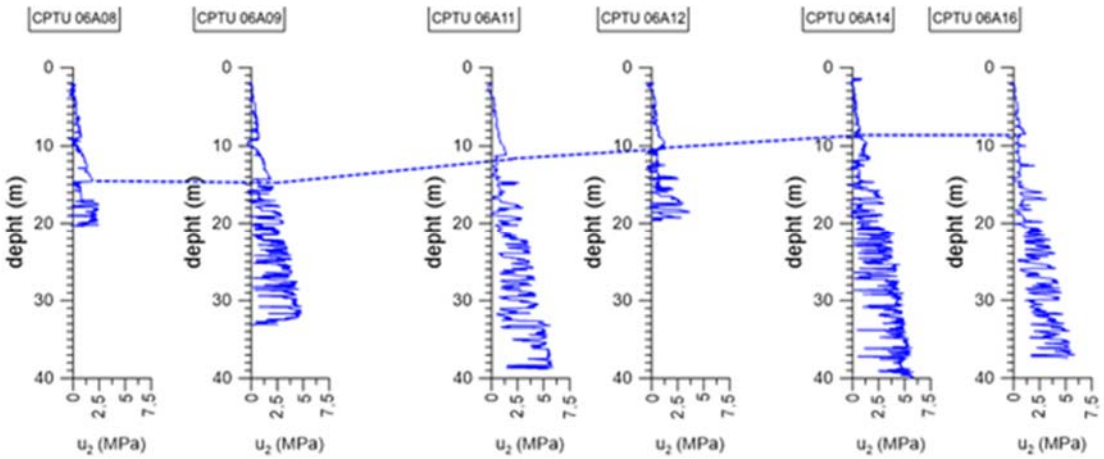

Figure 2.28. Cone pore pressures in a non-failed section CS-6A of Phase 1.

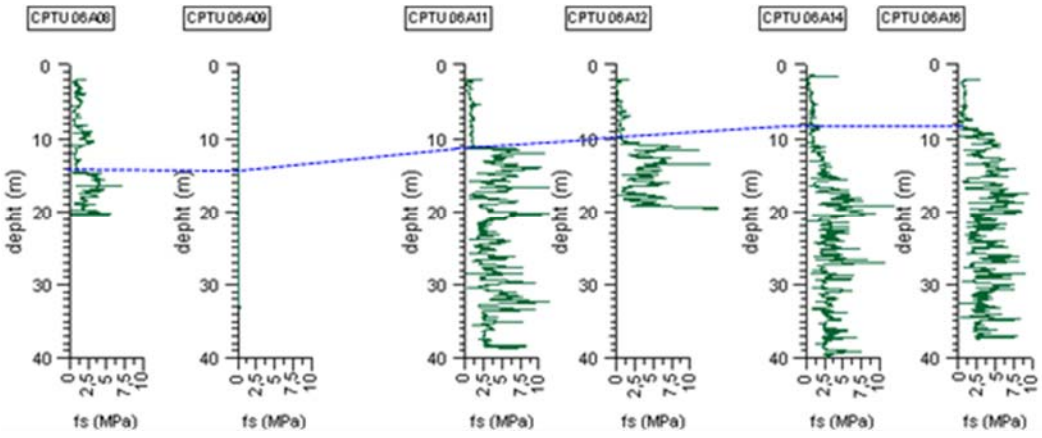

Figure 2.29. Cone sleeve friction in a non-failed section CS-6A of Phase 1.

Figure 2.30, Figure 2.31, Figure 2.32 and Figure 2.33 show in more detail CPTu observations of cone resistance (q_c), pore pressure (u_2) and sleeve friction (f_s) at four different locations. Hydraulic fill appears largely homogenous at each location with very low value of cone resistance. The CPTu results also show that the natural ground exhibits an interbedded sequence of low plasticity silty clays and silty fine sands.

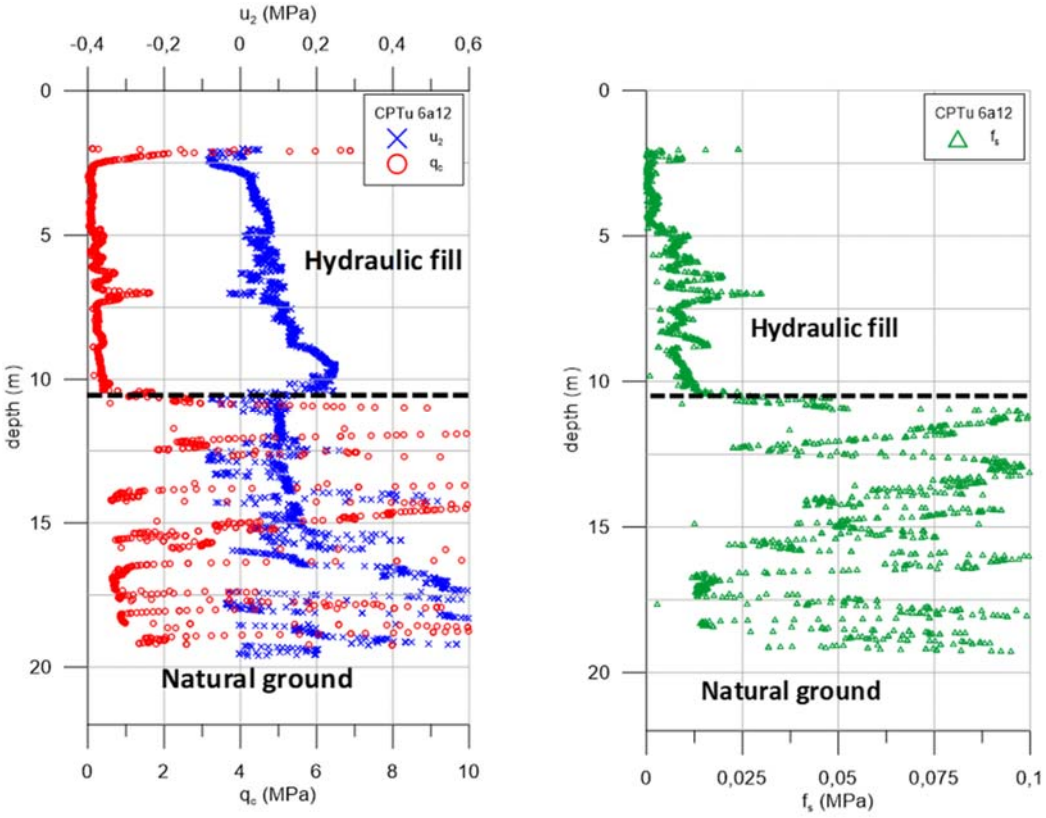

Figure 2.30. CPTu results of sounding 6a12.

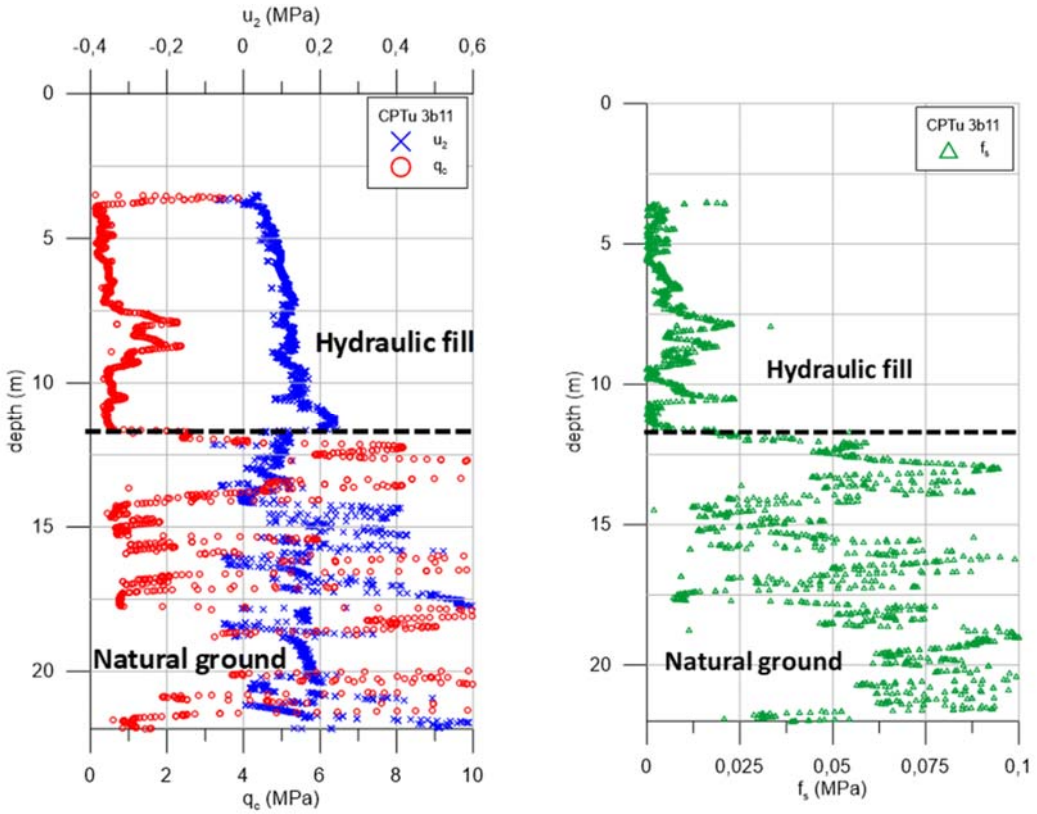

Figure 2.31. CPTu results of sounding 3b11.

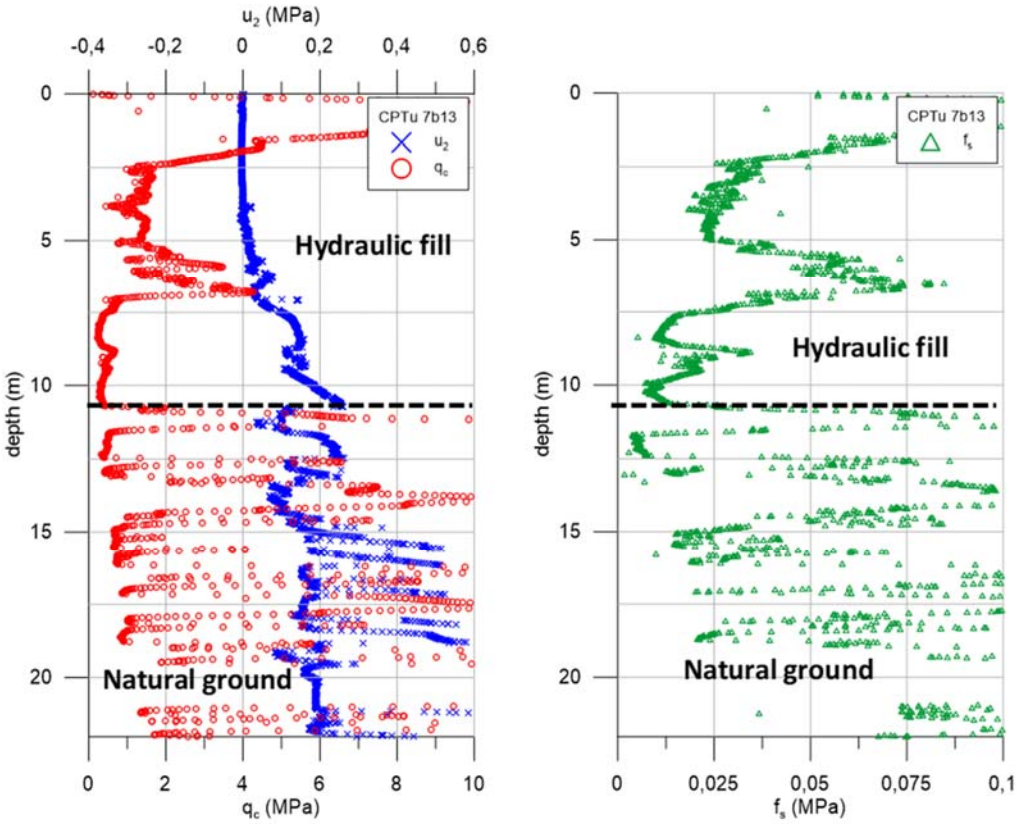

Figure 2.32. CPTu results of sounding 7b13.

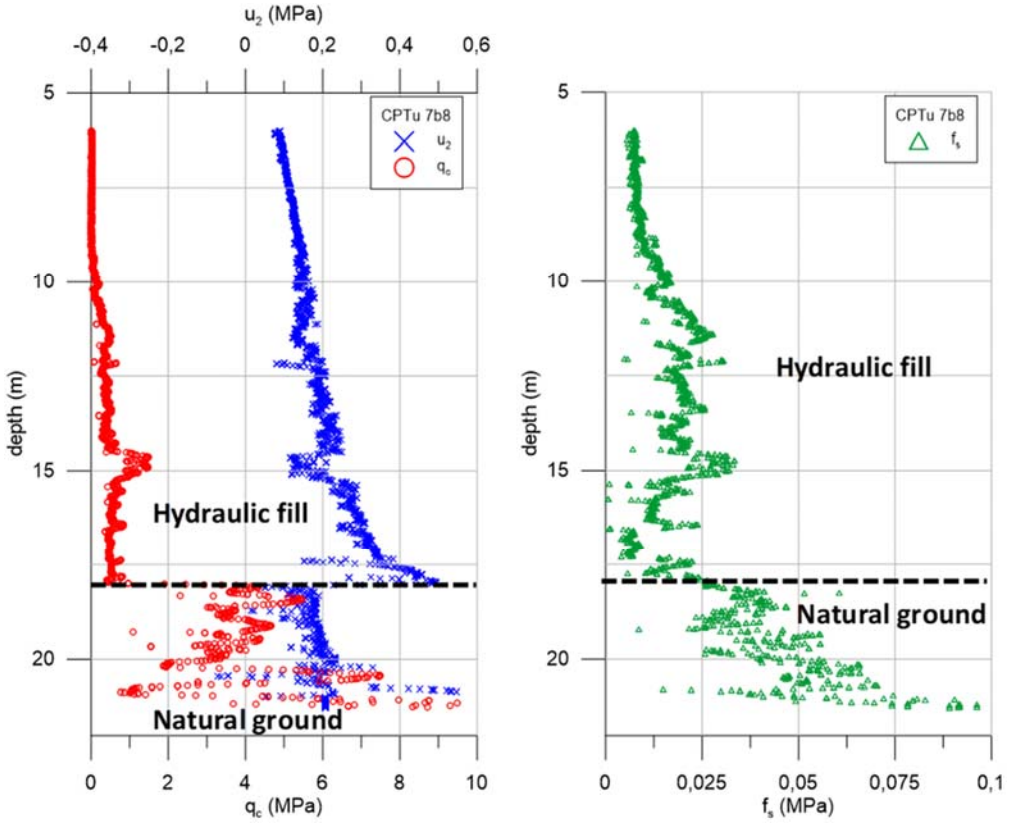

Figure 2.33. CPTu results of sounding 7b8.

Dissipation tests were performed systematically during the cone penetration tests. The horizontal coefficient of consolidation (c_h) were estimated using Houlsby and Teh (1988) approach. The results for Phases 1 and 2 are shown in Figure 2.34. It can be observed that there is a larger scatter in the hydraulic fills results compared with the natural ground. Values of c_h in the hydraulic fill are generally larger than those of the natural ground

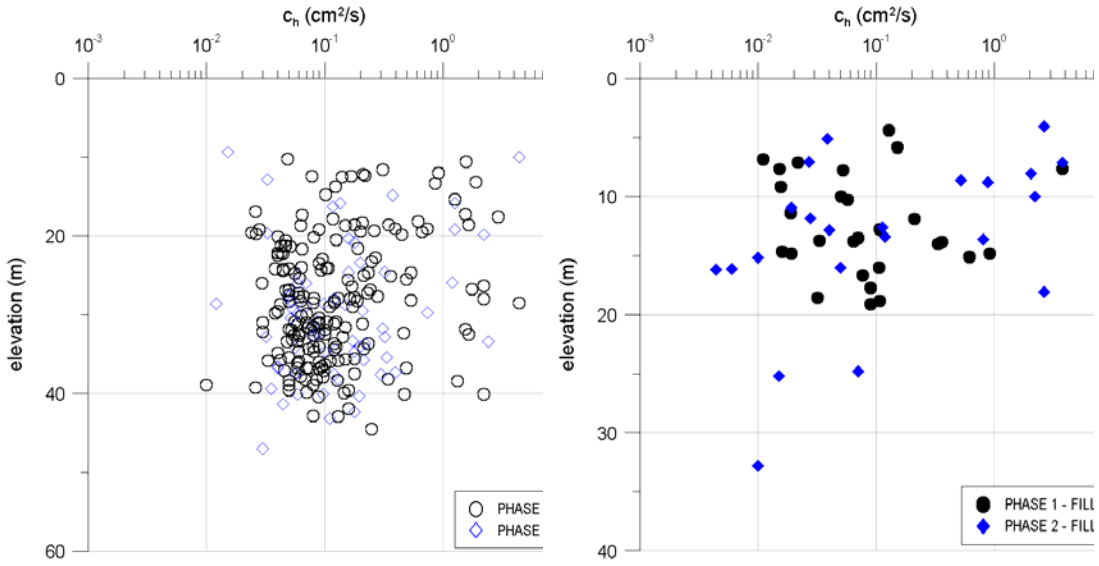

(a) (b)

Figure 2.34. Dissipation tests results, c_h in (a) natural ground and (b) hydraulic fill.

2.5.2.2. DMT tests

Marchetti Dilatometer tests (DMT) also performed, four in the Phase 1 area and two in the Phase 2 area. The DMT soundings were always carried out next to a CPTu test location. The Standard DMT parameters P_1 and P_0 were obtained from test results. They are combined to obtain the soil index (I_{DMT}) , the horizontal stress index (K_{DMT}) and the coefficient of earth pressure at rest (K_0):

$$I_{DMT}=(P_1-P_0) / (P_0-u_0) \quad [2.1]$$

$$K_{DMT}=(P_0-u_0) / \sigma'_{v0} \quad [2.2]$$

$$K_{0\,DMT} = 0.47 \cdot \left(\frac{K_{DMT}}{1.5}\right) - 0.6 \quad [2.3]$$

Selected results are plotted in Figure 2.35, Figure 2.36 and Figure 2.37.

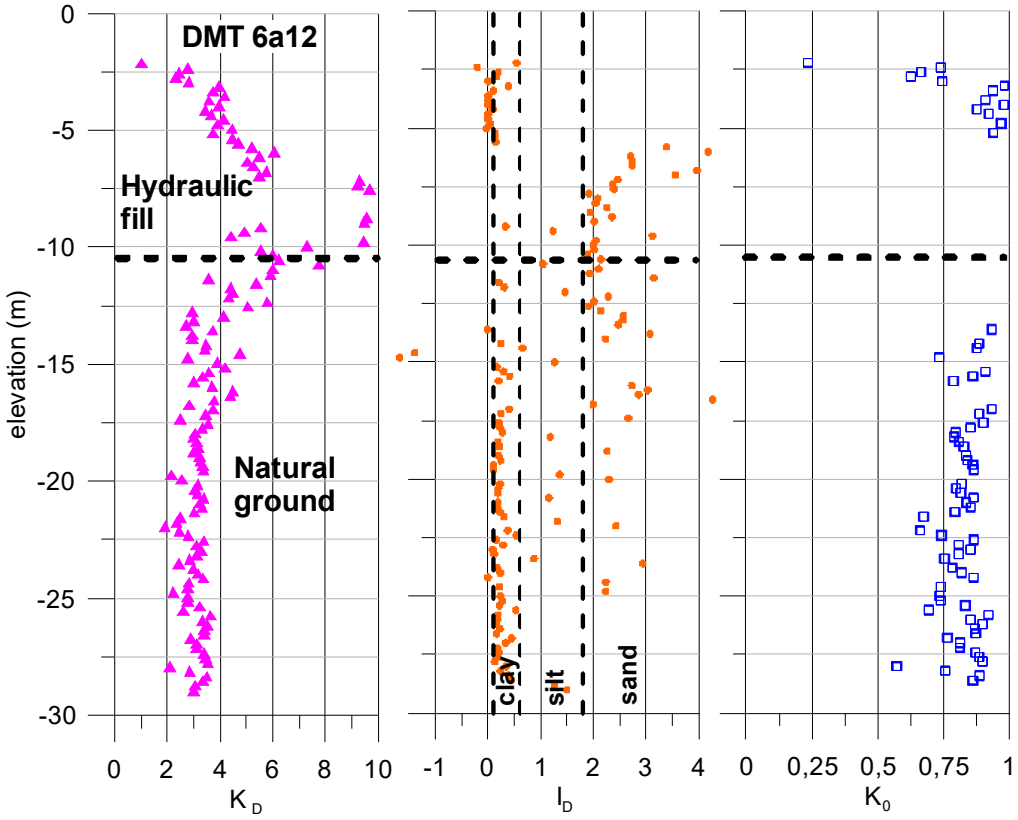

Figure 2.35. DMT results of sounding 6a12.

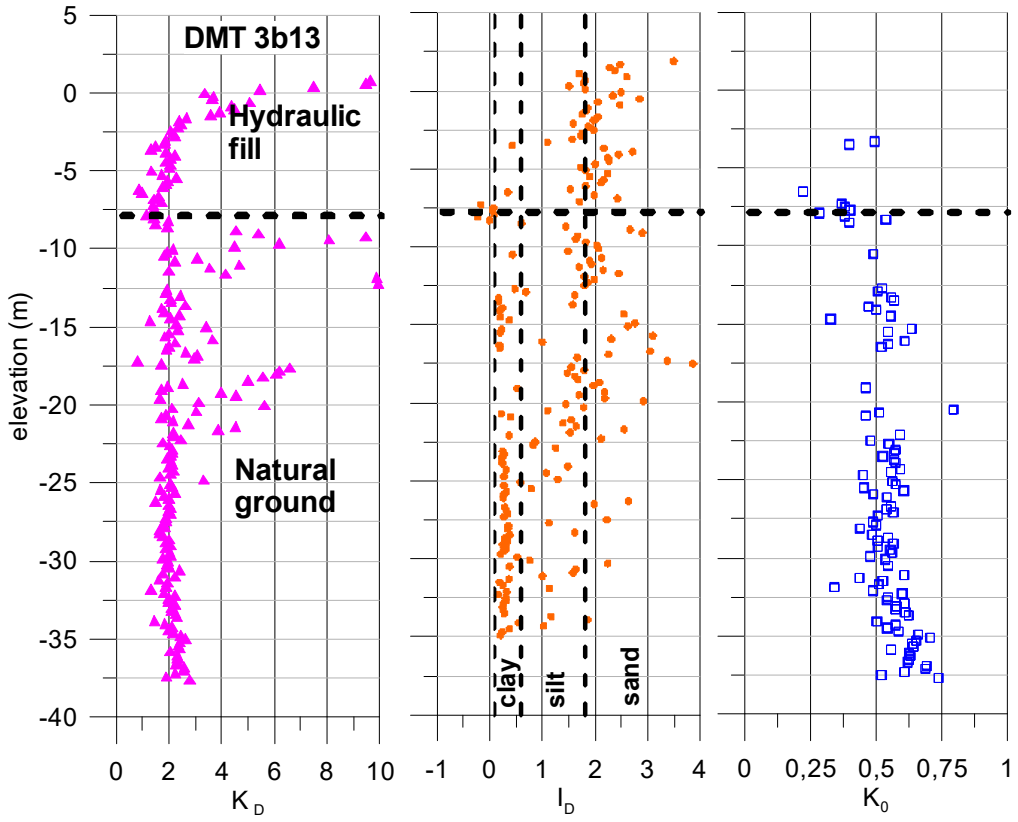

Figure 2.36. DMT results of sounding 3b14.

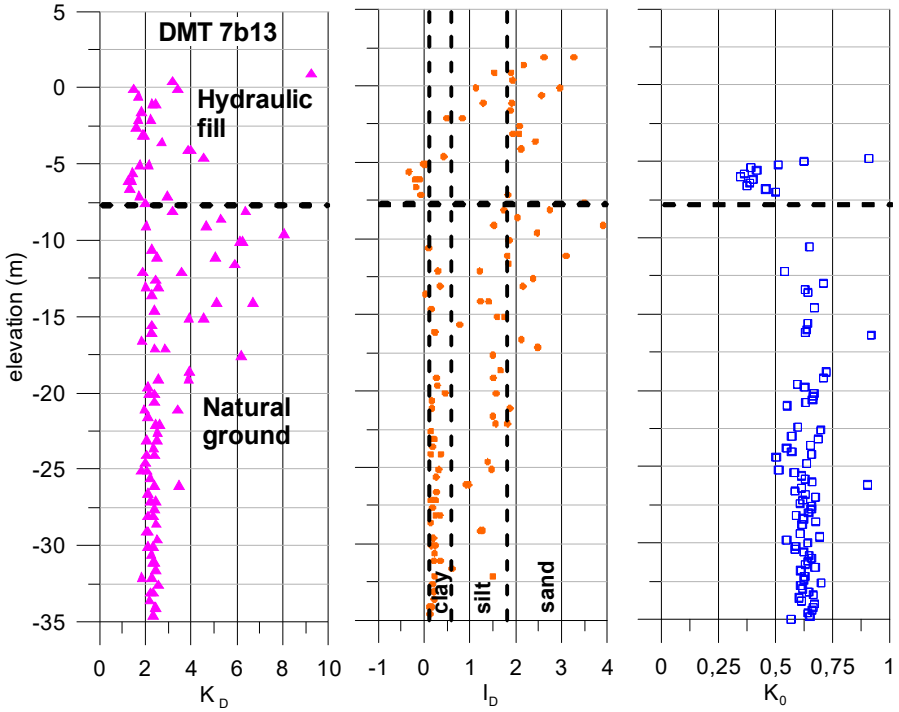

Figure 2.37. DMT results of sounding 7b13.

2.5.3. Laboratory tests

Results of laboratory tests performed to determine properties of the hydraulic fill, natural ground and rubble mound. Because of its relevance in a failure investigation, strength parameters are discussed separately in the next section.

The main physical and classification properties of the hydraulic fill are presented in Figure 2.38 and Figure 2.39. They are similar to those of the natural ground from which it derives. Gradings are quite variable with more sand present in the Phase 1 fill. Water contents in the clayey samples is close to the liquid limit. The material has a low plasticity with a plasticity index (I_P) generally lower than 10.

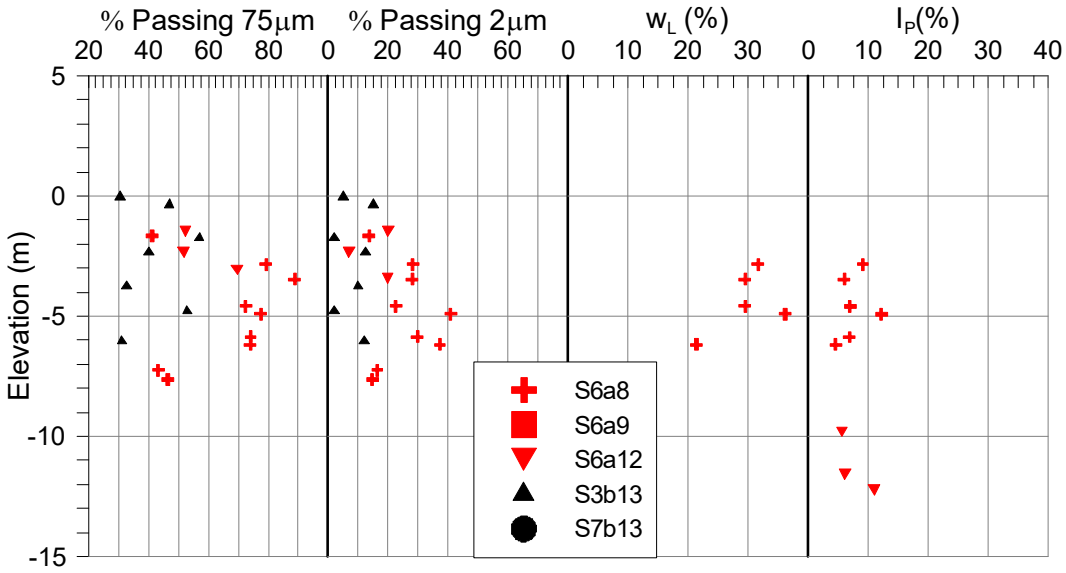

Figure 2.38. Fill properties in Phase 1 (red symbols) and Phase 2 (black symbols).

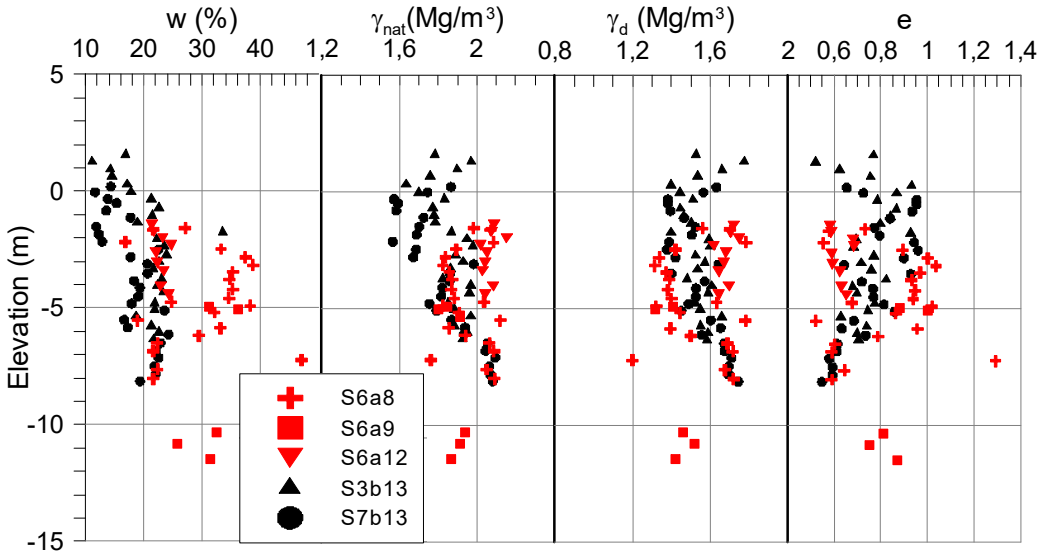

Figure 2.39. Fill properties in Phase 1 (red symbols) and Phase 2 (black symbols).

The grading of a hydraulic fill is often variable because it depends on the source material, the specific model of deposition and on the distance of a particular location from the discharge point. Figure 2.29 illustrates this point by showing the range of grading curves obtained in samples retrieved from a single borehole, 6a8. In any case, the proportion of fine particles is generally high.

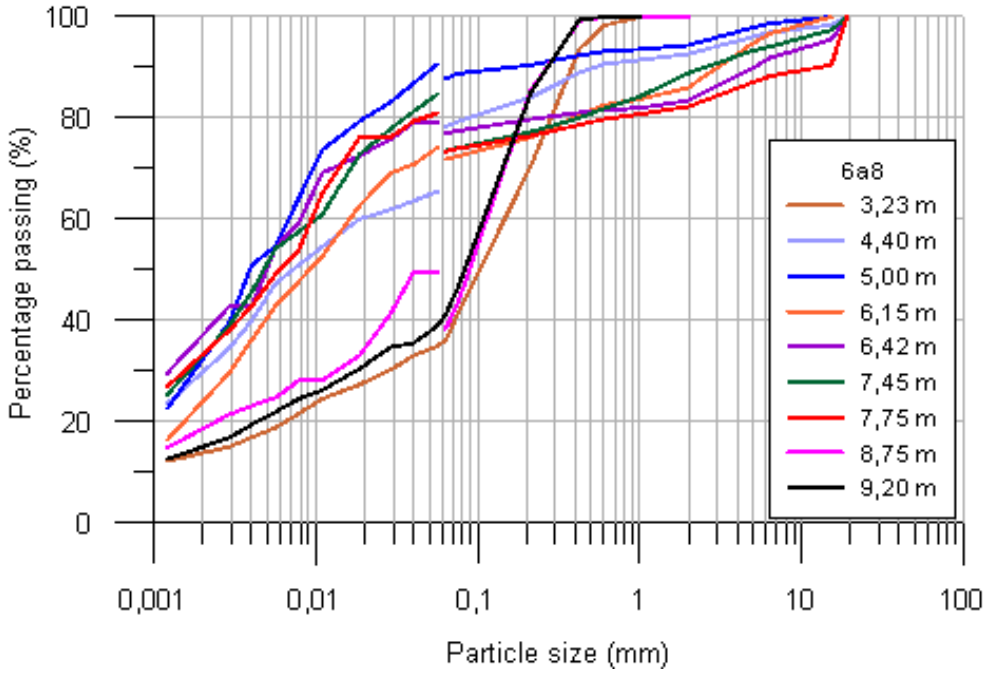

Figure 2.40. Particle size distributions from samples of hydraulic fill recovered from borehole 6a8.

The corresponding properties of the natural ground are presented in Figure 2.41. Index properties are similar to hydraulic fill values. Soils classify as low plasticity clays and silts or, locally, silty sands. Organic content is always below 1%.

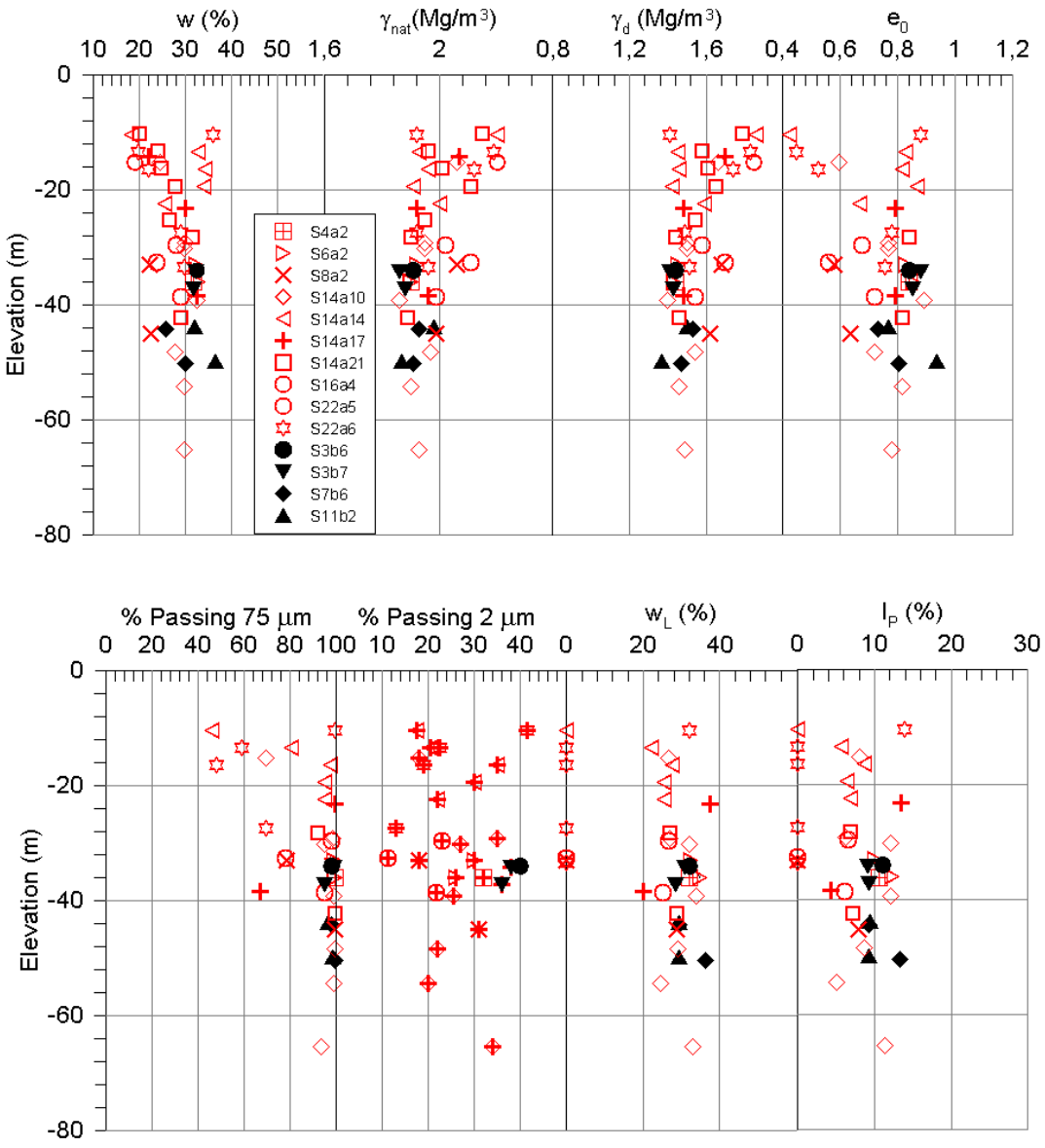

Figure 2.41. Natural ground properties in Phase 1 (green symbols) and Phase 2 (black symbols).

The mineralogical composition of the hydraulic fill was determined using powder X-Ray diffraction (XrD) (Figure 2.42). Results indicated that this soil contains typical mineral grains of sediment from the Llobregat River, mainly muscovite (32.7%), calcite (27.7%) and quartz (14.9%), but also halite (8.9%) kaolinite (5.9%), graphite (5.9%) and dolomite (4%), Tauler (2007). Clay minerals as muscovite and kaolinite are not active clay minerals or flocculants.

Additionally, in order to compare the mineral composition of the natural ground (fine-grained) and hydraulic fills, both powder XrD results are represented in Figure 2.43. Results are similar, both in peaks location (2θ) and in peak intensities which imply the same mineral phases and the same mineral phases proportion. It results from the fact that dredged material placed in the hydraulic fill derives from the natural ground at the same location.

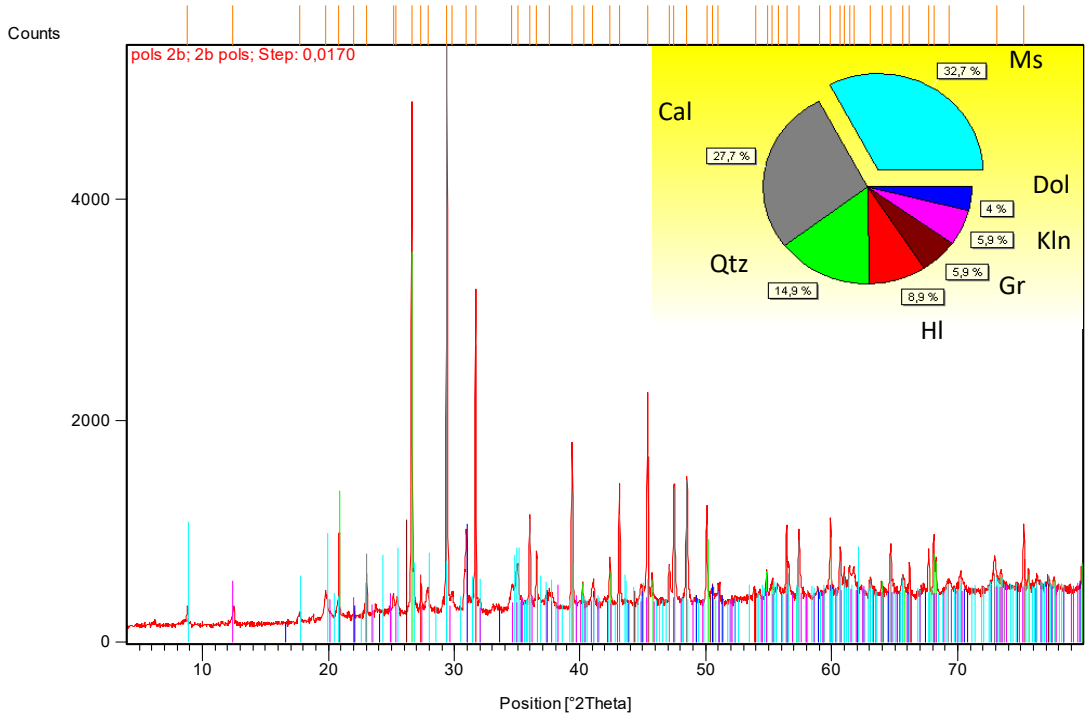

Figure 2.42. XRD powder diffraction and semi-quantitative analysis results from hydraulic fill soil. Mineral phases: Cal: calcite, Ms: muscovite, Dol: dolomite, Kln: kaolinite, Gr: graphite, Hl: halite and Qtz: quartz, Tauler (2007).

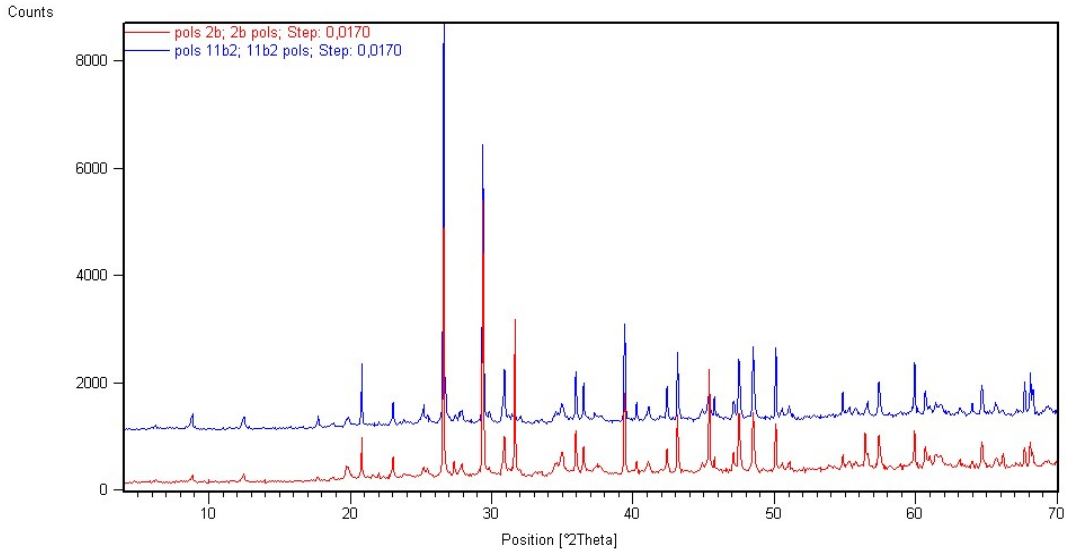

Figure 2.43. XRD powder diffraction natural ground (blue) and hydraulic fill (red), Tauler (2007).

Shelby samplers were used to obtain undisturbed specimens from the natural ground but they proved largely inadequate for the hydraulic fill where the Beguemann sampler was more successful. Oedometer tests were performed to obtain compression (C_C) and swelling (C_S) indices. They are plotted in Figure 2.44. Compression index values lie in the range of 0.12 to 0.21 for the natural ground, and 0.21 to 0.27 for the fill whereas the values of swelling index range from 0.002 to 0.004 for both materials. The void ratio (e_0) of the retrieved samples were higher in the hydraulic fill than in the natural ground silty clay.

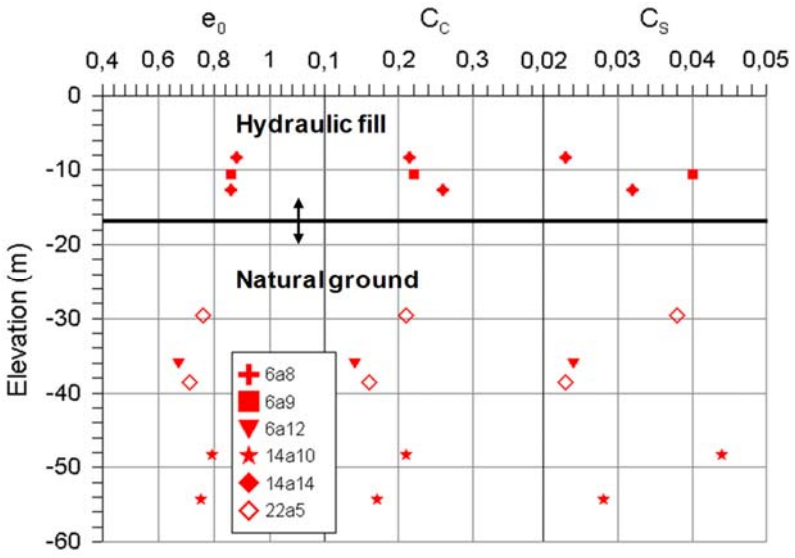

Figure 2.44. Void ratio, compression index and swelling index for fill and natural ground in Phase 1.

In addition, identification tests were performed on the quarry run used for the rubble mound. The grain size distribution presented in Figure 2.45 indicates that it is composed by more than 70% of gravels, 15 % of sand, 6% of silts and 4% of clay; D_{50} was close to 10 mm. This material is non plastic.

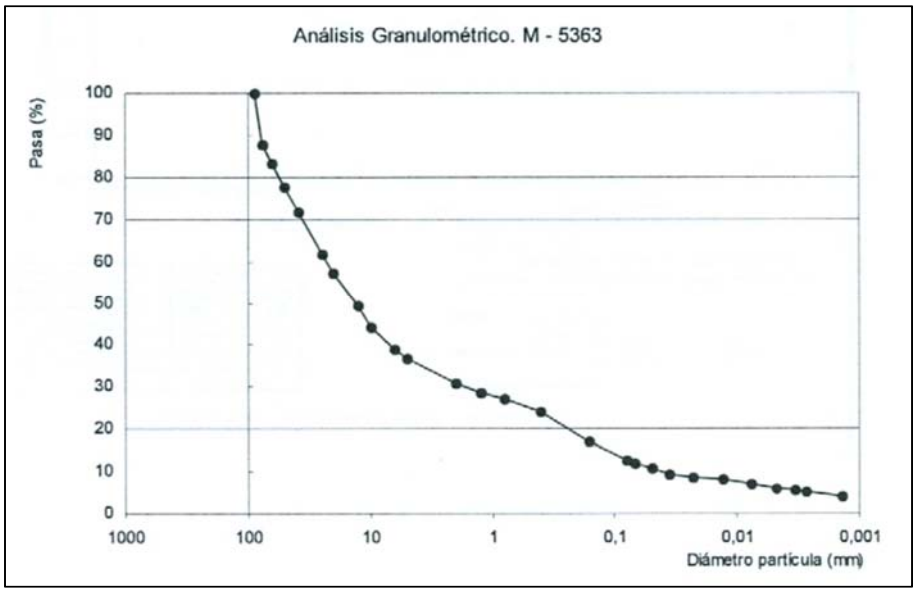

Figure 2.45. Particle size distributions from samples of rubble mound recovered from borehole 6a8, CEDEX 2007.

2.6. *Soil strength*

In the failure case investigated, the undrained shear strength of the natural ground and hydraulic fill is the key parameter controlling stability. Its determination is mainly based on the results of in-situ tests, CPTU tests and DMT tests but laboratory tests of natural ground samples have also been considered.

In the case of CPTu tests, the undrained shear strength, c_u, is computed as:

$$c_u = (q_t - \sigma_v) / N_{kt} \quad [1]$$

where q_t is the total cone resistance, σ_v is the total vertical stress and N_{kt} is an empirical parameter. A standard value of N_{kt} equal to 15 has been adopted. σ_v has been computed using an average saturated density value of 1.85 Mg/m^3.

For the DMT, c_u was determined using the expression from Marchetti (1980):

$$c_{u\,DMT}=0.22\ \sigma'_{v0}\ (0.5\cdot K_{DMT})^{1.25} \quad [2]$$

Again an average saturated density value of 1.85 Mg/m^3 was used.

Soil strength parameters for the rubble mound material was obtained from laboratory tests.

2.6.1. Hydraulic fill

Two typical profiles of undrained shear strength for the hydraulic fill are shown in Figure 2.46 and Figure 2.47. It can be noted that there are many records well below the usual range of 0.20-0.25 σ'_v, where σ'_v is the effective vertical stress. In some cases, the estimated value of c_u is even close to zero. These observations point out towards the hydraulic fill being a brittle material susceptible to flow liquefaction (Monforte et al., 2021). In the sandy areas of the profile, significantly larger shear strengths are measured. The same low values of undrained shear strength and its variation from location to location are also apparent in the results of CPTu tests of the Phase 2 materials (Figure 2.48).

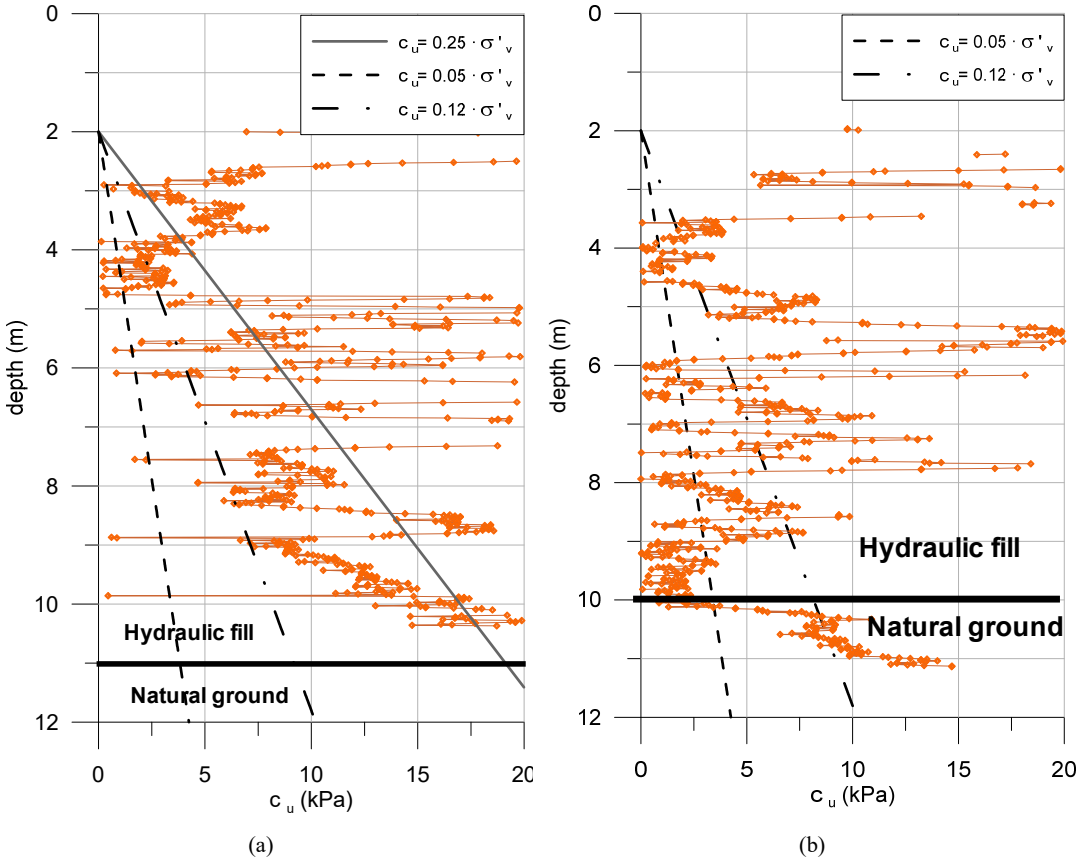

Figure 2.46. CPTu results in hydraulic fill (a) 6a12 and (b) 6a11, Phase 1.

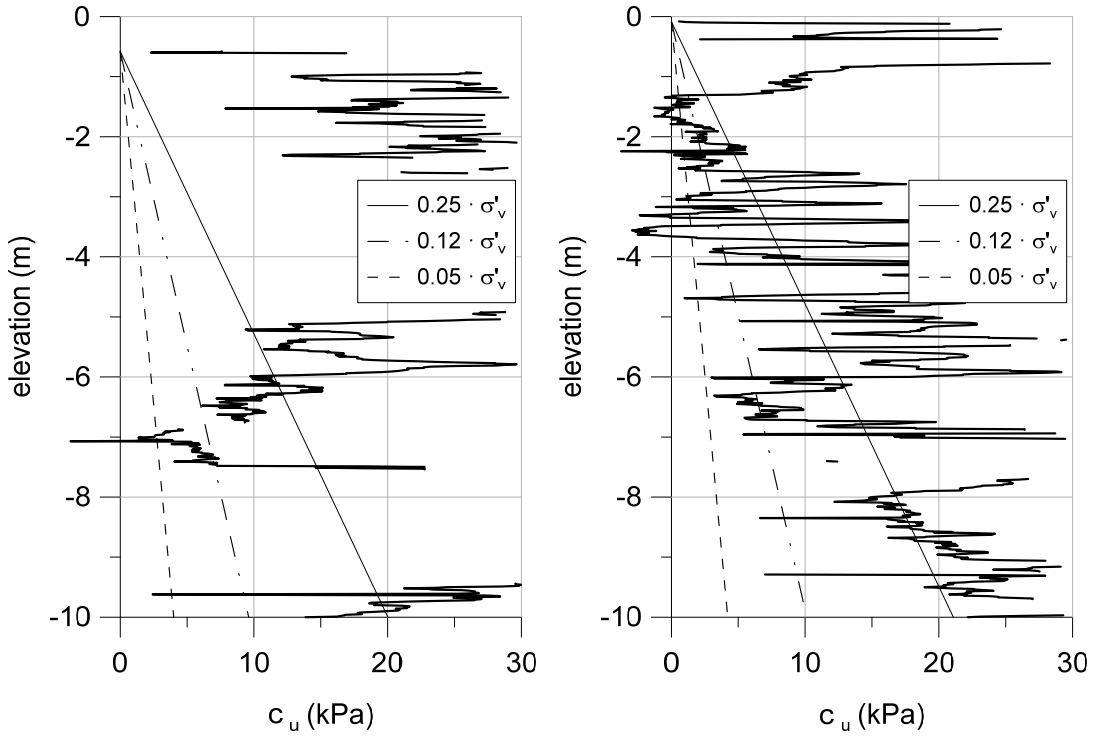

Figure 2.47. CPTu results in hydraulic fill (a) 6a8 and (b) 6a14, Phase 1.

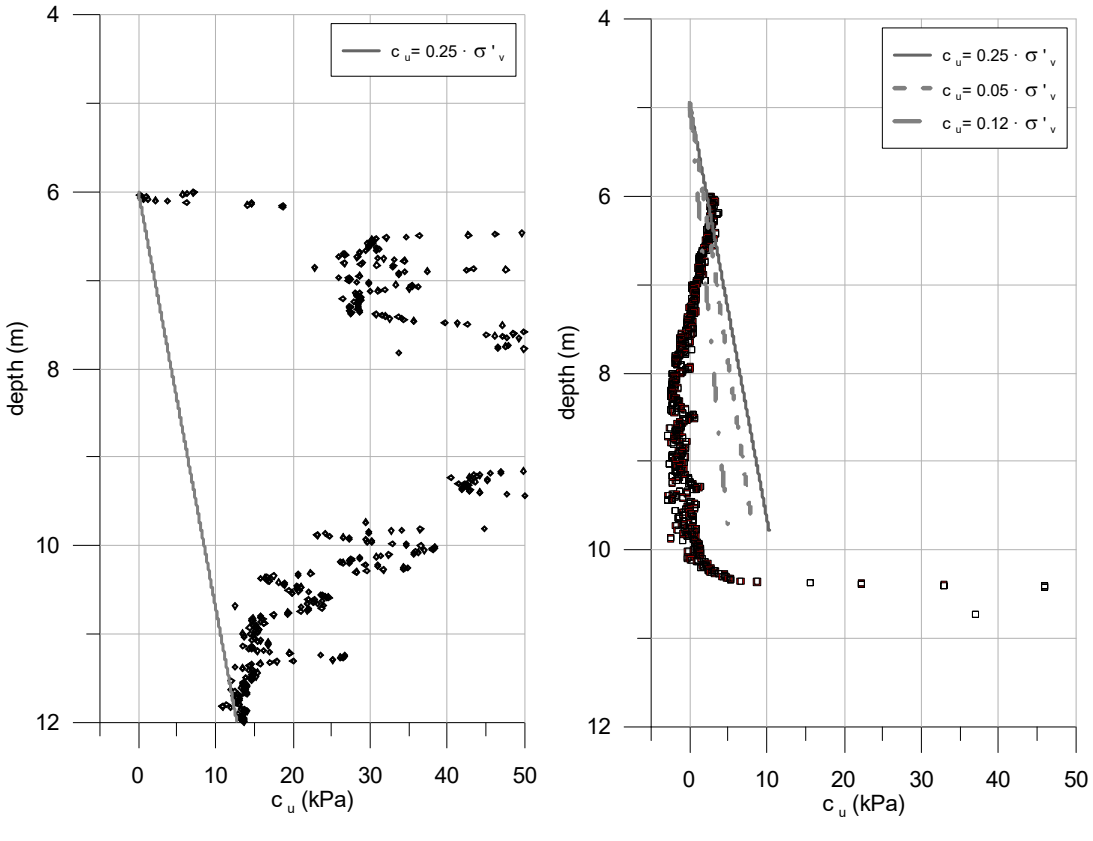

Figure 2.48. CPTu results in hydraulic fill, (a) 3b12 and (b) 7b12, Phase 2.

The undrained shear strength derived from DMT tests in three soundings are represented in Figure 2.49. Values lower than 0.20 - 0.25 σ'_v are determined but the very low values of the CPTu tests are not apparent in this case. This is consistent with the fact that the cone penetration creates much more disturbance in the soil than the DMT test.

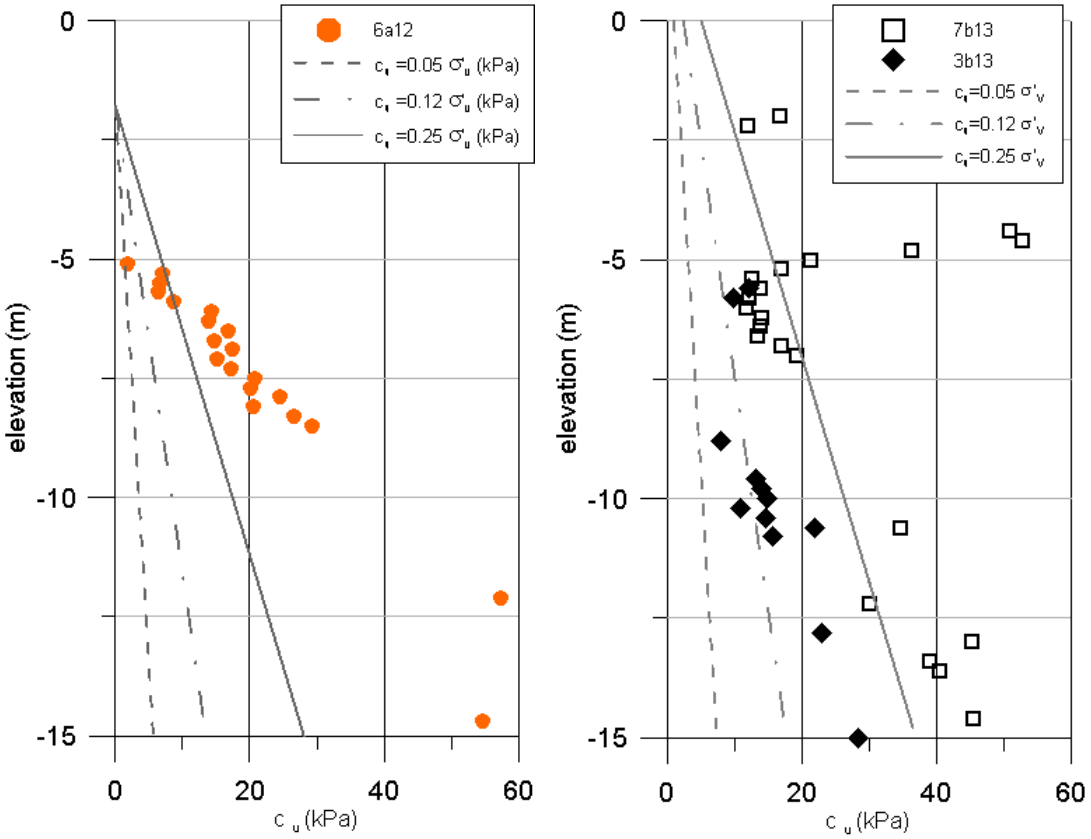

Figure 2.49. Undrained shear strength from DMT results in hydraulic fill, (a) 6a12 and (b) 3b13 and 7b13.

2.6.2. Natural ground

Typical profiles of CPTu-derived undrained shear strength for the natural ground are presented in Figure 2.50. It can be observed that now the values lie in the range of 0.20 - 0.25 σ'_v although some rather low values occasionally appear; a possible cause could be the presence of gas. The interbedded macrostructure of the material is also apparent in the profile. The undrained shear strength estimated from DMT tests confirms those results (Figure 2.51). The friction angle lies around 34º.

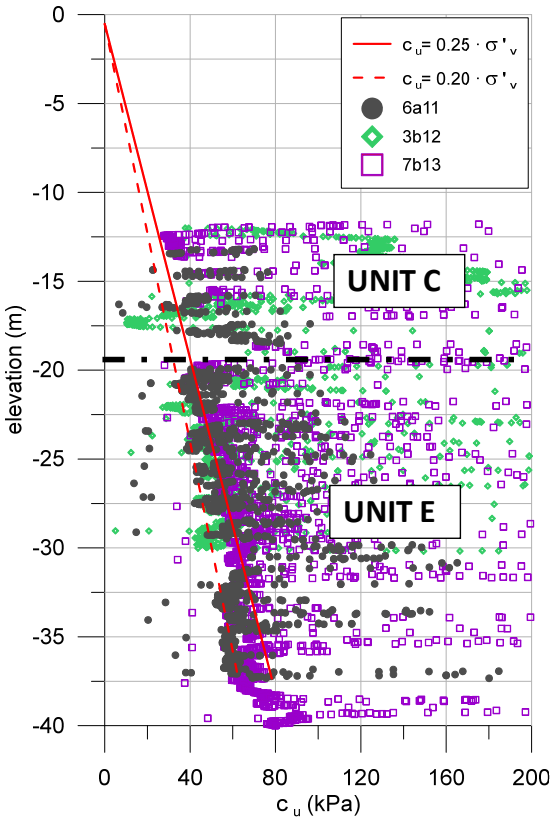

Figure 2.50. CPTu results, derived undrained shear strength, from CPTu 6a11, 3b12 and 7b13.

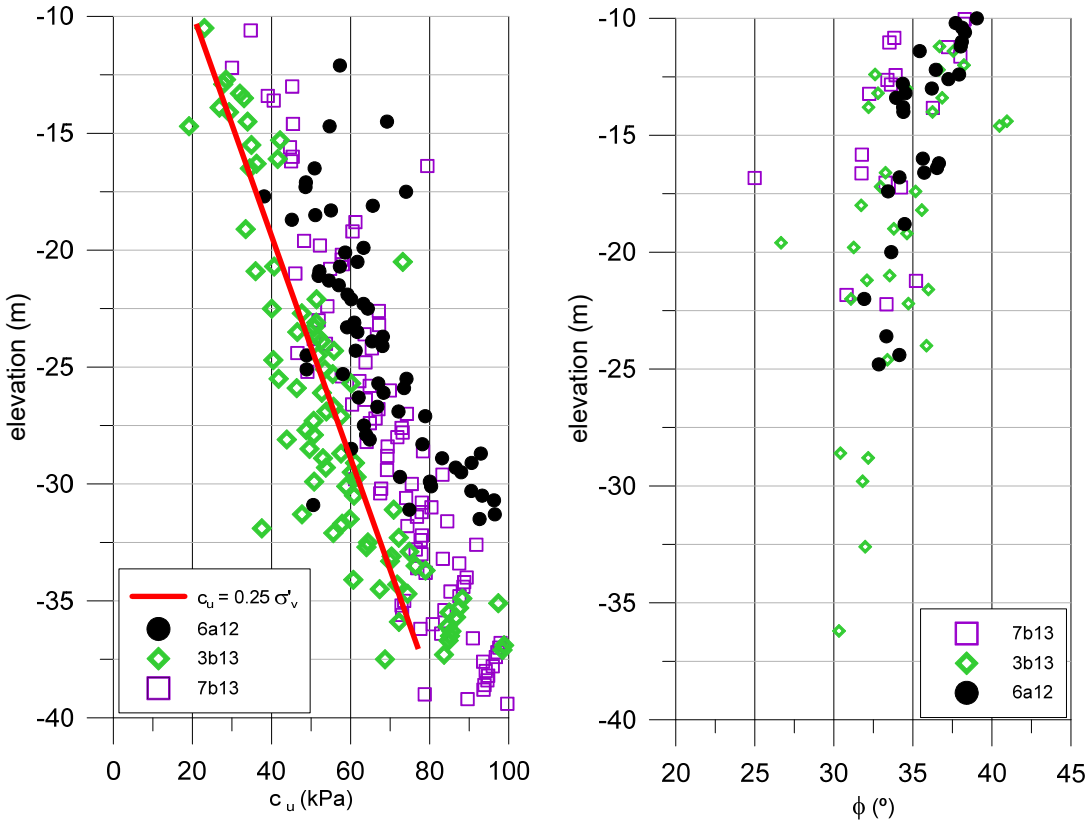

Figure 2.51. DMT results, derived undrained shear strength (left) and friction angle (right), from DMT 6a12, 3b13 and 7b13.

Simple shear tests on Shelby specimens were performed by the Norwegian Geotechnical Institute. It can be seen that the undrained strength results cluster around $0.25 \cdot \sigma'_v$ line although some values are noticeably larger. Similar results were also obtained in the site investigation of the South breakwater founded on the same material (Gens and Alonso, 2001), Figure 2.52.

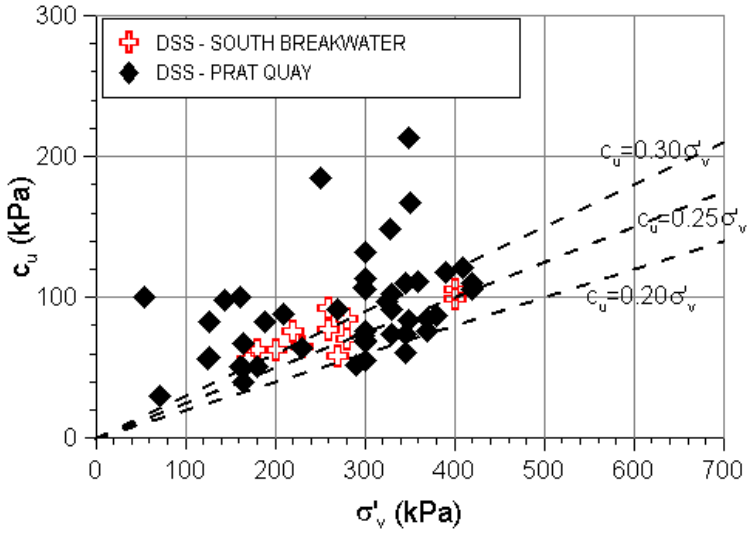

Figure 2.52. Results of simple shear tests soils of Prat quay and South breakwater, modified from Gens and Alonso (2001).

2.6.3. Rubble mound

The friction angle of the rubble mound material was measured in a large scale triaxial apparatus testing a 150 mm diameter reconstituted sample. A friction angle of 38º was obtained (Figure 2.53). The friction coefficient of the interface concrete - rubble mound material was also measured. A value of 0.42 was obtained that corresponds to a friction angle equal to 2/3 the friction angle of the rubble mound material.

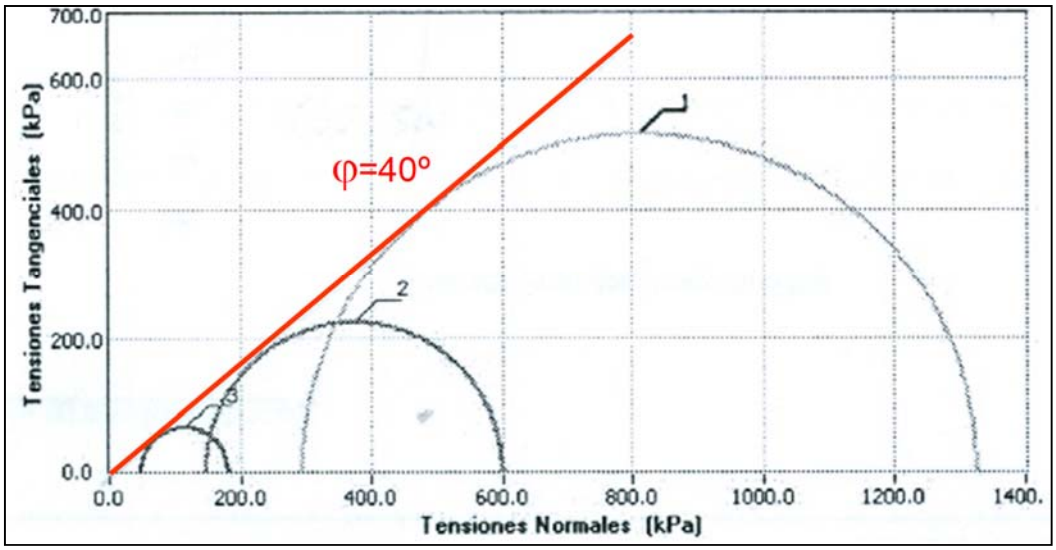

Figure 2.53. Quarry-run material of rubble mound. Triaxial CD –drained consolidated-test results, CEDEX (2007).

2.7. Evidence of flow liquefaction in Prat quay failure

No previous signs of instability were recorded or described during the construction of the Prat quay. The first one was the gas/water discharges ("geysers"), immediately followed by overall failure, large caisson displacements and flow of the hydraulic fill to the sea. Failure occurred during a very short time lapse; this behaviour was clearly linked to flow liquefaction. Additional evidence was found during the fieldwork after the failure. A first evidence of liquefaction was the fact that, a set of repeated steps on the crust on top of the Phase 1 fill resulted in a loss of strength that led the person to sink in the fill. There was also anecdotal evidence that the fill was liquefiable because, on occasions, small fine sand or fine grained volcanos appeared when the fill was loaded (Figure 2.54 and Figure 2.55).

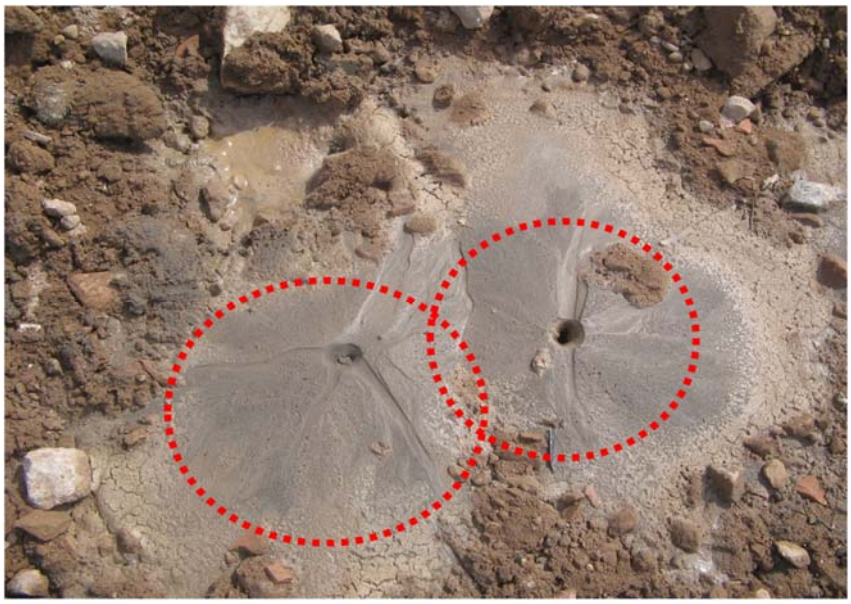

Figure 2.54. Fine sand volcanos from hydraulic fill

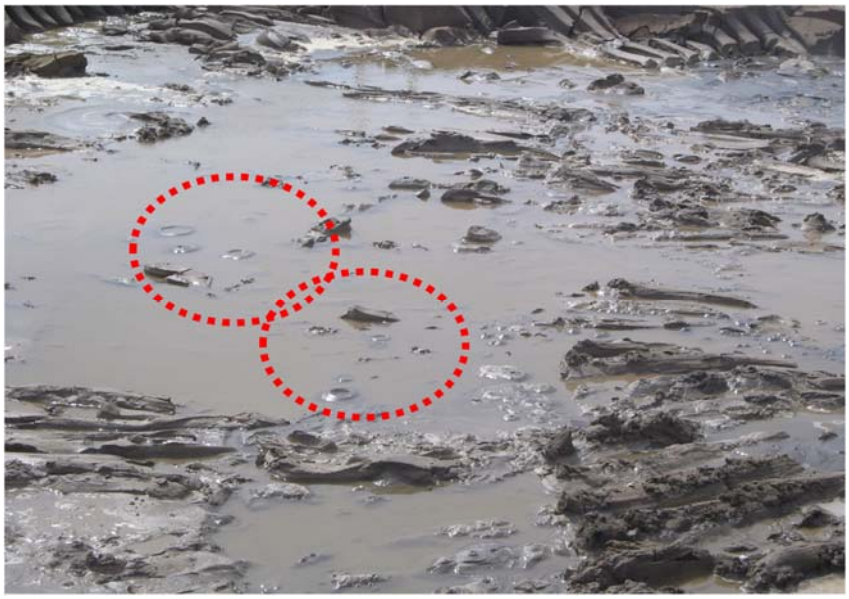

Figure 2.55. Fine grained soil volcanos from hydraulic fill

It is also clear that some of recurrent actions that sometimes trigger the failure can be excluded. Thus, there was no evidence of cyclic loading before the failure because: (i) seismograph placed in Barcelona did not recorded any seismic event prior to the failure and (ii) the buoy of placed in the inner harbour detected a variation of wave height only just after the failure, as shown above. The phenomenon that occurred was flow -sometimes called static-, liquefaction, not cyclic liquefaction.

2.8. Summary

A 600 m long section of a caisson quay failed catastrophically without apparent warning. Caissons were displaced long distances.

The quay was founded on soft deltaic deposits but the failure did not involve the natural ground. The mechanism of failure was by sliding of the caissons on the rubble mound placed underneath.

Failure involved the flow (static) liquefaction of the hydraulic fill deposited behind the caissons.

Low values of the undrained shear strength of the hydraulic fill -derived from CPTU tests-, suggest that the undrained behaviour of the material is brittle and therefore it may develop flow liquefaction.

There is additional observational evidence that the hydraulic fill was susceptible to flow liquefaction.

Because of the key role played in the failure of the Prat quay, the phenomenon of flow liquefaction is examined in detail in the next Chapter together with an evaluation of the hydraulic fill liquefaction potential according to on some commonly used criteria.

2.9. References

Alonso, B., Baraza, J., Ercilla, G., Estrada, F., Farrán, M., Palanques, A. 1995. Estudio Geofísico y sedimentológico en el área de ampliación del Puerto de Barcelona. CSIC report, internal document Barcelona Port Authority.

Bayó, A. 1985. Les aigües. Història Natural dels Països Catalans, vol. 3. Enciclopèdia Catalana, Barcelona, pp. 21– 41.

CEDEX - Centro de Estudios y Experimentación de Obras Públicas, 2007. Simple shear and triaxial tests of rock fills. Madrid, 2007.

Gàmez, D. 2007. Sequence Stratigraphy as a tool for water resources management in alluvial coastal aquifers: application to the Llobregat delta (Barcelona, Spain). PhD thesis. Technical University of Catalunya.

Gamez, D., Simó, J.A., Lobo, F.J., Barnolas, A., Carrera, J., Vazquez-Suñé, E. 2009. Onshore-Offshore correlation of the Llobregat deltaic system, Spain: Development of deltaic geometries under different relative sea-level and growth fault influences. Sedimentary geology 217, 65-84.

Gens, A., Alonso, E. E. 2001. Barcelona Port Authority. New dykes simple shear tests on shelby samples (NGI and CEDEX laboratories). UPC report. internal document Barcelona Port Authority.

Houlsby, G.T. and Teh, C.I. 1988. Analysis of the piezocone in clay. Penetration Testing 1988, Vol. 2, Balkema, Rotterdam: 777–783.

La Vanguardia (2009).Vivir. Printed, paper. 02/03/2009.

Lafuerza, S., Canals, M., Casamor, S.L., Devincenzi, J.M. 2005. Characterisation of deltaic sediment bodies based on in situ CPT/CPTU profiles: A case study on the Llobregat delta plain, Barcelona, Spain. Marine Geology 222-223 (2005) 497-510.

Liquete, C., Canals, M., De Mol, B., De Batist, M., Trincardi, F. 2008. Quaternary stratal architecture of the Barcelona prodeltaic continental shelf (NW Mediterranean). Marine Geology, 250, 234-250.

Marchetti, S. 1980. In-situ tests by flat dilatometer. Journal of Geotechnical Engineering 107 (GT3), 832-837.

Marquès, M.A. 1974. Las formaciones cuaternarias del delta del Llobregat. PhD thesis. University of Barcelona, Barcelona. 401 pp.

Monforte, L., Gens, A., Arroyo, M., Mánica, M., Carbonell, J.M. 2021. Analysis of cone penetration in brittle liquefiable soils. Computers and Geotechnics (accepted for publication).

Ventayol, A., 2003. Caracterización geotécnica de sedimentos deltaicos mediante piezoconos. In: Gimeno, López (Ed.), Aplicación al margen izquierdo del delta del Llobregat. Ingeniería del terreno, INGEOTER, vol. 2 (C), pp. 413– 433.

Tarragó, D., Gens, A. 2018. Gas effect on CPTu and dissipation test carried out on natural soft-soil of Barcelona Port. 4th International Symposium on Cone Penetration Testing, Delft, Nederland. Best poster award.

Tauler, E. 2007. Personal communication.

Urgeles, R., De Mol, B., Liquete, C., Canals, M., De Batist,M., Hughes-Clarke, J.E., Amblàs, D., Arnau, P.A., Calafat,A.M., Casamor, J.L., Centella, V., De Rycker, K., Fabrés,J., Frigola, J., Lafuerza, S., Lastras, G., Sànchez, A.,Zuñiga, D., Versteeg, W., Willmott, V. 2007. Sediment undulations on the Llobregat prodelta: Signs of earlyslope instability or sedimentary bedforms?. Journal of Geophysical Research, 112, B5, 102.

Urgeles, R., Cattaneo, A., Puig, P., Liquete, C., De Mol, B., Amblàs, D., Sultan, N., Tincardi, F. 2011. A review of undulated sediment features on Mediterranean prodeltas: distinguishing sediment transport structures from sediment deformation. Marine Geophysical Research,32, 49-69.

Chapter 3. Hydraulic fill liquefaction

3.1. Introduction

The phenomenon of soil liquefaction entails the total or partial loses of strength or stiffness, usually over a short period of time (Jefferies and Been, 2016). This phenomenon is often associated with catastrophic failure. Although some confusion in liquefaction terminology existed in the past, it is now generally accepted that flow (or static) liquefaction must be considered separately from cyclic liquefaction or cyclic mobility, as indicated in Figure 3.1 (Robertson and Wride, 1998).

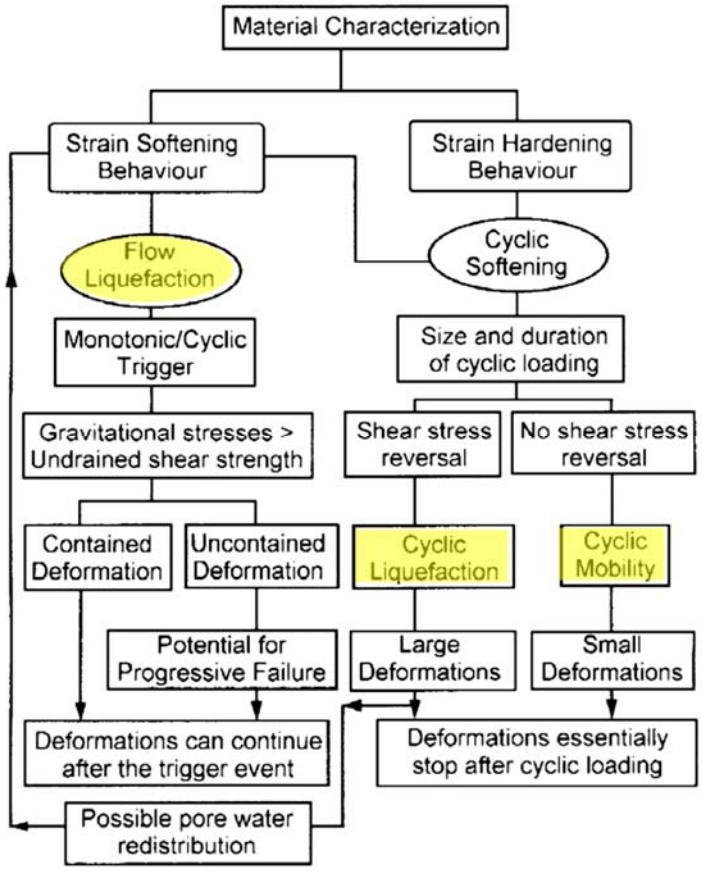

Figure 3.1. Flow chart to evaluate liquefaction potential of soils (Robertson and Wride, 1998).

Flow (or static) liquefaction is linked to undrained softening behaviour. The term flow liquefaction is preferred to static liquefaction because this type of liquefaction can in fact be triggered by cyclic loading (Gens, 2019).

Cyclic liquefaction or cyclic mobility results from the increment of water pore pressure during cyclic loading that can be due to various events such as earthquakes, vibrations or wave action during storms. In the case of cyclic liquefaction, the rise of pore pressure can take the soil to very low effective stresses where large deformations are produced. In contrast, cyclic mobility occurs at larger effective stresses and only small deformations are produced.

In Figure 3.2, different idealized undrained behaviour of a non-plastic soil is summarized. Flow liquefaction is associated with a behaviour in which an abrupt reduction of undrained shear strength occurs after the peak, associated with a generation of large pore pressures (Gens, 2019).

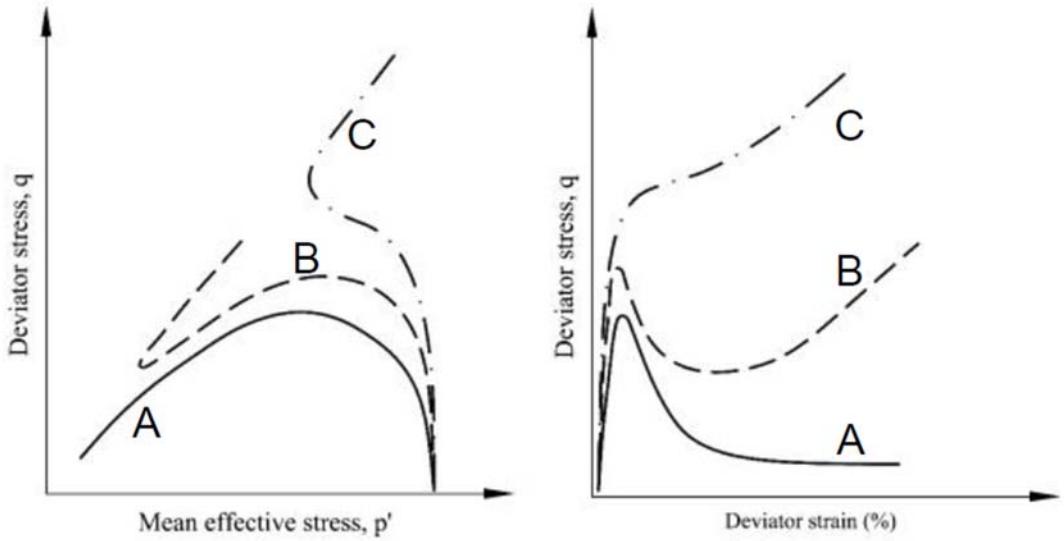

Figure 3.2. Typical undrained behaviour of non-plastic soils (Gens, 2019).

3.2. Flow liquefaction

Flow liquefaction behaviour is a recurrent failure cause. Reported failures of different civil and mining works mainly such as embankments, tailing dams, railways or hydraulic fills were triggered by static loading and earthquakes. In Table 3.1 and

Table 3.2 different cases of engineering projects from 1889 to 1997 compiled from Olson and Stark (2002), Yamamuro and Lade (1999), Jefferies and Benn (2006), and Gens (2019) are shown. Important instances of failure are, the Aberfan spoil slide that killed 144 people, Bishop et al. (1969) and Bishop (1973), the Merriespruit embankment failure that caused 17 fatalities and high economic losses (Figure 3.3), Fourie et al. (2001), or the recent Brumadinho embankment failure that caused more than 250 fatalities (Figure 3.4), Robertson et al. (2020).

Figure 3.3. The failure of the slurry dam of Merriespruit due to flow liquefaction, Fourie et al. (2001).

Figure 3.4. The failure of the tailings dam of Brumadinho due to flow liquefaction, source Youtube.

Table 3.1. Real cases of flow liquefaction, reported by Olson y Stark (2002), Yamamuro and Lade (1999) and Jefferies and Benn (2006).

Historical	Structure	Year	Involved soil and apparent failure cause	References
1	Wachusett Dam - North Dike	1907	During sand filling	Olson et al. (2000)
2	Calavera Dam	1918	Hydraulic fill	Hazen and Metcalf (1918) and Hazen (1918)
3	Sheffield Dam (earthen dams)	1925	Santa Barbara eq. (ML=6,3)	Seed (1969)
4	Helsinki Harbor	1936	Static liquefaction during construction	Andresen and Bjerrum (1968)
5	Fort Peck Dam	1938	Static liquefaction hydraulic fill	Middlebrooks (1942); Casagrande (1965)
6	Finnvika fjord railway embankment	1940	Static liquefaction silty sand embankment construction fill	Bjerrum (1971)
7	Solfatara Canal Dike	1940	Imperial Valley eq. (ML = 7,1)	Ross (1968)
8	Hemmelvika	1942	Static liquefaction man-made submarine sandy fill	Bjerrum (1971)
9	Lake Merced bank	1957	San Francisco eq. (ML=5,3)	Ross (1968)
10	Kawagishi-Cho building	1964	Niigata eq. (Mw = 7,5)	Yamada (1966); Ishihara and Koga (1981); Seed (1987)
11	Uetsu Railway embankment		Niigata eq. (Mw = 7,5)	Yamada (1966)
12	El Cobre Tailings Dam	1965	Chile eq. (ML=7-7,25)	Dobry and Alvarez (1967)
13	Aberfan spoil Tip (Wales)	1966	Static liquefaction mine waste	Bishop (1973)
14	Koda Numa highway embankment	1968	Tokachi-Oki eq. (ML=7,9)	Mishima and Kimura (1970)
15	Metoki Road embankment	1968	Tokachi-Oki eq. (ML=7,9)	Ishihara et al. (1990)
16	Hokkaido Tailings Dam	1968	Tokachi-Oki eq. (ML=7,9)	Ishihara et al. (1990); Ishihara (1993)
17	Lower San Fernando Dam	1971	After San Fernando eq.(MW=6,6) on silty sand of hydraulic fill	Seed et al. (1973); Castro et al. (1989); Seed et al. (1989); Vasquez-Herrera and Dobry (1989); Marcuson et al. (1990); Castro et al. (1992)
18	Tar Island Dyke	1974	Sand tailings	Mittal and Hardy (1977); Plewes et al. (1989); Konrad and Watts (1995)
19	Mochi-Koshi Tailings Dam	1978	Izu-Oshima-Kinkai eq. (ML=7,0)	Marcuson et al. (1979); Okusa and Anma (1980); Ishihara et al. (1990)
20	Nerlerk Berm failures	1982 1983	Static liquefaction of sands and foundation clay failure	Sladen et al. (1985a, 1985b, 1987); Been et al. (1987); Sladen (1989); Rogers et al. (1990); Konrad (1991); Hicks and Boughraruo (1998)
21	Hachiro-Gata Road embankment	1983	Nihon-Kai-Chubu eq. (M=7,7)	Ohya et al. (1985)

Table 3.2. Real cases of flow liquefaction, reported by Olson y Stark (2002), Yamamuro and Lade (1999), Jefferies and Benn (2006) and Gens (2019).

Historical	Structure	Year	Involved soil and apparent failure cause	References
22	Asele Road embankment	1983	Pavement repairs	Ekstrom and Olofsson (1985); Konrad and Watts (1995)
23	La marquesa Dam	1985	Chilean eq. (ML=7,8)	de Alba et al. (1987)
24	La Palma Dam	1985	Chilean eq. (ML=7,8)	de Alba et al. (1987)
25	Stava Mine	1985	Tailings	Chandler and Tosatti (1995)
26	Fraser River Delta	1985	Gas desaturation and low tide	Chillarige et al. (1997a, 19976); Christian et al. (1997)
27	Lake Ackerman highway embankment	1987	Seismic reflection survey	Hryciw et al. (1990)
28	Fill in Chonan Middle School	1987	Fill, Chiba-Toho-Oki eq. (M = 6,7)	Ishihara et al. (1990) ; Ishihara (1993)
29	Tailing dam	1988	Cerro Negro eq. on silty sand	Troncoso (1988)?
30	Tailing dam	1988	Veta del Agua eq. on silty sand	Troncoso (1988)?
31	Nalband Railway embankment	1988	Armenian eq. (ML = 6.8)	Yegian et al. (1994)
32	Sullivan Mine	1991	Static liquefaction tailings	Davies et al. (2002)
33	Shibecha-Cho embankment	1993	Kushiro-Oki eq. (ML = 7,8)	Miura et al. (1998)
34	Route 272 at Higashiarekinai	1993	Kushiro-Oki eq. (ML = 7,8)	Sasaki (1994)
35	Hydraulic fill	1994	Northridge eq. on silty sand	Kerwin & Stone (1997)
36	Merriespruit Dam	1994	Static liquefaction of tailings	Wagener et al. (1998); Fourie et al. (2001)
37	Alznalcollar Dam	1997	Static liquefaction tailings	Alonso and Gens (2006)

3.2.1. Critical states and state parameter

Flow liquefaction behaviour is best understood in the context of the critical state concept. The initial definition of critical state was proposed by Casagrande (1936), after observing that almost the same void ratio (critical void ratio, e_{ss}) is reached, when loose sand contracted and dense sand dilated in direct shear tests. No volume change was detected after critical void ratio.

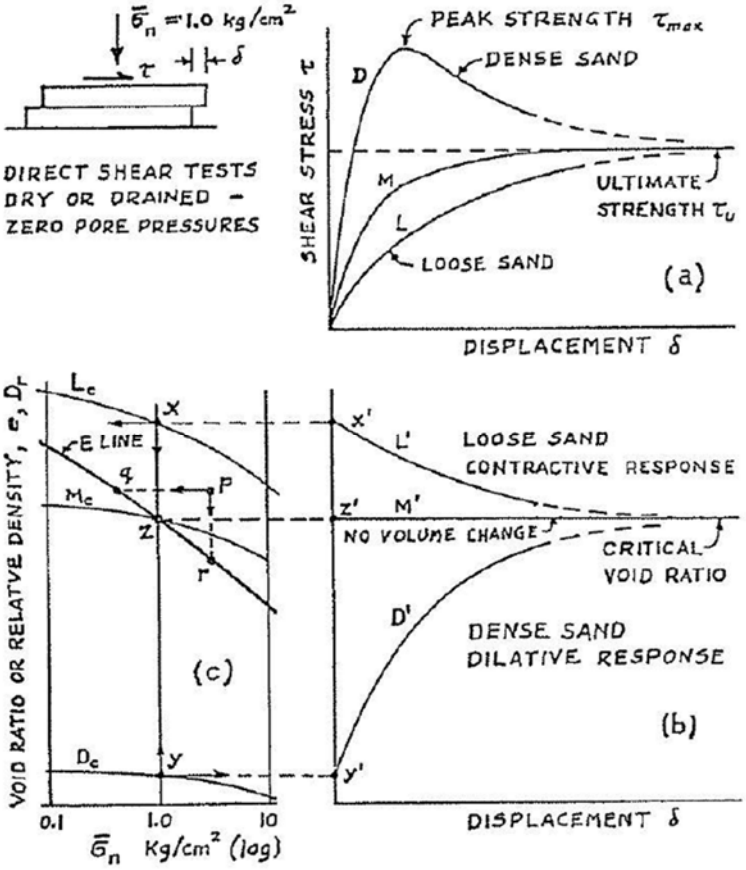

Figure 3.5. Critical void ratio for sands from direct shear tests, Casagrande (1975).

Schofield and Wroth (1968) stablished the concept of critical state line (CSL) of a soil. This line is defined by different critical void ratios (e_{cs}) reached during shear under different constant stress when no longer volume change occurs. Although vertical effective stress can be used, mean effective stress (p') is frequently used to represent CSL, as shown in [3].

$$e_{cs} = e_0 - \lambda \log_{10} \cdot p' \qquad [3]$$

where the mean effective stress (p') is defined as:

$$p' = (\sigma_1' + \sigma_2' + \sigma_3') / 3 \qquad [4]$$

σ'_1, σ'_2 and σ'_3 are the principal effective stresses. Initial void ratio (e_0) is a parameter of the soil.

Although the critical state line in the former definition is assumed a straight line in (e - $\log_{10} p'$) space (Figure 3.6), for real soils, the line is sometimes bilinear or curved as shown in Figure 3.7. This phenomenon is frequently associated with particle crushing.

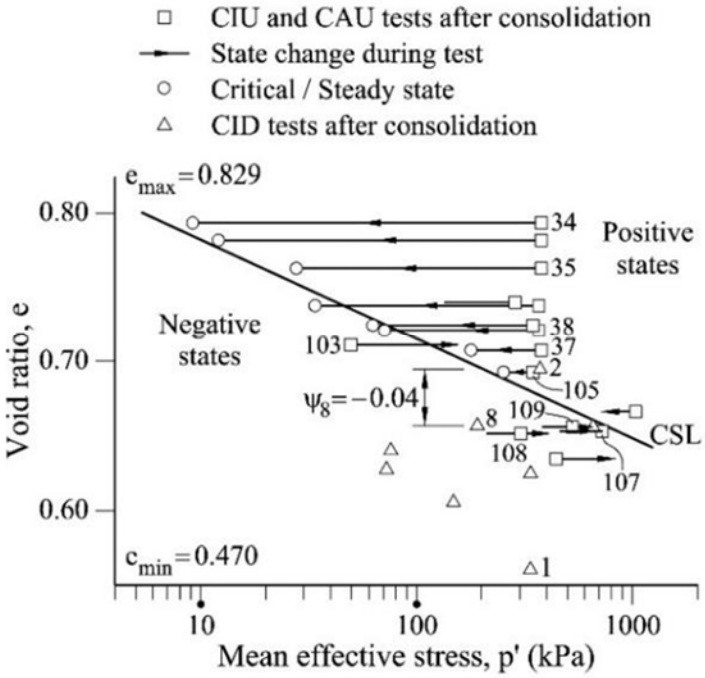

Figure 3.6. State diagram from Kogyuk 350/2 sand tests, Been and Jefferies (1985).

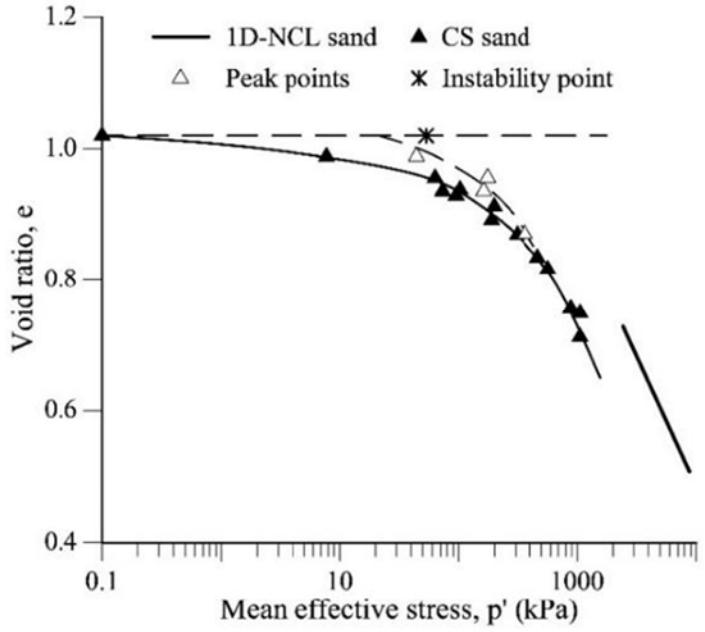

Figure 3.7. Critical state line from Stava tailings tests, Carrera et al. (2011).

A relevant parameter to evaluate the soil character is the state parameter. It was defined in Been and Jefferies (1985) although it had been stated previously by Wroth and Basett (1965). The state parameter (ψ) is defined as the difference between the current void ratio and the void ratio in the critical state line (e_{SS}) at the same value of mean effective stress (Figure 3.8). It is important to note that state points located above the CSL (i.e. in $\psi > 0$) are loose soils exhibiting contractive behaviour. In contrast state points located below the CSL $\psi < 0.$) correspond to dense soils showing dilatant behaviour.

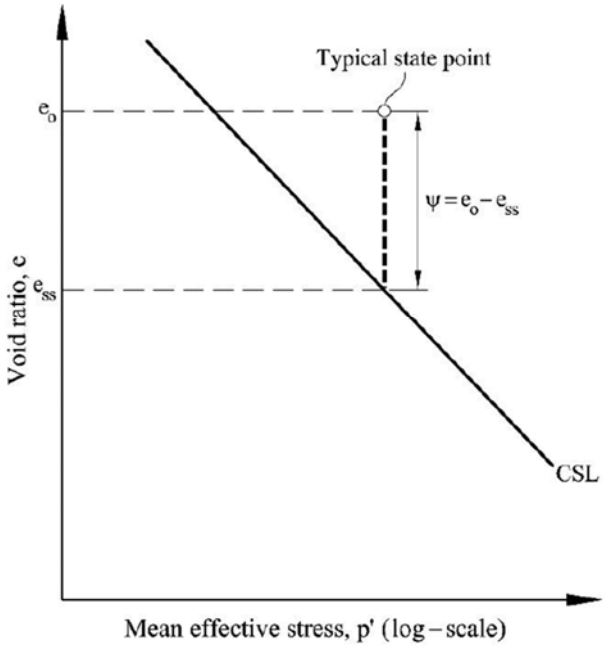

Figure 3.8. State parameter (ψ) definition, Been et al. (1991).

3.2.2. Undrained softening

As indicated above for path A of Figure 3.2, the undrained stress path and deviator stress-axial strain of a soil exhibiting undrained softening are represented in Figure 3.9 and Figure 3.10. This path reaches a peak on deviator stress followed by a drastic reduction of deviator stresses reaching finally its critical state. Of course, void ratio and mean effective stresses at the CS (or SS) lie on CSL.

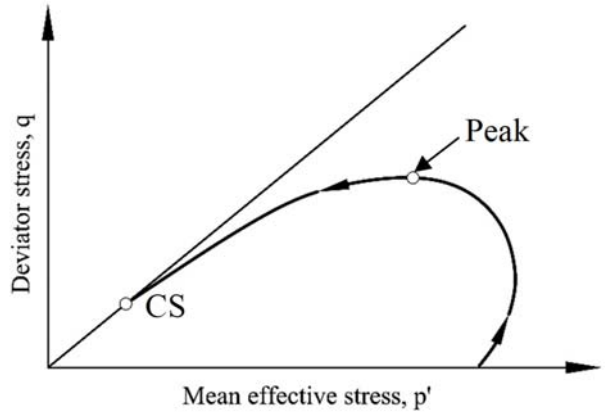

Figure 3.9. Undrained softening, effective stress path, Gens (2019).

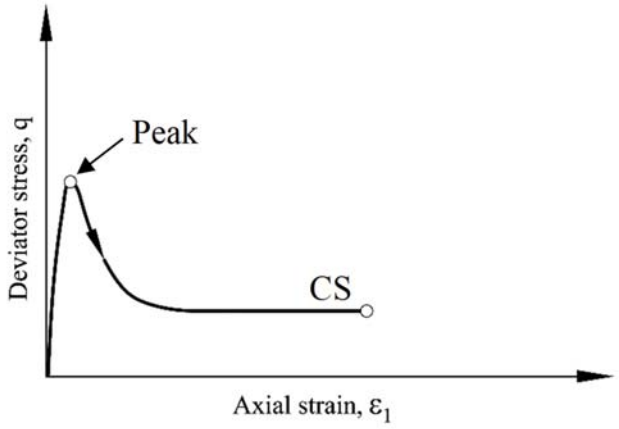

Figure 3.10. Undrained softening, stress-strain curve, Gens (2019).

During flow liquefaction, a large generation of pore water pressures is observed due to the contractive soil character -i.e. Castro (1969) tests showed in Figure 3.11-, as corresponds to positive values of the state parameter.

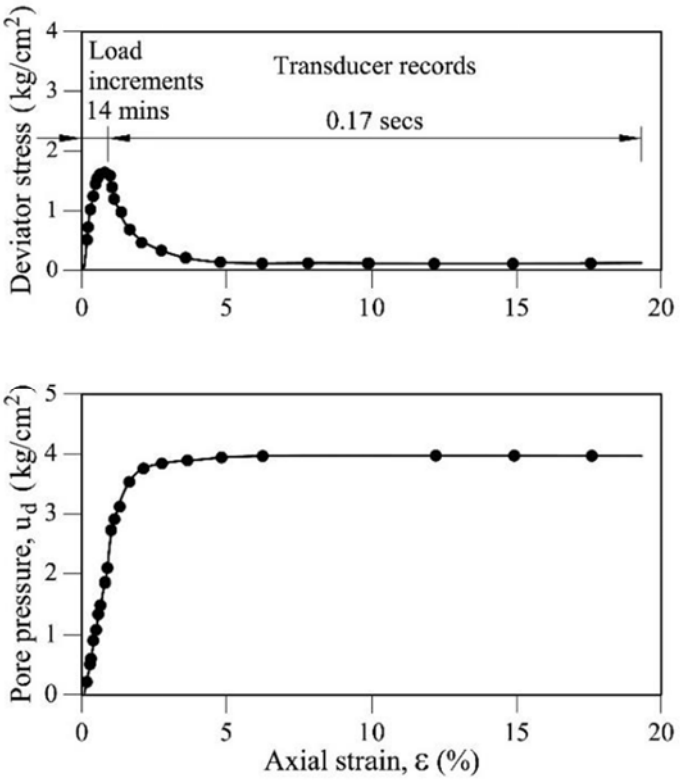

Figure 3.11. Results of a stress-controlled test on loose Banding sand, deviator stress-axial strain curve and pore pressure-axial strain curve. Bishop (1973), data from Castro (1969).

Different magnitudes of deviator stress at CS are obtained according to the location on the CSL. For very low p' values, high e_0 values often exists, hence deviator stress could be null at CS, if the CSL is curved Figure 3.6. In that case, the phenomenon has been called true liquefaction (Carrera et al., 2011). It is interesting to note that even if non-null values of deviator stress are reached, flow

liquefaction can also occur. However, failure consequences evidently will be more extreme in true liquefaction.

In connection with the investigation of the Aberfan failure, Bishop (1973) defined a brittleness index (I_B) to evaluate undrained softening in terms of undrained shear strength (c_u), [5].

$$I_B = \frac{c_{u\,peak} - c_{u\,SS}}{c_{u\,peak}} \quad [5]$$

Brittleness index indicates the susceptibility of a soil to reach flow liquefaction. The values of I_B are in the range of 0 to 1, and ductile corresponds to $I_B = 0$. True flow liquefaction would be associated with $I_B = 1$.

3.2.3. Critical /steady state

This CS is sometimes also called steady state (SS), although it has been claimed that the two concepts are not exactly the same. Poulos (1981) defined the steady state of deformation of any mass of particles is that state in which the mass is continuously deforming at constant volume, constant normal effective stress, constant shear stress and constant velocity. The difference between critical state and steady state lies in the existence of constant velocity in SS definition which it is not present in critical state (Gens, 2019). Nevertheless, both concepts are in fact quite equivalent.

Based on the ratio M = q / p' at critical state, a friction angle termed the critical state friction angle (φ_{cs}) can be derived. The deviator stress (q) is [6].

$$q = \sigma_1 - \sigma_3 \quad [6]$$

Where σ_1 and σ_3 are the major and minor principal total stresses, respectively.

The deviator stress at critical state is also called liquefied or residual strength. Significant problems -out of the PhD thesis scope-, exists to reach the CS value under experimental conditions in the laboratory triaxial apparatus (Gens, 2019).

3.2.4. Peak strength

Two different proposals have been made connecting the line that joins the peak undrained strength points: (i) Collapse line that goes from peak strength to steady state -Sladen et al. (1985a) and Ishihara (1993)-, and (ii) Flow liquefaction line that goes from peak strength to the origin of p'- q' space (Vaid and Chern, 1985 and Lade, 1993). The framework of state parameter has been proposed in Yang (2002) to merge both concepts. Gens (1982) has pointed out that peak strength depends on strain rate and consolidation stress path. Thus, it is better to consider peak strength as simply an undrained parameter unrelated to effective stress strength parameters.

Isotropic consolidation stress paths for laboratory tests on flow liquefaction have been usually adopted. However, this assumption does not match up real field conditions and it tends to reduce peak strength, as Castro (1969) demonstrates for the same sand subject to different initial consolidation stresses (Figure 3.12).

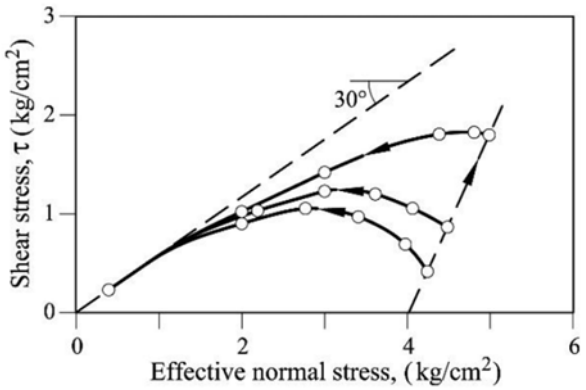

Figure 3.12. Triaxial undrained tests with different initial anisotropically consolidation stress paths, (Bishop 1973, data from Castro 1969).

Triaxial tests on isotropically and anisotropically consolidated samples were performed on tailings involved in the Merriespruit failure (Fourie and Tshabalala, 2005). Results showed that different stress ratios (η = q / p') at peak strength were reached depending on whether the consolidation stress path was isotropic and anisotropic. Isotropic consolidated tests reached a peak stress ratio close to 0.6 (Figure 3.13) whereas the stress ratio from anisotropic consolidated tests were, 0.9 (Figure 3.14).

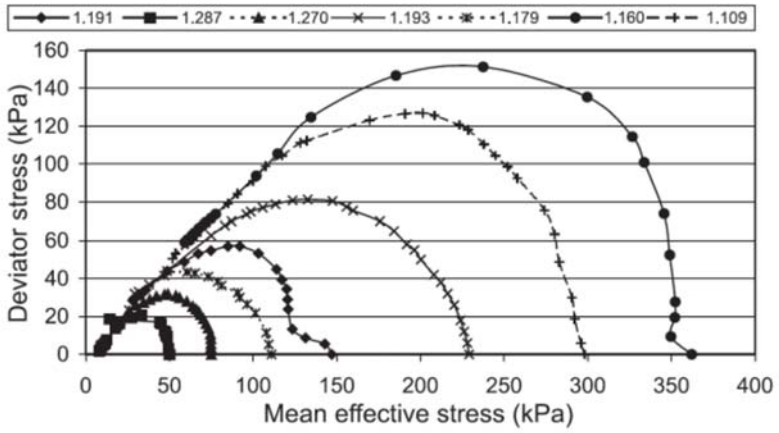

Figure 3.13. Undrained triaxial tests on isotropically consolidated samples (Fourie and Tshabalala, 2005).

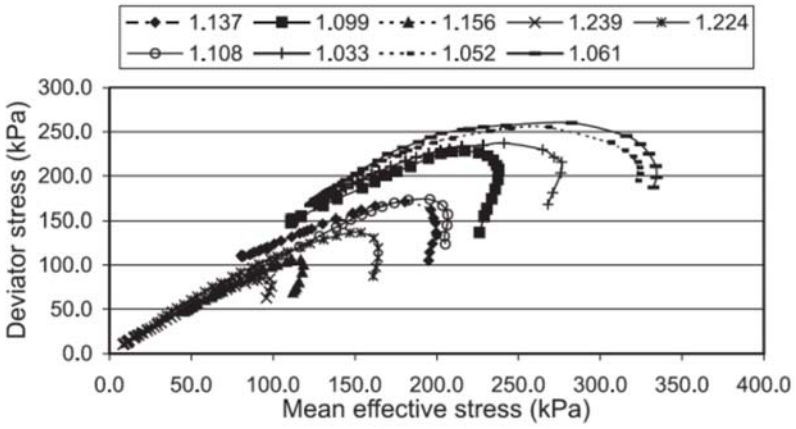

Figure 3.14. Undrained triaxial tests on anisotropically consolidated samples (Fourie and Tshabalala, 2005).

3.2.5. Triggering flow liquefaction

Although the triggering of flow liquefaction could be "spontaneous" as Terzaghi (1957) suggested when soil liquefy due to its emplacement over a slope with large enough inclination, soil it is more likely undergo flow liquefaction after an external load is applied that acts as liquefaction precursor or trigger (Gens, 2019). The applied deviator stress may be due associated with different total stress paths such as A or B in Figure 3.15. Path A is associated with an undrained rise of vertical stress, whereas path B corresponds to a reduction of horizontal stress. Gens (2019) indicated the all undrained total stress path are equivalent regarding the resulting effective stress path.

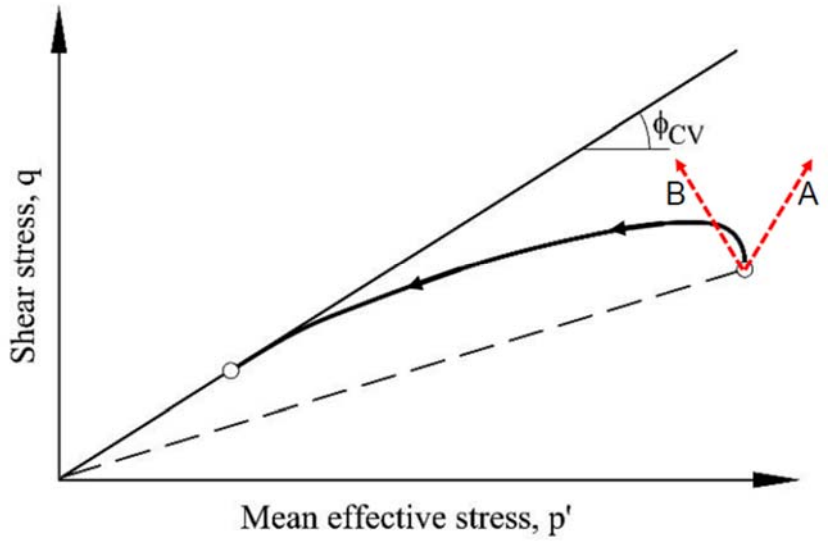

Figure 3.15. Undrained increment of deviator stress triggers flow liquefaction (Gens, 2019).

Another triggering event can be associated with a reduction of drained lateral (Figure 3.16). It is also possible in case of an increase of pore pressure from the variation in hydraulic conditions or from cyclic loading, as shown in Figure 3.17 and Figure 3.18 respectively, may also trigger flow liquefaction. Although peak strength is not attained in last three cases, the instability branch is reached and flow liquefaction follows.

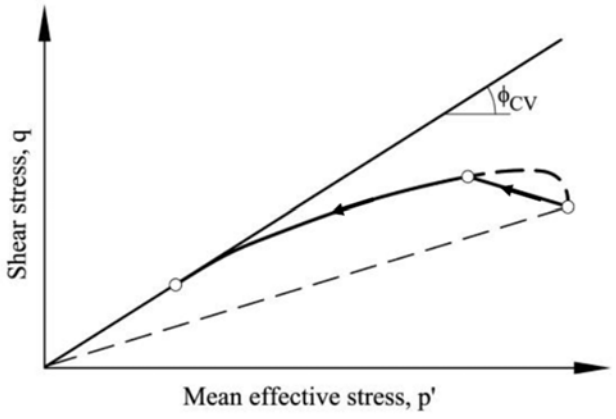

Figure 3.16. Drained unloading of lateral stress triggers flow liquefaction (Gens, 2019).

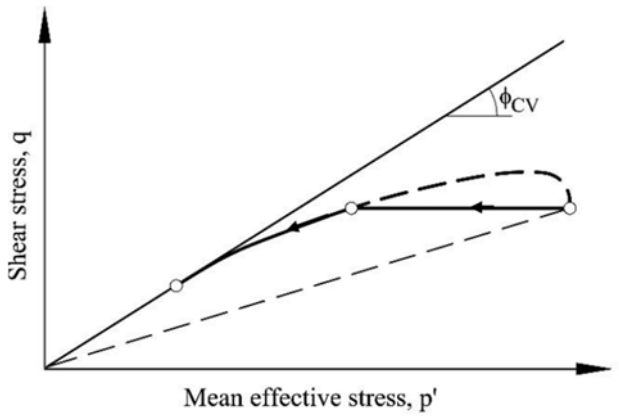

Figure 3.17. An increase of pore pressure by variation in hydraulic conditions triggers flow liquefaction (Gens, 2019).

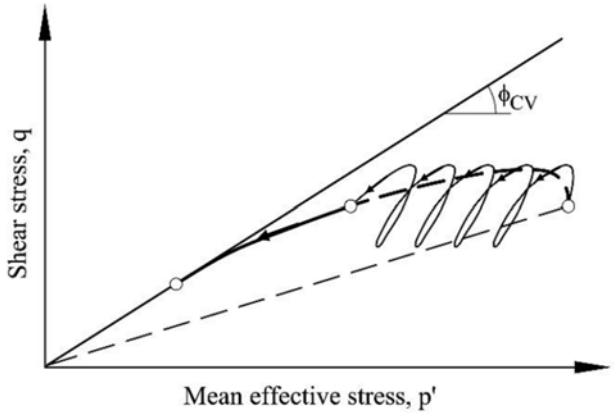

Figure 3.18. An increase of pore pressure by cyclic loading triggers flow liquefaction (Gens, 2019).

Gens (2019) linked the stress paths shown above with physical triggering mechanisms for flow liquefaction (Martin and McRoberts, 1999):

i) Path A (Figure 3.15) may be linked with an emplacement of material or construction.

ii) Unloading of lateral paths -undrained path B (Figure 3.15) for rapid event and drained path from Figure 3.16 for slow event-, may be linked with foundation sliding, dam overtopping, toe erosion or excavation.

iii) Variation in hydraulic conditions path (Figure 3.17) may be linked with increased pond levels, unfavourable weather conditions or pore pressure redistribution.

iv) Cyclic loading path (Figure 3.18) may be linked with any type of action involving vibration (from earthquakes to traffic or blasting).

3.3. *Evaluation of liquefied undrained strength*

High plasticity soils tend to have large strains to both peak and liquefied shear strength and therefore tend not to experience flow failures (Ladd et al., 1977), whereas, low plasticity soils tend to have smaller strains to both peak and residual strength. Most case histories of flow liquefaction -reported in Olson and Stark (2002)-, have occurred in low plasticity or non-plastic soils consistent with the small strain to peak strength and high brittleness. These cases have been back-calculated resulting in $c_{u\,SS}/\sigma'_v$ (or $c_{u\,liq}/\sigma'_v$) values in the range of 0.04 to 0.12, Figure 3.19. According to reported $c_{u\,peak}$, I_B values are higher than 0.4. Thus, it has been suggested that soil with I_B =0.4 can be called high brittleness soils (Robertson, 2017).

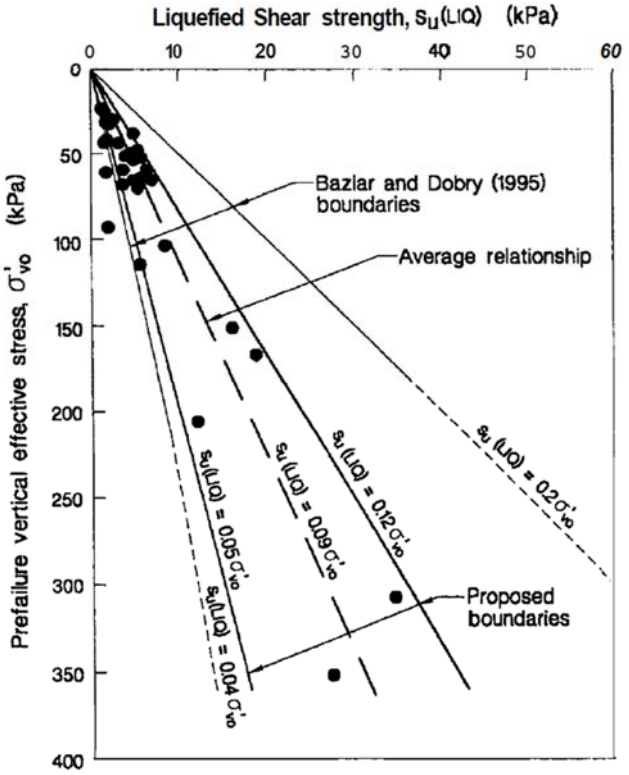

Figure 3.19. Vertical effective stress vs. liquefied shear stress of different case histories, Olson & Stark (2002).

From different study cases of flow liquefaction presented in Olson and Stark (2002), a relationship between q_c from CPTU and yield strength ratio ($c_{u\,yield}/\sigma'_v$) or ($c_{u\,peak}/\sigma'_v$) was proposed by Olson and Stark (2003).

$$\frac{c_u(yield)}{\sigma'_v} = 0.205 + 0.0143(q_{c1}) \pm 0.04 \qquad \text{for } q_{c1} \leq 6.5 \text{ MPa} \qquad [6]$$

$$\text{where:} \quad q_{c1} = \frac{1.8}{0.8+\frac{\sigma'_v}{p_a}} \cdot q_c \qquad [7]$$

where q_{c1} is the q_t normalized for overburden stress (MPa) and p_a atmospheric pressure (MPa).

The liquefied shear strength ratio was estimated by Olson and Stark (2002) to be:

$$\frac{c_u(LIQ)}{\sigma'_v} = 0.03 + 0.0143(q_{c1}) \pm 0.03 \quad \text{for } q_{c1} \leq 6.5 \text{ MPa} \qquad [8]$$

Peak and liquefied shear strength ratios have been derived for hydraulic fill CPTu results (Figure 3.20 to Figure 3.24). The obtained values of peak shear strength ratio lies close to 0.25. In contrast, the average of liquefied shear strength is lower, around 0.06. Results are similar in both Phases, although higher values due to the existence of sand layers are observed in Phase 2 fill.

This relationship has limitations for determining liquefied shear strength ratio because the original database was obtained analysing cases in which there was a recognizable post-failure geometry for the failed mass (Olson and Stark, 2002). It is not the case for Prat quay, where such analysis would have been impossible as the material flowed nearly more than a hundred meters. Nonetheless, this liquefied ratio will be used in following constitutive model calibration.

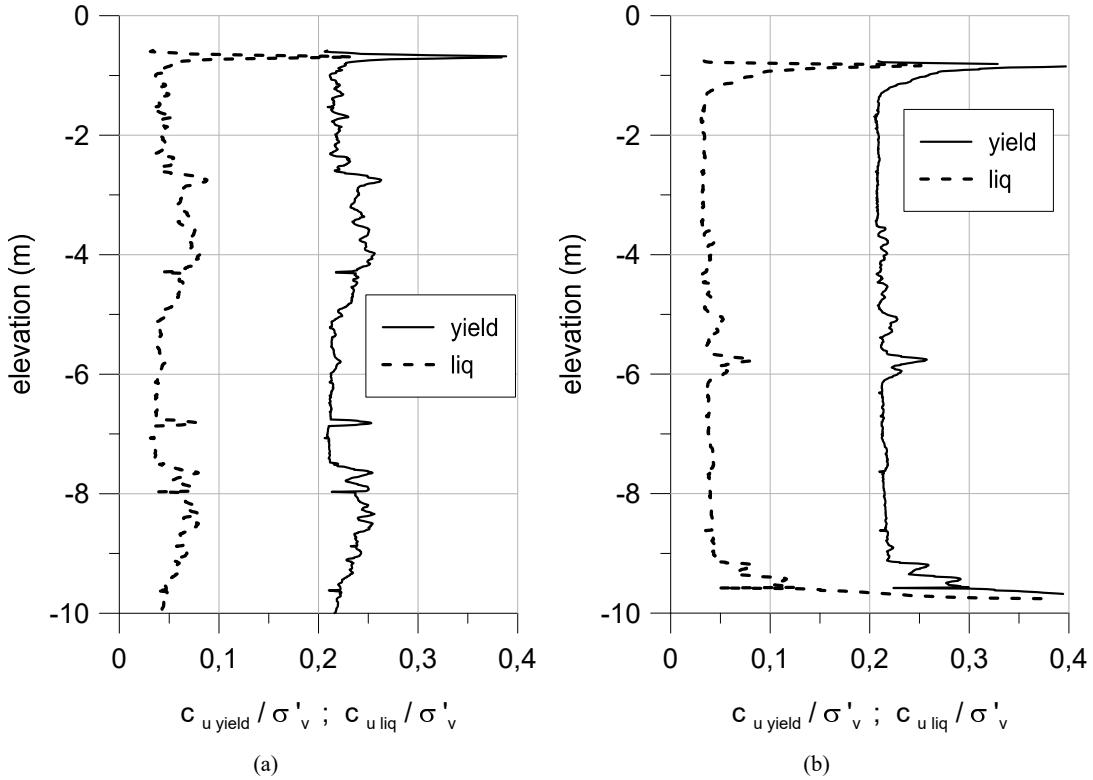

Figure 3.20. Results of peak and liquefied shear strength ratio from CPTu data, (a) 6a8 and (b) 6a12, Phase 1.

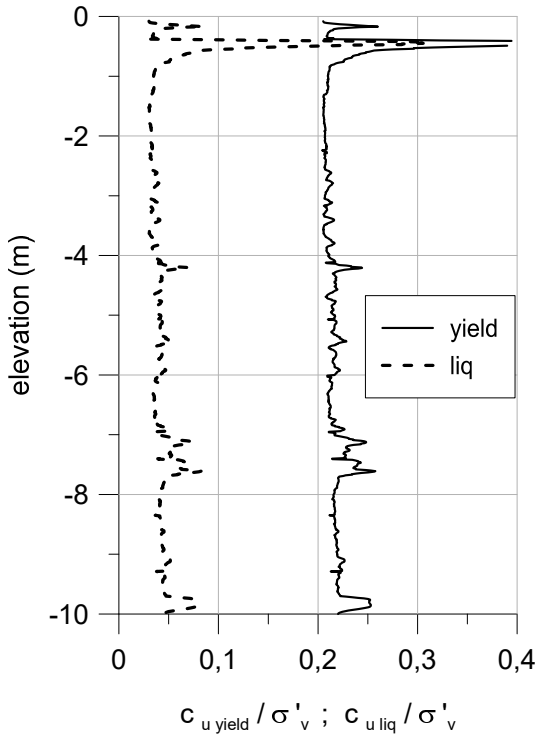

Figure 3.21. Results of peak and liquefied shear strength ratio from CPTu data, 6a14 Phase 1.

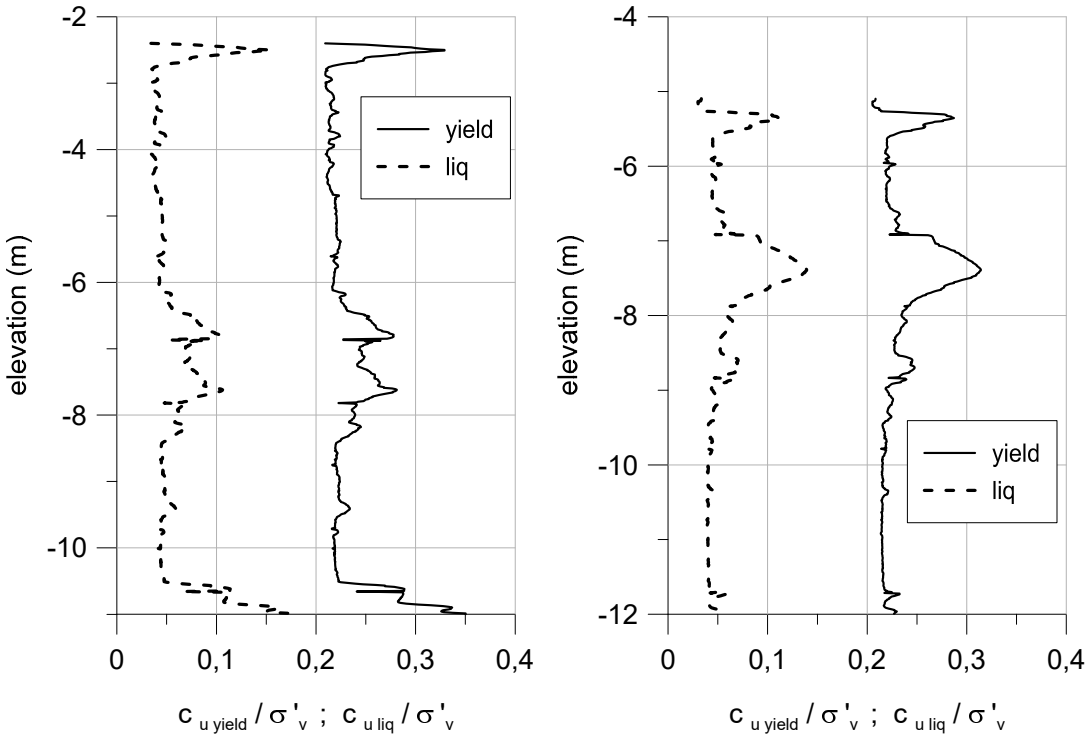

(a) (b)

Figure 3.22. Results of peak and liquefied shear strength ratio from CPTu data, (a) 3b11 and (b) 3b12, Phase 2.

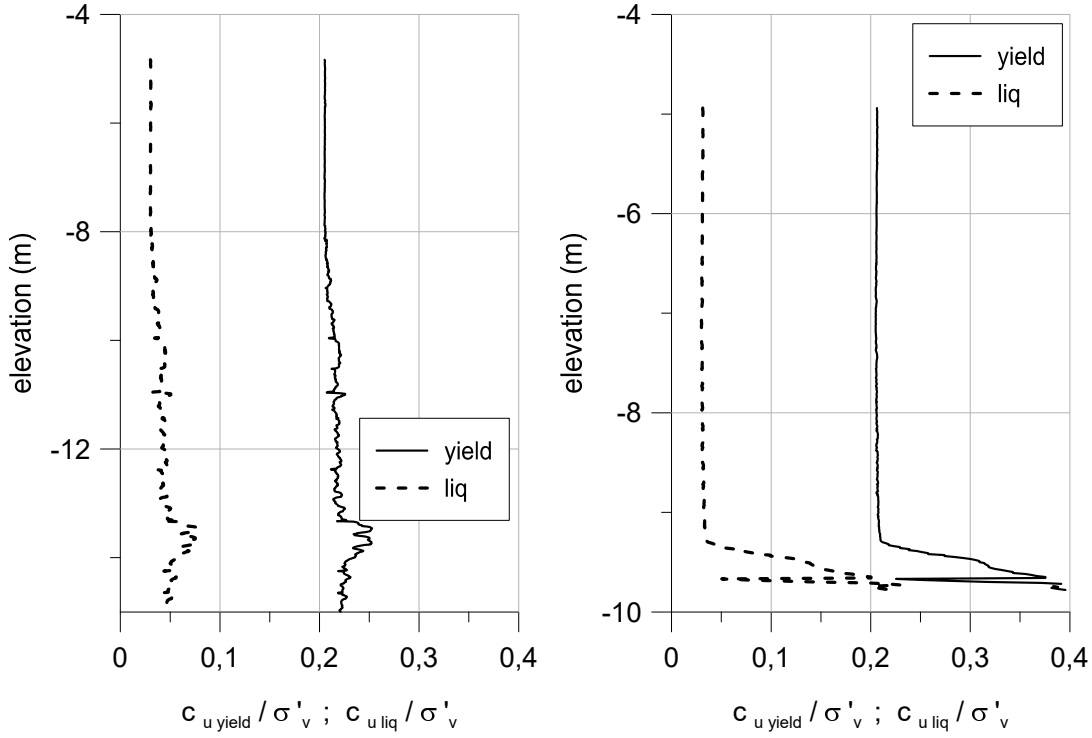

Figure 3.23. Results of peak and liquefied shear strength ratio from CPTu data, (a) 7b8 and (b) 7b12, Phase 2.

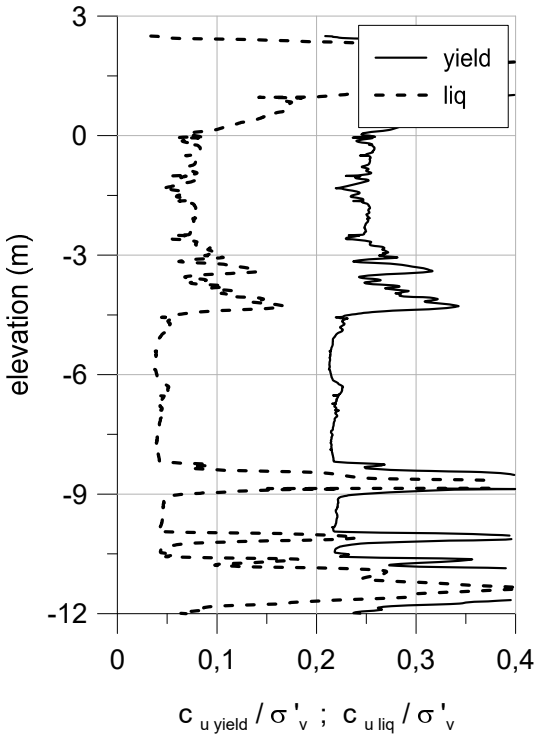

Figure 3.24. Results of peak and liquefied shear strength ratio from CPTu data, 7b13 Phase 2.

3.4. Criteria for flow liquefaction

Most liquefaction criteria have been developed in relation to seismic actions. Although an earthquake was not the trigger for the Part quay failure, such criteria have been applied to the hydraulic fill using the Barcelona seismic conditions (Appendix D). The results, using the criteria for cyclic liquefaction (Appendix E.2) are presented in Appendix E.3. In this section, the application of four different criteria for flow liquefaction to the Prat quay hydraulic fill is described. One of criteria is based on laboratory tests whereas the other three are based on CPTu results.

The criterion based on laboratory tests uses the values of plasticity index (I_P), liquid limit (LL) and water content (w_c). Seed et al. (2003) modified an existing Chinese criterion (Wang, 1979) to define three zones separating materials susceptible, moderately susceptible and not susceptible to liquefaction. The modified Chinese criterion indicates that zone A is limited by PI in the range of 0 to 10 and LL in the range of 0 to 37, while zone B is bounded by $10 < I_P < 12$ and $37 < LL < 47$. Additional soil conditions were imposed; materials in Zone A are prone to liquefaction if $w_c \geq 0.85$ LL (red shadowed) while soils within Zone B are potentially susceptible to liquefaction if $w_c \geq 0.80$ LL. The soils, which are not in Zone A or Zone B, are considered as no liquefiable. To simplify the application of the criterion, it was plotted by Bray et al. (2004) as in Figure 3.25 shows. Although the criterion was proposed for cyclic liquefaction, it is thought that it may also be applicable to flow liquefaction.

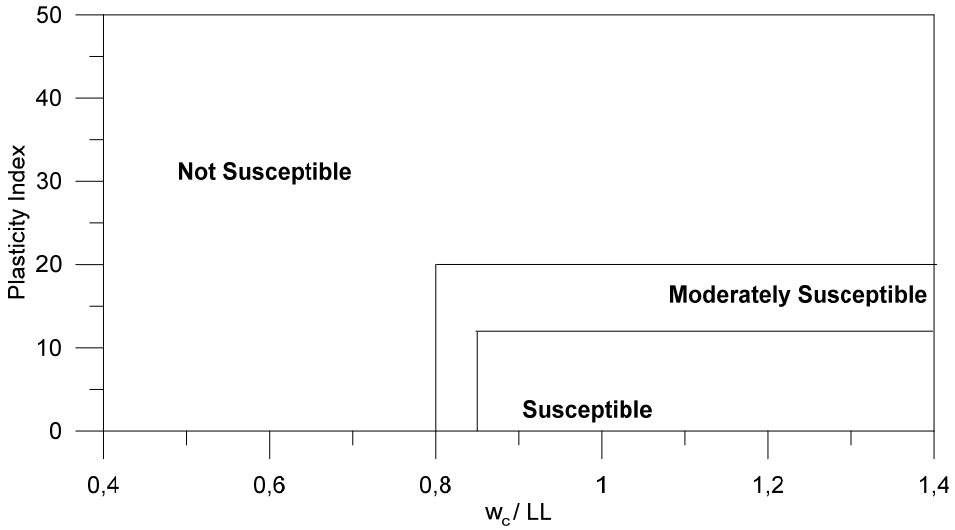

Figure 3.25. Liquefaction criterion Bray et al. (2004).

Since the extraction of undisturbed samples in hydraulic fill is difficult, soil characterization has been principally based on in-situ tests, especially cone penetration tests (Viana da Fonseca, 2013). Consequently, flow liquefaction potential evaluation has been mostly based on cone penetration results. To normalised parameters F_r: friction ratio, Q_t: normalized cone resistance ratio, and B_q: Pore pressure ratio are used for this purpose (Wroth, 1984; Houlsby and Teh, 1988). They are defined as

obtain a screening tool, q_c, f_s and u_2 were normalized as such as Q_t: normalized cone resistance ratio, F: friction ratio, and B_q: Pore pressure ratio:

$$Q_t = (q_t - \sigma_{vo}) / \sigma'_{vo} \quad [7]$$

$$F = f_s / (q_t - \sigma_{vo}) \quad [8]$$

$$B_q = (u_2 - u_o) / (q_t - \sigma_{vo}) \quad [9]$$

$$Q_t(1 - B_q) + 1 = (q_t - u_2)/\sigma'_{vo} \quad [10]$$

where q_t is the total cone resistance, f_s is the sleeve friction, u_2 is the pore pressure measured at the cone shoulder and u_0 is the initial pore pressure.

As indicated above, the value of the state parameter can be used as an indicator for the potential for flow liquefaction. Contours of ψ are plotted in a $Q_t \cdot (1\text{-}B_q)+1$ – F space. The state parameter is derived from Shuttle and Cunning (2008) that establishes the occurrence of flow liquefaction ($\psi > -0.05$).

The plot also shows contours of soil index behaviour (I_c) as defined by Robertson (1990) and reformulated in Robertson and Wride (1998) as:

$$I_c = [\ (3.47 - \log Q_t)^2 + (\log F + 1.22)2\ ]^{0.5} \quad [11]$$

The soil index behaviour delimits the regions occupied by different sol types.

However, the method designed by Plewes et al. (1992) is likely the most commonly applied method to evaluate ψ for fine-grained tailings (Shelbourn, 2010; Jefferies & Been, 2006 and Morgenstern et al., 2016). The Plewes et al. (1992) method is defined in following equations:

$$\lambda_{10} = \max\left[0.01; \frac{\min(F\ ; 7)}{10}\right] \quad [12]$$

$$k = M_{tc}\left(3 + \frac{0.85}{\lambda_{10}}\right) \quad [13]$$

$$m = 11.9 - 13.3\ \lambda_{10} \quad [14]$$

$$Q_{(group)} = \left(\frac{3}{1 + 2\ K_0}\right) \max\left[Q\ (1 - B_q) + 1\ ; 0.01\right] \quad [15]$$

$$\psi_{plewes} = -\frac{ln\left(\frac{Q_{(group)}}{k}\right)}{m} \quad [16]$$

where λ_{10} is the compressibility index on $\log_{10}$, M_{tc} is the critical friction ratio and, k and m values from an exponential trend line. Again, flow liquefaction is considered possible of the computed $\psi > -0.05$.

The flow liquefaction criterion of Robertson (2009) is based on the new concept of normalized cone resistance ratio, Q_{tn}, that incorporates a variable stress exponent n -that varies with I_c-, from Zhang et al. (2002). The iteration process to evaluate Q_{tn} is described in flow chart presented in Figure 3.26.

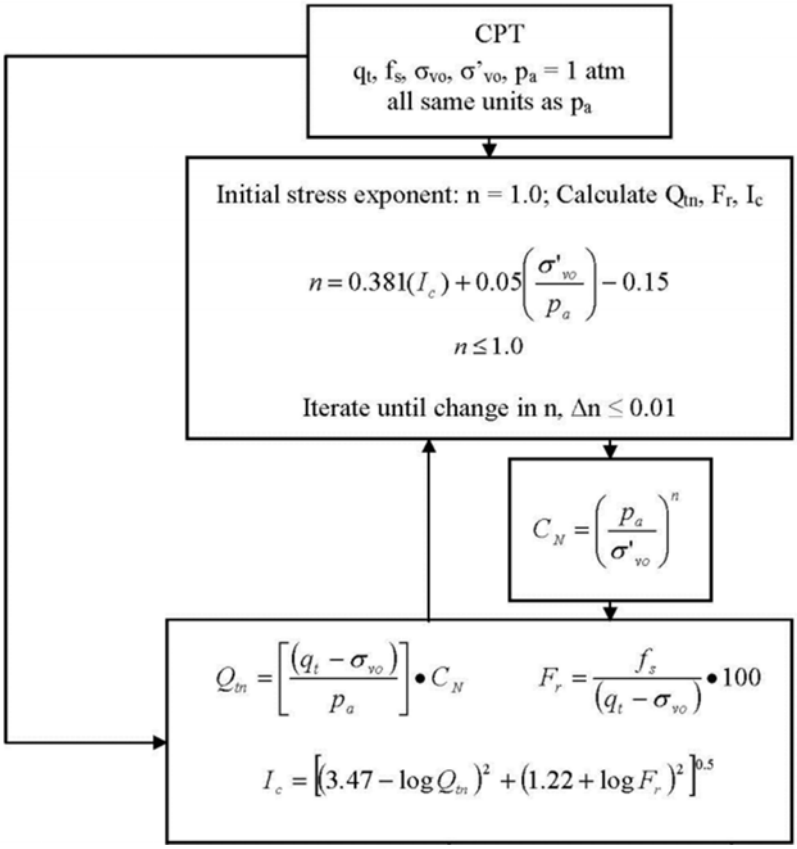

Figure 3.26. Flow chart to evaluate Q_{tn} (modified from Robertson, 2009).

Robertson (2009) and (2016) adopted the space of normalized cone resistance, Q_{tn}, vs friction ratio to distinguish the regions occupied with different material types (Figure 3.27): sand-like (S), transition materials (T) and clay-like material (C). The regions are also further distinguished depending on whether they are contractive (C) or dilatant (D). A special region is defined to accommodate sensitive contractive clay-like soils (CCS). Flow liquefaction is associated with soils with contractive behaviour that lie below the line defined by the equation $(Q_{tn} - 11)\cdot(1 + 0.06\cdot F) = 70$.

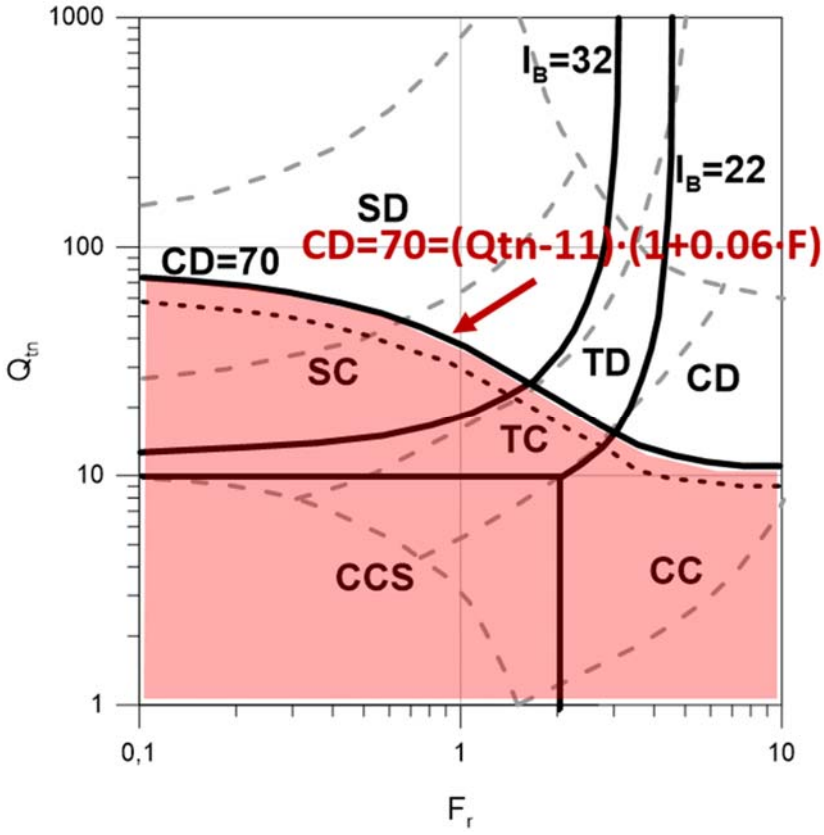

Figure 3.27. Screening soil behaviour chart, Robertson (2016) criteria.

The final flow liquefaction criterion to be considered has been defined in Mayne (2019) and Mayne and Sharp (2019). It is based on the yield stress ratio (YRS = σ'_p / σ'_{v0}), where σ'_p is the yield stress and σ'_{v0} is the initial vertical effective stress. The contractive – dilative behaviour boundary is related to an excess pore pressure is zero in undrained shear. Then YSR at critical state line is [17]:

$$YSR_{CSL} = (2/\cos\phi')^{1/\Lambda} \quad [17]$$

where: ϕ' is the effective stress friction angle, Λ is the plastic volumetric strain ratio (Λ=1-(C_s/C_c)), C_s is the recompression index and C_c is the compression index. A value of Λ =0.9 is usually adopted for sensitive clays (Mayne, 2008), ϕ' is derived from CPTu results according to expression [18] defined by Mayne (2007) for soft to firm clays restricted to 0.05 $\leq B_q \leq$ 1.1 and 20° $\leq \phi' \leq$ 45°.

$$\phi' = 29.5 \cdot B_q^{0.121} \cdot (0.256 + 0.336 \cdot B_q + \log Q_t) \quad [18]$$

The current YSR was related to normalized CPTu parameters for structured and sensitive clays. Three expression was derived using hybrid spherical cavity expansion and critical state soil mechanics (Mayne, 1991; Agaiby and Mayne, 2018 and Mayne et al., 2018). The following expression is used [19]:

$$YSR_{CPTU} = \left[\frac{Q_t - (M_{c1}/M_{c1}) \cdot (U^* - 1)}{1.95 \cdot M_{c1} + (M_{c1}/M_{c1})}\right]^{1/\Lambda} \quad [19]$$

where: U^* is normalized water pressure, $U^*=(u_2-u_0)/\sigma'_v$ and M_c is the friction parameter in p'- q space, $M_c = 6\cdot\sin(\phi') / (3 - \sin(\phi'))$. The M_{c1} value is defined for the normally-consolidated soil and [19] is the value for the intact structured soil. For non-structured soil, as hydraulic fills recently placed, will be supposed $M_{c1}=M_{c2}$. Soil behaves in a contractive way and flow liquefaction is possible, if $YSR_{CPTU} < YSR_{CSL}$.

3.5. *Application of flow liquefaction criteria*

The four criteria described above have been applied to results from the site investigation of Prat quay, Phases 1 and 2. To check the criteria based on CPTu tests, the observations obtained in tests 6a8, 6a12 and 6a14 (Phase 1), 3b11, 3b12, 7b8, 7b12 and 7b13 (Phase 2) have been be used. They provide a representative set of the results obtained in the hydraulic fill.

Additionally, cyclic liquefaction criteria are applied in Appendix E.3 using Barcelona seismic conditions (Appendix D).

3.5.1. Bray et al. (2004) criterion

The values of plasticity index and water content/Limit Liquid of a number of specimens extracted from the hydraulic fill are plotted in Figure 3.28. It can be noted that they classify as susceptible to liquefaction. To increase the database, a settling column was set up in the laboratory to simulate the deposition and settling process of the hydraulic fill (Appendix F). Samples were retrieved from the column and their results are also plotted in Figure 3.28. They lie in the moderately susceptible zone.

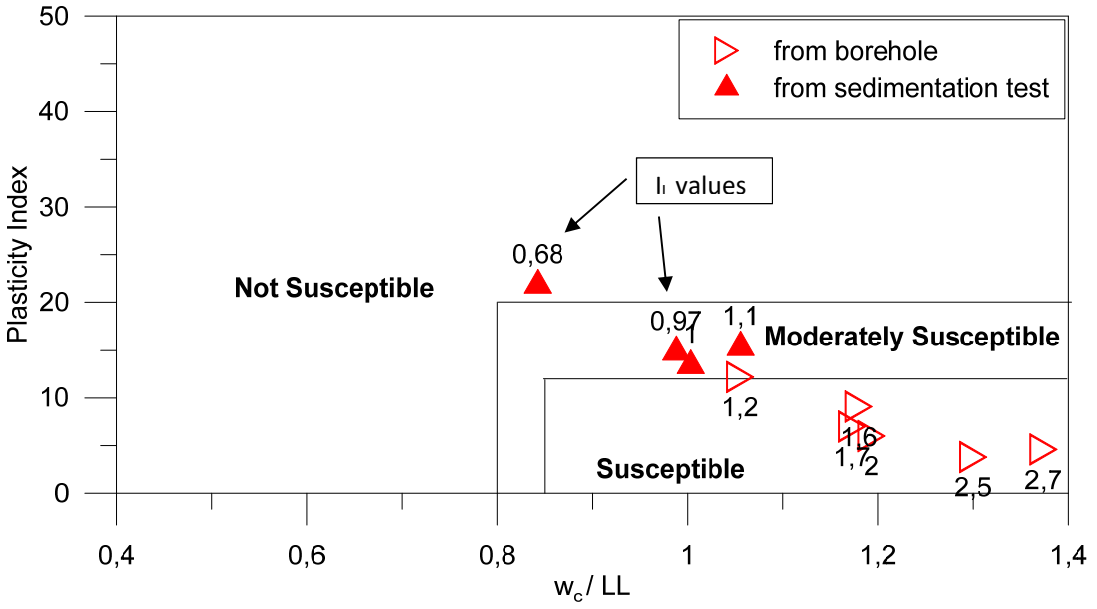

Figure 3.28. Liquefaction criterion (Bray et al., 2004) for hydraulic fill specimens, labels indicate I_L values for each specimen.

The criterion uses the same parameters of liquidity index (I_L), LL, LP and w, that were related to remoulded undrained shear strength -equivalent to $c_{u\,SS}$-, by Leroueil et al. (1983), with the following equation:

$$c_{u\,r} = 1 / (I_L\text{-}0{,}21)^2 \qquad [20]$$

Results confirm that high values of I_L are related with low values of $c_{u\,SS}$, which also correspond with the zone of susceptible soils as delimited by the criterion. Direct shear tests on samples taken from the settling column were carried out. This peak shear strength were close to 80 kPa. As the I_L was close to 1, $c_{u\,SS}$ is estimated as 1.6 from equation (16). Therefore, the resulting brittleness index is 0.98.

3.5.2. Plewes et al. (1992) criterion

The state parameter evaluation based on Plewes et al. (1992) method has been applied to the same CPTu tests that were used to estimate the liquefied shear strength according to Olson and Stark (2002). The results corresponding to the hydraulic fill are shown in Figure 3.29 to Figure 3.33. It can be noted that large zones of hydraulic fill yield values of the state parameter larger than -0.05 and are therefore susceptible to flow liquefaction. State parameters values in contractive region ($\psi > -0.05$), represent roughly half of derived values in both Phase 1 and Phase 2. Although, it is obvious existing heterogeneity on results.

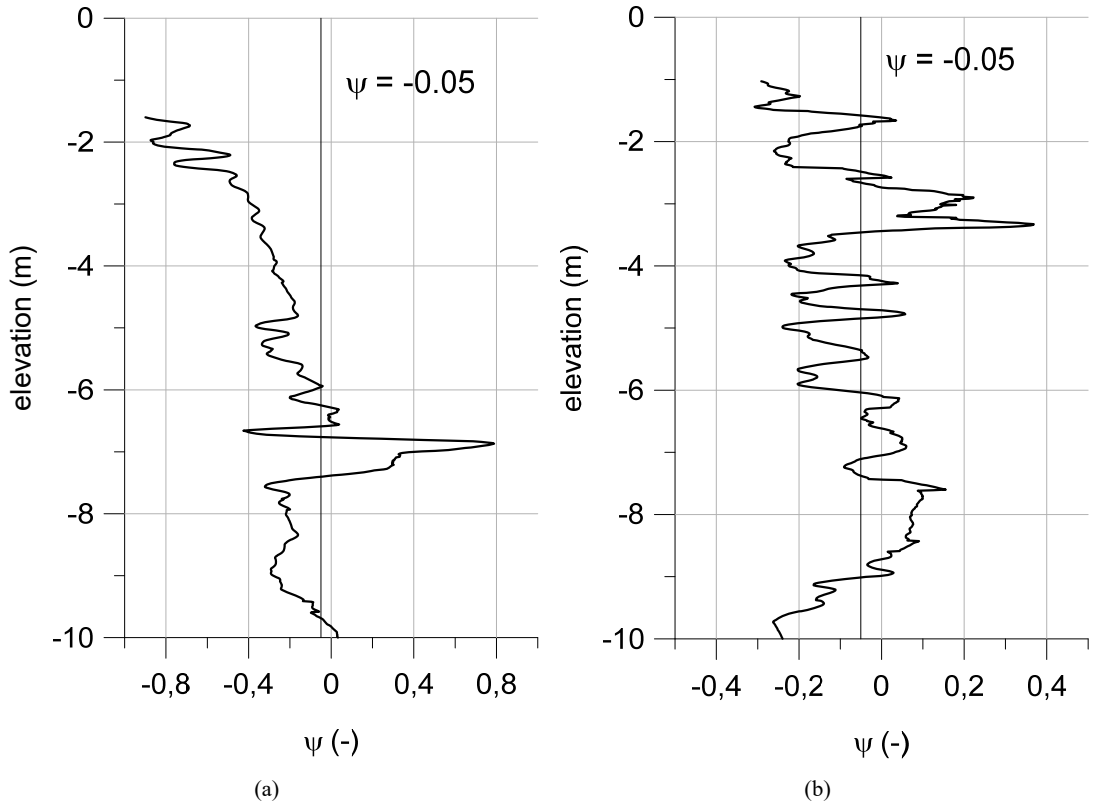

Figure 3.29.Results of applying Plewes et al. method for (a) 6a8 and (b) 6a12, Phase 1.

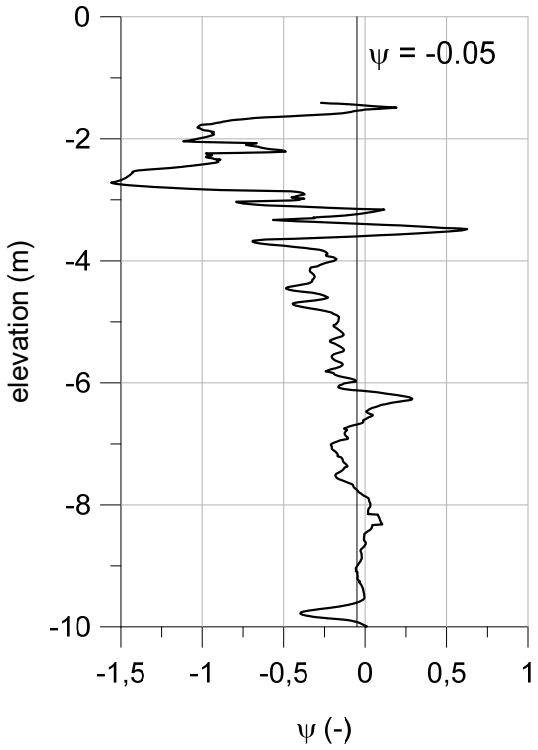

Figure 3.30. Results of applying Plewes et al. method for 6a14, Phase 1.

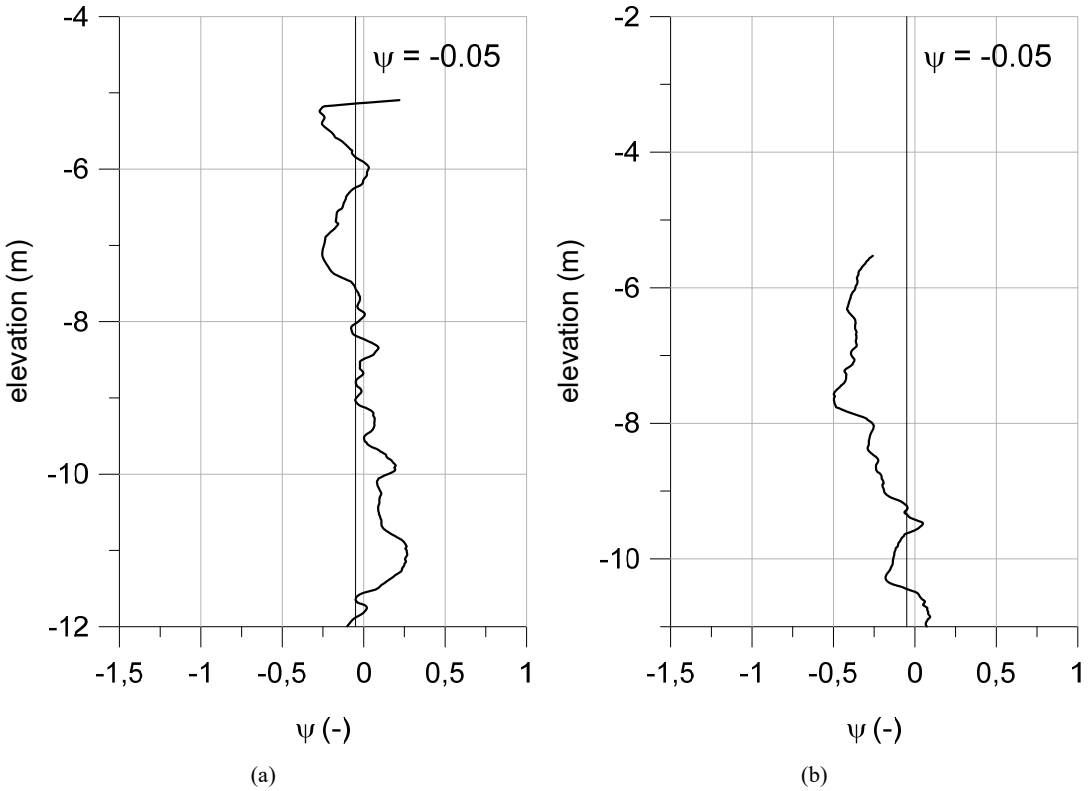

Figure 3.31. Results of applying Plewes et al. method for (a) 3b11 and (b) 3b12, Phase 2.

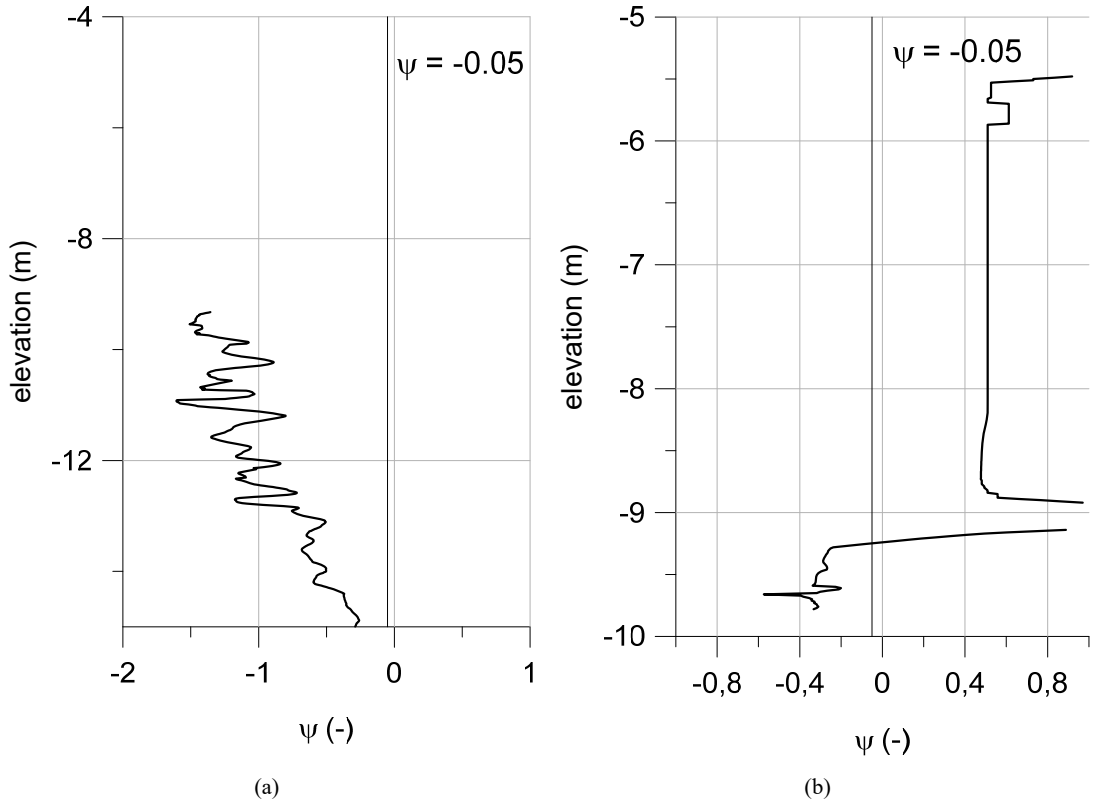

Figure 3.32. Results of applying Plewes et al. method from (a) 7b8 and (b) 7b12, Phase 2.

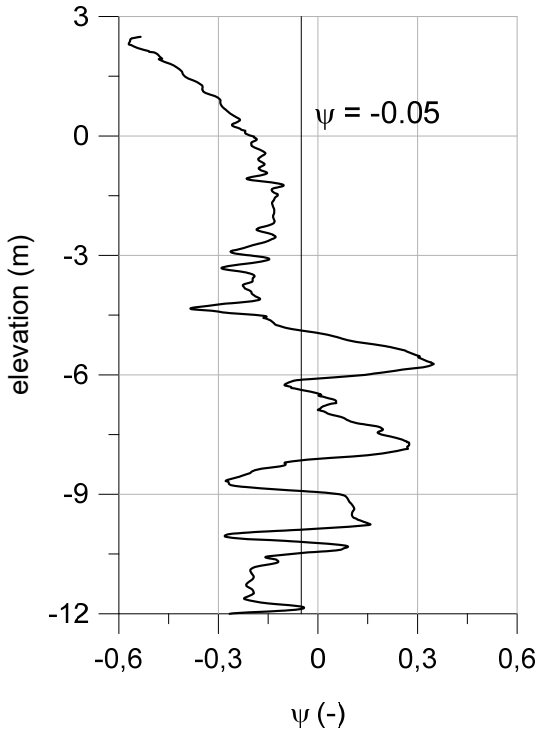

Figure 3.33. Results of applying Plewes et al. method for 7b13, Phase 2.

3.5.3. Robertson (2016) criterion

The results of the same CPTu results are plotted in the Robertson (2016) charts in Figure 3.34 to Figure 3.38. Again, a large majority of points lie in the contractive, and therefore, potentially liquefiable zones. Approach indicate contractive soils essentially over the full depth. It is interesting to note that a substantial number of points correspond to the region of sensitive contractive clay-like soils (CCS). Punctually, F-Q_{tn} values are out of the criterion range, however many points of a CPTu (Figure 3.37b) can not be characterized by this criterion, because extremely low Q_{tn} and high F values are obtained.

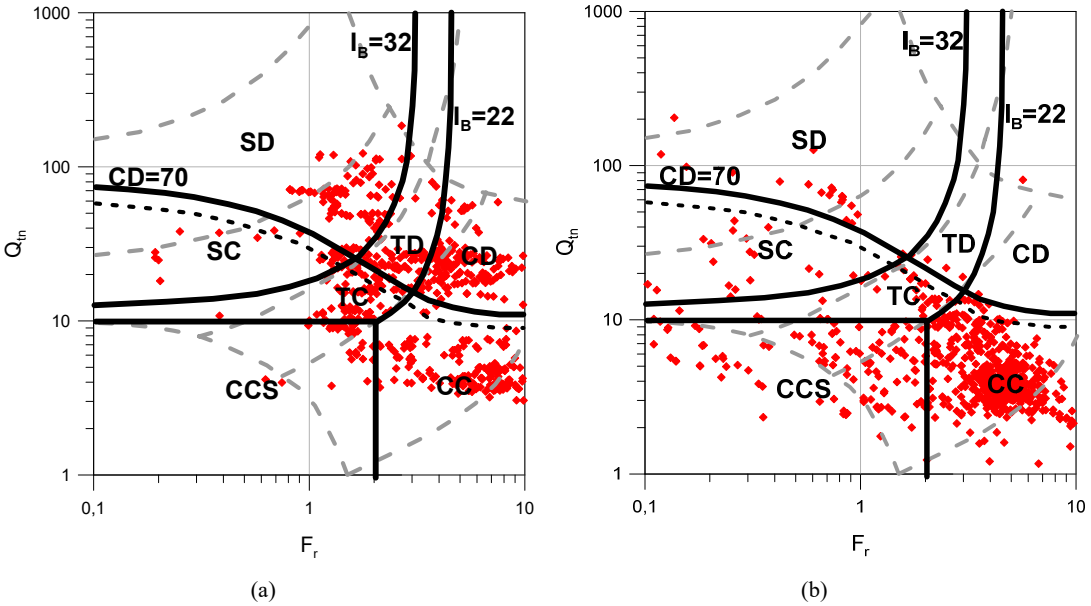

Figure 3.34. Location of the results of two CPTu tests in Roberson (2016) chart: a) CPTu 6a8 and CPTu 6a12 from Phase 1.

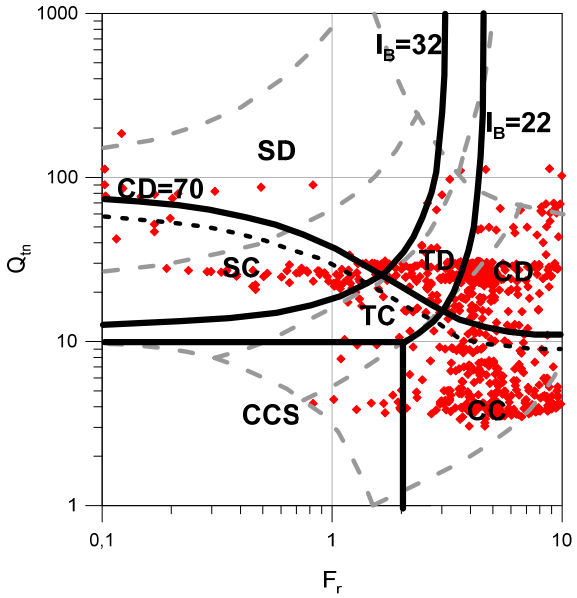

Figure 3.35. Location of the results of a CPTu test in Roberson (2016) chart: a) CPTu 6a14, from Phase 1.

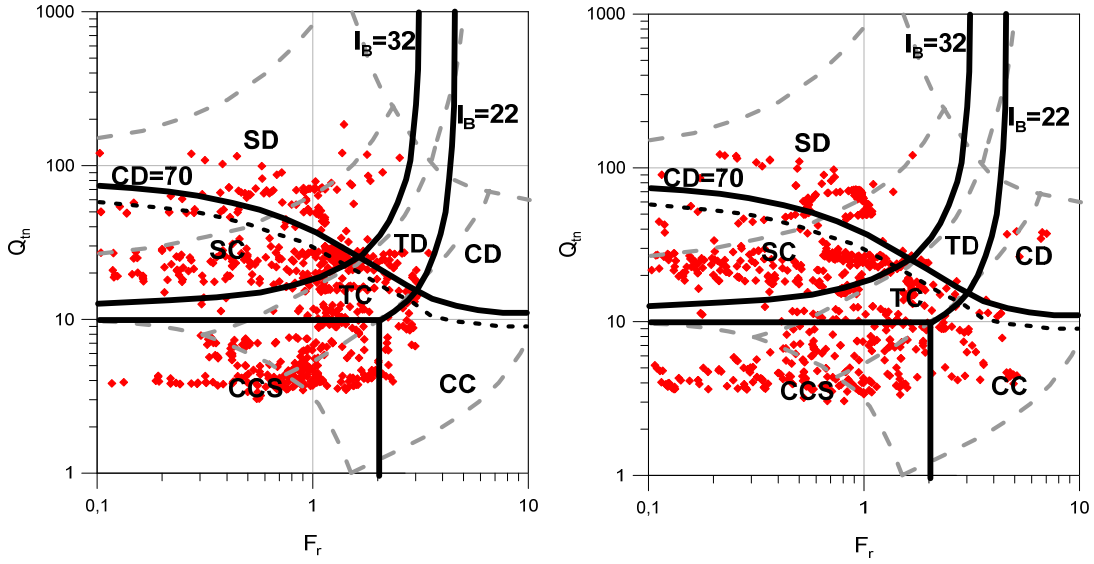

Figure 3.36. Location of the results of two CPTu tests in Roberson (2016) chart: a) CPTu 3b11 (Phase 2) and b) CPTu 3b12, from Phase 2.

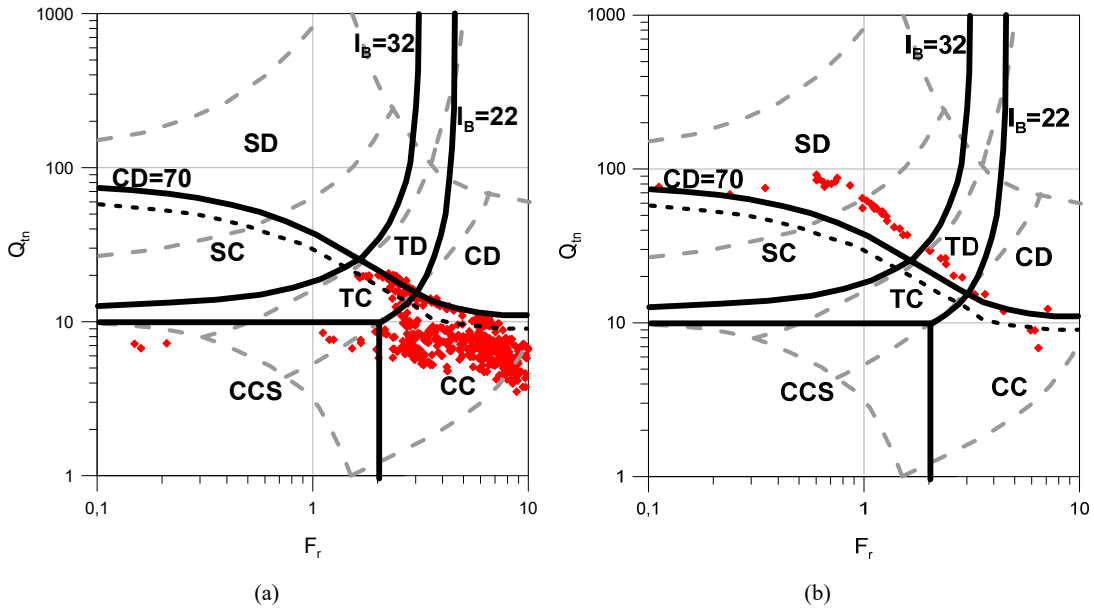

Figure 3.37. Location of the results of two CPTu tests in Roberson (2016) chart: CPTu 7b8 and CPTu 7b12 from Phase 2.

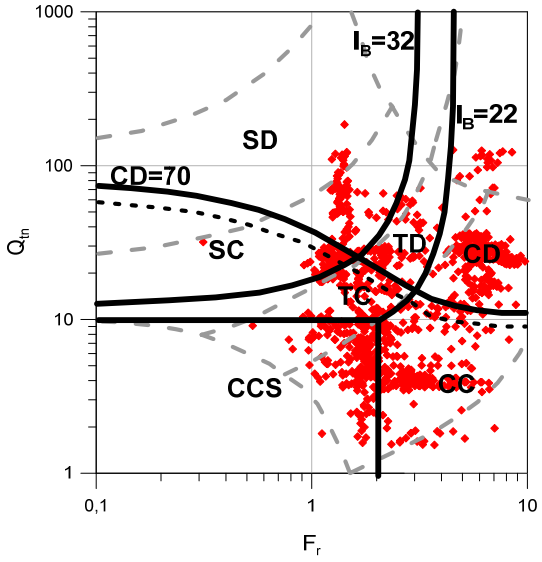

Figure 3.38. Location of the results of a CPTu test in Roberson (2016) chart: CPTu 7b13 from Phase 2.

3.5.4. Mayne (2019) criterion

The screening method proposed by Mayne (2019) has also been applied to the same CPTu profiles in previous criteria, large parts of the hydraulic fill classify as potentially liquefiable (Figure 3.39 to Figure 3.43). It should be noted that some points indicate that the YSR<1, described by Mayne and Sharp (2019) as "a higher warning of soils in an under-consolidated state with more imminent risks of instability and failure".

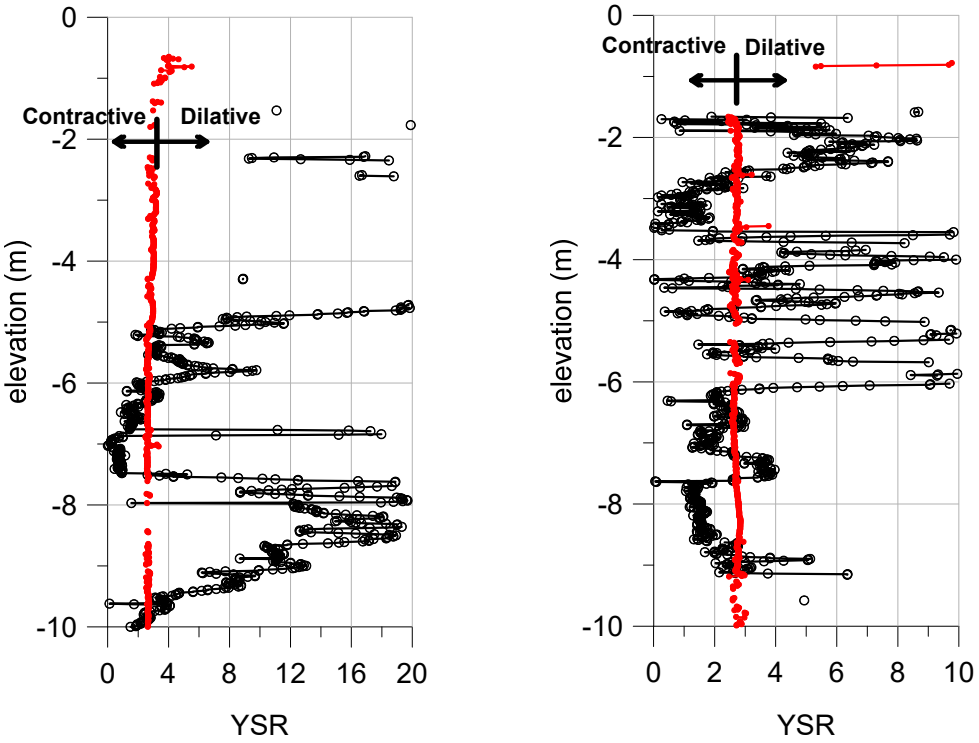

Figure 3.39. Application of Mayne (2019) criterion: YSR_{CSL} (red) and YSR_{CPTU} (black), from (a) 6a8 and (b) 6a12, Phase 1.

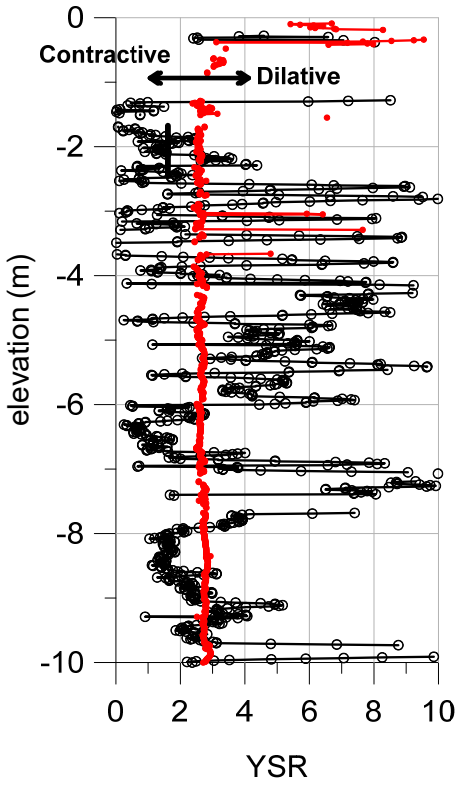

Figure 3.40. Application of Mayne (2019) criterion: YSR_{CSL} (red) and YSR_{CPTU} (black), from 6a14, Phase 1.

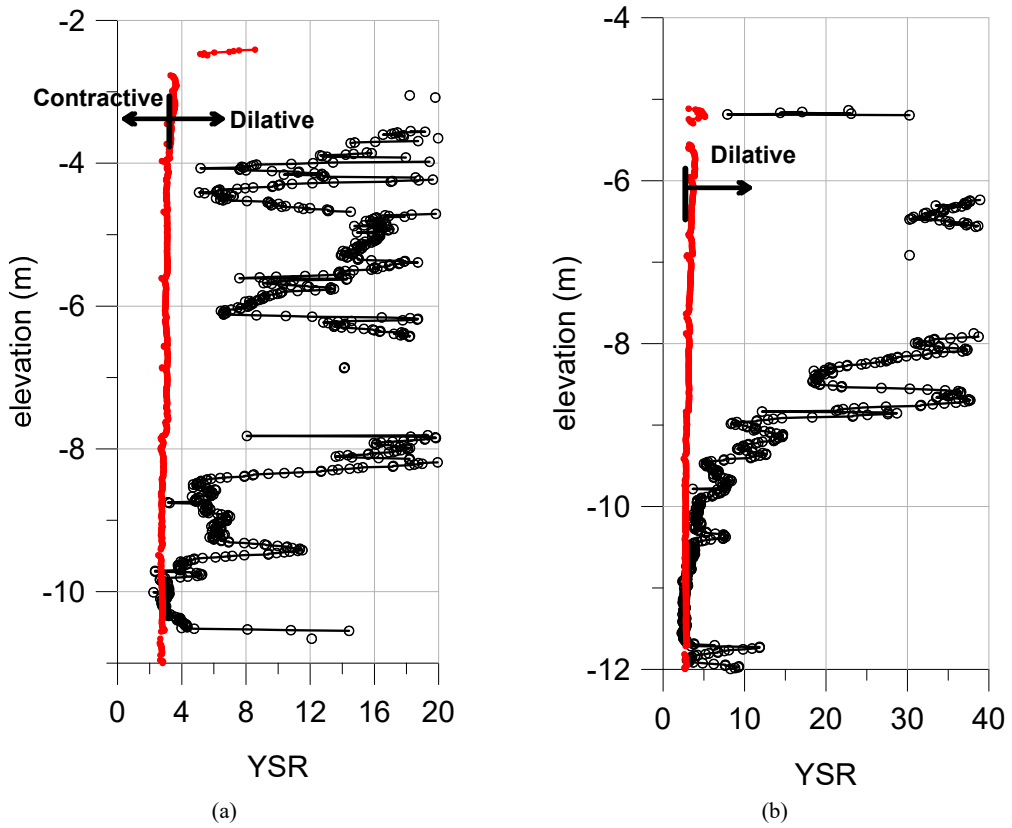

Figure 3.41. Application of Mayne (2019) criterion: YSR_{CSL} (red) and YSR_{CPTU} (black), from (a) 3b11 and (b) 3b12, Phase 2.

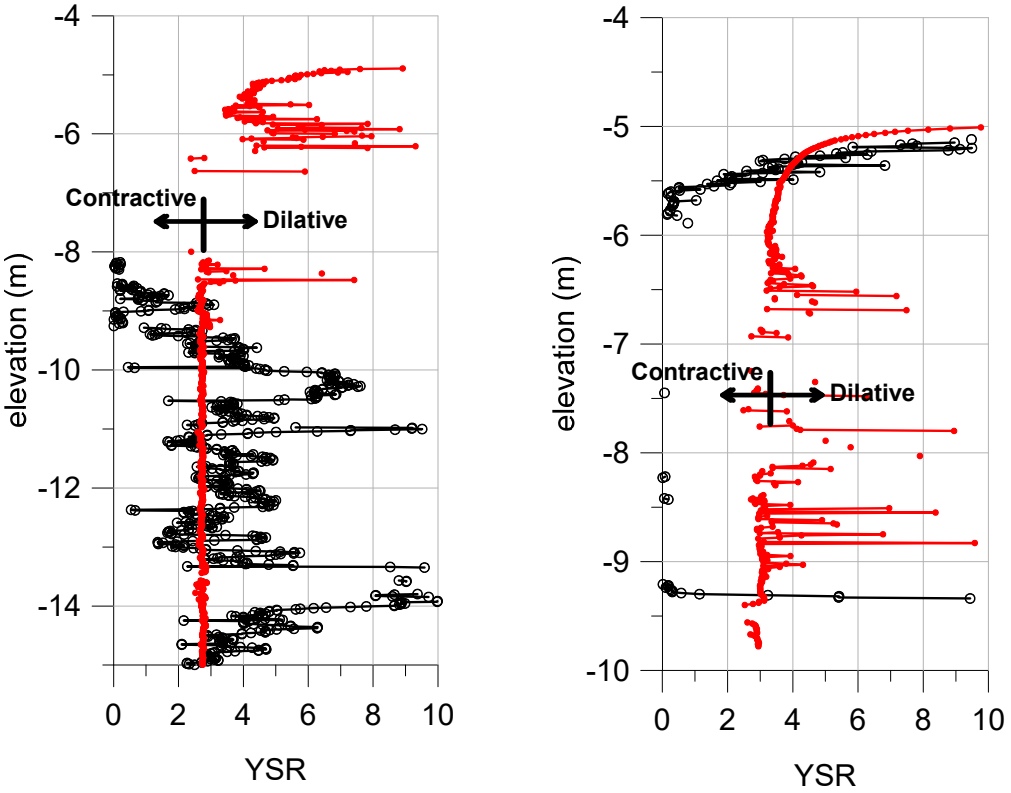

Figure 3.42. Application of Mayne (2019) criterion: YSR_{CSL} (red) and YSR_{CPTU} (black), from (a) 7b8 and (b) 7b12, Phase 2.

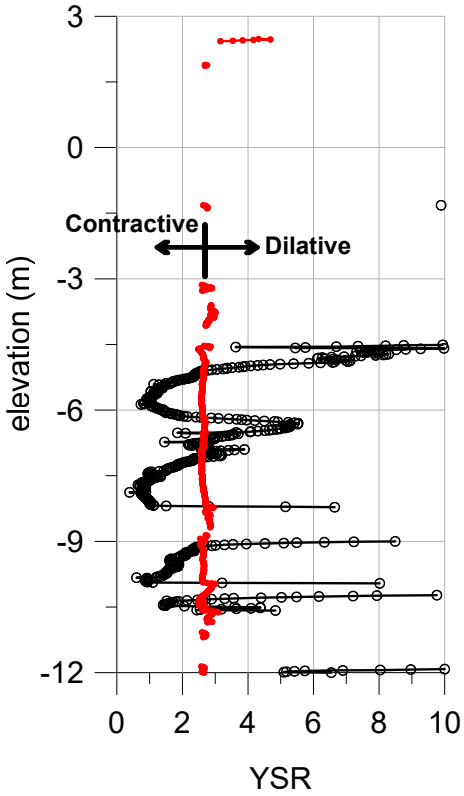

Figure 3.43. Application of Mayne (2019) criterion: YSR_{CSL} (red) and YSR_{CPTU} (black), from 7b13, Phase 2.

3.5.5. Criteria comparison

For comparison, the results of applying the Plewes et al. (1992), Robertson (2016) and Mayne (2019) criteria results are plotted together. Note that the profile of Robertson (2016) criteria is plotted in a Q_{tn} plot, with the boundary between dilative (D) and contractive (C) for CD=70. Thus, all three approaches indicate soils prone to flow liquefaction if: (i) $\psi > -0.05$, (ii) $Q_{tn} < Q_{tn}$ for CD=70 and (iii) $YSR_{CPTU} < YSR_{CSL}$ for the Plewes, Robertson and Mayne criteria respectively.

From Phase 1:

- 6a8: Criteria of Plewes and Mayne delimited the same region (-6 to -7.5 m) as a contractive soil. In contrast, the deeper 6 meters from this profile are defined as contractive soil by Robertson criteria.

- 6a12: Again, Plewes and Mayne criteria are roughly coincident, but in this case Robertson approach indicate contractive soils essentially over the full depth

- 6a14: Although Plewes and Mayne criteria coincide on the general prediction of contractive behaviour, more contractive points from the Mayne criterion are obtained than for the Plewes criterion. As previously, the results of Robertson criterion tend to indicate a large number of contractive points in the profile.

From Phase 2

- 3b11: The values obtain with the Plewes method do not coincide with those from the Mayne criterion. However a small zone around z = -10 m is contractive. In contrast, Robertson criterion indicates contractive soils essentially over the full depth.

- 3b12: In this case, the Plewes criterion provides contractive behaviour in zones that Mayne does not. Mayne criterion only defined as contractive soils the lower part of the fill. Unlike a number of other cases, Robertson criterion is quite similar to Plewes criterion.

- 7b8: Plewes and Robertson criteria coincide only for the last meters of the profile. The top part of the soil exhibited friction ratios (F_r) less than 10. Plewes criterion defines this region as dilative soil, in contrast Robertson as a contractive. Top part is identified as dilative by the Mayne criterion and the rest of the profile is placed between contractive and dilative region.

- 7b12: The results of this hydraulic fill profile are different for each criterion. Plewes criterion indicates that over the full depth is contractive. Robertson give values for the lower part of the profile that indicate dilative soil, as Plewes and Mayne (YSR>10) also do. Results of Robertson are not present for full depth because upper part have F_r <10. In contrast, Mayne criterion does not provide values over 3 meters because the data are outside the criterion

scope. The top part of the profile, however, is classified as a transition zone from dilative to contractive.

- 7b13: In this case, the results of the different criteria match quite well. Although Mayne criterion do not show values in the upper part of the profile, the estimated values of YSR are higher than 10.

In summary, there are differences in the results obtained applying the various criteria to the same CPTu data. This is not surprising given the basic empirical bases on which they are founded. It appears that the Robertson criterion is more conservative than those of Plewes et al. and Mayne. In all cases, however, they all indicate large zones of hydraulic fill that can potentially undergo flow liquefaction if a triggering action occurs. It should be noted that the flow liquefaction potential is largely attributed to fine grained soils according to F-Q classification charts (Figure 3.44 to Figure 3.51).

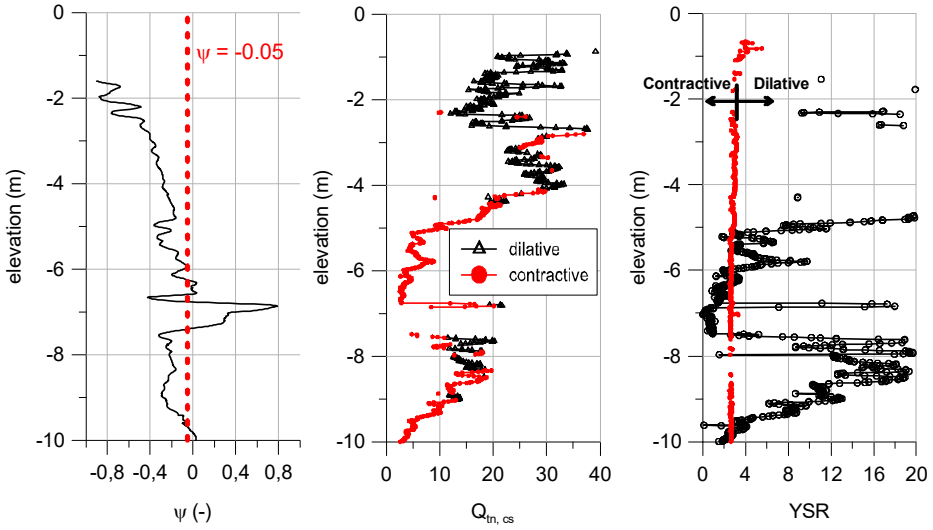

Figure 3.44. (a) Plewes criterion, (b) Robertson criterion and (c) Mayne criterion for CPTu 6a8, Phase 1.

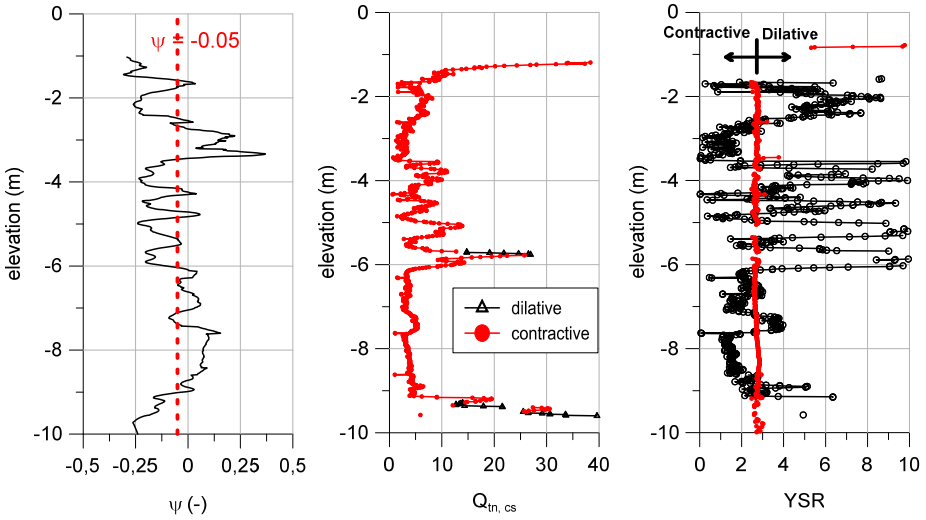

Figure 3.45. (a) Plewes criterion, (b) Robertson criterion and (c) Mayne criterion for CPTu 6a12, Phase 1.

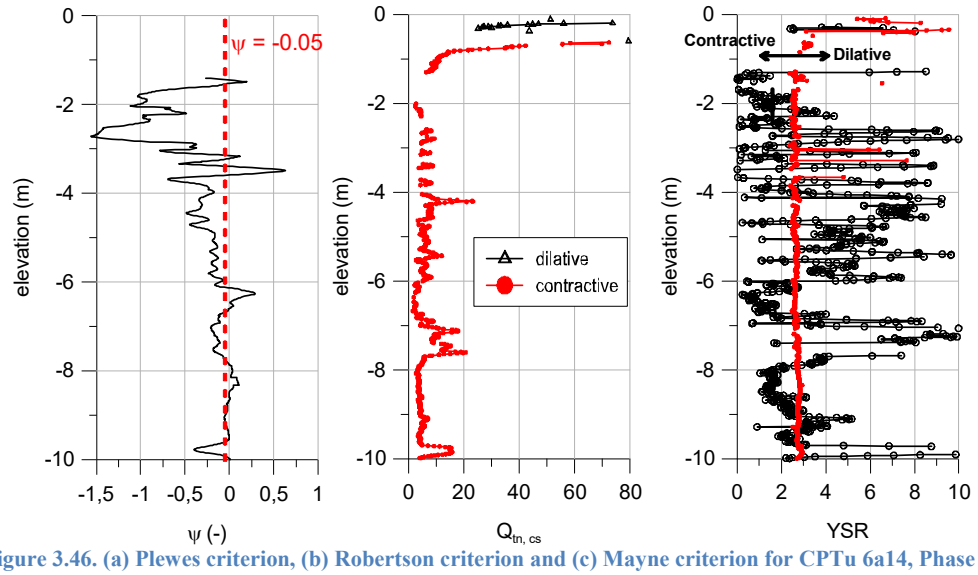

Figure 3.46. (a) Plewes criterion, (b) Robertson criterion and (c) Mayne criterion for CPTu 6a14, Phase 1.

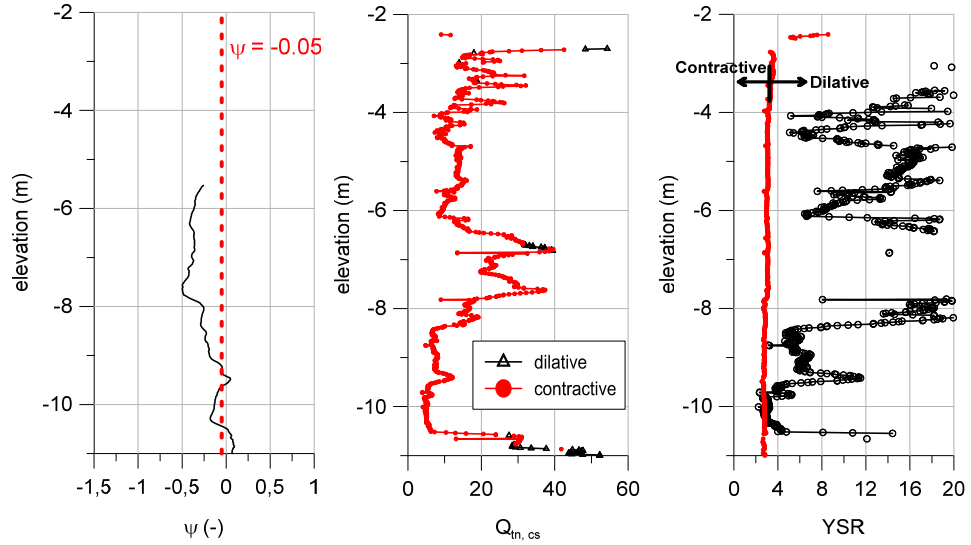

Figure 3.47. (a) Plewes criterion, (b) Robertson criterion and (c) Mayne criterion for CPTu 3b11, Phase 2.

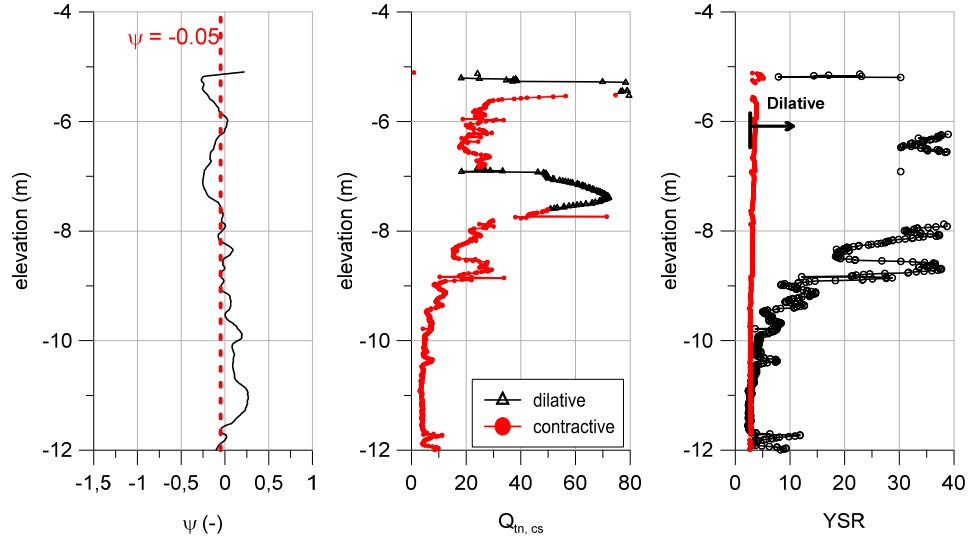

Figure 3.48. (a) Plewes criterion, (b) Robertson criterion and (c) Mayne criterion for CPTu 3b12, Phase 2.

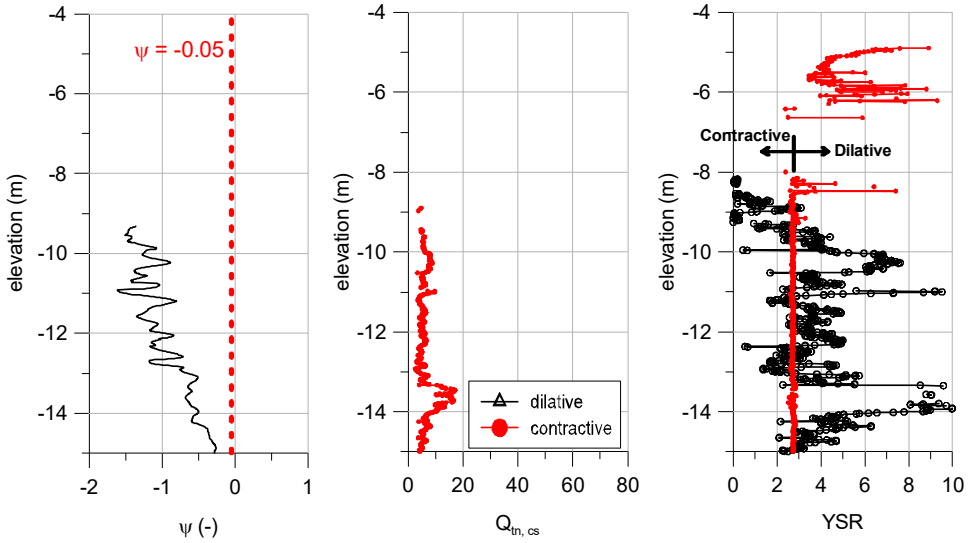

Figure 3.49. (a) Plewes criterion, (b) Robertson criterion and (c) Mayne criterion for CPTu 7b8, Phase 2.

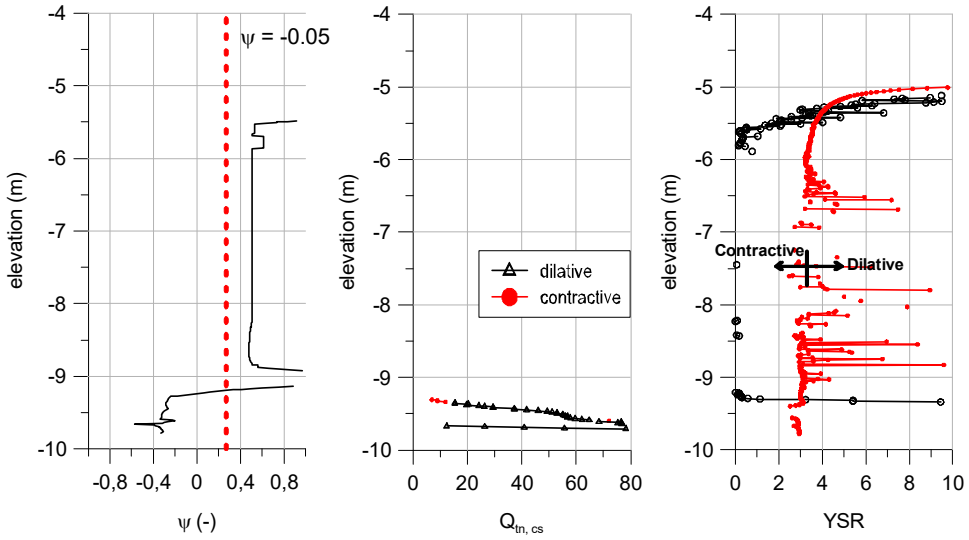

Figure 3.50. (a) Plewes criterion, (b) Robertson criterion and (c) Mayne criterion for CPTu 7b12, Phase 2.

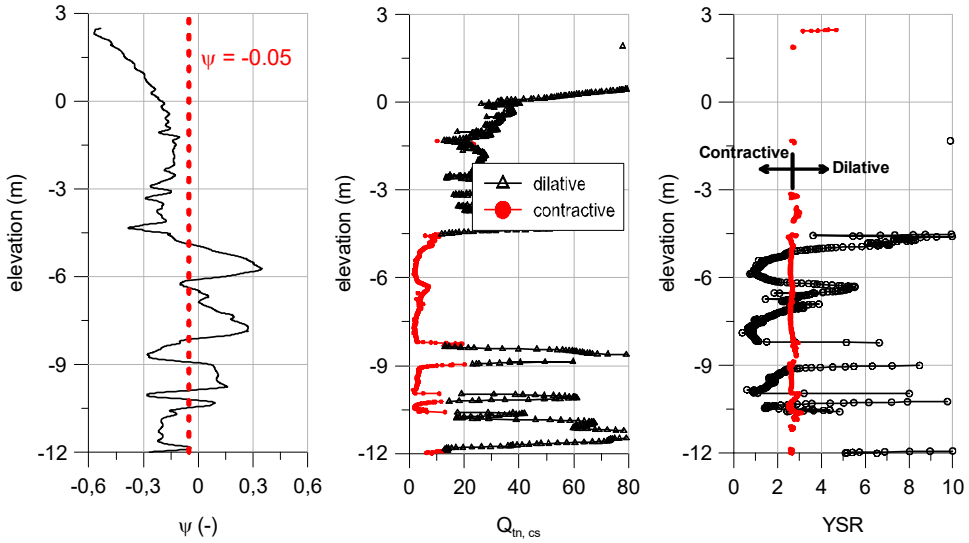

Figure 3.51. (a) Plewes criterion, (b) Robertson criterion and (c) Mayne criterion for CPTu 7b13, Phase 2.

3.6. *A constitutive model for flow liquefaction*

A substantial number of constitutive models exist that are capable of simulating undrained softening and therefore flow liquefaction (e.g. Jefferies 1993, Manzari and Dafalias 1997, Yu 1998, Pestana and Whittle 1999, Gajo and Wood 1999, Imam et al. 2005). Usually these models are isotropic, however, the MIT-S1 model can also represent anisotropic behaviour (Pestana et al., 2002). In this PhD thesis, the CASM model (Yu, 1998) will be used in a modified form to reproduce the hydraulic fill behaviour, including the phenomenon of flow liquefaction.

The CASM model has a number of advantages:

- It incorporates the state parameter concept in the model formulation.
- It is consistent with the critical state concept.
- It allows modelling a wide range of behaviour from strong undrained softening to ductile or dilatant material.
- It is relatively simple, using only a single yield surface.
- It assumes non-associated plasticity so that instability phenomena can be adequately reproduced.
- Classical Cam-Clay models result if appropriate parameters are selected.

The unified state parameter model for clay and sand (CASM) is based on a reinterpretation of the Cam-Clay model involving the state parameter (ξ), Yu (1998). In Figure 1, the definition of ξ is presented as the difference between the current specific volume and the specific volume on the critical state line (CSL) for identical effective mean stress (Figure 3.52).

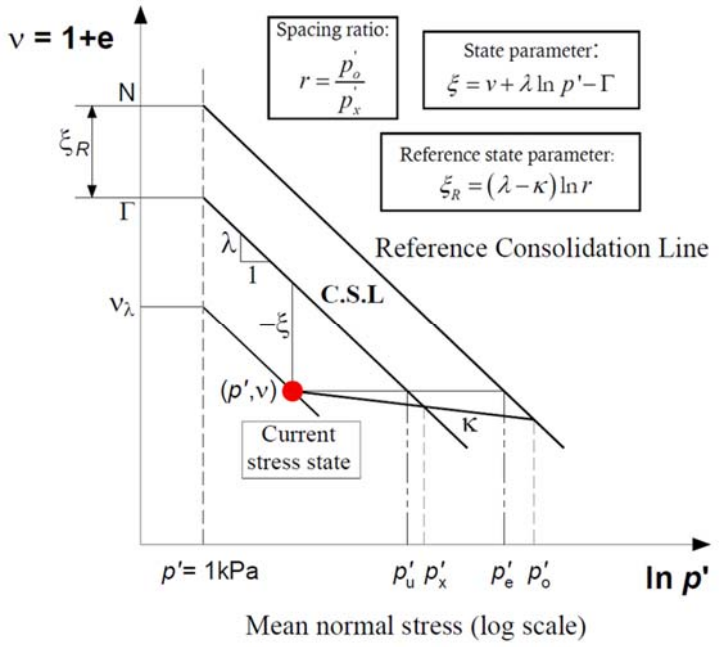

Figure 3.52. Definitions of state parameter, critical state constants, and reference state parameter (Yu, 1998).

At critical state, the following conditions prevail:

$$\frac{\partial p'}{\partial \varepsilon_q} = \frac{\partial q}{\partial \varepsilon_q} = \frac{\partial v}{\partial \varepsilon_q} = 0 \qquad [21]$$

where: p' is the effective mean stress, q is the deviatoric stress ($\sigma_1 - \sigma_3$ for triaxial conditions), v is the specific volume (v = e + 1), e is the void ratio and ε_q is the deviatoric strain.

Under drained conditions if a positive value of ξ exists, a volume contraction is needed to reach the CSL. Similarly, under undrained conditions, CSL is reached after a pore water pressure increase (Figure 3.6).

The critical state coincides with the peak deviatoric stress in Cam-Clay model -thus in CASM-, for undrained loading on the wet side of the yield surface. This behaviour is valid for many normally consolidated clays. However, in other cases, the increase of water pressures is still able to continue after peak strength. Thus, it can lead to a reduction on strength that continues until reaching the critical state (strength at CS, Figure 3.53).

A general stress ratio-state parameter relationship to define the state boundary surface of soils is assumed by the CASM constitutive model to be used for both clay and sand. By assuming a non-associated flow rule, the model can reach critical state conditions beyond the peak strength and, therefore, flow liquefaction can be correctly simulated by the CASM model.

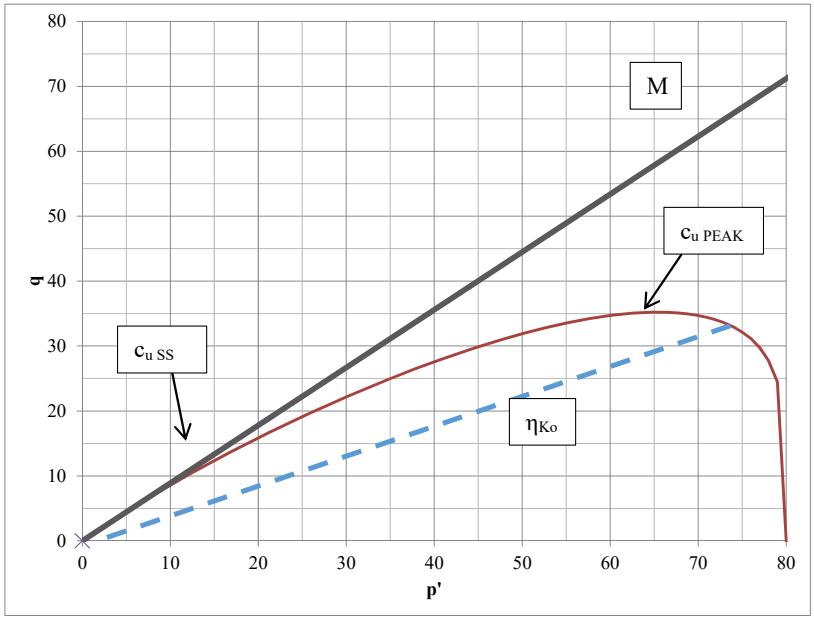

Figure 3.53. Undrained softening, effective stress path.

The rate-independent version of the implementation is now described. In the following, the soil mechanics convention (compressive stresses and strains are positive) is adopted and stresses refer

always to effective stresses. The stress integration algorithm and the viscoplastic extension are described in Mánica (2020) and will not be discussed here.

3.6.1. Elastic behaviour

The model assumes an isotropic nonlinear elasticity in the yield surface, thus a linear behaviour is obtained in the $\upsilon - \ln p$ space, where the slope is κ, a soil parameter. In equation [22], the bulk resulting modulus (K) expression is presented.

$$K = \frac{\nu \cdot p}{\kappa} \quad [22]$$

In this case, a constant Poisson's ratio (υ) is assumed to define the full elastic stiffness matrix.

3.6.2. Yield surface

In terms of the state parameter, an expression for the yield function of the CASM constitutive model is given by

$$f = \left(\frac{\sqrt{3}J}{M_\theta p}\right)^n + \frac{\xi}{\xi_R} - 1 \quad [23]$$

where J is the second invariant of the deviatoric stress tensor, M_θ is the slope of the CSL in the q – p' plane that depends on the Lode's angle θ, n is a parameter that controls the shape of the yield function, and ξ_R is the reference state parameter controlling the separation between the CSL and the reference consolidation line (Fig. 1).

The yield function can also be represented in terms of the spacing ratio r, defined also in Figure 3.52,. The spacing ratio r defines the separation between the CSL and the reference consolidation line. In that case, the yield function becomes:

$$f = \left(\frac{\sqrt{3}J}{M_\theta p}\right)^n + \frac{1}{\ln r}\, ln\frac{p}{p_0} \quad [24]$$

The shape of the yield function is influenced by n; the effect is presented in Figure 3.54. As mentioned above, the critical state may not coincide with the maximum of the function (peak strength), thus undrained softening behaviour can be simulated depending on the selected parameters.

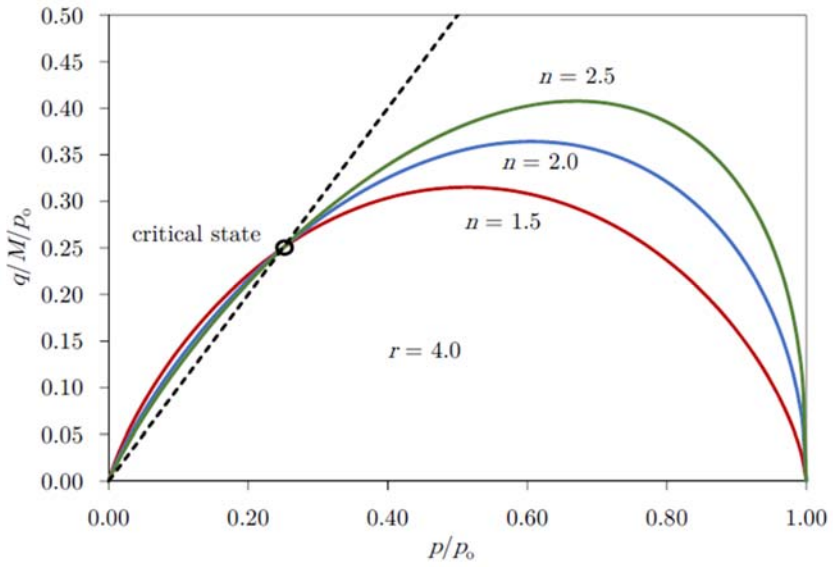

Figure 3.54. Normalised state boundary surfaces for different values of n, Manica (2020).

It is important to note that the yield function (or steady state parameter) can be modified and adapted to impose the desired degree of undrained softening, Figure 3.55. However, the soil sensitivity is mainly controlled by r, the spacing ratio parameter (Figure 3.52) as depicted in Figure 3.56.

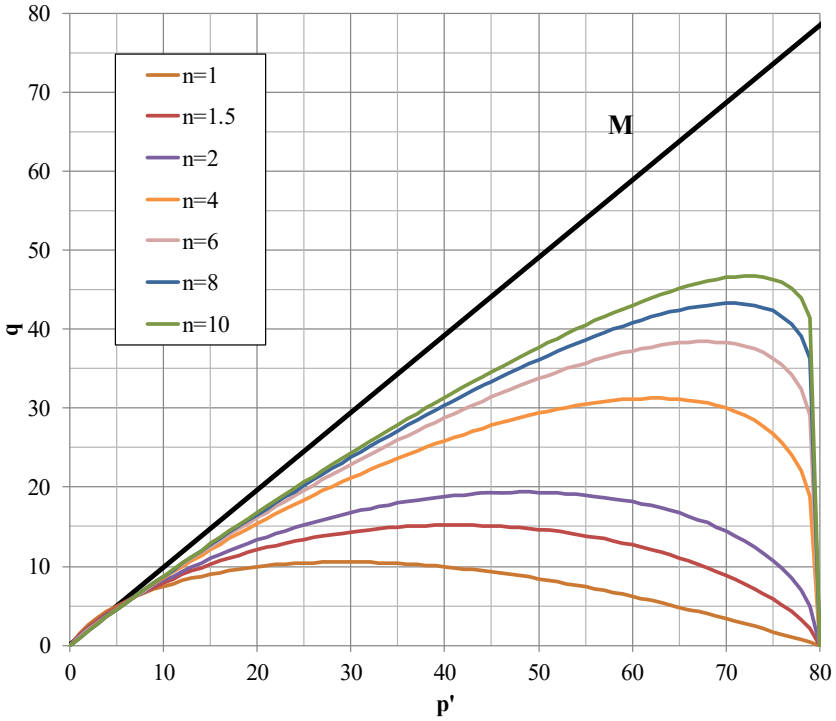

Figure 3.55. CASM sensibility of steady state parameter (n), r=12.

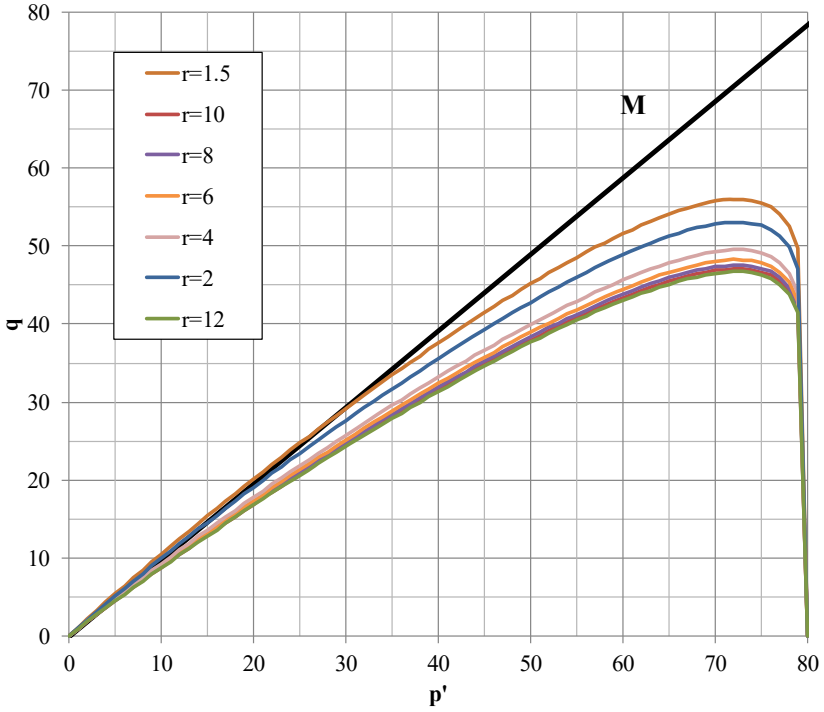

Figure 3.56. CASM sensibility of spacing ratio parameter (r), n=10.

In the original CASM model, the slope of the CSL was assumed constant and, therefore, it traces a circle in the deviatoric plane. M_θ is expressed as function of the Lode's angle, using the relationship proposed by Sheng et al. (2000), [25].

$$M_\theta = M\left(\frac{2\alpha^4}{1+\alpha^4+(1-\alpha^4)\sin 3\theta}\right)^{\frac{1}{4}} \quad [25]$$

where M is the slope of the CSL in the p' - q plane under triaxial compression and α is a parameter that modifies the function shape in the deviatoric plane. It results in a different value of M between triaxial compression and extension, i.e. between θ = -30º and θ = 30º, respectively .

Moreover, M and α can be selected to coincide with the Mohr-Coulomb envelope for triaxial compression and extension loading conditions (Gonzalez, 2011) [26] and [27].

$$M = \frac{6\sin\phi_{cs}}{3-\sin\phi_{cs}} \quad [26]$$

$$\alpha = \frac{3-\sin\phi_{cs}}{3+\sin\phi_{cs}} \quad [27]$$

where ϕ_{cs} is the friction angle at critical state for triaxial compression.

The adopted function in the deviatoric plane is depicted in Figure 3.57, along with the Mohr-Coulomb envelope and an envelope with α = 1. In the latter case, a constant value of M_θ is obtained and, therefore, a circular shape is recovered.

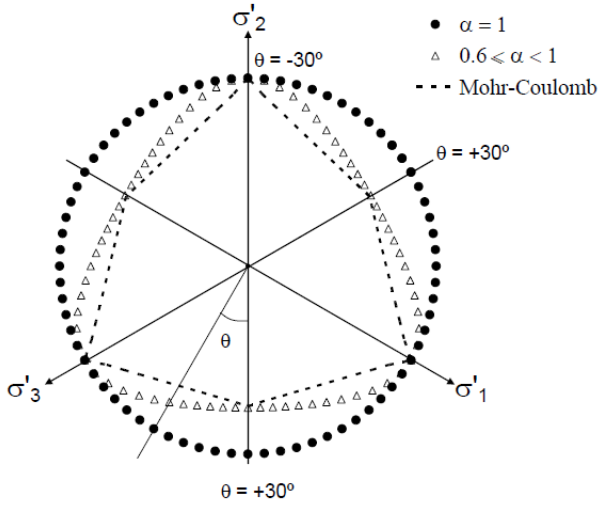

Figure 3.57. Shape of the yield function in the deviatoric plane, Gonzalez (2011).

3.6.3. Plastic potential

The plastic potential was derived by integrating the stress-dilatancy relationship of Rowe (1962) in the original CASM formulation (Yu, 1998). However, Rowe's (1962) stress-dilatancy relation is accurate for high stress ratios, but it is not particularly realistic for stress paths with low stress ratios such isotropic consolidation and 1D consolidation, Yu (2006). He suggested an alternative potential function, similar in shape to the CASM yield function, but resulting in null plastic volumetric strains at reaching critical state [28].

$$\frac{d\varepsilon_v^p}{d\varepsilon_q^p} = \frac{{M_\theta}^n - \eta^n}{m\eta^{n-1}} \qquad [28]$$

where: ε_v^p is the volumetric plastic strains, ε_q^p is the shear plastic strains, n is a constant defined previously and m may be considered a material constant independent of n and r. m should be selected to ensure that flow rule predicts zero lateral strain for stress states corresponding to Jaky's (1948) K_0 condition:

$$K_0 = 1 - \sin\varphi_{cs} = (6 - 2M) / (6 + M) \qquad [29]$$

In p - q' plane, K_0 condition induces the following expression in stress ratio:

$$\eta_{K_0} = \frac{3\cdot(1-K_0)}{1+2K_0} = \frac{3\cdot M}{6-M} \qquad [30]$$

Otherwise, assuming lateral strain (ε_3) as zero:

$$\frac{d\varepsilon_v^p + d\varepsilon_v^e}{d\varepsilon_q^p + d\varepsilon_q^e} = \frac{d\varepsilon_1}{\frac{2}{3}d\varepsilon_1} = \frac{3}{2} \qquad [31]$$

Taking into account a negligible elastic shear strains, equation [31] gives:

$$\frac{d\varepsilon_v^p}{d\varepsilon_q^p} = \frac{3}{2}\Lambda \qquad [32]$$

where: $\Lambda = 1 - \frac{\kappa}{\lambda}$.

The soil behaviour during hydraulic fill deposit will follow a K_0 path during consolidation. The CASM implementation of Gonzalez (2011) defines an alternative plastic potential [33] that leads the following stress-dilatancy relation [34] slightly different from proposed by Yu (2006) equation [28].

$$g = \left(\frac{\beta\sqrt{3J}}{M_\theta p'}\right)^n + \frac{1}{\ln r} ln \frac{p'}{P_0'} = 0 \qquad [33]$$

$$\frac{d\varepsilon_v^p}{d\varepsilon_q^p} = \frac{{M_\theta}^n - m\eta^n}{m\eta^{n-1}} \qquad [34]$$

where ε_v^p is the volumetric plastic strains, ε_q^p is the shear plastic strains and $m=n\ ln\ r\ (\beta)^n$. If β is 1 then the flow rule is associated and $m=n\ ln\ r$.

The parameter to adjust the K_0 is β when eq [34] is zero for $M_\theta=\eta$. Therefore [35]:

$$\beta = \left(\frac{1}{n \cdot \ln r}\right)^{1/n} \qquad [35]$$

Gonzalez (2011) assumption involves that r and n control the anisotropic stress path during consolidation. This proposal give a K_0 for a set of parameters that do not fulfil with stress-dilatancy relation [31] because stress-dilatancy relation equal to 2/3 corresponds with η=0.85 (Figure 3.58). The correct η would be 0.59 which is consistent with Jaky's equation.

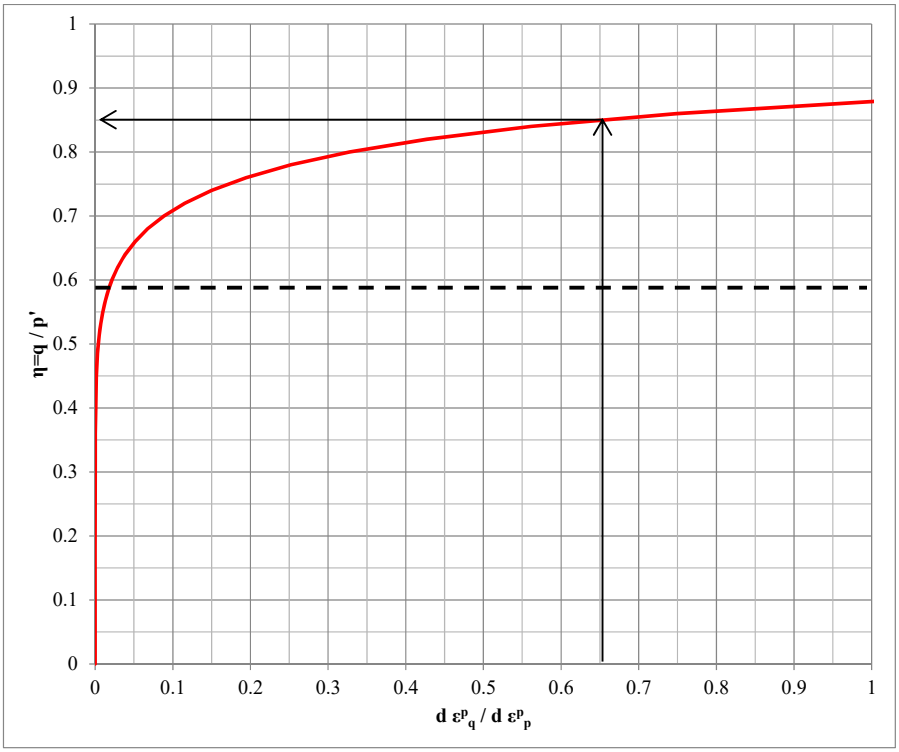

Figure 3.58. Stress-dilatancy relation by stress ratio with prescribed CASM parameters.

Therefore, in this PhD thesis, a modification of the constitutive model has been performed changing the plastic potential function to:

$$\frac{d\varepsilon_v^p}{d\varepsilon_q^p} = \frac{w(M_\theta{}^n - m\eta^n)}{m\eta^{n-1}} \quad [36]$$

The new parameter w helps to obtain a relation between plastic shear strains and plastic volumetric strains of 2/3 for a specified value of K_0. The effect of w parameter can be seen in Figure 3.59 where η_{Ko} corresponds with $d\varepsilon_v^p / d\varepsilon_q^p = 2/3$.

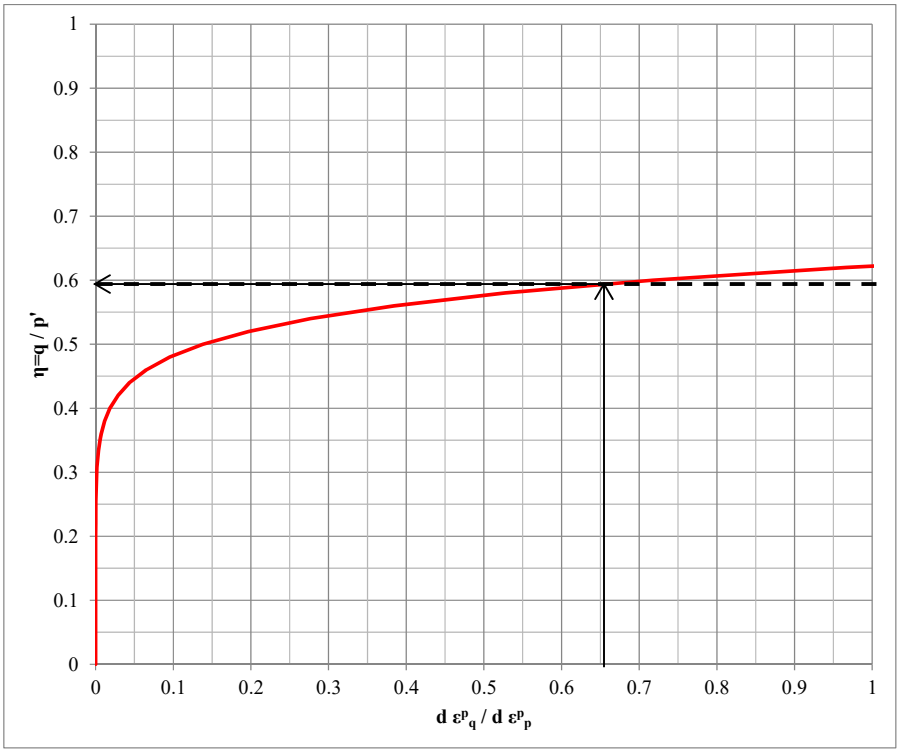

Figure 3.59. Stress-dilatancy relation by stress ratio with new parameter *w* and the prescribed CASM parameters.

CASM model improvement parameters should simulate properly undrained shear strength, post-liquefaction undrained shear strength, strain softening and K_0. In Chapter 4 where Prat quay failure is simulated, the parameters calibration will be presented.

3.6.4. Hardening rule

The CASM constitutive model uses the same isotropic volumetric plastic strain hardening rule than the modified Cam-Clay model [37].

$$\frac{\partial p_0}{\partial \varepsilon_v^p} = \frac{\nu p_0}{\lambda - \kappa} \quad [37]$$

where $\varepsilon^p{}_v$ is the volumetric plastic strain and λ is the slope of the CSL and reference consolidation line in the $\upsilon - \ln p$.

3.7. Summary

The general description of the flow liquefaction phenomenon is prompted by the clear evidence of its occurrence described in Chapter 2. The flow liquefaction susceptibility of the hydraulic fill has been verified using a number of proposed criteria. It appears that the Robertson criterion is more conservative than those of Plewes et al. and Mayne that identify a lower percentage of liquefaction-susceptible soil. It is worth mentioning that the flow liquefaction potential was largely attributed to fine grained soils according to F-Q classification charts. In addition, the liquefied undrained strength ($c_{u\,SS}$) and the $c_{u\,peak}$ for the hydraulic fill have been estimated. All these results are consistent with the tests results of Chapter 2, were brittle behaviour was detected.

In addition, the unified state parameter model for clay and sand model (CASM) has been selected for the flow liquefaction simulation of the hydraulic fill. The parameters of CASM can be calibrated to obtain the specific brittle index derived from the values of $c_{u\,SS}$ and $c_{u\,peak}$. A modification of the constitutive law (Gonzalez, 2011) to obtain a more realistic stress path for K_0-consolidation has been incorporated into the formulation,

Using the developments presented in this Chapter, it is now possible to undertake the simulation of the Prat quay Phase 1 and Phase 2, as described in the following Chapter 4 and Chapter 5 respectively.

3.8. References

Agaiby, S.S., Mayne, P.W. 2018. Interpretation of piezocone penetration and dissipation tests in sensitive Leda clay at Gloucester test site. Canadian Geot. J. 55(12): 1781-1794.

Alonso, E. E., Gens, A. 2006. Aznalcóllar dam failure. Part 1: Field observations and material properties. Géotechnique 56, No. 3, 165–183.

Andresen, A., Bjerrum, L. 1968. Slides in subaqueous slopes in loose sand and silt. Norwegian Geotechnical Institute, Publication 81, pp. 1–9.

Been, K., Jefferies, M. G. 1985. A state parameter for sands. Géotechnique 35, 99–112.

Been, K., Conlin, B.H., Crooks, J.H.A., Fitzpatrick, S.W., Jefferies, M.G., Rogers, B.T., Shinde, S. 1987. Back analysis of the Nerlerk berm liquefaction slides: Discussion. Canadian Geotechnical Journal, 24: 170-179.

Been, K., Jefferies, M.G., Hachey, J. 1991. The critical state of sands, Géotechnique 41, 365–381.

Bishop, A.W., Hutchinson, J.N., Penman, A.D.M., Evans, H.E. 1969. Geotechnical investigation into the causes and circumstances of the disaster of 21st October 1966. A selection of Technical Reports submitted to Aberfan Tribunal, Welsh Office, Her Majesty's Stationery Office (HMSO), London.

Bishop, A. W. 1973. The stability of tips and spoil heaps, Quaterly Journal of Engineering Geology 6, 335–376.

Bjerrum, L. 1971. Subaqueous slope failures in Norwegian fjords. In: Proceedings of the First International Conference on Port and Ocean Engineering Under Arctic Conditions, 1:24–47.

Bray, J. D., Sancio, R. B., Riemer, M. F., Durgunoglu, T. 2004. Liquefaction susceptibility of fine-grained soils. 11th Int. Conf. on Soil Dynamics and Earthquake Engineering and 3rd Int. Conf. on Earthquake Geotechnical Engineering, D. Doolin et al., eds., Stallion Press, pp 655-662.

Carrera, A., Coop, M.R., Lancellotta, R. 2011. The influence of grading on the mechanical behaviour of Stava tailings. Géotechnique 61, 935–946.

Casagrande, A. 1936. Characteristics of cohesionless soils affecting the stability of earth fills. J. Boston Society of Civil Engineers 23, 257–276.

Casagrande, A. 1965. The role of the 'calculated risk' in earthwork and foundation engineering. Soil Mech. Found. Engrg. Div., ASCE, 91(4) 1-4.

Casagrande, A. 1975. Liquefaction and cyclic deformation of sands: A critical review. Proceedings of the Fifth Pan-American Conference on Soil Mechanics and Foundation Engineering 5, 79-133. Buenos Aires, Argentina.

Castro, G. 1969. Liquefaction of sands. Harvard Soil Mechanics Series, No. 81. Cambridge, MA: Harvard University.

Castro, G., Keller, T.O., Boynton, S.S. 1989. Re-evaluation of the Lower San Fernando Dam: Report 1, an investigation of the February 9, 1971 slide. Army Corps of Engineers Contract Report GL-89-2, Volumes 1 and 2. U.S. Army Corps of Engineers Waterways Experiment Station, Vicksburg, Mississippi.

Castro, G., Seed, R.B., Keller, T.O., Seed, H.B. 1992. Steadystate strength analysis of Lower San Fernando Dam slide. Journal of Geotechnical Engineering, ASCE 118(3) 406-427.

Chandler R.J., Tosatti, G. 1995. The Stava tailings dams failure, Italy, July 1985. Proceedings of the Institution of Civil Engineers-Geotechnical Engineering 113, 67-79.

Chillarige, A.V., Robertson, P.K., Morgenstern, N.R., Christian, H.A. 1997a. Evaluation of the in situ state of Fraser River sand. Canadian Geotechnical Journal, 34: 510-519.

Chillarige, A.V., Morgenstem, N.R., Robertson, P.K., Christian, H.A. 1997b. Seabed instability due to flow liquefaction in the Fraser River delta. Canadian Geotechnical Journal, 34:520-533.

Christian, H.A., D.J., Robertson, P.K., Courtney, R.C. 1997. Site investigation to evaluate flow liquefaction slides at Sand Heads, Fraser River delta. Canadian Geotechnical Journal, 34: 384-397.

Davies, M., McRoberts, E., Martin, T. 2002. Static liquefaction of tailings – Fundamentals and case histories. Tailings Dams 2002. ASDSO/USCOLD, Las Vegas, Nevada.

de Alba, P., Seed, H.B., Retamal, E., Seed, R.B. 1987. Residual strength of sand from dam failures in the Chilean earthquake of March 3, 1985. Earthquake Engineering Research Center Report No. UCB/EERC-87-11, University of California, Berkeley, CA.

Dobry, R., Alvarez, L. 1967. Seismic failures of Chilean tailings dams. Journal of the Soil Mechanics and Foundations Division 93 (1967) 237-260.

Ekstrom, A., Olofsson, T. 1985. Water and frost – stability risks for embankments of fine-grained soils. In Proceedings of the Symposium on Failures in Earthworks, Institution of Civil Engineers, London, 6-7 March, Vol. 1, pp. 155-166.

Fourie, A.B., Blight, G.E., Papageorgiou, G. 2001. Static liquefaction as a possible explanation for the Merriespruit tailings dam failure. Canadian Geotechnical Journal 38, 707–719.

Fourie, A.B., Tshabalala, L. 2005. Initiation of static liquefaction and the role of K0 consolidation. Canadian Geotechnical Journal 42, 892–906.

Gajo, A., Wood, D. 1999. Severn-Trent sand, a kinematic hardening constitutive model: The q-p formulation. Géotechnique 49, 595- 614.

Gens, A. 1982. Stress–strain and strength of a low plasticity clay. PhD thesis. Imperial College, London.

Gens, A. 2019. Hydraulic fills with special focus on liquefaction. Proceedings of the XVII ECSMGE-2019 Geotechnical Engineering foundation of the future ISBN 978-9935-9436-1-3.

González, N. A. 2011. Development of a family of constitutive models for geotechnical applications. PhD thesis, Universitat Politècnica de Catalunya, Barcelona, Spain.

Jaky, J. 1948. Pressure in soils. 2nd ICSMFE, London, Vol 1, pp 103-107.

Jefferies, M.G. 1993. Nor-Sand: a simple critical state model for sand, Géotechnique 43, 91–103.

Jefferies, M., Been, K. 2006. Soil Liquefaction. A critical state approach. Taylor & Francis Book.

Hazen, A. 1918. A study of the slip in the Calaveras Dam. Engineering News-Record, 81(26): 1158-1164.

Hazen, A., Metcalf, L. 1918. Middle section of upstream side of Calaveras Dam slips into reservoir. Engineering News-Record, 80(14): 679-681.

Hicks, M.A., Boughrarou, R. 1998. Finite element analysis of the Nerlerk underwater berm failures. Géotechnique, 48(2): 169-185.

Houlsby, G.T., Teh, C.I. 1988. Analysis of the piezocone in clay. Penetration Testing 1988, Vol. 2, Balkema, Rotterdam: 777–783.

Hryciw, R.O., Vitton, S., Thomann, T.G. 1990. Liquefaction and flow failure during seismic exploration. Journal of Geotechnical Engineering, ASCE, 116(12): 1881-1899.

Imam, S.M.R., Morgenstern, N.R., Robertson, P.K., Chan D.H. 2005. A critical-state constitutive model for liquefiable sand. Canadian Geotechnical Journal 42, 830-855.

Ishihara, K., Koga, Y. 1981. Case studies of liquefaction in the 1964 Niigata earthquake. Soils Found., 21(3), 35-52.

Ishihara, K., Yasuda, S., Yoshida, Y. 1990. Liquefaction-induced flow failure of embankments and residual strength of silty sands. Soils and Foundations, 30(3): 69-80.

Ishihara, K. 1993. Liquefaction and flow failure during earthquakes, Géotechnique 43, 351–451.

Kerwin, S., Stone, J. 1997. Liquefaction failure and remediation: King Harbor Redondo Beach, California. ASCE Journal of Geotechnical and Geoenvironmental Engineering 123 (8), 760 – 769.

Konrad, J.M. 1991. Toe Nerlerk berm case history: sorne consideration for the design of hydraulic sand fills. Canadian Geotechnical Journal, 28: 601--612.

Konrad, J.M., Watts, B.O. 1995. Undrained shear strength for liquefaction flow failure analysis. Canadian Geotechnical Journal, 32: 783-794.

Koppejan, A.W., van Wamelen B. M., Weinberg, L. J. H. 1948. Coastal flow slides in the Dutch Province of Zeeland. Procs. 2nd International Conference on Soil Mechanics and Foundation Engineering, Rotterdam, Holland, 5:89–96.

Ladd, C.C., Foott, R., Ishihara. K., Schlosser, F., Poulos, H.G. 1977. Stress-deformation and strength Characteristics. State-of-the-art-report, Proceedings 9th International Conference on Soil Mechanics and Foundation Engineering, Tokyo, 2, 421-94.

Lade, P.V. 1993. Initiation of static instability in the submarine Nerlerk berm. Canadian Geotechnical Journal 30, 895–904.

Lee, K. L. 1974. Earthquake induced permanent defonnations of embankments. Report to the National Science Foundation, Project GI 38521, School of Engineering and Applied Science, University of California, Los Angeles.

Leroueil, S., Tavenas, F., Lebihan, J. P. 1983. Proprietes caracteristiques des argiles de l'est du Canada," Canadian Geotech. Journal, Vol. 20(4), pp. 681-705.

Mánica, M.A. 2020. Implementation of the CASM constitutive model within the context of the project: Análisis numérico de la rotura de la Presa I de la Mina de Corrego de Feijao en Brumadinho April 17, 2020. CIMNE - DECA Internal Report.

Manzari, M.T., Dafalias, Y.F. 1997. A critical state two-surface plasticity model for sands. Géoteclmique 47, 255-272.

Marcuson, W.F., Ballard, R.F., Ledbetter, R.H. 1979. Liquefaction failure of tailings dams resulting from the N ear Izu Oshima earthquake, 14 and 15 January 1978. In Proceedings of the 6th Pan-American Conference on Soil Mechanics and Foundation Engineering, Lima Peru, Vol. 2, pp. 69-80.

Marcuson, W.F., Hynes, M.E., Franklin, A.G. 1990. Evaluation and use of residual strength in seismic safety analysis of embankments. Earthquake Spectra, 6(3): 529–572.

Martin, T.E., McRoberts, E.C. 1998. Some considerations in the stability analysis of upstream tailings dams 287-302. Tailings and Mine Waste ’99, Fort Collins, Colorado.

Mayne, P.W. 1991. Determination of OCR in clays by piezocone tests using cavity expansion and critical state concepts. Soils and Foundations 31 (2): 65-76.

Mayne, P.W. 2007. NCHRP Synthesis 368: Cone Penetration Testing, Transportation Research Board, Washington, DC: 118 p. www.trb.org.

Mayne, P.W. 2008. Piezocone profiling of clays for maritime site investigations. Geotechnics in Maritime Engineering, Vol. 1 (Proc. 11th Baltic Sea Geot. Conf., Gdansk), Polish Committee on Geotechnics: 333-350.

Mayne, P.W., Greig, J., Agaiby, S. 2018. Evaluating CPTu in sensitive Haney clay using a modified SCE-CSSM solution. Proc. GeoEdmonton, 71st Canadian Geot. Conf., Paper ID No. 279: www.cgs.ca.

Mayne, P.W., Sharp, J. 2019. CPT Approach to Evaluating Flow Liquefaction Using Yield Stress Ratio. Proceedings of Tailings and Mine Waste 2019. November 17–20, 2019, Vancouver, Canada. Published by the University of British Columbia, 2019.

Mayne, P.W. 2019. Analytical CPTu model for sensitive clay at Tiller-Flotten site, Norway. Proceedings of the XVII ECSMGE-2019 Geotechnical Engineering foundation of the future ISBN 978-9935-9436-1-3 © The authors and IGS: All rights reserved, 2019 doi: 10.32075/17ECSMGE-2019-0153.

Middlebrooks, T. A. 1942. Fort Peck slide. Transactions of the American Society of Civil Engineers, 107: 723–764.

Mishima, S., Kimura, H. 1970. Characteristics of landslides and embankrnent failures during the Tokachioki eaiihquake. Soils and Foundations, 10(2): 39-51.

Mittal, H.K., Hardy, R.M. 1977. Geotechnical aspects of a tar sand tailings dyke. In Proceedings of the Conference on Geotechnical Practice for Disposal of Solid Waste Materials, ASCE Specialty Conference of the Geotechnical Engineering Division, Vol. 1, pp. 327-347.

Miura, K., Yoshida, N., Nishimura, M., Wakamatsu, K. 1998. Stability analysis of the fill embankment damaged by recent two major earthquakes in Hokkaido, Japan. Geotech. Special Pub. 75, ASCE, 926-937.

Morgenstern, N. R., Vick, S. G., Watts, B. D.,Viotti, C. 2016. Fundão tailings dam review panel. Report on the immediate causes of the failure of the Fundão Dam. New York, NY, USA: Cleary Gottlieb Steen & Hamilton LLP.

Ohya, S., lwasaki, T., Wakamatsu, M. 1985. Comparative study of various penetration tests in ground that underwent liquefaction during the 1983 Nihon-Kai-Chubu and 1964 Niigata earthquakes. In Proceedings of the Workshop on ln-Situ Testing Methods for Evaluation of Soil Liquefaction Susceptibility, San Francisco, California, Vol. 1, pp. 56-88.

Okusa, S., Anma, S. 1980. Slope failures and tailings dam damage in the 1978 Izu-Ohshima-Kinkai earthquake. Engineering Geology, 16: 195-224.

Olson, S.M., Stark, T.D., Walton, W.H., Castro, G. 2000. 1907 Static liquefaction flow failure of the North Dike of Wachusett Dam. Journal of Geotechnical and Geoenvironmental Engineering, ASCE 126, 1184-1193.

Olson, S. M., Stark, T. D. 2002. Liquefied strength ratio from liquefaction flow failure case histories. Canadian Geotechnical Journal 39, 629–647.

Olson, S. M., Stark, T. D. (2003). Yield strength ratio and liquefaction analysis of slopes and embankments. J. Geotech. Geoenviron. Engng ASCE 129, No. 8, 727–737.

Pestana, J.M., Whittle, A.J. 1999. Formulation of a unified constitutive model for clays and sands, International Journal for Numerical and Analytical Methods in Geomechanics 23, 1215–1243.

Pestana, J.M., Whittle, A.J., Salvati, L. 2002. Evaluation of a constitutive model for clays and sands: Part I Sand behavior, International Journal for Numerical and Analytical Methods in Geomechanics 26, 1097–1121.

Plewes, H.D., O'Neil, G.D., McRoberts, E.C., Chan, W.K. 1989. Liquefaction considerations for Suncor tailings pond. In Proceedings of the Dam Safety Seminar, Edmonton, Alberta, Sept., Vol. 1, pp. 61-89.

Plewes, H.D., Davies, M.P., Jefferies, M.G., 1992. CPT based screening procedure for evaluating liquefaction susceptibility. In Proceedings of the 45th Canadian Geotechnical Conference, pp. 41-49.

Poulos, S.J. 1981. The steady state of deformation, Journal of the Geotechnical Engineering Division, ASCE 107, 553–562.

Robertson, P.K., Wride, C.E., 1998. Evaluating cyclic liquefaction potential using the cone penetration test. Canadian Geotechnical Journal, Ottawa, 35(3): 442-459.

Robertson, P. K. 2009. Interpretation of cone penetration tests - A unified approach. Can. Geotech. J., 46, 1337–1355.

Robertson, P.K. 2016. Cone penetration test (CPT)-based soil behaviour type (SBT) classification system - an update. Canadian Geotechnical Journal 53, 1910-1927.

Robertson, P.K., Melo, L., Williams, D.J., Wilson, G.W., 2020. Report of the Expert Panel on the Technical Causes of the Failure of Feijão Dam I.

Rogers, B.T., Been, K., Hardy, M.D., Johnson, G.J., Hachey, J.E. 1990. Re-analysis of Nerlerk B-67 berm failures. In Proceedings of the 43rd Canadian Geotechnical Conference – Prediction of Performance in Geotechnique, Quebec, Canada, Vol. pp. 227-237.

Ross, G. A. 1968. Case studies of soil stability problems resulting from earthquakes. PhD thesis University of California, Berkeley, Calif.

Rowe, P. W. 1962. The stress-dilatancy relation for static equilibrium of an assembly of particles in contact. Proceedings of the Royal Society of London A, 269(1339):500-527.

Sasaki, Y. 1994. River dike failure due to the Kushiro-Oki Earthquake of January 15, 1993, Proc. International Workshop on Remedial Treatment of Liquefiable Soils, Public Works Research Institute, Tsukuba.

Schofield, A. N., Wroth, C. P. 1968. Critical state soil mechanics, McGraw-Hill, London.

Seed, H.B. 1969. Analysis of Sheffield Dam failure. Journal of the Soil Mechanics and Foundations Division, Proceedings ofthe ASCE, 95(SM 6): 1453-1490.

Seed, H.B., Lee, K.L., Idriss, I.M., Makdisi, F. 1973. Analysis of the slides in the San Fernando Dams during the earthquake of Feb. 9, 1971. Earthquake Engineering Research Center Report No. EERC 73-2, University of California, Berkeley, Calif.

Seed, H.B. 1987. Design problems in soil liquefaction. Journal of Geotechnical Engineering Division, ASCE, 113(8): pp 827–845.

Seed, H.B., Seed, R.B., Harder, L.F., Jong, H.L. 1989. Reevaluation of the Lower San Fernando Dam: Report 2, examination of the post-earthquake slide of February 9, 1971. Army Corps of Engineers Contract Report GL-89-2, Amy Corps of Engineers Waterways Experiment Station, Vicksburg, Mississippi.

Seed, R.B., Cetin, K.O., Moss, R.E.S., Kammerer, A., Wu, J., Pestana, J. and Riemer, M., Sancio, R.B., Bray, J.D., Kayen, R.E., Faris, A. 2003. Recent Advances in Soil Liquefaction Engineering: A Unified and Consistent Framework. Earthquake Engineering Research Center Report No. EERC 2003-06. http://eerc.berkeley.edu/reports/.

Shelbourn, M. 2010. Geotechnical design verification and performance assessment of tailings storage facilities, in R Jewell & AB Fourie (eds), Proceedings of the First International Seminar on the Reduction of Risk in the Management of Tailings and Mine Waste, Australian Centre for Geomechanics, Perth, pp. 3-14.

Sladen, J.A., D'Hollander, R.D., Krahn, J. 1985a. The liquefaction of sands, a collapse surface approach. Canadian Geotechnical Journal, 22: 564-578.

Sladen, J.A., D'Hollander, R.D., Krahn, J., Mitchell, D.E. 1985b. Back analysis of the Nerlerk berm liquefaction slides. Canadian Geotechnical Journal, 22: 579-588.

Sladen, J.A., D'Hollander, R.D., Krahn, J., Mitchell, D.E. 1987. Back analysis of the Nerlerk berm liquefaction slides: Reply. Canadian Geotechnical Journal, 24: 179-185.

Sladen, J.A. 1989. Problems with interpretation of sand state from cone penetration test. Géotechnique 1989; 39(2):323–332.

Terzaghi, K. 1957. Varieties of submarine slope failure. Norwegian Geotechnical Institute, Publication no. 25, 1–16.

Troncoso, J. H. 1988. Evaluation of seismic behavior of hydraullic structures, in Hydraulic Fill Structures. Geotech. Spec. Pub. No. 21, ASCE, D. J. A. Van Zyl and S. G. Vick eds, pp. 475-491, 1988.

Vaid, Y. P., Chern, J. C. 1985. Cyclic and monotonic undrained response of saturated sands. Advances in the Art of Testing Soils under Cyclic Conditions, 120–147. American Society of Civil Engineers.

Vasquez-Herrera, A., Dobry, R. 1989. Re-evaluation of the Lower San Fernando Dam: Report 3, the behavior of undrained contractive sand and its effect on seismic liquefaction flow failures of earth structures. US Army Corps of Engineers Contract Report GL-89-2, U.S. Army Corps of Engineers Waterways Experiment Station, Vicksburg, Mississippi.

Viana da Fonseca, A. 2013. Application of in situ testing in tailing dams, empahsis on liquefaction. Geotechnical and Geophysical Site Characterization 4 (Eds. Coutinho, Mayne), 181-203. Taylor & Francis Group, London.

Wagener, F., Craig, H.J., Blight, G.E., McPhail, G., Williams, A.A.B., Strydom, J.H. 1998. The Merriespruit tailings dam failure — a review. In Proceedings of the Conference on Tailings and Mine Waste ‘98, Colorado State University, Fort Collins, January 1998, pp. 925–952.

Wang, W. S. 1979. Some Findings in Soil Liquefaction. Water Conservancy and Hydroelectric Power Scientific Research Institute, Beijing, China.

Wroth, C.P., Bassett, R.H. 1965. A stress–strain relationship for the shearing behaviour of a sand. Géotechnique 15, 32–56.

Wroth, C.P. 1984. The interpretation of in-situ soil tests: Rankine Lecture. Géotechnique, 34(4): 449-489.

Yamada, G. 1966. Damage to earth structures and foundation by the Niigata earthquake, June 16, 1964. Soils Found., 6(1), 1-13.

Yamamuro, J. A., Lade, P. L. 1998. Steady-state concepts and static liquefaction of silty sands. J. Geotechmical Geoenvironmental Engineering ASCE 124, 868–877.

Yamamuro, J.A., Lade, P.V. 1999. Experiments and modelling of silty sands susceptible to static liquefaction. Mechanics of Cohesive-Frictional Materials, 4(6): 545–564.

Yang, J. 2002. Non-uniqueness of flow liquefaction line for loose sand. Géoteclmique 52, 757-760.

Yegian, M.K., Ghahraman, V.G., Harutinunyan, R.N. 1994. Liquefaction and embankment failure case histories, 1988 Armenia earthquake. Journal of Geotechnical Engineering, ASCE, 120(3): 581-596.

Yu, H.S. 1998. CASM: A unified state parameter model for clay and sand. International .Journal for Numerical and Analytical Methods in Geomechanics 22, 621-653.

Chapter 4. Pray quay failure analysis

4.1. Introduction

The failure of the Prat quay and additional background information covering the geotechnical properties of the materials involved have been described in previous chapters. The brittle nature of the fill and the characteristics of the failure indicate that flow liquefaction has played a relevant role in reducing the available quay wall stability.

Further insight into the soil parameters, conditions and processes that led to the failure are presented in this Chapter. The starting point is a definition of suitable constitutive models and parameters for the simulation of the main materials properties specified in Chapter 2. Two dimensional numerical analyses using finite element methods (FEM) have been performed. Hypotheses derived from the information collected in Chapters 2 and Chapter 3 are implemented in these analyses. The as-built geometry and construction stages from quay are incorporated in the numerical model to examine the quay wall behaviour until failure. The results of FEM analyses allow the study of soil behaviour during the quay wall construction and can provide insights into the rupture mechanisms.

Additionally, this Chapter seeks to explore two triggering mechanisms of flow liquefaction simulation that could trigger the failure. These analyses are complemented by a parametric study that provides additional information for the interpretation of the failure cause.

Finally, the reasons leading to the failure are discussed in perspective by comparing them with two precursors used.

4.2. Constitutive models and material properties

The selected constitutive models and material parameters for hydraulic fill, natural ground, rubble mound, and concrete caissons are presented in the following sections.

4.2.1. Hydraulic fill

The hydraulic fill constitutive model and associated parameters must provide an adequate simulation of flow liquefaction. For this purpose, the CASM constitutive model has been calibrated to obtain suitable values of K_0, undrained shear strength at peak, undrained shear strength at CSL and compressibility.

Thus, parameters β=0.73 and w=0.04 are selected to result in a value of K_0=0.54, estimated from a friction angle of around 28º and Jaky's (1948) formula. Parameters r=12 an n=10 have been calibrated to yield an undrained shear strength ratio at peak $c_{u\,peak} / \sigma'_v = 0.25$ and an undrained shear strength ratio at the CSL $c_{u\,SS} / \sigma'_v = 0.06$ (Chapter 3.3). The results of a simulation of a triaxial test under anisotropic consolidation (K_0=0.54) followed by undrained loading (triaxial CAU) are shown in Figure 4.1 and Figure 4.2. It can be noted that undrained softening is well reproduced in terms of stress path (p'- q) and of deviatoric stresses (q) versus axial strain (ε_1).

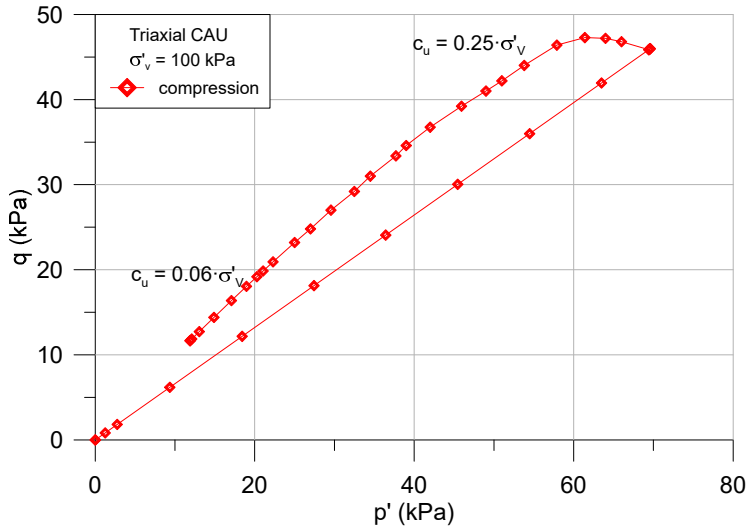

Figure 4.1. Stress path p' - q for triaxial CAU consolidation and undrained shear.

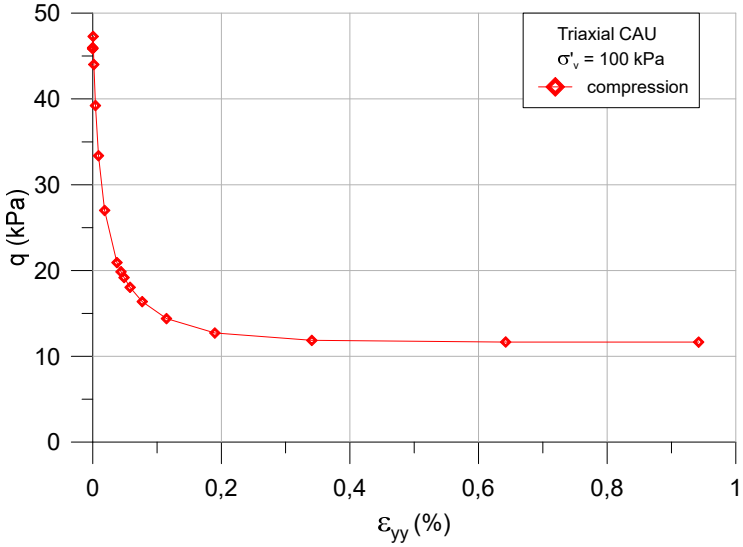

Figure 4.2. ε_1 (ε_{yy}) vs. q curve during shear for triaxial CAU conditions.

Natural density, initial void ratio and compression index of the hydraulic fill were established according to values from laboratory tests (Chapter 2) and the settling column (Appendix F). To estimate an average value for permeability, the c_h values from dissipation tests results were used. The parameters are provided in Table 4.1. An interface element is provided between the caisson and the hydraulic fill with a friction angle of 9º.

Table 4.1.Parameters in CASM constitutive model.

Properties	**Hydraulic fill**
Saturated unit weight (kN/m^3)	18 / 19
Poisson's ratio (ν)	0.3
Void ratio (e)	1
Coefficient of earth pressure at rest (K_0)	0.54
Compression index (c_c)	0.23
Swelling index (c_s)	0.07
Permeability (m/s)	$5 \cdot 10^{-8}$
Undrained shear strength ratio at peak ($c_{u\ peak}/\sigma'_v$)	0.25
Undrained shear strength ratio at critical state ($c_{u\ SS}/\sigma'_v$)	0.06

4.2.2. Natural ground

The Soft soil model (Plaxis, 2020) is used to reproduce natural ground behaviour. The parameters adopted are given in Table 4.2. Natural density, initial void ratio and compression index were obtained from laboratory results. They resulted in a value of undrained shear strength $c_u = 0.25 \cdot \sigma'_v$. The permeability was obtained from dissipation tests results.

Table 4.2. Parameters in Soft Soil constitutive model.

Properties	**Natural ground**
Saturated unit weight (kN/m^3)	19
Poisson's ratio (ν)	0.3
Void ratio (e)	0.8
Compression index (c_c)	0.18
Swelling index (c_s)	0.05
Permeability (m/s)	10^{-8}
Undrained shear strength ratio (c_u/σ'_v)	0.25

4.2.3. Rubble mound and earth bund

These materials are cohesion-less and coarse grained materials that was used in the foundations of the caissons and on the top of caissons. The Mohr-Coulomb (elastic perfectly plastic) model has been

adopted for these materials. Some parameters have been obtained from the site investigation; other parameters have been estimated from standards. In this way, shear strength parameter of the rubble mound was determined from test results but standard values of rigidity were chosen. There are no tests on the materials of the earth bund placed on the caissons that included uncompacted granular soil and dredged fill. Standard values of 18 kN/m^3 for density and of 28° for friction angle (φ) have been used. The main parameters values are shown in Table 4.3. An interface element was provide between the caisson and the rubble mound with a friction angle of R_{inter}· tan (φ).

Table 4.3. Adopted parameters for cohesion less materials.

Material	**γ [kN/m^3]**	**E [kN/m^2]**	**ϕ [°]**	**R inter [-]**
Rubble mound	20	35000	38	0.6
Earth bund & lateral trench fill	18	15000	28	-

4.2.4. Concrete caissons

Concrete caissons used in quay wall were not made of massive concrete but they contained cylindrical hollow cells inside. The floor view of a Phase 1 caisson is presented in Figure 4.3.

When a caisson was installed with the cells full of water the overall density was 16 kN/m^3. When the cells were subsequently filled with sand the density increased to 20.2 kN/m^3. Caissons are assumed as nonporous material (i.e. no flow is allowed).

The caisson was model with a linear elastic constitutive law based on concrete properties.

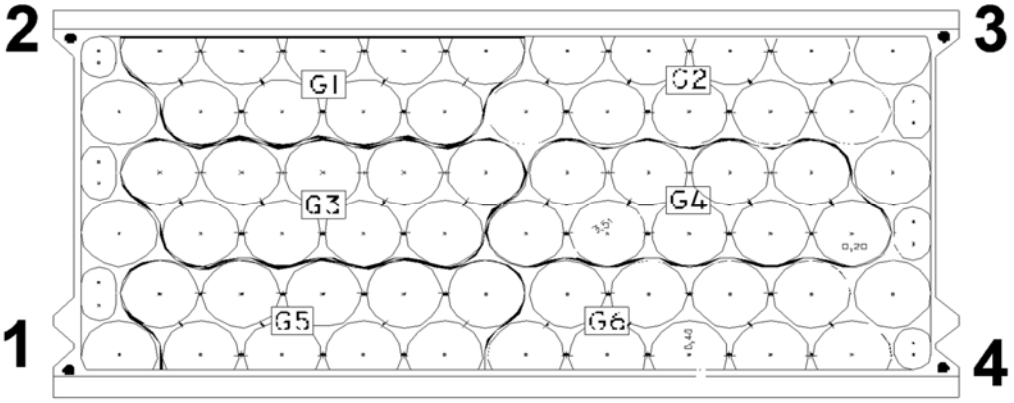

Figure 4.3. Plan view of Phase 1 caisson.

4.2.5. Parameters overview

As a summary, the constitutive models and parameters used to simulate the behaviour each material are presented in Table 4.4.

Table 4.4. Material properties for FE analysis.

Symbol & Units	Natural ground	Hydraulic fill	Caissons	Rubble mound	Earth bund
Constitutive model	Soft soil	CASM	Elastic	M-C	M-C
γ_{nat} [kN/m^3]	19	18.0 [(1)] / 19.0 [(2)]	20.2 [(3)] / 16.0 [(4)]	20	18
e [-]	0.8	1			
c_c	0.18	0.23	-	-	-
c_s	0.05	0.07	-	-	-
E' [kPa]	-	-	$2 \cdot 10^7$	35000	15000
ν [-]	0.3	0.3	0.3	0.3	0.3
k [m/s]	10^{-8}	$5 \cdot 10^{-8}$	-	10^{-2}	10^{-3}
$c_{u\ peak}$ / σ'$_v$	-	0.25	-	-	-
$c_{u\ SS}$ / σ'$_v$	0.25	0.06	-	-	-
φ [°]	-	-	-	38	28
$R_{interface}$	-	0.66	-	0.6	-

[(1)] Upper part from fill; [(2)] Lower part from fill; [(3)] Filled caisson; [(4)] Empty caisson.

4.3. Geometry and material distribution

The geometry of the numerical model is based on the representative cross-section of the as-built project that had been presented previously in Figure 2.14. This geometry is presented in Figure 4.4. It has been discretized to simulate each quay construction stage. The domain of analysis is 250 m long and 64 m high and comprises by 9998 15-noded elements.

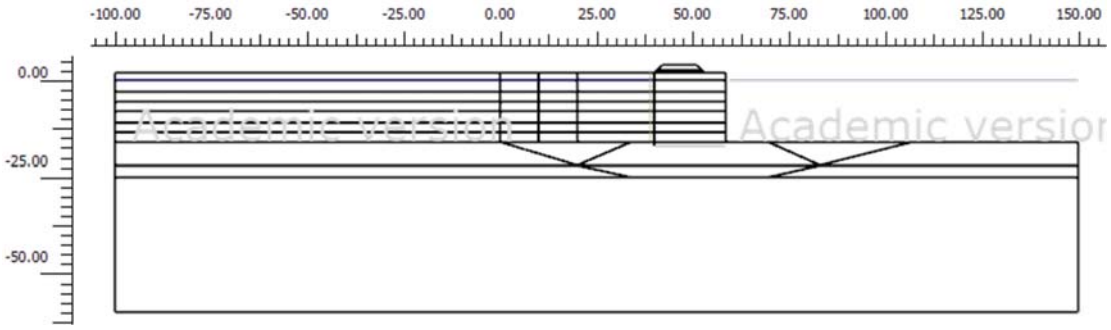

Figure 4.4. Geometry of Prat quay Phase 1.

It can be noted the horizontal lines corresponding to the various hydraulic fill levels. The resulting distribution of the materials is indicated in Figure 4.5. The same material has been assumed for the core and the rock armour in the rubble mound. According to the settling column result, the unit weight of the hydraulic fill depends on the vertical stress (or equivalently on depth). For this reason, a density of 18 kN/m^3 in the upper part and of 19 kN/m^3 in the lower part 19 kN/m^3 have been used.

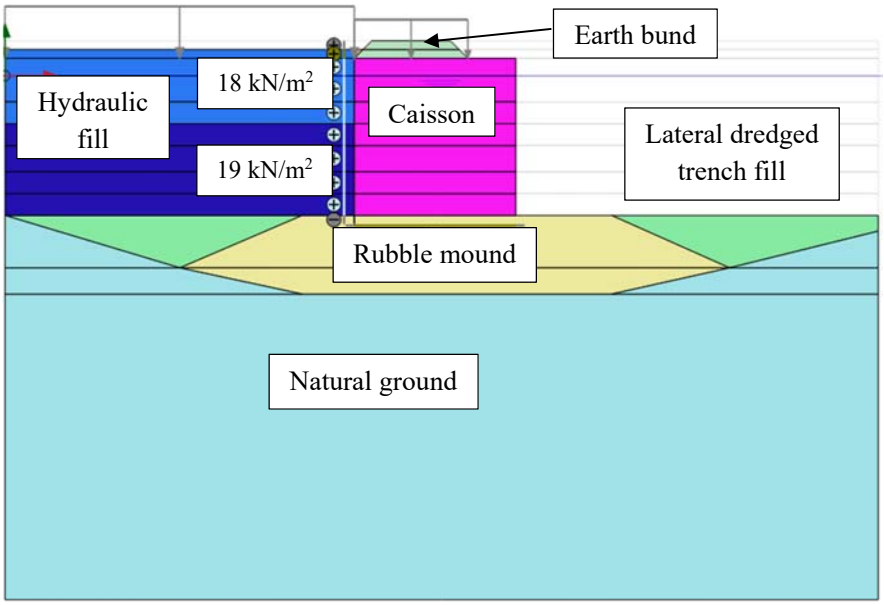

Figure 4.5. Geometry of hydraulic fill up to +3 m elevation, Phase 1.

4.4. Boundary conditions

The displacement boundary conditions are as follows: zero vertical and horizontal displacements are prescribed on the lower horizontal boundary whereas zero horizontal displacements are prescribed on the two vertical boundaries. A no-stress condition is applied to the top surface of the domain in all construction steps.

Concerning water flow conditions, on the vertical boundary, a constant water head corresponding to an elevation of +0 m (mean sea level) has been applied. This water head elevation also applied on the land side while the hydraulic fill was below sea level. Subsequently, there was about 0.5 m of water above the hydraulic fill top elevation, i.e. when the hydraulic fill was at +2 m, water level was at +2.5 m and, of course, sea water remained at level +0 m, see Figure 4.6. In addition, the lower horizontal boundary down to -60 m, a constant water head corresponding to an elevation of +0 m (mean sea level) has been applied. The boundary is impermeable in the land side.

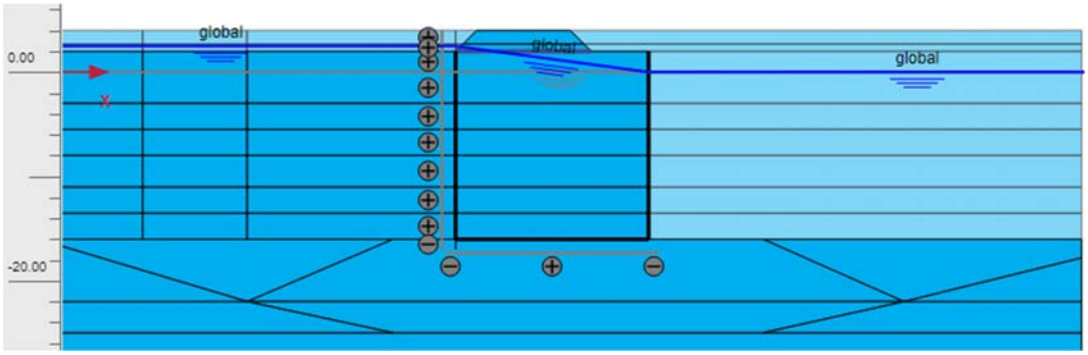

Figure 4.6. Hydraulic conditions, water level in hydraulic fill +2 m.

4.5. Stages of analysis

The analysis simulates the construction of the quay wall; it involved 14 stages until the hydraulic fill reached the level of +3 m. The name, the number and the time interval of the various stages are collected in Table 4.5.

Table 4.5. Description of construction stages of Phase 1.

Description	Stage	Time interval (day)
Initial K_0 phase	0	-
Trench dredging	1	120
Construction of the rubble mound	2	180
Caisson placement and filling	3	86
Consolidation	4	127
Trench filling next to caissons	5	90
Hydraulic fill up to -13.5 m	6	4
Hydraulic fill up to -11 m	7	7
Hydraulic fill up to -8 m	8	10
Hydraulic fill up to -5.5 m	9	31
Hydraulic fill up to -3 m	10	44
Hydraulic fill up to +0 m	11	68
Hydraulic fill consolidation (+ 0m)	12	32
Hydraulic fill up to +2 m	13	27
Hydraulic fill up to +3 m	14	8 (up to failure)

The first phase of analysis considers only the natural soil in order to establish the initial conditions of the analysis. Displacements generated up to stage 3 are reset to zero so that they do not interfere with the displacements computed and recorded during construction. Afterwards, the quay wall is constructed step-by-step following the actual construction sequence. For all phases, consolidation analyses are performed that incorporate the hydromechanical interactions and the time-dependent dissipation of pore pressures over the period considered.

The final stage (14) of the calculation -"up to failure"-, corresponds to the period of 8 days prior to the failure. The only processes considered in this calculation stage are the hydraulic fill raising up to +3 m.

4.6. Triggering flow liquefaction in Prat quay

In Chapter 3, a number of potential flow liquefaction triggering mechanisms have been identified. For the Prat quay case, two different scenarios are possible. The first one simply involves the continuation of construction of the hydraulic fill until a sliding failure condition of the caisson is reached. At that moment, the caisson starts to displace laterally, reducing the horizontal stress in the backfill and thereby triggering undrained flow liquefaction. The second one postulates that liquefaction occurs locally that then propagates causing the liquefaction of most of the hydraulic fill

mass and the failure of the quay. A zone close to the tip of the South embankment being constructed at the time of failure is a likely location for the initiation of liquefaction if embankment instability was the initiation event.

Both precursors of flow liquefaction have been implemented in the analysis. In fact, for the first hypothesis no changes in the simulation is required. For the second hypothesis a limited zone of the hydraulic fill has been assumed to have undergone liquefaction. To simulate this local liquefaction, the undrained shear strength of the material is reduced to the ultimate undrained shear strength ratio of 0.06 by changing the constitutive law to Soft Soil model (Plaxis, 2010) with the parameters presented in Table 4.6, the parameter determination is presented in Appendix B.2.

Table 4.6. Liquefied hydraulic fill parameters in Soft soil constitutive model.

Properties	**Liquefied hydraulic fill**
Saturated unit weight [kN/m^3]	18
Void ratio (e)	2
Compression index (c_c)	0.20
Swelling index (c_s)	0.02
Permeability [m/s]	10^{-8}
Undrained shear strength (c_u / σ'_v)	0.06

4.7. Results of Phase 1 analysis

As described above, the numerical analyses performed incorporate the available information concerning soil behaviour, material parameters, geometry, hydraulic boundary conditions and construction history.

4.7.1. Analysis before failure

The analysis performed provides data relating to the evolution of water pressures and deformations. There were no piezometers installed in the works at the time of failure but surveying records provide useful information for comparison. Figure 4.7 shows the computed settlements compared with the observed settlements of Phase 1 caissons during construction. The agreement is quite satisfactory suggesting a good estimate of deformation parameters of the natural ground and rubble mound. The comparison between computed and observed horizontal displacements is presented in Figure 4.8. The magnitude and tendency of the calculated horizontal movements are similar to the field records. Nevertheless, there are differences regarding stages 11, 12 and 13.

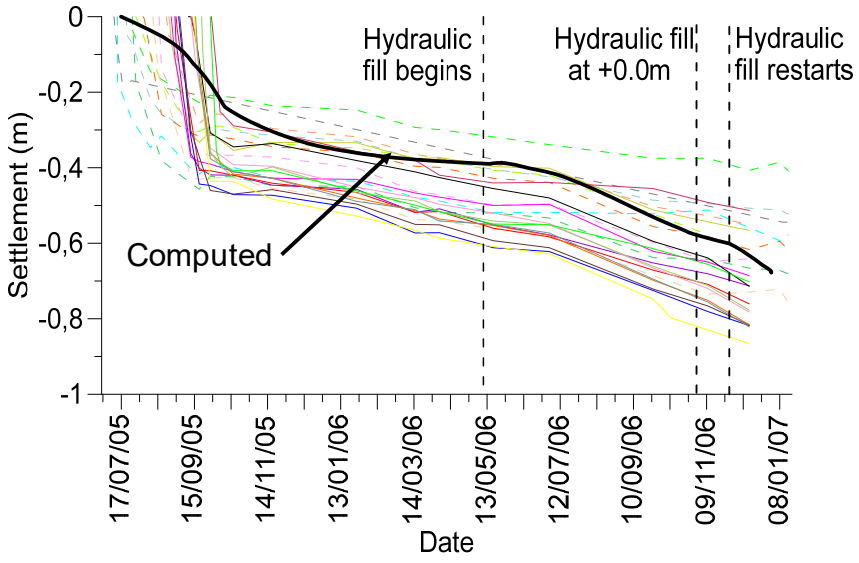

Figure 4.7. Observed caisson settlements vs. computed settlements during quay wall construction.

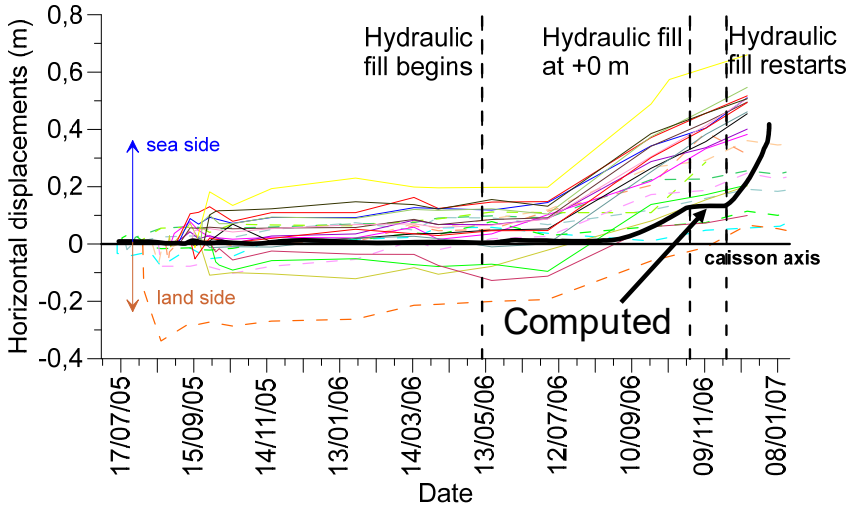

Figure 4.8. Observed caisson horizontal displacements vs. computed horizontal displacements during quay wall construction.

The computed contours of excess pore pressures (EPP) are presented in Figure 4.9. Maximum excess pore pressures before the failure are reached in the natural ground below the hydraulic fill, although a secondary peak is visible under the caisson. Significantly, lower values of EPP (around 40 kPa) have been computed in hydraulic fill close to quay wall.

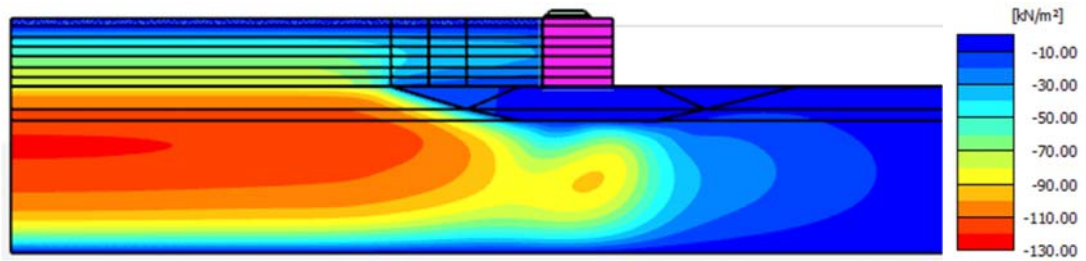

Figure 4.9. Contour of excess pore pressures at the stage before the failure, Stage 13.

Figure 4.10 shows the mobilized shear stresses at stage 13, when the hydraulic fill had reached an elevation of +2.0 m. It can be noted that there is a higher mobilized shear stresses in the rubble mound below the caisson toe on the sea side, although this is insufficient to lead to a bearing capacity instability of the rubble mound.

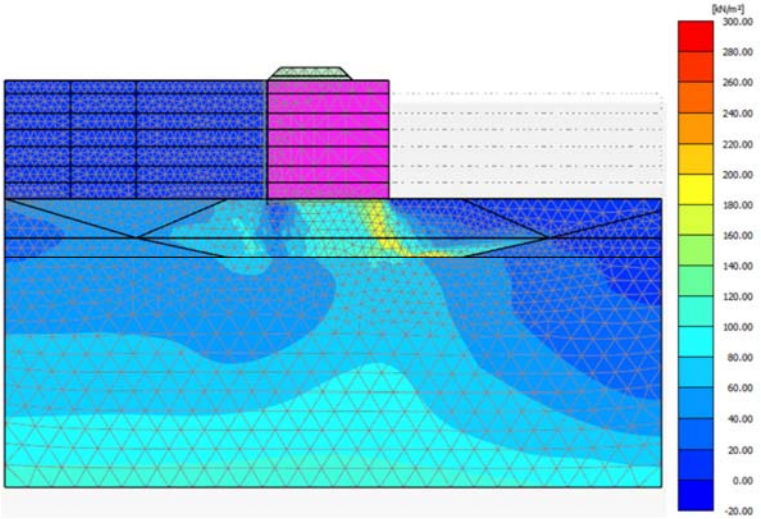

Figure 4.10. Mobilized shear stresses, stage 13, before failure.

A check on the shear stress in the interface between caisson and rubble mound is performed for the same stage 13 (Figure 4.11). The blue area represents the mobilized shear stresses on the caisson base whereas the dashed line is maximum theoretical shear stresses along the interface. It can be observed that about, 13 meters (70%) have reached a failure condition; only the region from 13 m to 18.5 m (30%) has not reached failure yet.

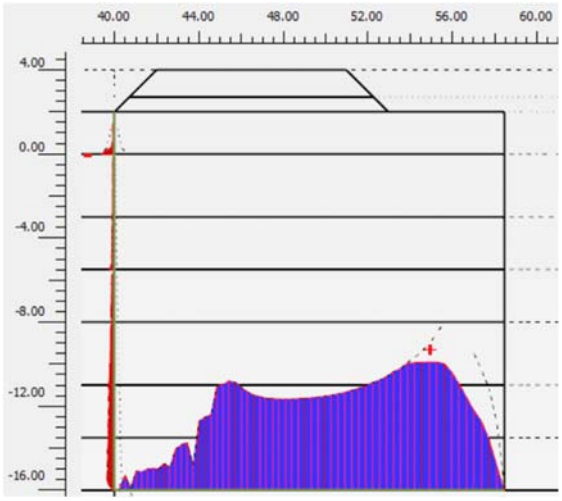

Figure 4.11. Mobilized (red line) and maximum (dashed black line) shear stresses on backfill and caisson base, at the stage before the failure, 12.

To examine the stability evolution during construction, factors of safety (FoS) have been computed using the phi-c reduction method. Although reduction on Mohr Coulomb and Soft Soil models could be directly applied in the software used, a special procedure had to be developed for the CASM

model, as described in detail in Appendix A. The computed values of FoS for the final stages of the analysis are presented in Table 4.7.

Table 4.7. FoS of previous stages before the failure.

Stage	Identification	FoS Manual φ - c reduction
11	Hydraulic fill up to 0m	1.12
12	Hydraulic fill consolidation up to 0m	-
13	Hydraulic fill up to +2.0m	1.08

Quay stability is being reduced by the rise of the hydraulic fill. It is interesting to note that the two failure mechanisms, corresponding to stages 11 and 13, are quite similar in shape, see Figure 4.12 and Figure 4.13, respectively.

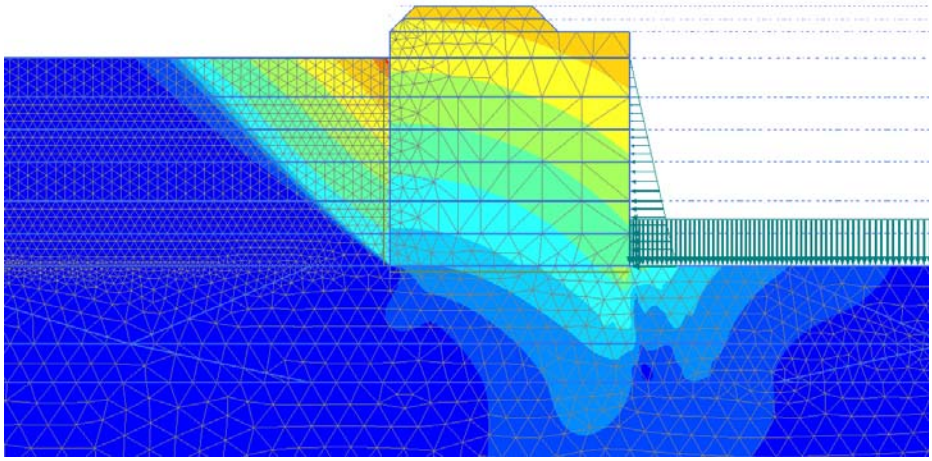

Figure 4.12. Phase displacements in FoS analysis of the stage with fill at elevation +0 m, stage 11.

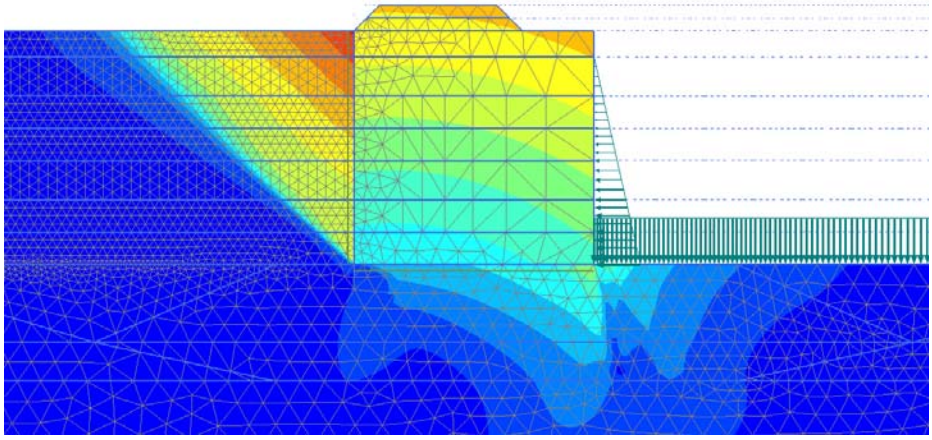

Figure 4.13. Phase displacements in FoS analysis at the stage before failure, stage 12.

4.7.2. Liquefaction triggered by fill emplacement (Mechanism 1)

This analysis attempts to simulate failure as a consequence of continuing the process of fill emplacement. A new computation stage (Stage 14) is performed where the hydraulic fill is raised from elevation +2.0 m to +3.0 m. This analysis predicts failure when the calculation reaches 75% of the total calculation stage. This would correspond to the hydraulic fill reaching a +2.75 m elevation,

a figure that agrees quite well with the fact that, at the time of failure, the hydraulic fill had reached an elevation of +2.50 m.

The mechanism of failure is shown in Figure 4.14 in terms of incremental displacements. It involves an active pressure wedge behind the caisson where the fill has liquefied. Naturally, the liquefaction would progress landwards as more hydraulic fill becomes unstable and liquefies but this subsequent evolution of the failure is beyond the capabilities of the analysis. In addition, a limited sinking of the caisson toe on the sea side can also be noticed.

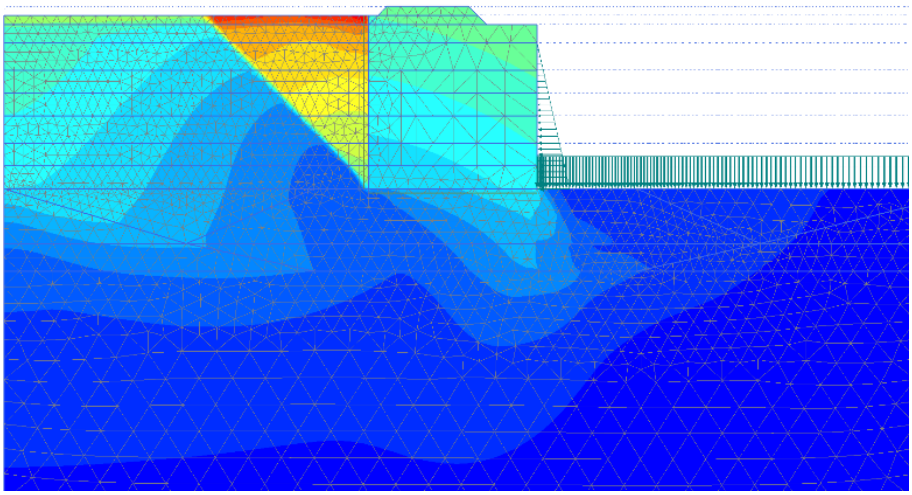

Figure 4.14. Contours of incremental displacements at the failure stage (14).

The shear surface of the failure mechanism, identified by means of incremental shear strains, is shown in Figure 4.15. This surface crosses the hydraulic fill from top to bottom. In addition, a slightly small contour of incremental shear strains can be perceived in the rubble mound next to the caisson toe on the sea side possibly related to incipient bearing capacity. No incremental shear stains have been detected in the base of the caisson because of the interface presence. For this reason, it is important to check again the caisson interfaces for stage 14.

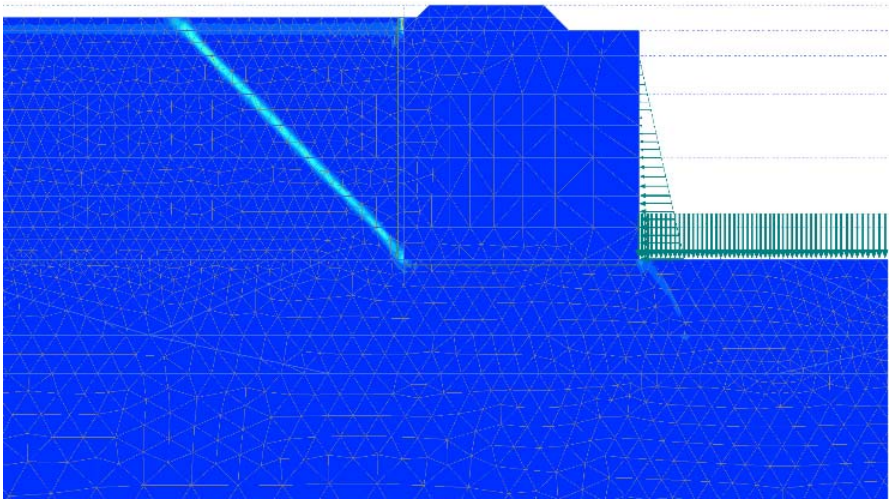

Figure 4.15. Incremental shear strains at failure stage, 14.

The computer code does not plot the shear strain contour in the interface but the interface shear stresses are plotted directly in Figure 4.16. As in Stage 13, only 70% of the interface has reached the available strength.

Observing the interface displacement directions in the final stage helps to understand the mechanism of the failure (Figure 4.17). It involves sliding along most of the interface combined with a downward movement around the sea side edge of the caisson.

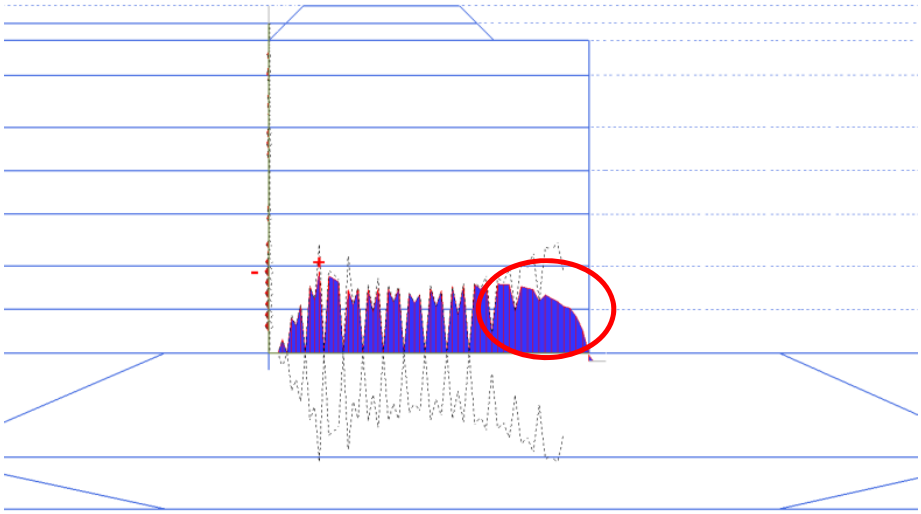

Figure 4.16. Shear strength at the caisson interface. Stage 14, hydraulic fill at elevation +3m.

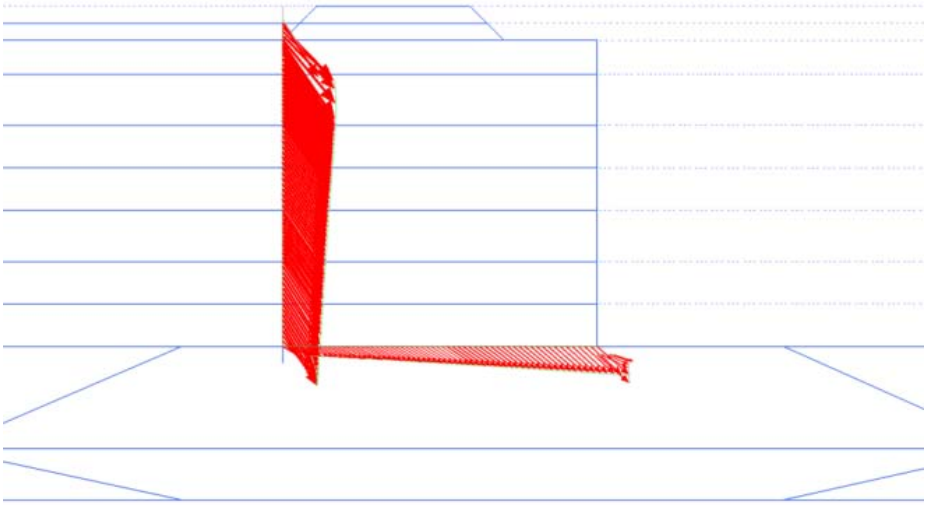

Figure 4.17. Displacements at the interface of the caisson. Stage 14, hydraulic fill at elevation +3m.

For reference, the results just presented can be compared with those of a preliminary analysis in which the liquefied strength of the hydraulic fill was assumed throughout (Appendix B). It can observed that a similar failure mechanism is obtained.

4.7.3. Liquefaction triggered by local liquefaction (Mechanism 2)

This failure mechanism is analysed assuming that, after the hydraulic fill has reached elevation +2.50 m, a limited zone in the hydraulic fill undergoes liquefaction (Figure 4.18). This area is located 20 m away from the rear part of the quay wall in an area near the end of the South embankment.

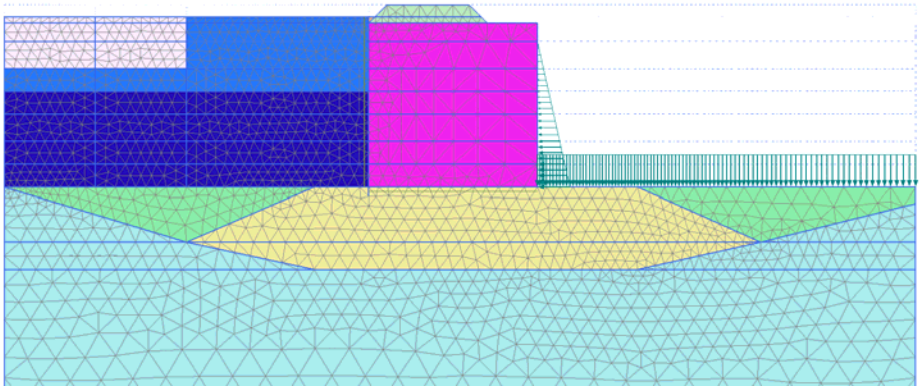

Figure 4.18. Geometry of the new cluster defined to simulate liquefied material due to embankment failure.

The analysis shows that a general quay failure ensues. The development of failure after the initial liquefaction is illustrated in Figure 4.19. It can be observed how the displacements associated with failure spread from the initial liquefaction region (a and b) until producing the complete failure of the caisson wall (f).

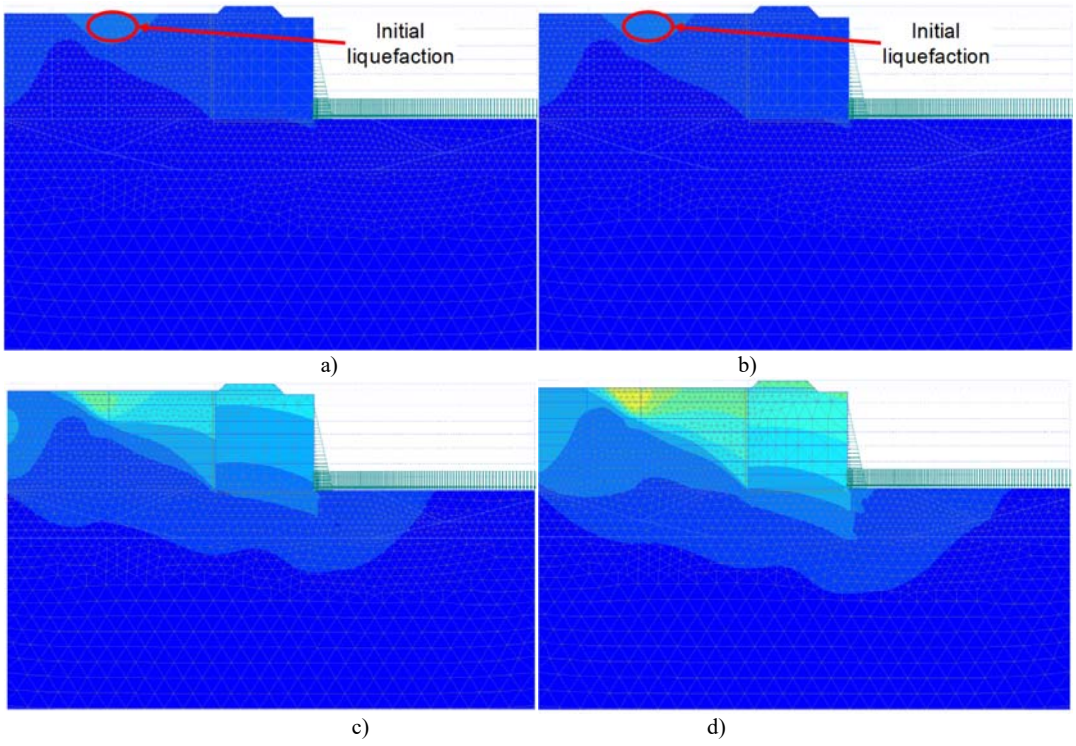

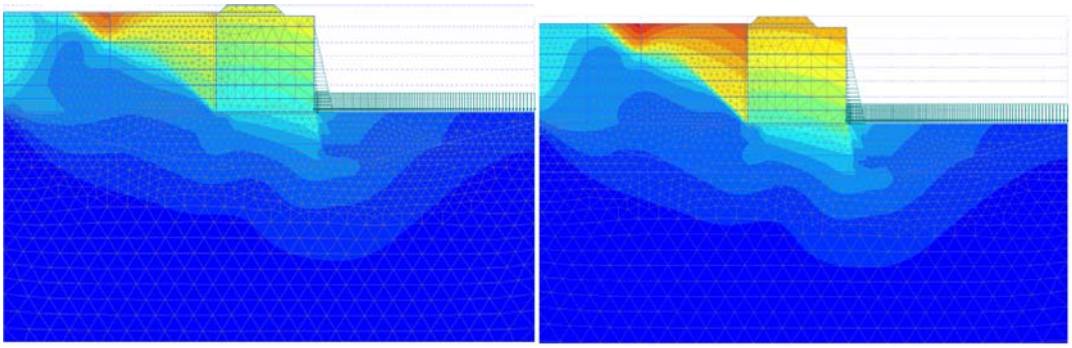

e) f)

Figure 4.19. Succession of computed displacements contours during failure.

The vectors of computed displacements during failure are depicted in Figure 4.20. The kinematics of the failure can be clearly seen: the initial flow liquefaction mobilized the hydraulic fill wedge behind the caisson, part of the caisson interface undergoes partial sliding and a localised bearing capacity failure occurs at the sea side edge of the rubble mound.

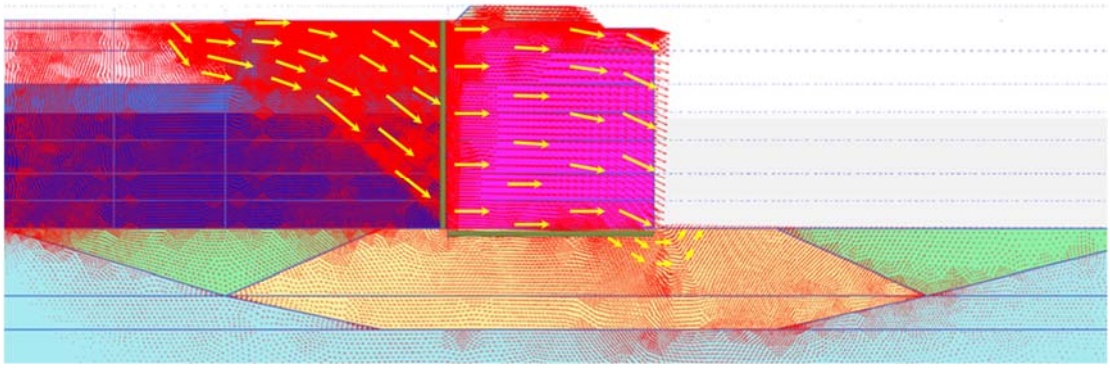

Figure 4.20. Vectors of computed displacements during failure.

4.8. Parametric study

A parametric study has been undertaken to examine how the variation on a single parameter can influence the quay wall failure. Furthermore, it will help to understand better the circumstances that may lead to instability in this particular case.

Failure is the result of the interplay of the stabilizing and destabilizing forces. The main stabilising forces are the caisson weight and the friction on the caisson base whereas the main destabilising force is the thrust of the fill. The parametric study involves two cases modifying the stabilizing forces: (i) the caisson weight and (ii) rubble mound friction angle and on case that changes the destabilizing force by varying hydraulic fill parameters such as soil brittleness and soil weight. The analyses described above will be considered as the Base case for comparison.

4.8.1. Friction angle of rubble mound

Result of parametric study for rubble mound shows that this variation produces a slightly change on the hydraulic fill level of the failure. A change of ± 3° in friction angle implies a variation of about 0.4 m, as summarised in Table 4.8.

Table 4.8. Results of friction angle of rubble mound parametric study.

Material	φ [°]	Hydraulic fill level [m]
Rubble mound*	38	+2.75
Less resistant rubble mound	35	+2.41
More resistant rubble mound	41	+2.86

* Base case.

4.8.2. Caisson weight

An increment or a reduction of 1 kN/m^3 in caisson weight involves changes on the failure hydraulic fill level on the order of 0.80 m, the results are presented in Table 4.9. It is expected that the caisson weight variation would be more influential than the change in friction angle of the rubble mound, because of the direct influence on stabilising forces.

Table 4.9. Results of weight of caissons parametric study.

Caisson material	γ [kN/m^3]	Hydraulic fill level [m]
Filled caisson*	20.2	+2.75
Light filled caisson	19.2	+2.09
Heavy filled caisson	21.2	> +3.00

* Base case.

4.8.3. Brittleness index of hydraulic fill

Undrained shear strength ratio at steady state was determined by back analysis in Olson and Stark (2002) obtaining values lying in the range of $0.05 \cdot \sigma'_v$ to $0.12 \cdot \sigma'_v$. Thus result in brittleness indices (I_B) between 0.52 and 0.80 if $c_{u\ peak}/\ \sigma'_v$=0.25 was assumed. In this parametric study, analyses were performed using values of brittleness index of 0.76 -the analysis already described-, 0.56 -upper boundary of liquefied shear strength-, 0.36 -a brittle soil but outside the usual range of liquefied shear strength-, and 0 (ductile behaviour).

The sensitivity analyses have been performed considering the two alternative liquefaction triggers. The results of parametric study assuming Mechanism 1 indicate that failure is not reached for any of the values of brittleness index tried (0.56, 0.36 or 0). In contrast, Mechanism 2 results showed that failure is reached if I_B is 0.56, but again it is not reached if I_B=0.36 or I_B=0. It should be noted that a FoS= 1.25 is computed for a ductile hydraulic fill (I_B=0) and $c_{u\ peak}/\sigma'_v$=0.25. A summary of the results of this set of analyses are presented in Table 4.10.

Table 4.10. Results of flow liquefaction susceptibility of hydraulic fill parametric study.

Fill material	Brittleness index (I_B)	Hydraulic fill c_u / σ'_v	Mechanism 1	Hydraulic fill level [m]	Mechanism 2	Hydraulic fill level [m]
High brittleness*	0.76	$c_{u\,peak} / \sigma'_v = 0.25$ $c_{u\,SS} / \sigma'_v = 0.06$	Failure	2.75	Failure	+2.5
Medium brittleness	0.56	$c_{u\,peak} / \sigma'_v = 0.25$ $c_{u\,SS} / \sigma'_v = 0.11$	Stable	>+3	Failure	+2.5
Low brittleness	0.36	$c_{u\,peak} / \sigma'_v = 0.25$ $c_{u\,SS} / \sigma'_v = 0.16$	Stable	>+3	Stable	>+2.5
No brittleness	0	$c_u / \sigma'_v = 0.25$	Stable	-	Stable	-

*Base Case analysis.

The shape of the failure for both Mechanism 1 (Figure 4.21) and Mechanism 2 are similar to those obtained in the Base Case analyses. However, the degree of brittleness has a strong influence on the value of FoS or the elevation level of hydraulic fill that can be reached. As expected, if brittleness reduces, the quay stability increases.

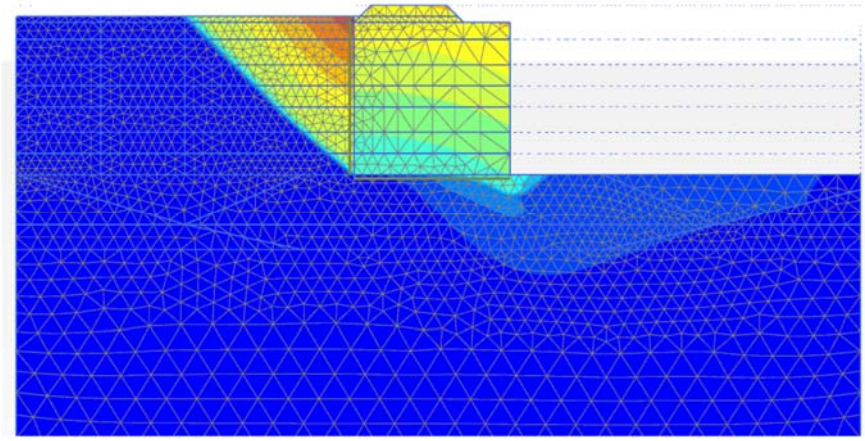

Figure 4.21. Contours of incremental displacements at stage 14 in FoS analysis. Hydraulic fill at elevation+3 m, I_B=0, FoS=1.25.

4.8.4. Saturated unit weight of hydraulic fill

A distribution of hydraulic fill density was postulated in the Base case analyses. The upper layer (from the surface to -5m) was assigned a density of 18 kN/m^3 and the lower layer (from -5 m to -16 m) a density of 19 kN/m^3.

A set of analyses has been performed varying the density of the upper layer; values of 17 and 19 kN/m^3 have been used. The results are shown in Table 4.11. As expected, a lower fill density increases stability and vice versa.

Table 4.11. Results of saturated unit weight of hydraulic fill parametric study.

Material	Upper hydraulic fill		Lower hydraulic fill		Failure
	γ_{sat} [kN/m^3]	Elevation [m]	γ_{sat} [kN/m^3]	Elevation [m]	Elevation [m]
Hydraulic fill*	18.0	Hydraulic fill level from top to -5 m	19.0	-5 m to -16 m	+2.75
Dense hydraulic fill	19.0	Hydraulic fill level to -5 m	20.0	-5 m to -16 m	+2.17
Loose hydraulic fill	17.0	Hydraulic fill level to -5 m	18.0	-5 m to -16 m	> +3.0

*Base case.

In addition, the elevation of the boundary between the upper and lower fill was also varied. It was changed from -5.0 m to -3 m (high level) and -8 m (low level). Results from high, medium and low levels achieved different elevations of failure +2.27 m, +2.75 m and 2.50 m, respectively, as shown in Table 4.12. It is apparent that the fill elevation at which failure occurs, it is rather insensitive to the location of the boundary between upper and lower fill.

Table 4.12. Results of level of hydraulic fill contact between layers' elevation sensitivity.

Level	Upper hydraulic fill		Lower hydraulic fill		Failure top level
	γ_{sat} [kN/m^3]	Elevation [m]	γ_{sat} [kN/m^3]	Elevation [m]	Elevation [m]
Medium*	18.0	Hydraulic fill level to -5 m	19.0	-5 m to -16 m	+2.75
Low	18.0	Hydraulic fill level to -8 m	19.0	-8 m to -16 m	+2.50
High	18.0	Hydraulic fill level to -3 m	19.0	-3 m to -16 m	+2.27

*Base Case analysis.

4.9. Comparison with field failure observations

The sequence of the failure includes: a flow liquefaction mechanism, the initiation of general failure initial instability and the final post-failure state of the quay wall. Leaving the flow liquefaction mechanism aside because it has been described in detail above, the initial instability and the final post-failure state of the quay wall will be discussed in this section.

Regarding the initial instability, the profile of the rubble mound determined after the failure can be compared to the shape of the failure mechanism from numerical analysis. The two results have been plotted together in Figure 4.22. It is interesting to note that the small portion of the rubble mound at the sea side edge that was missing in a number of sections corresponds to the computed shape of the failure surface in that area. Evidently, the final shape of the hydraulic fill after failure cannot be reached with this analysis.

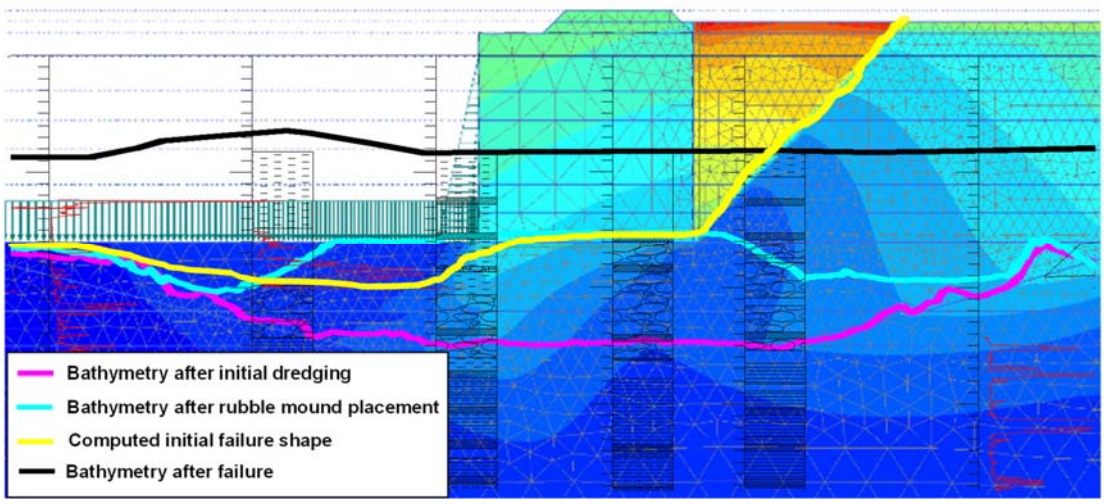

Figure 4.22. Computed incremental displacements at failure and observed ground profiles before and after failure.

A 3D post-failure analysis was carried out by Celigueta et al. (2007) using the Particle Finite Element Method (PFEM). Several hypothesis of liquefaction initiation were tried. The only analysis that resulted in caisson displacements similar to those observed in the field was the case in which liquefaction was initiated close to the tip of the South embankment followed by a second liquefaction episode close to the East embankment (Figure 4.23).

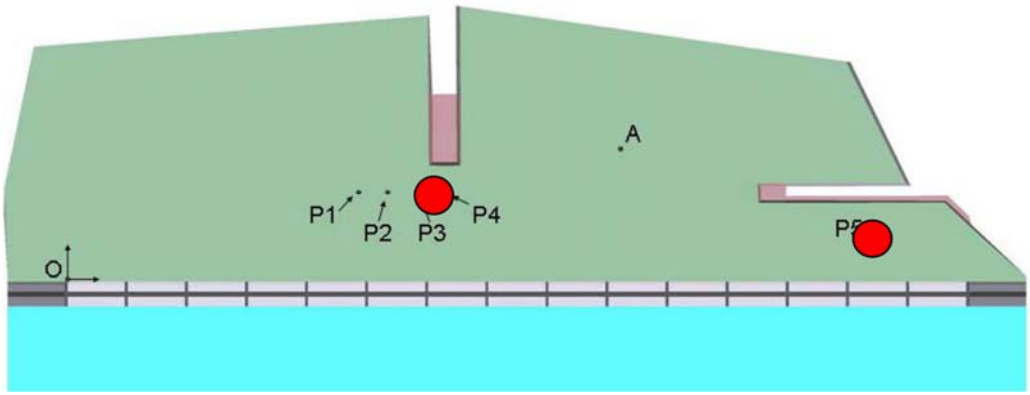

Figure 4.23. Assumed locations of liquefaction initiation, Celigueta et al. 2007.

Figure 4.24 shows the evolution of the distribution of the computed displacements of the caissons from the analysis. It can be seen that the final state is achieved after 41 seconds. The observed displacements are also plotted for reference.

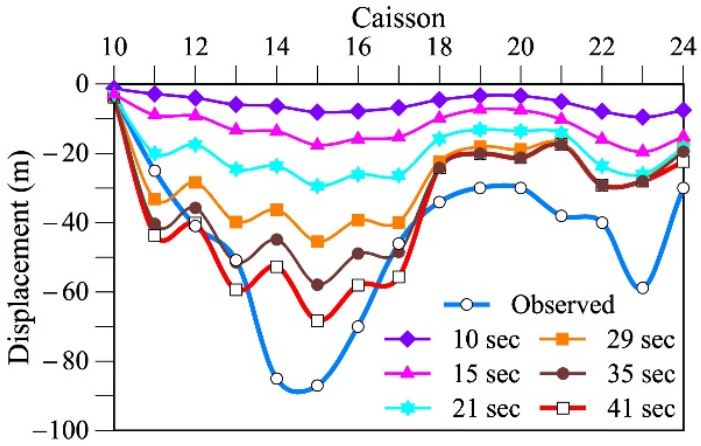

Figure 4.24. Evolution of computed caisson displacements with time. Observed caisson displacements are added for reference, Celigueta et al. 2007.

This analysis appears to suggest that the initial liquefaction of the backfill was associated with the failure of the South embankment. It also indicates that when liquefaction reached the zone of the East embankment, an additional failure provided a new liquefaction focus. It should be noted however, that the analyses performed is necessarily a quite simplified one but it is capable to provide a quite reasonable account of the movements of the caissons after failure.

4.10. Summary

The most significant conclusions from this Chapter are listed below.

(a) The simulation of the construction and failure of the Part quay based on the information presented in Chapter 2 and Chapter 3, provides a suitable framework to examine the events associated with the failure of the quay. Implementation of CASM model to simulate flow liquefaction has been a key feature.

(b) The simulation has reproduced satisfactorily the quay wall behaviour that includes the wall displacements before failure, the fill elevation at the moment of failure the shape of the initial failure surface.

(c) Two possible mechanisms for flow liquefaction triggering have been considered: continuing fill emplacement (Mechanism 1) or the occurrence of a local liquefaction as precursor of the general failure (Mechanism 2).

(d) The parametric study shows that a number of parameters have an influence on the moment and characteristics of the failure. For instance, the saturated unit weight of caisson or hydraulic fill or the friction angle of rubble mound affect the degree of stability of the quay wall. However, the stronger effect corresponds to degree of brittleness of the hydraulic fill. For Mechanism 1, if the brittleness index reduces, failure requires a higher level of fill emplacement to. In the case of Mechanism 2, failure still takes place if the ultimate strength is within the usual range of liquefied shear strengths.

(e) Liquefaction of the hydraulic fill was not triggered by a conventional sliding failure underlying the site or by a pore pressure increase. On this occasion, it was the hydraulic fill liquefaction that initiated the horizontal sliding of the caissons.

Results from this Chapter have made available a consistent explanation of Phase 1 failure of Prat Quay. Nevertheless, to study the reasons why Phase 2 did not fail in the same manner, require a detailed study and analysis that is presented in Chapter 5. The same Chapter also includes a consideration of the issues related to the completion of the construction of the Phase 2 quay and the reconstruction of Phase 1 quay.

4.11. References

Celigueta, M.A., Oñate, E., Suárez, B. 2007. Trabajos realizados por CIMNE en relación con la rotura del muelle del Prat del puerto de Barcelona. Informe Técnico, CIMNE IT-514. CIMNE, Barcelona.

Jaky, J. 1948. Pressure in soils. 2nd ICSMFE, London, Vol 1, pp 103-107.

Olson, S. M., Stark, T. D. 2002. Liquefied strength ratio from liquefaction flow failure case histories. Canadian Geotechnical Journal 39, 629–647.

Plaxis 2010. Materials Models Manual.

Chapter 5. Completion of the construction of Phase 2 and reconstruction of Phase 1

5.1. Introduction

This Chapter describes the changes in the design of Phase 2 incorporating the lessons derived from the study of the failure previously described. It also includes an account of the reconstruction of Phase 1.

The design and construction that allow the completion of Phase 2 are presented in this Chapter. A 2D FEM analysis of Phase 2 is presented first corresponding to the stages carried out up to the failure of Phase 1. This analysis is performed with the stages, geometry and materials defined in Chapter 2 and Chapter 4. The results of analysis allow the study of soil behaviour during the quay wall construction and can suggest the suitability of soil improvement to avoid another failure.

A summary of soil improvement used to mitigate soil liquefaction in practice is then presented. The implemented solution of soil improvement is described, as well as the monitoring system to check the quay wall behaviour. To check the results of the soil improvement, two additional site investigations have been before and after the implementation of the soil improvement measures.

New design and construction stages are defined for the completion of the Phase 2 quay construction that are also incorporated in the analysis. The definition of these stages is closely linked with the application of the observational method until the end of the quay construction. This requires a constant comparison between analysis results and the observation from the monitoring system.

The lessons learned from Phase 2 were used in the design of Phase 1 reconstruction that involved significant modifications.

Finally, a protocol for the evaluation liquefaction potential for hydraulic fill is proposed that includes actions to be taken before, during and after fill emplacement. The aim is to provide a structured tool for use in practice.

5.2. Phase 2 analysis

Although Phase 2 was not affected by failure, it was of some concern that this quay wall constructed with narrower caissons (11.5 m) had not failed in the same way as Phase 1 did. An insight into the reasons that led to a stable situation are presented in following sections. Again, 2D numerical analyses using FEM have been performed incorporating the new geometry and construction stages. Most constitutive models and parameters are the same as those presented in Chapter 4. The results of the analysis of Phase 2 quay allow to examine its behaviour before the failure and to check its degree of stability after the failure. The analysis is also used to define the soil improvement measures and the constructions stages required to complete the Phase 2 construction safely.

5.2.1. Constitutive models and material properties

The constitutive model and material parameters for natural ground (Soft Soil), rubble mound, lateral trench or dike (Mohr-Coulomb) and hydraulic fill (CASM) were already established for Phase 1, (Chapter 4). However, new materials, such as rock fill material and natural ground sand have been incorporated in the analysis. These materials have been simulated according to Mohr-Coulomb (M-C) model and the parameters are presented in Table 5.1. Rock fill had similar proprieties as the rubble mound defined above. In this case, an interface element was provided between the caisson and the rock fill with a friction angle of $R_{inter} \cdot \tan(\varphi)$. The parameters of the sands have been obtained from the site investigation.

The densities of Phase 1 and 2 caissons were similar. Thus, this material parameter was not modified.

Table 5.1. Adopted parameters for cohesion less materials.

Symbol & Units	Rock fill	Sands (natural ground)
Model	M-C	M-C
γ_{nat} [kN/m^3]	20	18
E' [kPa]	35000	15000
υ	0.3	0.3
k [m/s]	10^{-2}	10^{-4}
φ [°]	38	28
$R_{interface}$	0.6	-

5.2.2. Geometry and material distribution

The geometry of numerical model is based on the representative cross-section of the as-built project that previously had been presented in Figure 2.15. This geometry has been discretized to simulate each construction stage of the quay, as shown in Figure 5.1. The analysis domain is 200 m long and 64 m high and composed by 10012 elements of 15 nodes.

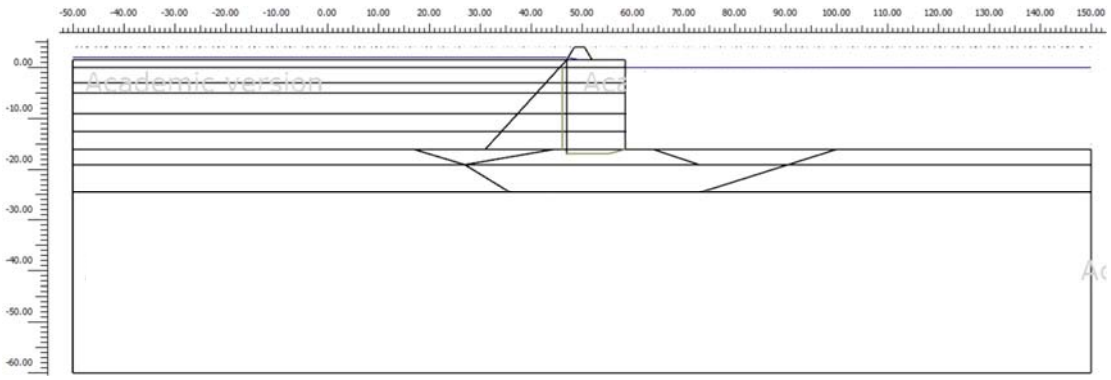

Figure 5.1. Geometry of Prat quay Phase 2.

The resulting distribution of the materials is presented in Figure 5.2.

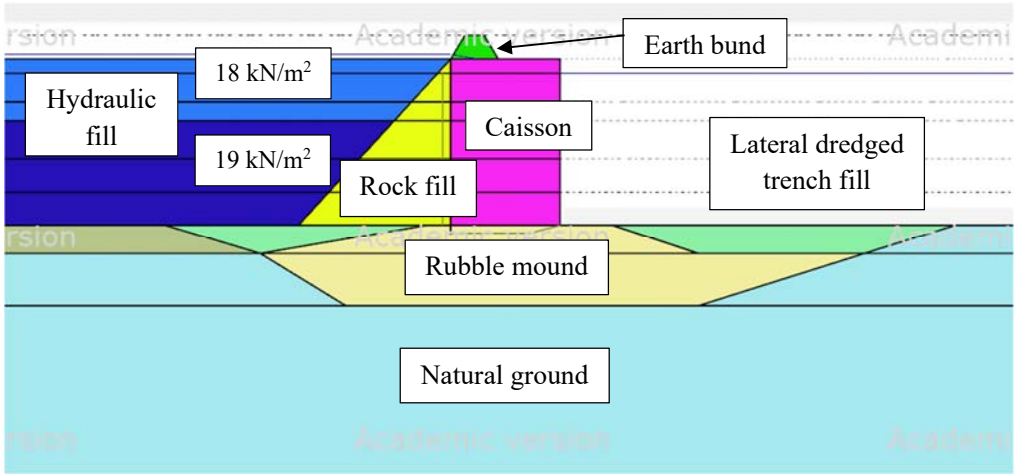

Figure 5.2. Geometry with hydraulic fill at elevation +1.5 m, Phase 2.

5.2.3. Boundary conditions

The displacement boundary conditions are as follows: zero vertical and horizontal displacements are prescribed at the lower horizontal boundary whereas zero horizontal displacements are prescribed on the two vertical boundaries. A no-stress condition is applied to the surface of the domain in all construction steps.

Concerning water flow conditions, on the vertical boundary, a constant water head corresponding to an elevation of +0 m (mean sea level) has been applied.. As done in Phase 1, this water head elevation also applied for the land-side material while the hydraulic fill was below sea level. Subsequently, there was about 0.5 m of water above the hydraulic fill top elevation, i.e. when the hydraulic fill was at +1.5 m, water level was at +2 m and, of course, sea water remained at level +0 m, see Figure 5.3. In addition, the lower horizontal boundary down to -60 m, a constant water head corresponding to an elevation of +0 m (mean sea level) has been applied. The boundary is impermeable in the land side

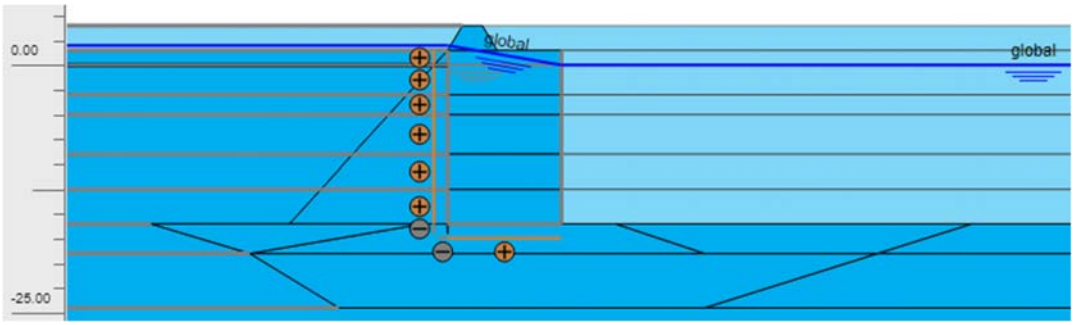

Figure 5.3. Hydraulic conditions, water level in hydraulic fill at elevation +1.5 m.

5.2.4. Stages of analysis

The analysis simulates the 10 construction stages until the time of the failure of Phase. They are listed in Table 5.2 together with the time corresponding to each stage. There is an additional stage that includes the reduction of the water level in the fill to +0 elevation and fill removal to elevation -3.5 m.

Table 5.2. Description of construction stages of Phase 2.

Description	Stage	Time interval (days)
Initial K_0 phase	0	-
Trench excavation	1	60
Rubble mound and rock fill sea side	2	105
Caisson anchoring and filling	3	30
Rock fill	4	20
Rock fill and hydraulic fill -12.5 m	5	10
Rock fill and hydraulic fill -9 m	6	10
Hydraulic fill -6 m and dike over the caissons	7	10
Hydraulic fill -3 m	8	20
Hydraulic fill 0 m	9	25
Hydraulic fill +1.5 m	10	30 (up to failure)
Reduction of water level to +0 and fill -3.5 m (a day after Phase 1 failure)	11	15

As established in Phase 1 simulation, the stage 0 of analysis considers only the natural soil in order to establish the initial conditions of the analysis. Displacements generated during stage 0, 1, 2 and 3 are reset to zero so that they do not interfere with the displacements computed during construction. Afterwards, the quay wall is constructed step-by-step following the actual construction sequence. For all phases, consolidation analyses are performed that incorporate the hydromechanical interactions and the time-dependent dissipation of pore pressures over the period considered. The stage (10) of the calculation -"up to failure"-, corresponds to a period of 30 days before the failure.

5.2.5. Results of Phase 2 analysis

As described previously, the numerical analyses performed incorporate the available information concerning soil behaviour, material parameters, geometry, hydraulic boundary conditions and construction history.

5.2.5.1. Analysis before failure

The analysis supplies data regarding to the evolution of water pressures and deformations. As in Phase 1, topographic surveys were used to provide caissons displacements. The comparison between observed (blue lines) and computed (red line) settlements of Phase 2 caissons during construction are presented in Figure 5.4. The agreement is quite good.

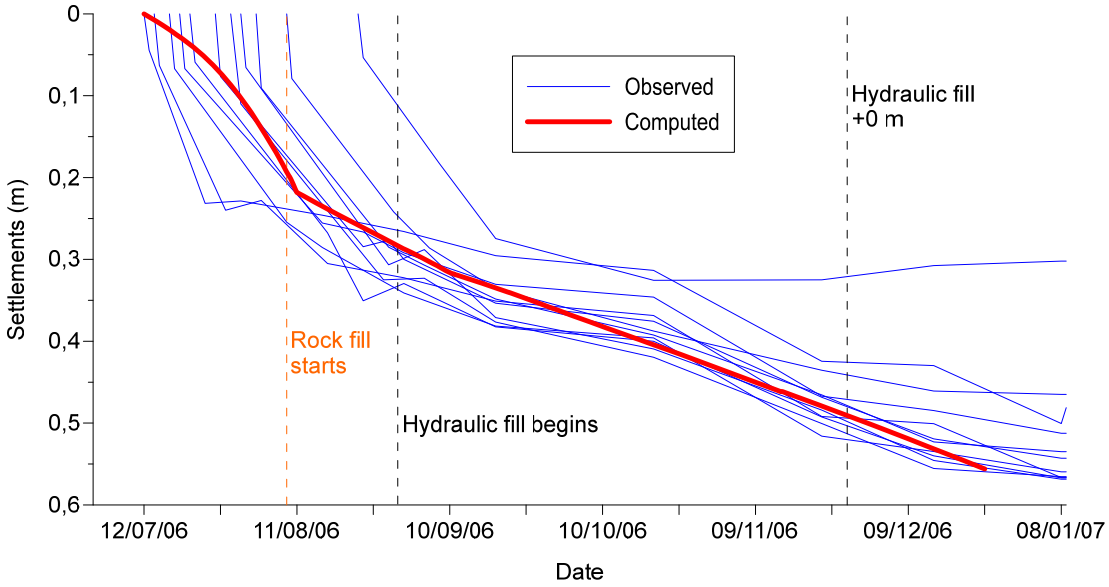

Figure 5.4. Caissons settlements along the quay wall during construction of Phase 2.

The computed contours of excess pore pressure during stage 10 -just before failure of Phase 1-, and 11 -after failure of Phase 1-, are presented in Figure 5.5 and Figure 5.6. At stage 10, as occurred in Phase 1, maximum excess pore pressures are reached in natural ground below the hydraulic fill, although a secondary peak is noted under the caissons. Lower values of EPP (around 20 kPa) have been computed in the hydraulic fill close to quay wall due to the presence of the rock fill. In contrast, a significant reduction on EPP is visible in stage 11. It is important to note that, now, the maximum computed EPP in the hydraulic fill is negligible.

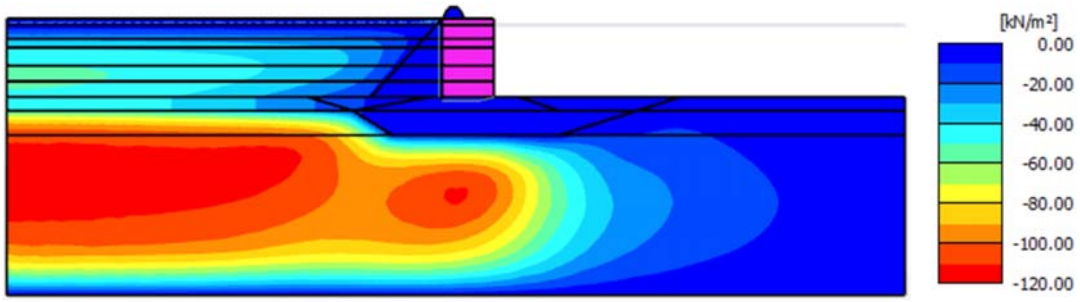

Figure 5.5. Contours of excess pore pressure at the stage before failure, Stage 10.

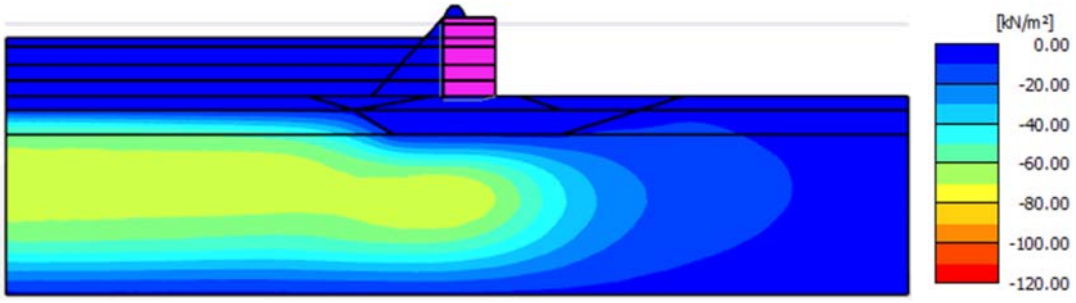

Figure 5.6. Contours of excess pore pressure at the stage after reduction of water level to +0 and fill to elevation -3.5 m, Stage 11.

5.2.5.2. Stability analysis

A stability check has been performed for Stage 10. As indicated above, the hydraulic fill is modelled using the CASM constitutive law. In this way, a potential for fill liquefactions is included in the analysis. This is the same hypothesis made for Mechanism 1 (Chapter 4) in Phase 2. In Phase 2, there were not embankments being constructed as in Phase 1; so, Mechanism 2 is not applicable.

As described in Chapter 4, FoS calculation was performed following the manual phi-c reduction method (Appendix A). The computed value of FoS for Stage 10 -once failure of Phase 1 had occurred-, is 1.12. The displacement contours presented in Figure 5.7 indicate that a deep failure has been obtained. It is interesting to realise that the 25% of the failure surface go through the hydraulic fill. Although it has been assumed that the hydraulic fill was liquefied, the quay wall failure mechanism of Phase 2 involves mainly the natural ground.

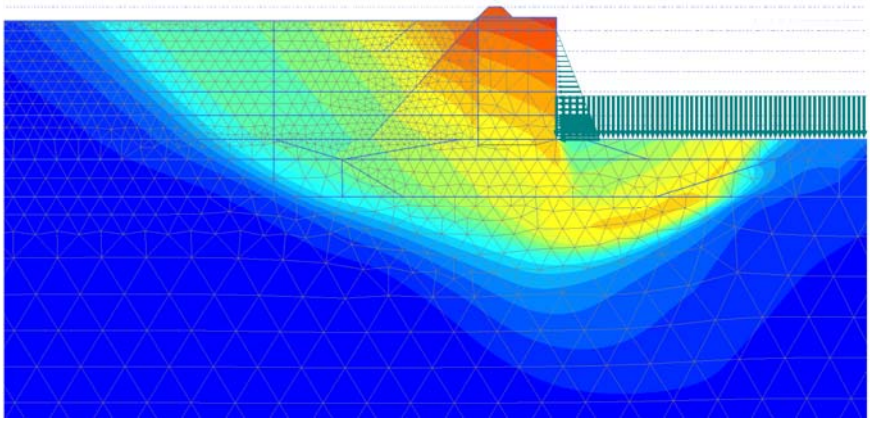

Figure 5.7. Contour of stage displacements in FoS analysis of Stage 10, FoS=1.12.

Further insight into quay wall stability is gained, if the same analysis is performed assuming that the hydraulic fill has not liquefied, i.e. the undrained shear strength is c_u/σ'_v = 0.25. Under those conditions, the value of FoS is 1.25. Stability is marginal only if the hydraulic fill liquefies.
These results are reinforced by the simulation results using the initial hypothesis of soil liquefaction from the beginning of construction presented in Appendix C.2.

5.3. Soil improvement

The results of the analyses presented in the previous section showed that the Phase 2 quay stability was rather precarious in case of hydraulic fill liquefaction. It was thus necessary to undertake soil improvement procedures to increase the resistance of the fill to liquefaction. A number of different techniques were used as described below.

There are numerous procedures for soil improvement (Phear & Harris, 2008), a number of them are in fact suitable for liquefaction mitigation. For instance, Yang (2002), Carrera et al. (2011), Castro (1969), Yamamuro & Lade (1998) and Fourie & Tshabalala (2005) argued that some soil improvement methods could avoid flow liquefaction due to enhanced drainage or improvement of the undrained shear strength. In this context, case histories or experiments of soil improvement used for liquefaction mitigation have been reported, e.g. Priebe (1989) & (1991), Seed and Booker (1977), Baez and Martin (1995), Boulanger et al., (1998), Andrus and Chung (1995), Seed et al. (2003), Yasuda et al. (1996), Adalier and Elgamal (2004) and Simpson et al. (2008). They involve a variety of procedures: (i) compaction grouting, (ii) permeation grouting, (iii) jet grouting, (iv) in-situ or deep soil mixing, (v) compaction with vibratory probes, (vi) dynamic consolidation, (vii) compaction piles, (viii) deep densification by blasting, (ix) drains (gravel drains, sand drains, prefabricated strip drains), (x) surcharge pre-loading or (xi) structural fills. The cases of liquefaction mitigation by soil improvement are more limited in the case of fine grained soils: (i) stone columns -Adalier et al. (2003) for non-plastic silts-, (ii) dynamic compaction, (iii) permeations techniques and (iv) electrokinetic injection of grouts, Thevanayagam and Martin (2002).
New soil improvement techniques have been developed for soil liquefaction mitigation, although during Prat quay remediation project many of these techniques were not readily available. Examples are: (i) nanomaterials as colloidal silica (Hamderi and Gallagher, 2015), bentonite (Santagata et al., 2014; Ochoa-Cornejo et al. 2014; Drnevich et al., 2014; Mohtar et al. 2008 and 2012) or laponite (p.e. Huang and Wang, 2016), (ii) short synthetic fibers (p.e. Karakan et al., 2018; Liu et al., 2011; Ibraim et al., 2010; Noorzad and Amini, 2014) and (iii) Recycled materials (p.e. Bahadori and Manafi, 2015; Bahadori and Farzalizadeh, 2016; Kaneko et al., 2013; Hazarika et al., 2010; Otsubo et al., 2016), (iv) Biological materials (p.e. DeJong et al., 2013; Xiao et al.,,2018), (v) Chemical grouting (p.e. Porcino et al., 2015), Microfine cement (p.e. Yao et al. 2018; Pantazopoulos & Atmatzidis, 2012), (vi) Partial saturation method (p.e. He et al., 2013; Yegian et al., 2007), also other materials as p.e. biochar (Pardo et al., 2019).

In spite of this large number of soil improvement methods, three key factors limited the feasibility of soil improvement implementation in Prat quay Phase 2: (i) the material is mainly fine-grained hydraulic fill, (ii) instability of the quay wall has to be avoided and (iii) a large surface area (540000 m^2) had to be treated. Finally, three methods were selected: stone columns by vibro-replacement, prefabricated strip drains and surcharge pre-loading. The objective was twofold: to increase resistance against liquefaction and to increase the undrained shear strength of the hydraulic fill and the natural ground.

Installation of stone columns by vibro-replacement (Figure 5.8) can reduce or remove the liquefaction potential: (i) by increasing the density of surrounding soil, (ii) by allowing drainage for the control of pore pressures, (iii) by introducing stiff elements (stone columns) which can potentially transmit higher stresses causing reduction in stress levels in the surrounding soil (Priebe, 1989 and 1991), and (iv) by providing a deformation restricting effect.

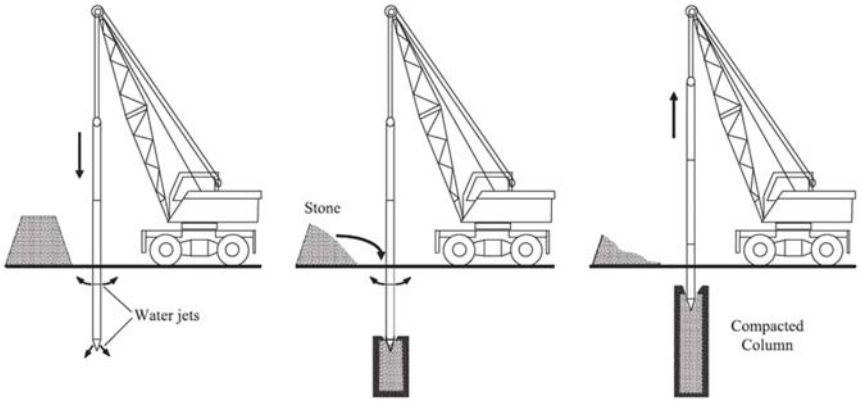

Figure 5.8. Gravel drain construction by vibro-replacement, Adalier and Elgamal (2004).

The application of prefabricated vertical drains (PVD) provides considerably shortened horizontal drainage paths for pore water flow, thereby accelerating soil consolidation (Hansbo, 1981). Prefabricated strip drains usually consist of a core of plastic and a filter sleeve or jacket of nonwoven geotextile, paper, fibrous material, or porous material, Yeung (1997). Some designs include a loose sleeve enclosing the core while others are fixed to the core. Detailed evaluations of laboratory and field performance of different types of prefabricated vertical drains are readily available in the literature (Atkinson and Eldred 1981; Davis and Humpheson 1981; McGown and Hughes 1981; Nicholson and Jardine 1981; Hansbo 1983; Long and Hover 1984; Robertson et al. 1988; Holtz et al. 1991; Kamon et al. 1992; Long and Fontaine 1992; Long et al. 1994; Indraratna and Redana, 2000; Bergado et al., 2002; Arulrajah et al. 2004; Arulrajah and Bo, 2008 and Almeida et al. 2010).

Precompression is the deliberate act of compressing the ground under an applied pressure prior to placing or completing the permanent load. It is described as surcharging where the stress intensity from the preloading (or precompression) is greater than the intensity from the permanent loading

(Mitchell and Jardine, 2002). Since the earliest recorded uses of pre-compression ground improvement in the UK (Tomlinson, 1956), this type of improvement has been carried out in civil works around the world. In this context, a detailed study for improving fine-grained dredged material after hydraulic fill deposition using consolidation was described in Bishop and Vaughan (1972). They clearly demonstrated the suitability of a hydraulic clayey fill as construction material. An appropriate case to prove the efficiency of the surcharge pre-loading was provided by the pre-loading embankments located in two areas close to Prat quay esplanade presented in Alonso et al. (2000) and (2010). They described the capabilities of well instrumented preloading trials: (i) to investigate consolidation in deltaic soils and (ii) to determinate the variation of secondary settlement rates with the OCR.

In practice, it is frequent to use PVD, horizontal drainage layer and surcharging preloading together to reduce the time of consolidation. Thus, the excess pore-water pressures, created by preloading, lead to preferential flow in the horizontal direction towards the PVD and along it vertically into the permeable drainage layers, i.e. Holtz (1987), Bergado et al. (2002) and Ma et al. (2011), as shown in Figure 5.9.

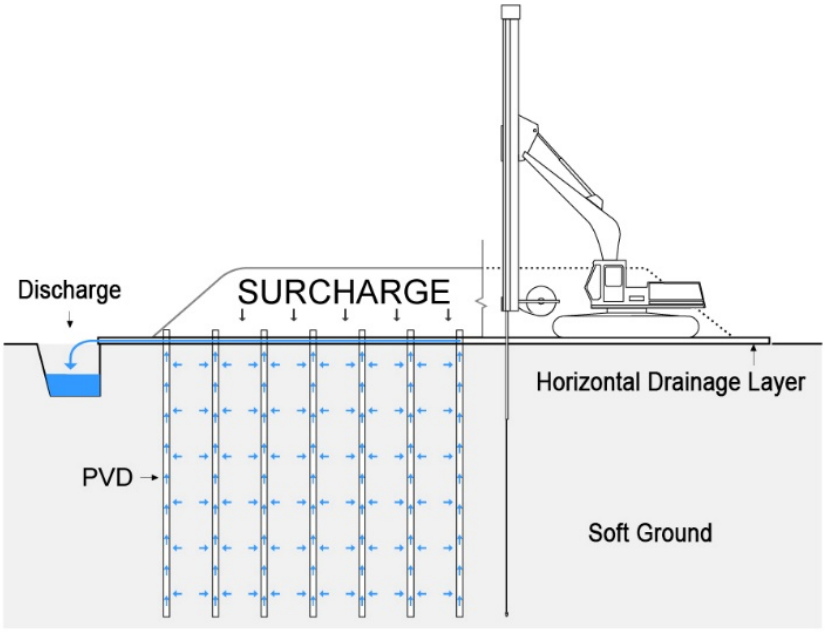

Figure 5.9. Improvement using PVD, horizontal drainage layer and surcharging preloading, source greencosmos.com.

This leads to an increase in soil density, undrained shear strength (Ladd et al., 1972 and Lad, 1991) and the rate of pore pressure dissipation. All these effects contribute to soil liquefaction mitigation.

The layout of the prefabricated strip drains, horizontal drainage layer, surcharge pre-loading and the zone improved with stone columns is shown in Figure 5.10. It was obtained from two studies out of the scope of this PhD thesis:

(i) A trial embankment in the storage area of Phase 2 (latterly shown in Figure 5.12.) to obtain a prelaminar idea of the effect of the proposed soil improvement (Alonso et al. 2008 and Gens et al. 2009b).

(ii) Different calculations to reach an optimal design for stone columns treatment and spatial arrangement of surcharge preloading (Gens et al., 2009a).

The stone columns by vibro-replacement were implemented in the backfill of the quay-wall, limited by the rock fill, and up to 20 m inland. The designed columns were 30 m long -or until to reach the rock fill-, and 0.5 m diameter, placed in a triangular grid with a spacing of 2 m. From the inland limit of stone columns to the end of the esplanade, 30 m long PVD were installed in a square grid with 1.5 m spacing. The designed preloading is composed by different embankments heights in different areas of the quay: quay line 3 m, manoeuvring 4.5 m and storage areas 8 m, it will be described later in Chapter 5.6.3. In addition, the preloading is composed by 0.5 m thick horizontal drainage layer, a water discharge system and geo-membrane sheet between terrestrial fill and drainage layer to avoid its contamination.

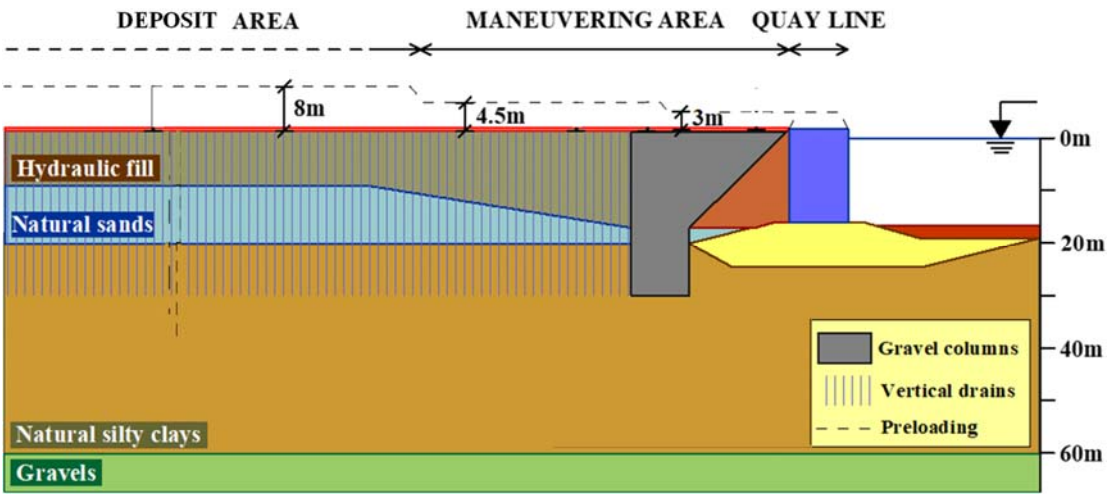

Figure 5.10. Cross section of Phase 2 including soil improvement measures, modified from Tarragó et al. (2012).

The improvement work was carried out in the following chronological order: (i) an initial land levelling, (ii) installation of PVDs, (iii) sequential placing of preload embankments and installation of stone columns.

5.4. Monitoring system

After the Phase 1 failure, the monitoring system of Phase 2 was significantly reinforced. In addition to providing useful information on the behaviour of the quay, the instrumentation was aimed towards the use of the observational method (Peck, 1969) to ensure a safe completion of the construction.

The monitoring system included inclinometers, clinometers, piezometers, sliding extensometers and settlement plates. These instruments were implemented in two stages: (i) just after the failure of

Phase 1 quay and (ii) once the esplanade had been levelled. The installed instrumentation is presented in the cross-section shown in Figure 5.11. Topographic markers were installed at the four top corners, of all the caissons together with a clinometer on the seaside face in order to control movements. Open piezometers were installed in the rock fill at the back of the every caisson to record a variation of pore pressures as a result of fill liquefaction. Chains of fixed inclinometers down to an elevation of -60 m, were installed in alternating caissons, together with chains of settlement gauges and chains of piezometers down to an elevation of -40 m.

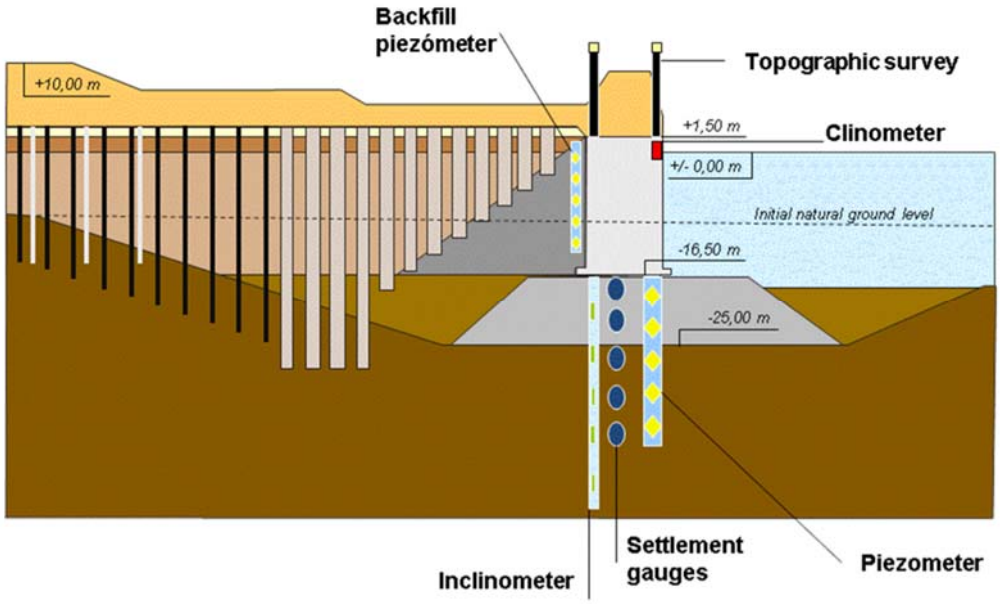

Figure 5.11. Cross section of Phase 2 with soil improvement measures and monitoring system, modified from Tarragó et al. (2012).

A general view of the monitoring system layout is presented in Figure 5.12. The esplanade instrumentation consisted of: (i) settlement plates with a grid spacing of 80 m, (ii) piezometers chains placed at distances of 30 m from each other, (iii) piezometers chains and sliding extensometers separated 160 m. Each piezometer chain had 4 piezometers and reached down to an elevation to -40 m the same as the sliding extensometers. The Phase 2 instrumentation also incorporated the monitoring system used in the performance of the trial embankment.

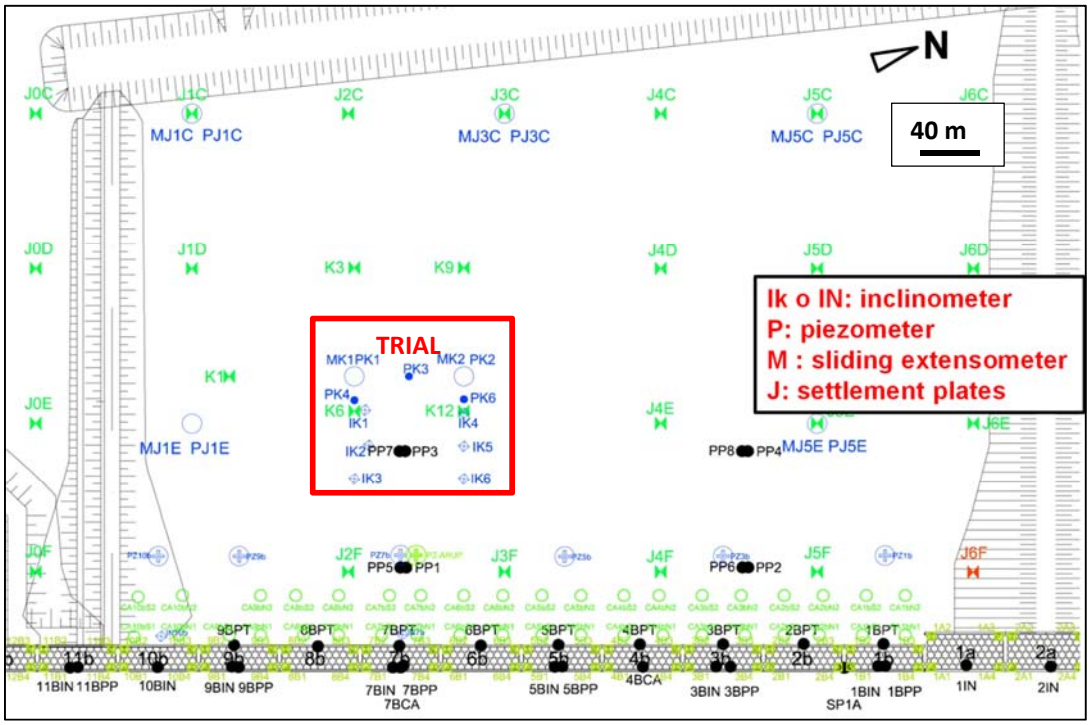

Figure 5.12. Layout of monitoring system of Phase 2, modified from APB (2008).

Monitoring results were fully described in Tarragó et al. (2012). It is important to note the results consistency according to improvement sequence.

5.5. *Evaluation of hydraulic fill improvement*

Soil improvement performed to enhance the resistance of the hydraulic fill was a key aspect towards completing the construction of Phase 2 safely. To assess the change in the state of the hydraulic fill, two additional site investigations were carried out before and after the soil improvement measures. The evaluation of the results obtained from these additional site investigations are presented in following sections. The degree of improvement is assessed in terms of undrained shear strength increase and of flow liquefaction criteria.

5.5.1. *Additional site investigations*

After the failure and subsequent land levelling to elevation +2 m, a site investigation based on more than 50 CPTu tests was carried out before any soil improvement was performed. The site investigation carried out after soil involved drilling of boreholes and the performance of 40 CPTu tests. On purpose, some of the new CPTu tests were placed in the same locations as CPTu tests performed before soil improvement. The distribution of CPTu tests performed before and after soil improvement is presented in Figure 5.13.

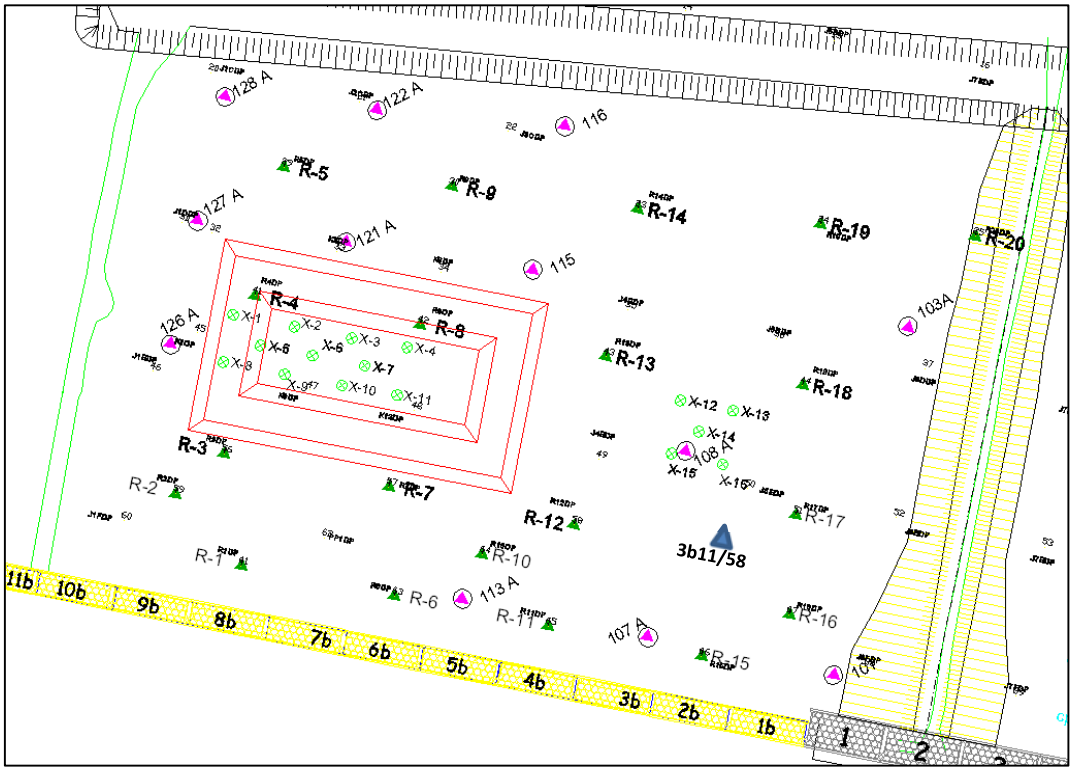

Figure 5.13. Location of additional CPTu tests in Phase 2 esplanade, APB (2008).

Results from two representative CPTu tests (3b11 and r5) before and after soil improvement are presented together in Figure 5.14 and Figure 5.15. The zones corresponding to dumped fill, hydraulic fill and natural ground are indicated. Only the results concerning the hydraulic fill are discussed here.

It is apparent that soil improvement was effective in the hydraulic fill. A large increase of cone resistance is obtained whereas sleeve frictions are also much higher than before. Pore water pressures generated in the hydraulic fill, u_2, also show an increase in some cases responding to the higher cone resistance.

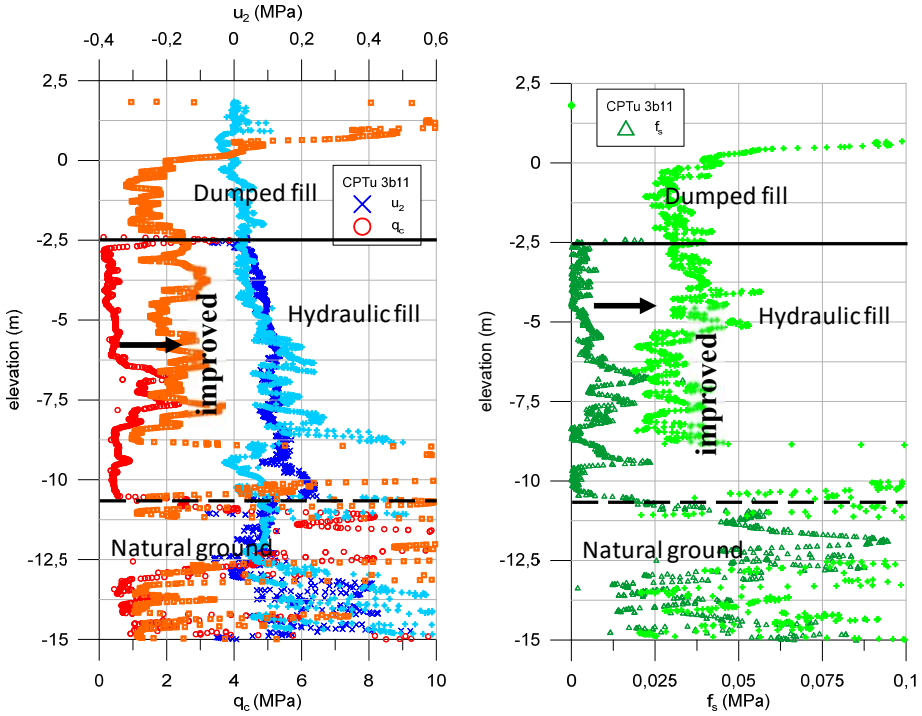

Figure 5.14. CPTu results from 3b11 before and after preloading surcharge.

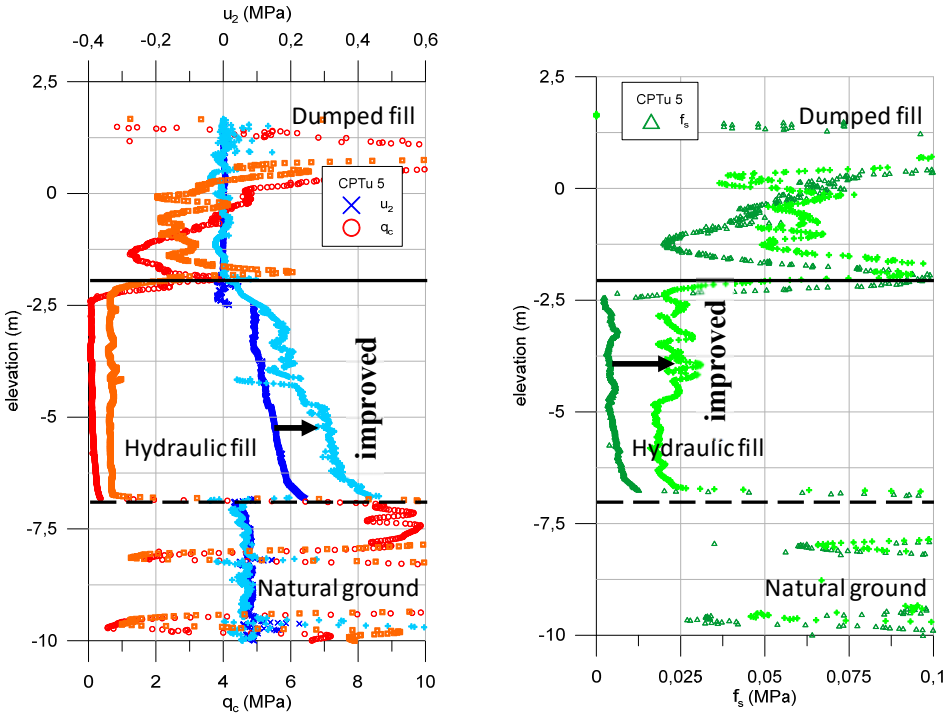

Figure 5.15. CPTu results from r5 before and after preloading surcharge.

5.5.2. Hydraulic fill strength

Representative profiles of undrained shear strength for the hydraulic fill before and after soil improvement are shown in Figure 5.16, Figure 5.17 and Figure 5.18. All records are above 0.25 σ'_v

which is consistent with an overconsolidation state induced by preloading, Ladd (1991). The very low values of undrained shear strength in some zones of the hydraulic fill before soil improvement reflect the brittle liquefiable nature of the material. It is noteworthy, that those very low values have disappeared after the soil improvement measures.

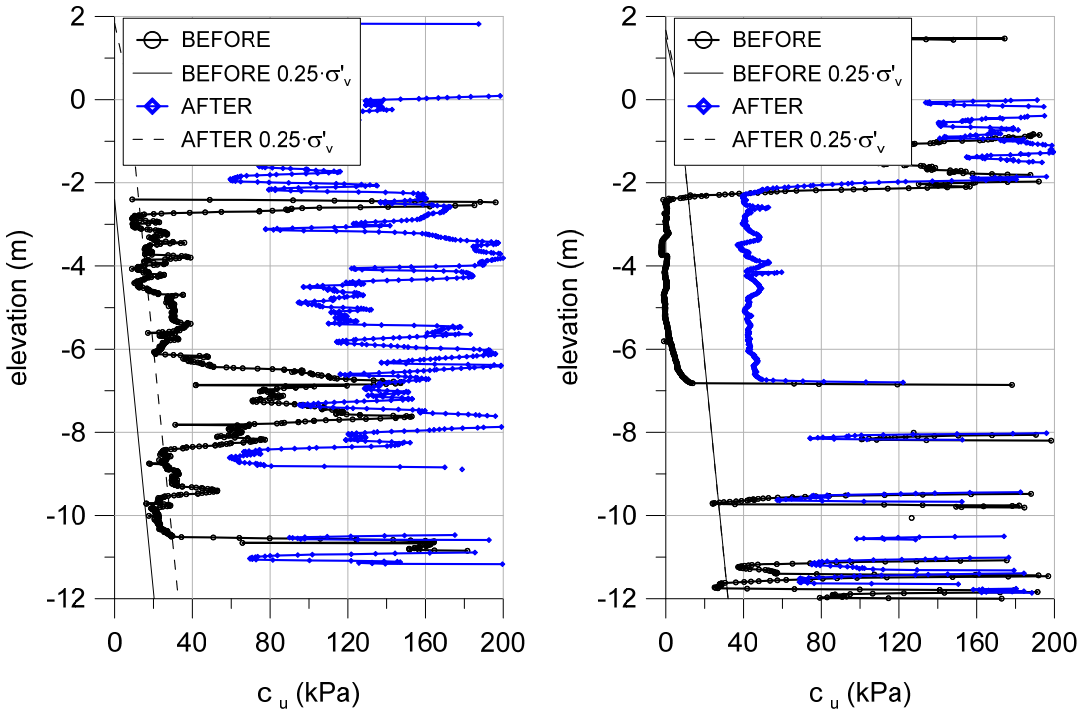

Figure 5.16. CPTu results from 3b11 (left) and r5 (right) before and after preloading.

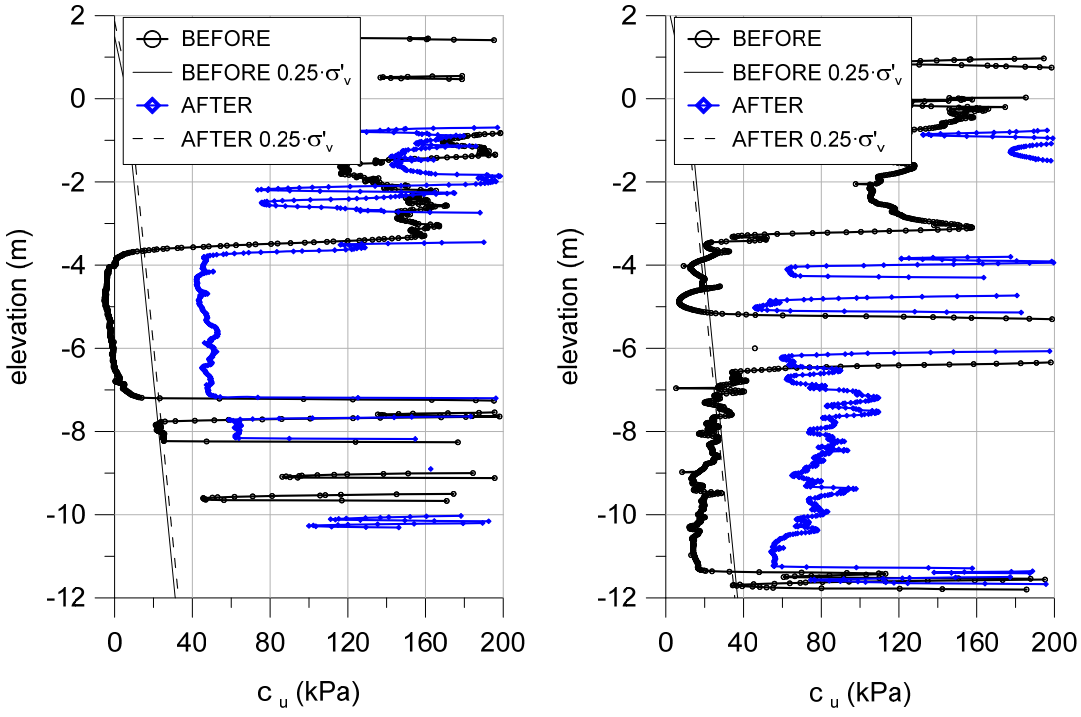

Figure 5.17. CPTu results from r9 (left) and r2 (right) before and after preloading.

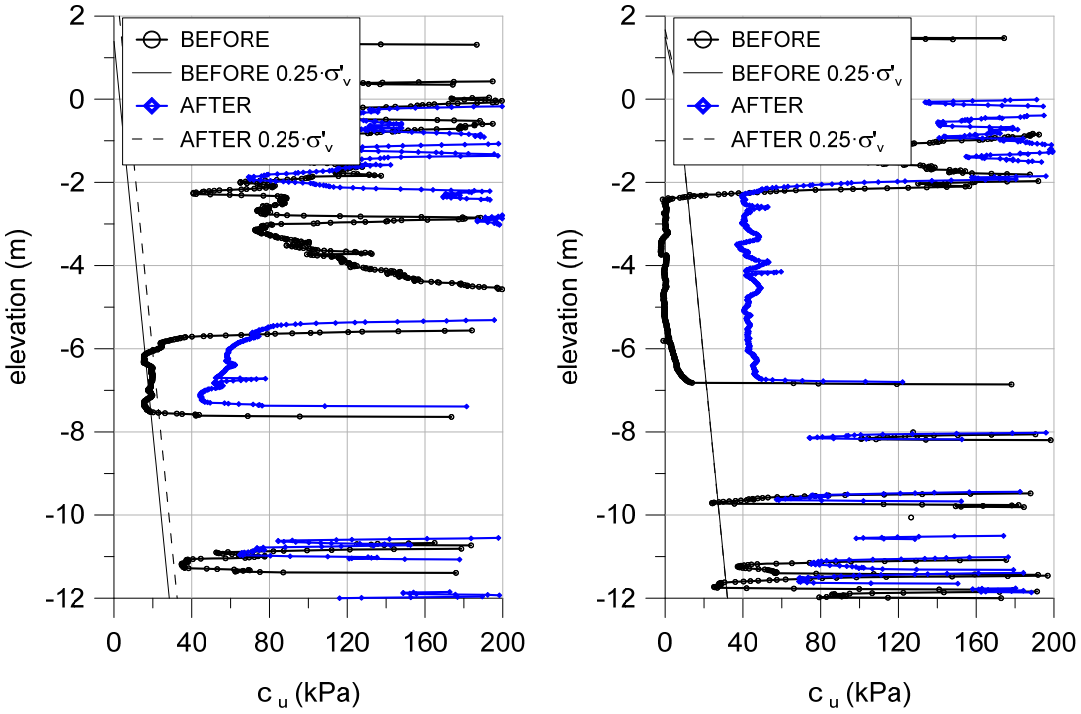

Figure 5.18. CPTu results from x2 and x6 before and after preloading.

5.5.3. *Application of flow liquefaction criteria*

The improvement in liquefaction resistance can be assessed more readily applying well-known flow liquefaction criteria. The same ones already applied in Chapter 3 -Bray et al. (2004), Plewes et al. (1992), Robertson (2016) and Mayne (2019)-, will be applied now.

5.5.3.1. *Bray et al. (2004) criterion*

The values of plasticity index and water content/Limit Liquid of a number of specimens extracted from the hydraulic fill after soil improvement are plotted in Figure 5.19. For the state of the fill before improvement, results from settling column samples -from Figure 3.28 in Chapter 3-, are used. It can be noted that the results without soil improvement lie in the moderately susceptible zone. In contrast, after soil improvement, the w_c/LL values have reduced and the corresponding points move to non-susceptible zone.

The existence of sand layers in the hydraulic fill limited the representatively of the results with respect to this criterion. There were non-plastic specimens (PI=0) that have not been represented in the plot.

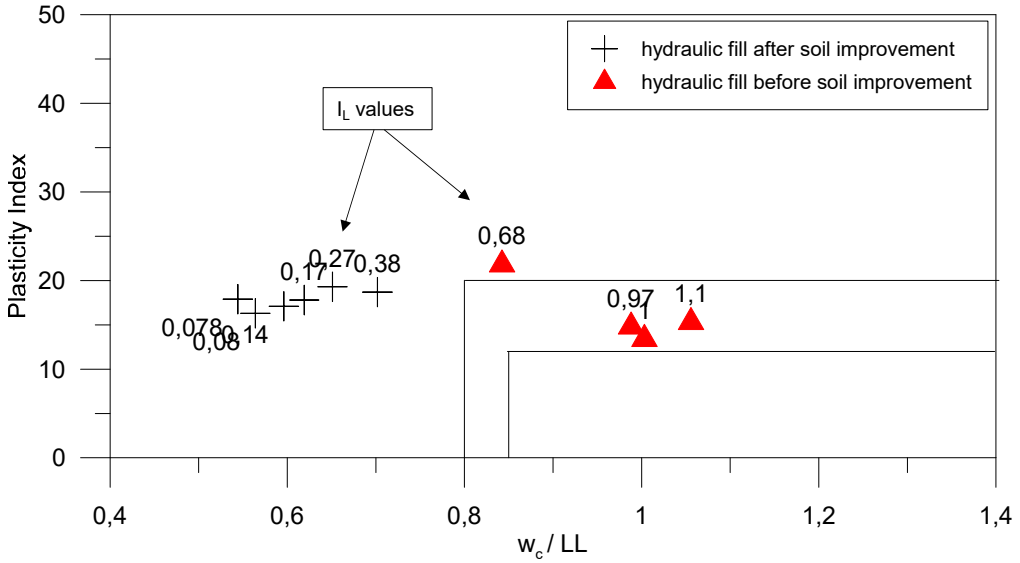

Figure 5.19. Liquefaction screening (Bray et al., 2004) of fill specimens before and after soil improvement, I_L values are indicated for each specimen

The results of some simple direct shear tests from hydraulic fill specimens of which soil index were presented above (before soil improvement). They are included in Figure 5.19 together with the results obtained after soil improvement. The values of $c_{u\,peak}$ and of remoulded undrained shear strength (or $c_{u\,SS}$), computed from the I_L according to (Leroueil et al. 1983) before and after soil improvement are represented in Figure 5.20. In addition, the brittleness indexes are calculated, and included in Figure 5.20. It is apparent that, soil brittleness was eliminated by soil improvement.

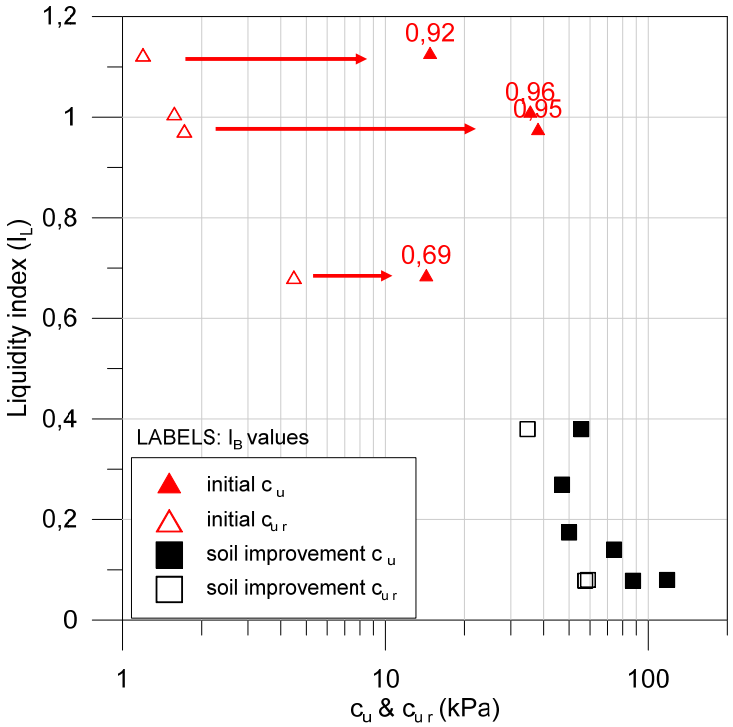

Figure 5.20. Peak and remoulded undrained shear strength vs. liquidity index before and after soil improvement. Remoulded strengths estimated according to Leroueil et al. (1983)

5.5.3.2. CPTu criteria

The criteria of Plewes et al. (1992), Robertson (2016) and Mayne (2019) have been applied to a representative set of CPTu observations. The results are plotted side by side in Figure 5.21 to Figure 5.26, in which Figures (a) corresponds to tests performed before soils improvement, and (b) corresponds to tests performed after soil improvement.

The Plewes criterion results indicate that, after soil improvement, the state parameters are lower than -0.05 or at least close to that value although there are three profiles (
Figure 5.22, Figure 5.24 and Figure 5.25) in which ψ reduction is more evident.
Although a significant increase of Q_{tn} values were obtained after soil improvement, using Robertson's chart, many points remain on the contractive region close to normally consolidated line after soil improvement (Figure 5.21 to Figure 5.24).
Profiles of YSR before improvement from Mayne criterion show that contractive behaviour is restricted to localized zone in some profiles (Figure 5.22 to Figure 5.24 and Figure 5.26). In contrast, after soil improvement, the criterion indicates that dilative soils are present over the full depth of the profile. It is important to note that YSR_{CPTU} after the improvement is generally higher than 10 and it is not represented in the plot.

As expected, results of the different criteria are not coincident. Whereas Plewes and Mayne criteria yield similar results, Robertson criterion seems to be more conservative. The beneficial effects of the soil improvement can be clearly seen in the comparison in the F-Q chart between the CPTu tests performed before and after preloading shown Figure 5.27. It can be noted that the points in the contractive area (SC-TC-CC) zone have moved much closer to the contractive/dilation boundary. Also, only a few points remain in the sensitive contractive clays (CCS) zone. It is also worth remembering that a contractive behaviour is a necessary but not a sufficient condition for undrained brittle behaviour.

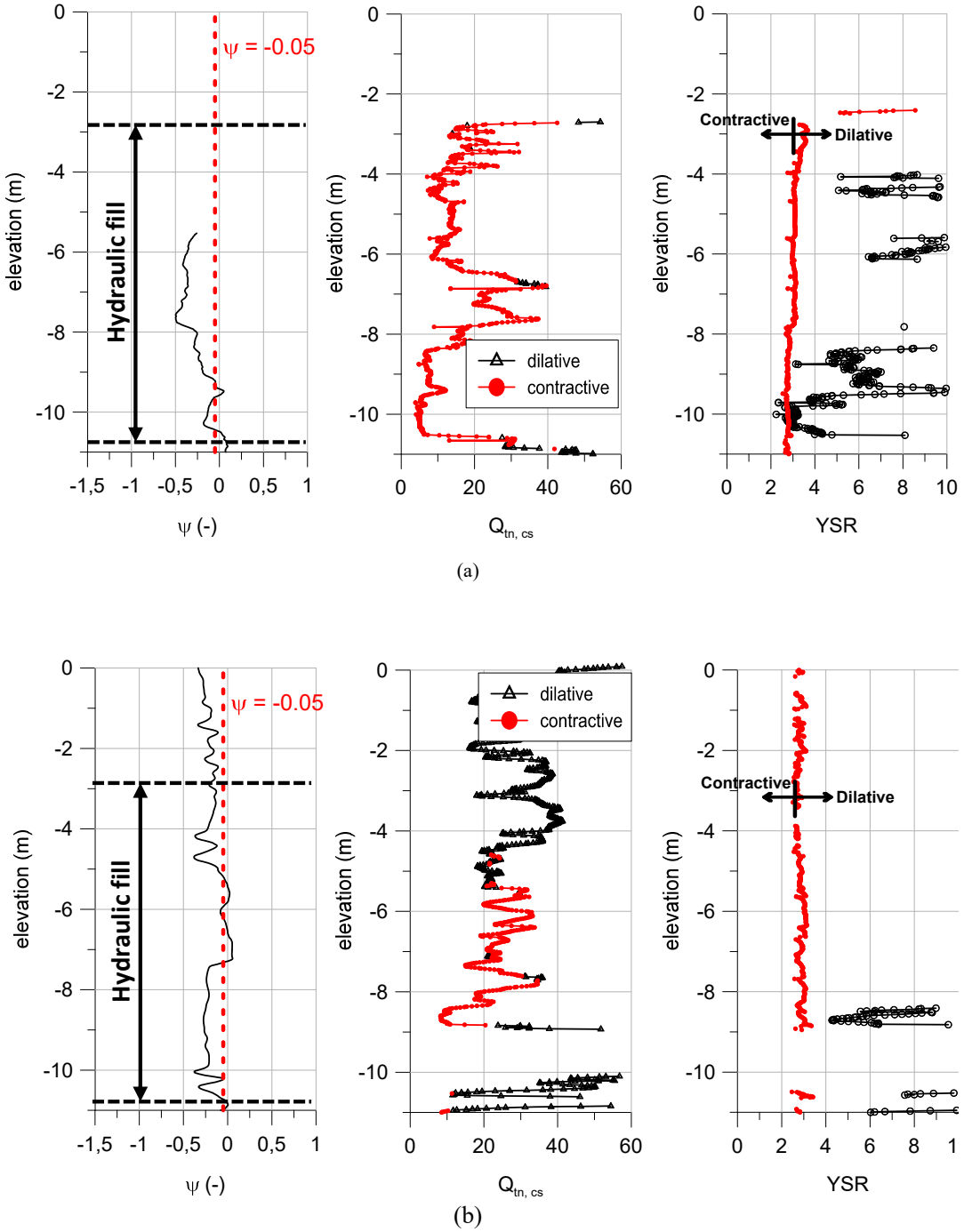

Figure 5.21. Plewes criterion (ψ), Robertson criterion (Q_{tn}) and Mayne criterion (YSR) for CPTu test 3b11, (a) before and (b) after soil improvement.

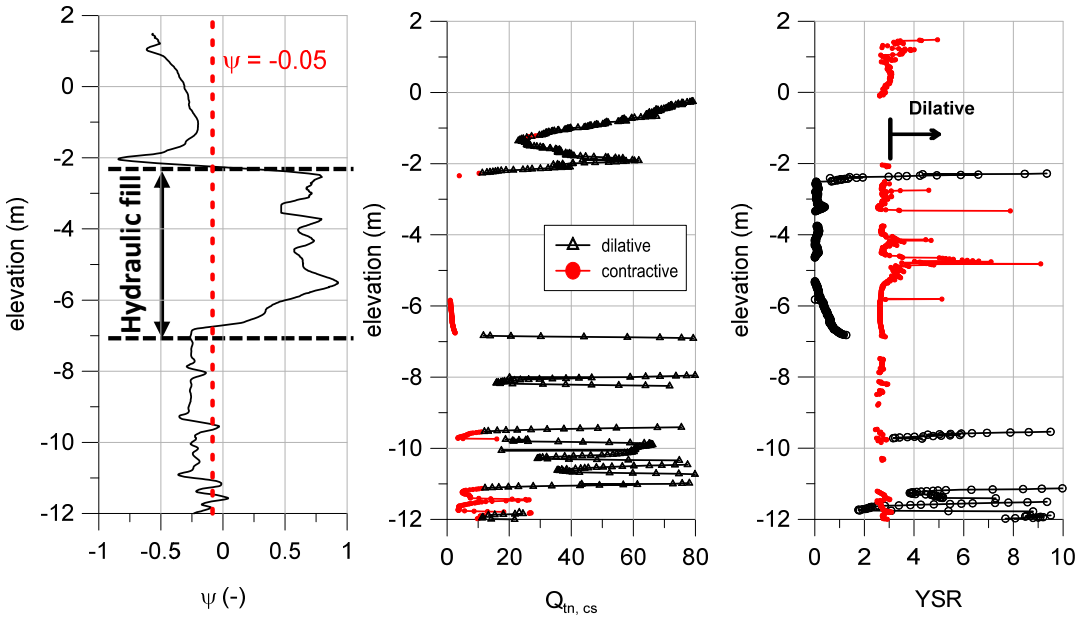

(a)

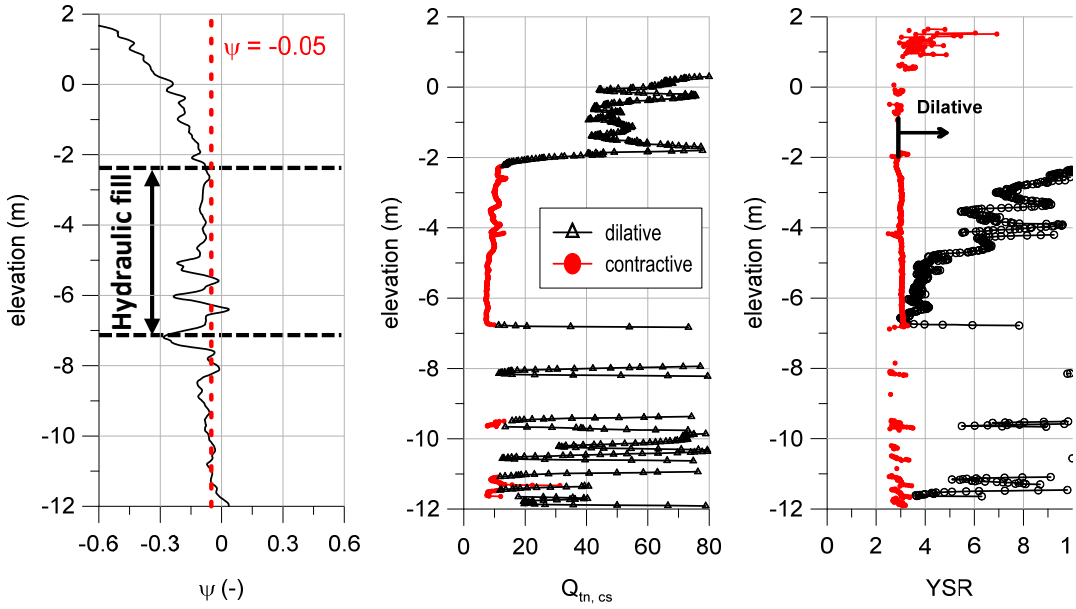

(b)

Figure 5.22. Plewes criterion (ψ), Robertson criterion (Q_{tn}) and Mayne criterion (YSR) for CPTu test r5 (a) before and (b) after soil improvement.

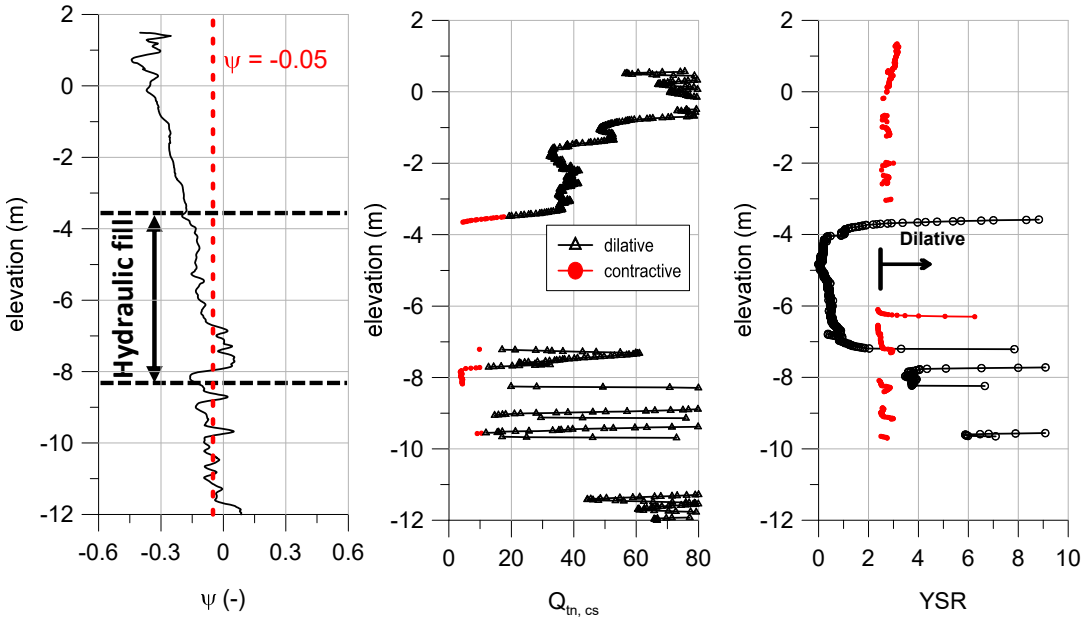

(a)

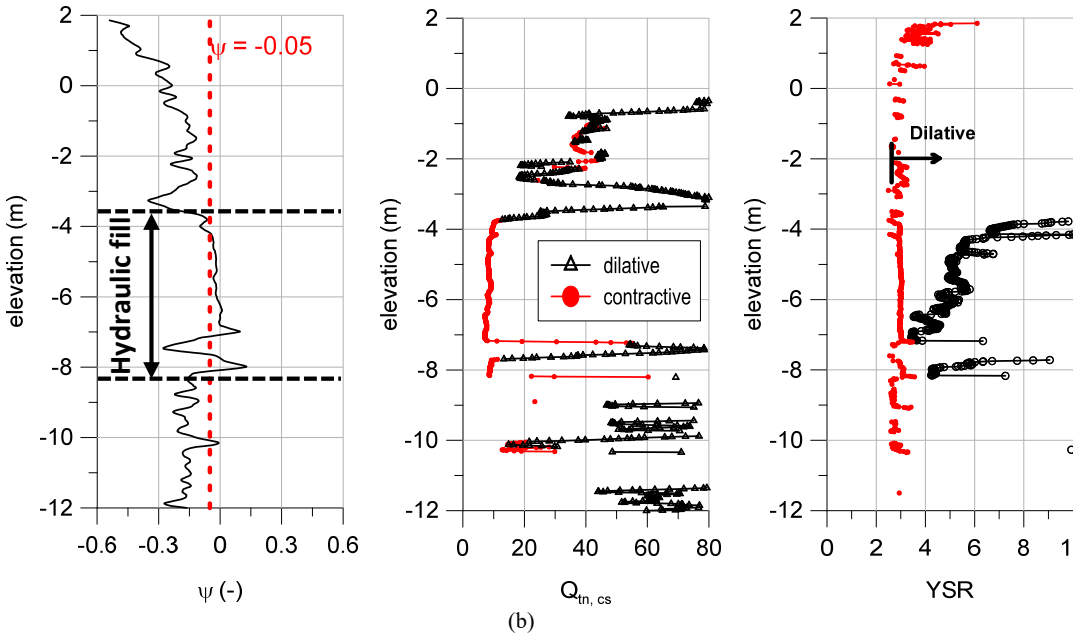

(b)

Figure 5.23. Plewes criterion (ψ), Robertson criterion (Q_{tn}) and Mayne criterion (YSR) for CPTu test r9, (a) before and (b) after soil improvement.

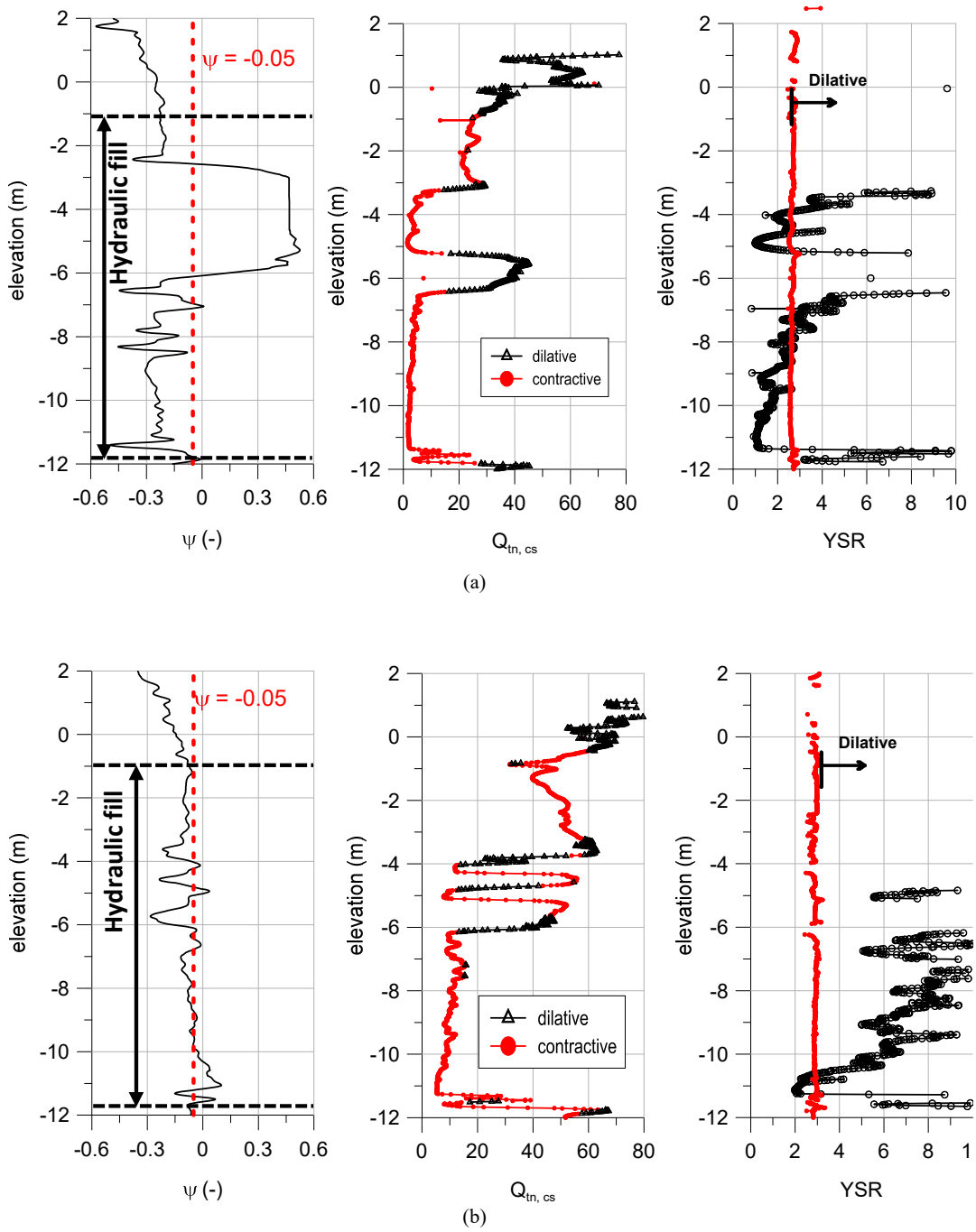

Figure 5.24. Plewes criterion (ψ), Robertson criterion (Q_{tn}) and Mayne criterion (YSR) for CPTu test r2, (a) before and (b) after soil improvement.

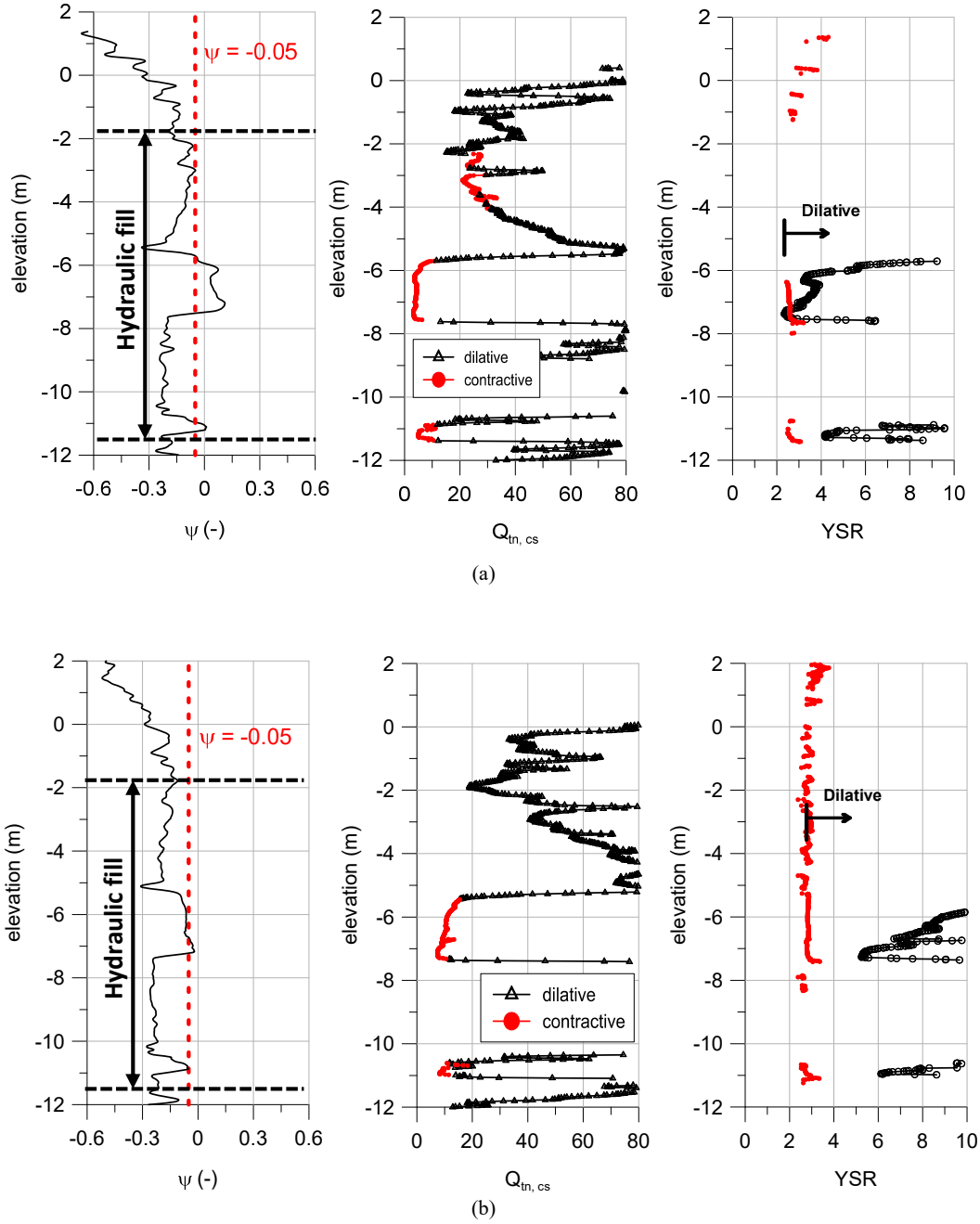

Figure 5.25. Plewes criterion (ψ), Robertson criterion (Q_{tn}) and Mayne criterion (YSR) for CPTu test x2, (a) before and (b) after soil improvement.

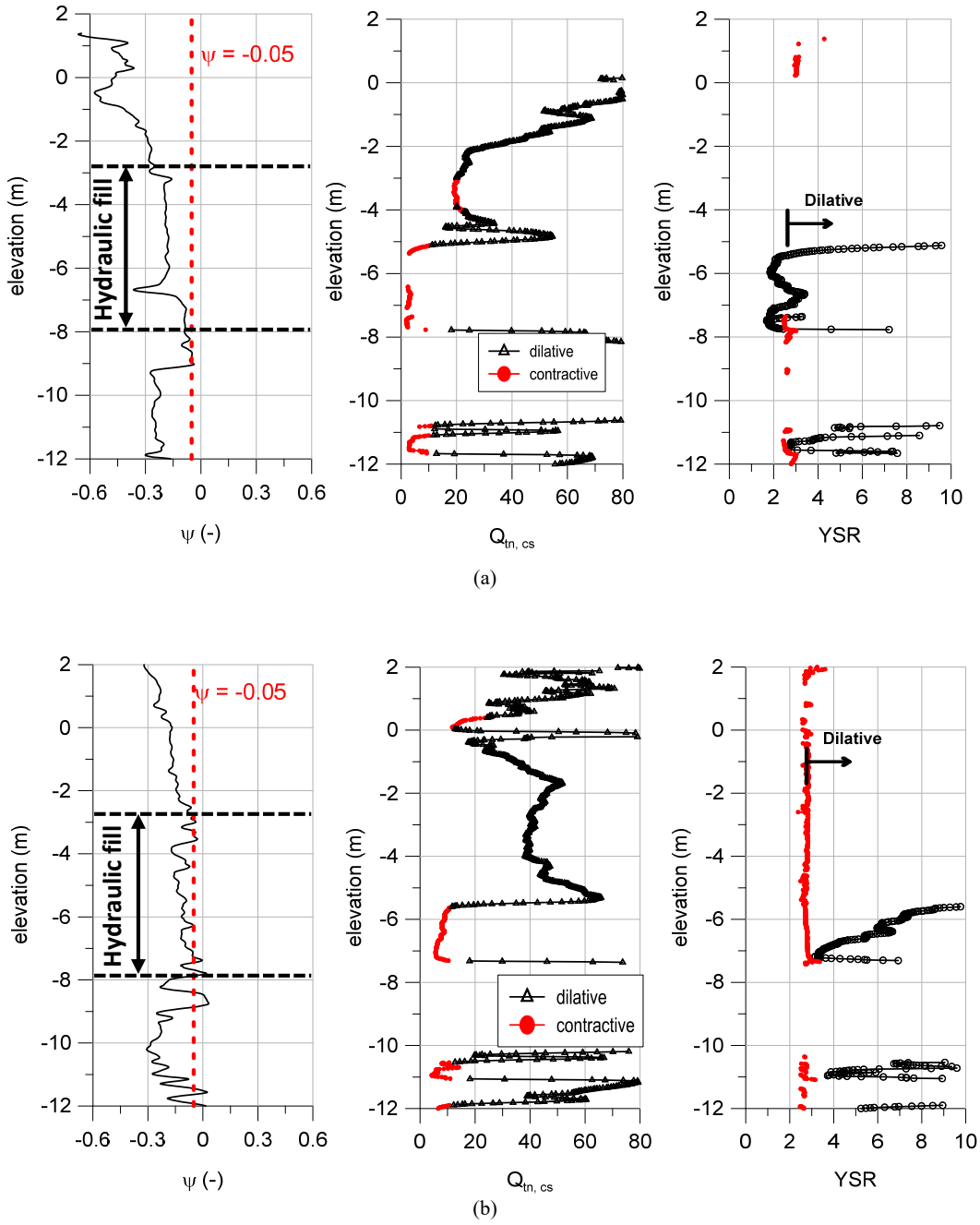

Figure 5.26. Plewes criterion (ψ), Robertson criterion (Q_{tn}) and Mayne criterion (YSR) for CPTu test x6, (a) before and (b) after soil improvement.

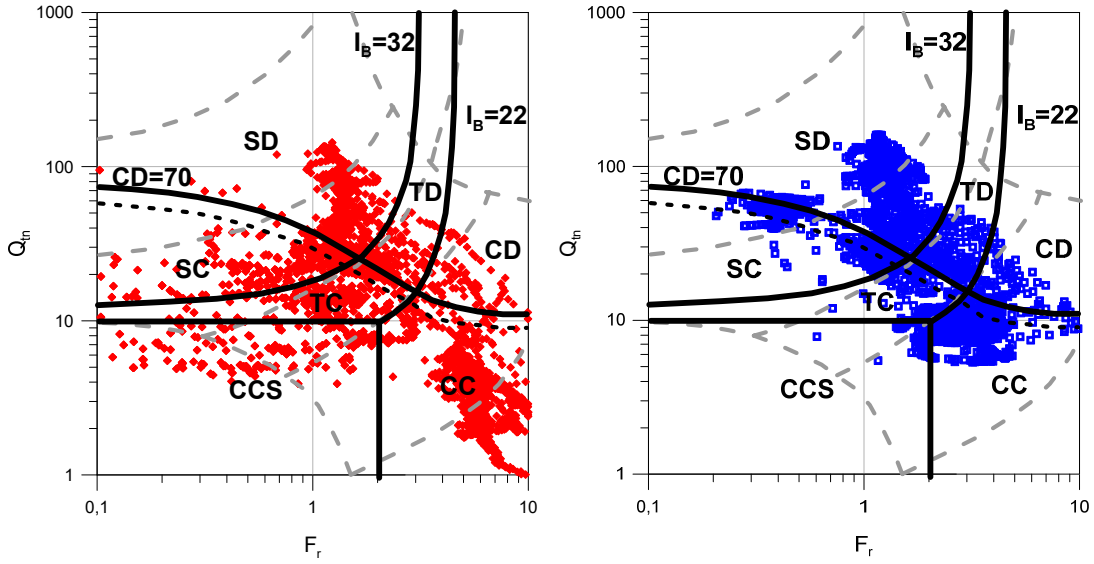

Figure 5.27. Application of Robertson criterion before (left) and after (right) soil improvement.

5.6. Analysis of Phase 2 after soil improvement

Firstly, the design of the construction process with observational method during soil improvement implementation in Phase 2 was originally performed with the numerical analysis presented in Appendix C.3. Although hydraulic fill had a constrained volume after emptying (Stage 11), flow liquefaction had to be avoided during soil improvement. As occurred in Appendix C.2, the initial hypothesis of soil liquefaction was again established in the analysis. Thus, hydraulic fill was under liquefied state from the beginning of construction. However, according to tests results, liquefaction criteria results and soil behaviour during construction, the removing of flow liquefaction potential of the hydraulic fill can be accepted after the soil improvement.

Further insights into new inputs for materials behaviour that led to the hydraulic fill improvement are presented in this section. The modified section and the new design of construction process are incorporated in the numerical analysis to evaluate the quay wall behaviour and final stability. It is important to note that the analysis presented in this section is used to confirm the performed design of the construction process using CASM model for hydraulic fill simulation.

5.6.1. Constitutive models and materials properties

The only constitutive model and associated parameters that are modified for this analysis correspond to the hydraulic fill after improvement. The CASM model was used before to be able to represent brittle behaviour and flow liquefaction. As shown in the previous section, it is concluded that flow liquefaction is no longer possible. The material is assumed ductile with an undrained shear strength of $0.25 \cdot \sigma'_v$. In that case, the Soft Soil constitutive model (Plaxis, 2010) is adopted. The corresponding model parameters are given in Table 5.3.

While the fill is undergoing consolidation during preloading, it is still assumed liquefiable, probably a conservative hypotheses at least in the later stages of pore pressure dissipation.

The effects of prefabricated strip drains and geotextile membrane on strength have been neglected. This hypothesis can be considered conservative, because both tend to induce strength increase, see for instance Rowe and Li (2002) or recently in Da Silva (2017). Note that, although effective stress strength parameters of hydraulic fill are not modified during preloading, hydraulic fill permeability have been calibrated from results of piezometers installed into hydraulic fill obtained during the preloading. This piezometer was likely to be located in the less permeable hydraulic fill making the parameter probably conservative.

A new material is also defined to represent the hydraulic fill from the failed zone that ended outside in an area outside the caissons. There were not tests performed in this material but divers described it as an extremely soft mud.

Table 5.3. New hydraulic fill properties for FE analysis.

Symbol & Units	Hydraulic fill with vertical strip drains	Improved hydraulic fill	Hydraulic fill from Phase 1 (sea side)
Constitutive model	CASM	Soft Soil	Soft Soil
γ_{nat} [kN/m^3]	18.5	19	16
e [-]	1	0.8	2
c_c	0.23	0.23	0.4
c_s	0.07	0.07	0.02
v [-]	0.3	0.3	0.3
k [m/s]	$2 \cdot 10^{-7}$	$2 \cdot 10^{-7}$	$5 \cdot 10^{-8}$
$c_{u\ peak}$ / σ'_v	0.25	-	-
$c_{u\ SS}$ / σ'_v	0.06	0.25	0.06

In addition, the Mohr-Coulomb constitutive model has been adopted for a set of coarse grained materials that have been used to improve stability conditions: sandy dumped fill, upper rock fill, stone columns and preloading material. Some parameters have been obtained from the site investigation; other parameters have been estimated from calibration or standards. Thus, shear strength and rigidity parameters of the dumped fill that was placed by land means was determined from in-situ tests results. There are no tests on the materials of the upper rock fill, soil with stone columns and preloading material. The same properties than for rubble mound are selected for the upper rock fill. The parameters of soil with stone columns were adjusted according to the equivalent area method (Tan et al., 2008). Standard values of 18 kN/m^3 for density and of 30° for friction angle have been used for simulating preloading material. The main parameters values are shown in Table 5.4.

Table 5.4. Adopted parameters for cohesion less materials.

Symbol & Units	Preloading material	Dumped fill	Upper rock fill	Improved soil with stone columns
γ_{nat} [kN/m^3]	18	18	20	19
E' [kPa]	10000	15000	35000	30000
ν [-]	0.3	0.3	0.3	0.3
φ [°]	30	28	38	27
$R_{interface}$	-	-	0.6	-

5.6.2. Geometry and material distribution

The original geometry for Phase 2 above (Figure 5.1) is modified to take into account the modifications implemented in the section in Figure 5.10. The new geometry is presented in Figure 5.28. The domain of analysis is 200 m long and 70 m high and comprises by 12307 elements of 15 nodes.

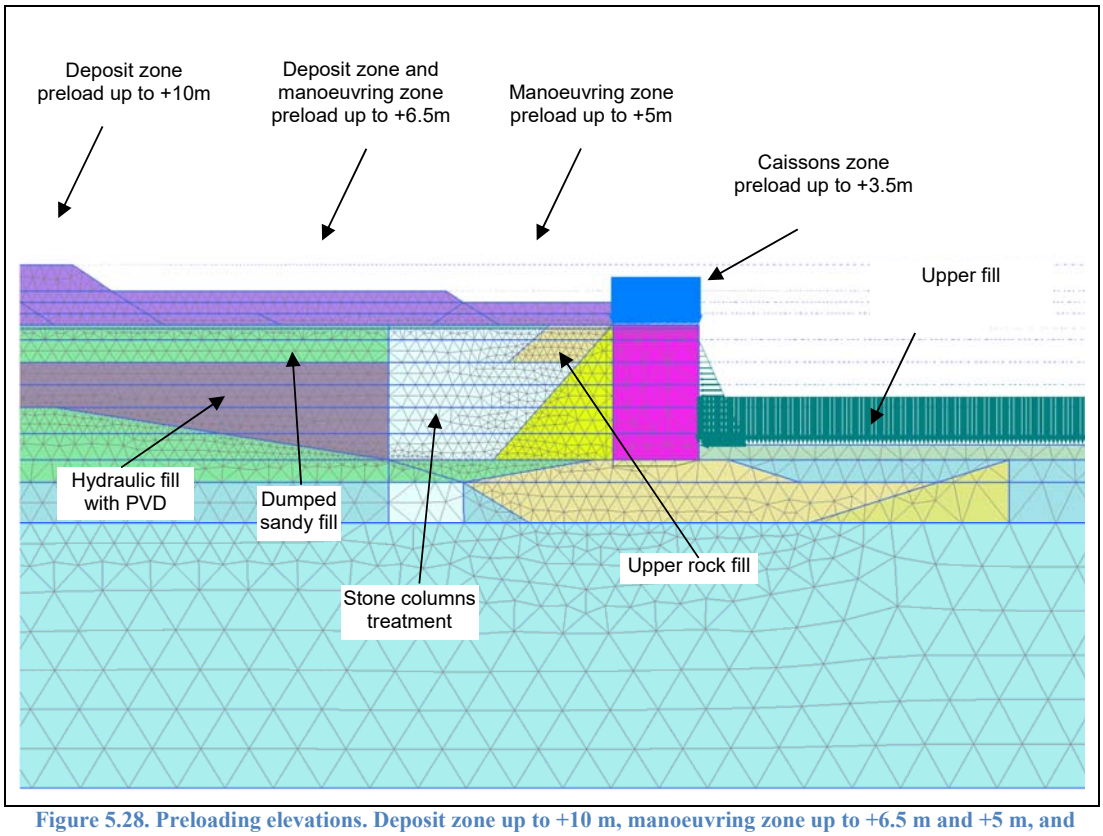

Figure 5.28. Preloading elevations. Deposit zone up to +10 m, manoeuvring zone up to +6.5 m and +5 m, and caissons up to +3 m for numerical simulation.

It is worth noting that the preloading geometry was specified to provide the loading distribution defined for each stage. The deposit and the manoeuvring zones preloading are simulated by material; whereas a simple line surface simulates caisson preloading.

Finally, note that a conservative assumption is when the effect of the gravel columns in the sand layer is not considered.

5.6.3. Phases of analysis

The model simulates all the events before and after the failure including soil improvement activities. The model is continued until the end of construction and includes the application of service loads. It involves 11 stages before the failure (Table 5.2) and 23 stages after the failure. The stages corresponding to the events after the failure after the failure are listed in Table 5.5. The sequence and stages after the failure were established using to observational method. It can be observed that, to ensure quay stability, the preload was applied sequentially. in two steps: (i) preloading of caissons and deposit zones (stage 17 to stage 25), and (ii) preloading of manoeuvring and deposit zones (stage 26 to stage 31).

Table 5.5. Description of construction stages of Phase 2 after Phase 1 the failure.

Description	Stage	Time (days)
Removal of the earth bund over the caissons	12	80
Granular Fill up to -0.5 m (placement by terrestrial means)	13	50
Granular Fill up to +1 m (placement by terrestrial means)	14	30
Drainage layer up to +1.5 m	15	50
Vertical prefabricated strip drains installation (+1.5 m)	16	110
Deposit zone preloading up to +6.5 m	17	20
Deposit zone preloading consolidation	18	45
Preloading up to +8.5 m, in part of the deposit zone. Caisson preloading with 6 layers of 0.5 m of soil	19	15
Preloading up to +10 m, in part of the deposit zone. Caisson preloading with 6 layers of 0.5 m of soil	20	20
Deposit zone and caissons preloading consolidation	21	45
Deposit zone preloading consolidation. Caissons preloading with 7 layers of 0.5 m of soil	22	4
Deposit zone and caissons preloading consolidation. Stone columns installation	23	55
Deposit zone and caissons preloading consolidation.	24	85
Deposit zone preloading consolidation. Unloading caissons preloading reduced to 3 layers of 0.5 m soil	25	10
Deposit zone and caissons preloading consolidation.	26	50
Deposit zone and caissons preloading consolidation. Manoeuvring zone preloading up to +5 m and +3 m.	27	10
Deposit zone, manoeuvring zone and caissons preloading consolidation	28	15
Deposit zone and caissons preloading consolidation. Manoeuvring zone preloading up to +6.5 m and +5 m.	29	20
Manoeuvring zone and caissons preloading consolidation. Unloading deposit zone preloading	30	60
Manoeuvring zone and caissons preloading consolidation	31	60
Preloads unloading to final height, 3m	32	30
Pavement, capping beam construction and dredge in the sea side to -16.5 m	33	360
Service loads	34	90

5.6.4. Results of the analysis

From a general perspective, it can be stated that the numerical analysis performed exhibited any convergence difficulties.

5.6.4.1. Construction

This analysis provides results of the evolution of deformations and water pressures. The monitoring system recorded data from piezometers and surveying that is useful to check the quay behaviour. The results of the instrumented section of a representative caisson are compared.

Figure 5.29 shows the computed vertical and horizontal displacements compared with the observed displacements of Phase 2 during various stage constructions. Caisson observations (red and black lines) and computed (blue line) of vertical and horizontal displacements are presented in Figure 5.29 for the main preloading stages, 17, 20, 27 and 29. The agreement is good in both terms of displacements at the end of construction. Nevertheless, stone columns performance generated movements that are not simulated.

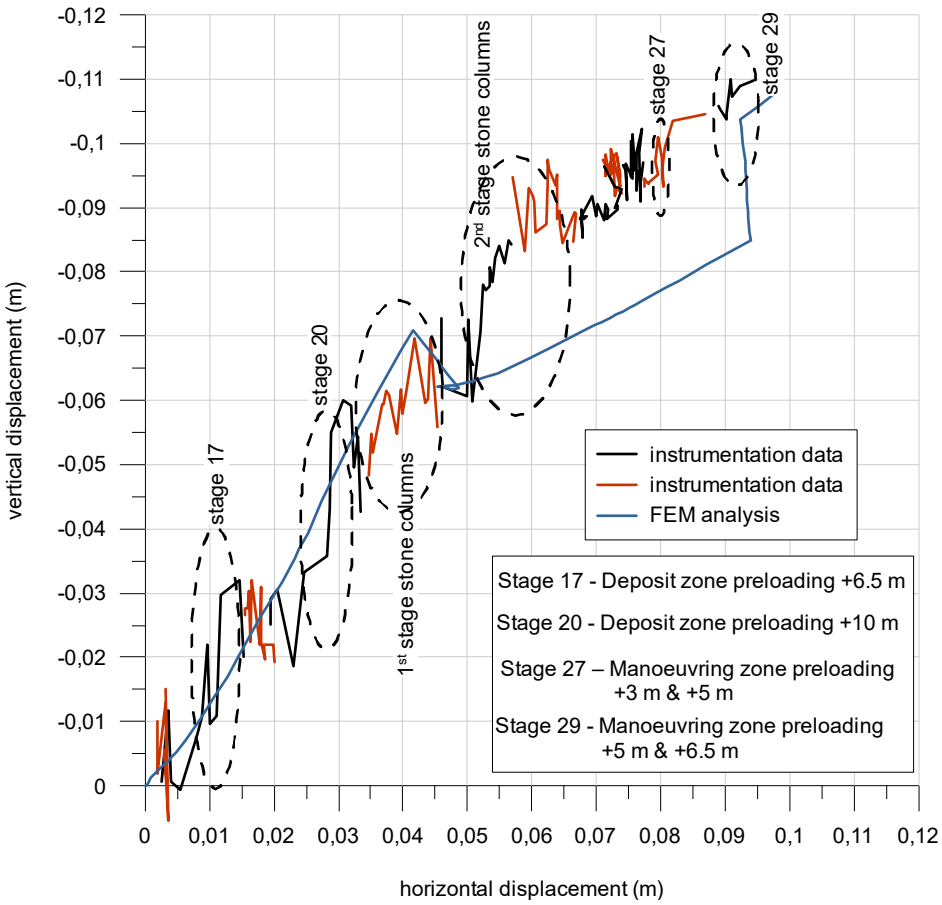

Figure 5.29. Vertical vs. horizontal displacements during Phase 2 quay construction. Results from topographic survey and numerical analysis.

The computed and measured excess pores pressures are represented in the quay cross-section in Figure 5.30. Excess pore pressure in hydraulic fill and natural ground are compared for the most

critical stages, 29 and 30. The water pressure dissipation in the hydraulic fill is faster than in the simulation. This behaviour is likely to be due to hydraulic fill heterogeneities.

In summary, a quite good agreement between analysis and monitoring results has been obtained indicating that the hydro-mechanic conditions during construction have been properly simulated.

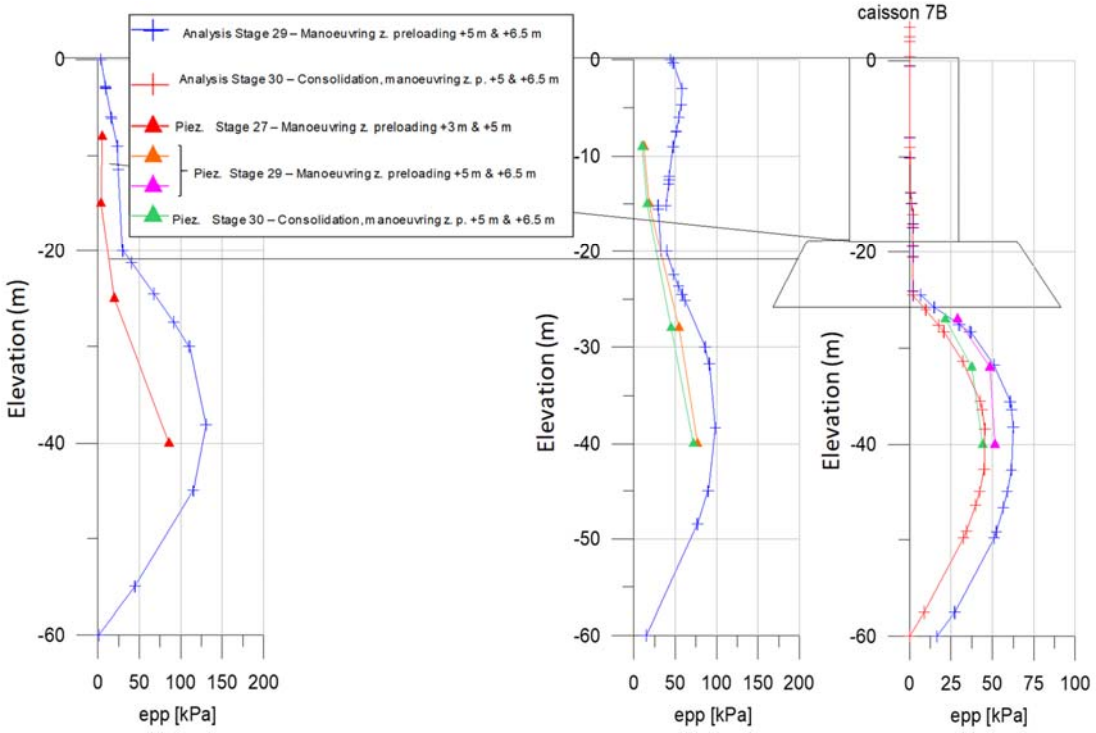

Figure 5.30. Excess pore pressure profiles from piezometers and numerical analysis results- Phase 2 quay construction.

5.6.4.2. Stability analysis

The factors of safety obtained with the hydraulic fill modelled using CASM are higher than 1.25. Unfortunately, with the manual φ – c reduction required when using the CASM model, it is not possible to calculate higher values of FoS and the failure mechanisms cannot be visualised. Once the CASM model is replaced by the soft soil model (i.e. after the end of the preloading), the service loading stage (34) is computed using the manual φ – c reduction (Appendix A). The computed FoS is 1.28. The full list of computed FoS during construction stages and service loading (bollard, crane and deposit loads) are presented in Table 5.6.

Additional stability analyses in critical stages were performed using the conservative initial hypothesis of complete hydraulic fill liquefaction as described in Appendix C.3. The results obtained in this way met the design requirements that FoS ≥ 1.25. Therefore, the design is likely to be conservative because the total liquefaction of the fill is quite an extreme assumption.

Table 5.6. FoS for construction stages and service loading.

Description	Stage	FoS Manual φ – c reduction
Deposit zone preloading up to +6.5 m	17	>1.25
Deposit zone preloading up to +10m, using a trench up to +6.5m. Caissons preloading consolidation with 6 layers of 0.5m of soil	20	>1.25
Deposit zone preloading consolidation. Caissons preloading with 7 layers of 0.5m of soil	22	>1.25
Deposit zone preloading consolidation. Unloading caissons preloading reducing to 3 layers of 0.5m soil (2.7 t/m^2).	25	>1.25
Deposit zone and caissons preloading consolidation. Manoeuvring zone preloading up to +5m and +3m.	27	>1.25
Deposit zone and caissons preloading consolidation. Manoeuvring zone preloading up to +6.5m and +5m.	29	>1.25
Service loads	34	1.28

The mechanism of failure during service loading (Figure 5.31) crosses the zone improved with stone columns, rock fill, rubble mound and natural ground. It is interesting to note that there is a considerable change of failure shape between stage 11 without soil improvement and the service loading stage. In addition, a failure shape similar to that obtained for Phase 1 (Figure 4.14) can be observed.

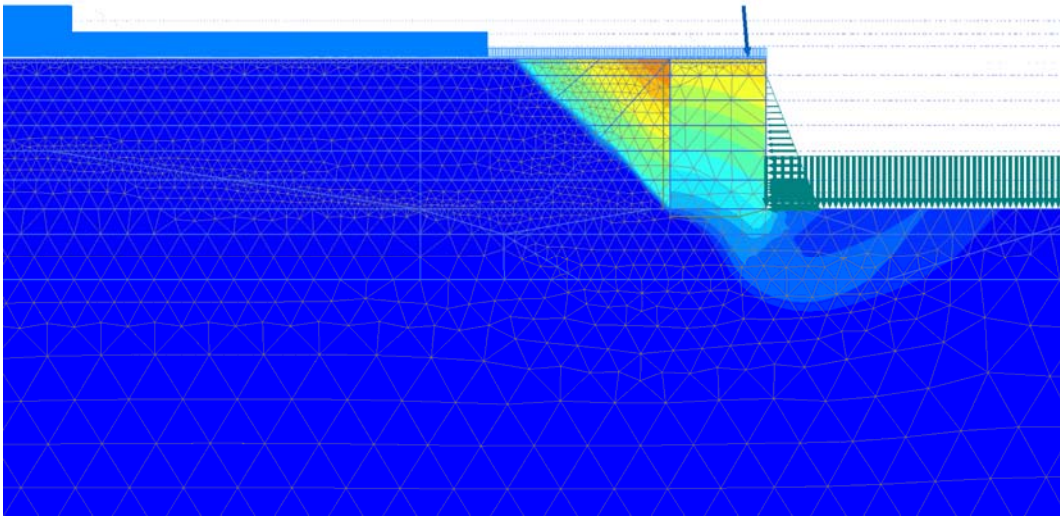

Figure 5.31. Contours of incremental displacements in stability analysis at stage 34, FoS=1.28.

In summary, the numerical analyses indicate an adequate stability of the Phase 2 of Prat quay under both construction and service conditions.

5.7. Phase 1 reconstruction

The construction of Phase 2 quay provided relevant information for the rebuilding the Phase 1 quay after the failure. The Phase 1 reconstruction was carried out in two stages: (i) Stage 1 involving the 9 caissons not affected by the failure, (ii) Stage 2 involving the part of the quay that had been directly

affected by the failure. Stage 1 started immediately after finishing the construction of the Phase 2 quay while Stage 2 started during the preloading of Stage 1. Stage 2 used the caissons that could be recovered, new caissons were built to replace those that could not be retrieved.

The design of the Stage 1 of Phase 1 had substantial changes with respect to the original cross-section design. The main ones are:

(i) Part of the already emplaced hydraulic fill was dredged out from the zone depicted in Figure 5.32.

(ii) The construction of a new dike.

(iii) A rock-fill wedge was emplaced behind the quay wall.

(iv) The raising of the fill up to elevation +2 m using dry coarse grained soil.

(v) Installation of prefabricated vertical strip drains.

(vi) Surcharge preloading improvement (Figure 5.33).

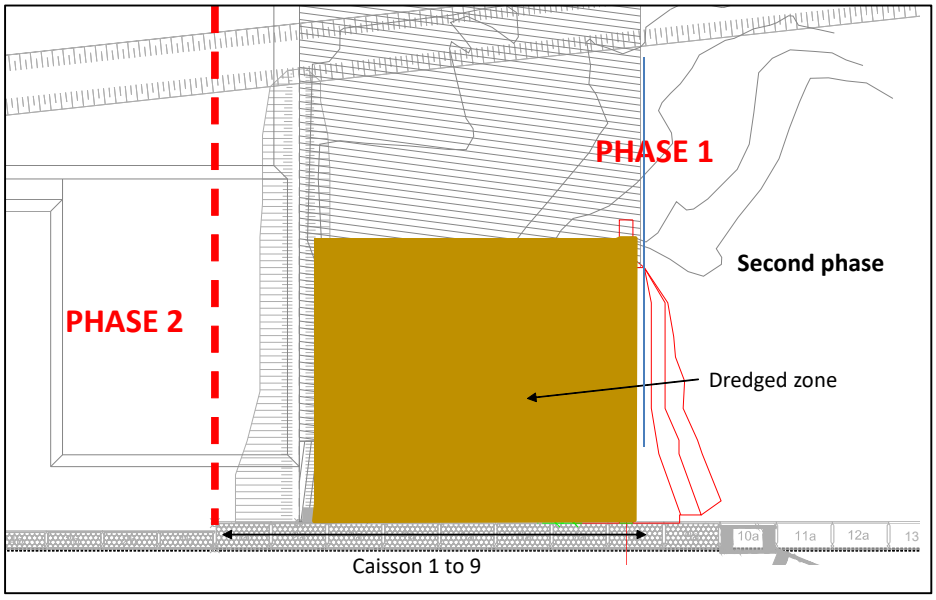

Figure 5.32. Plan view of Stage 1 of Phase 1 reconstruction, APB (2009).

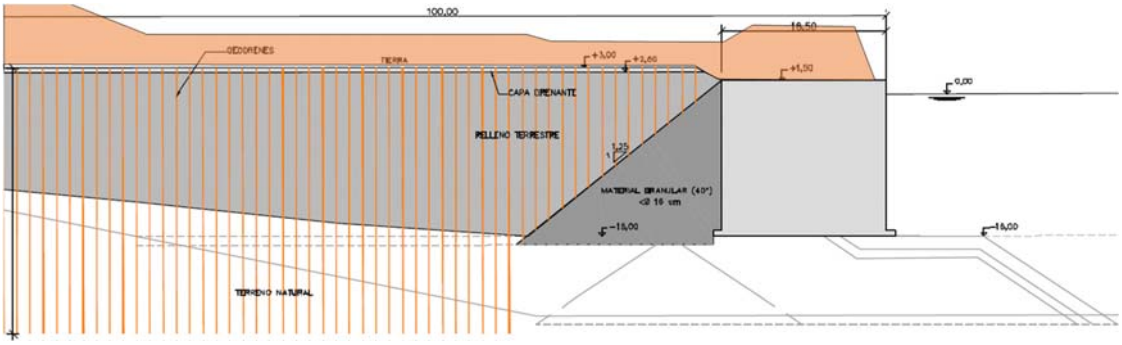

Figure 5.33. Cross-section of Stage 1 of Phase 1 reconstruction, APB (2009).

To check the characteristics of the new fill, four additional CPTu test were carried out before preloading. The new backfill is composed mainly by coarse grained soils. Excess water pore

pressures (u_2) were not generated and high values of q_c (>10 MPa) and f_s (>0.08 kPa) are measured in the CPTu soundings, as shown in Figure 5.34.

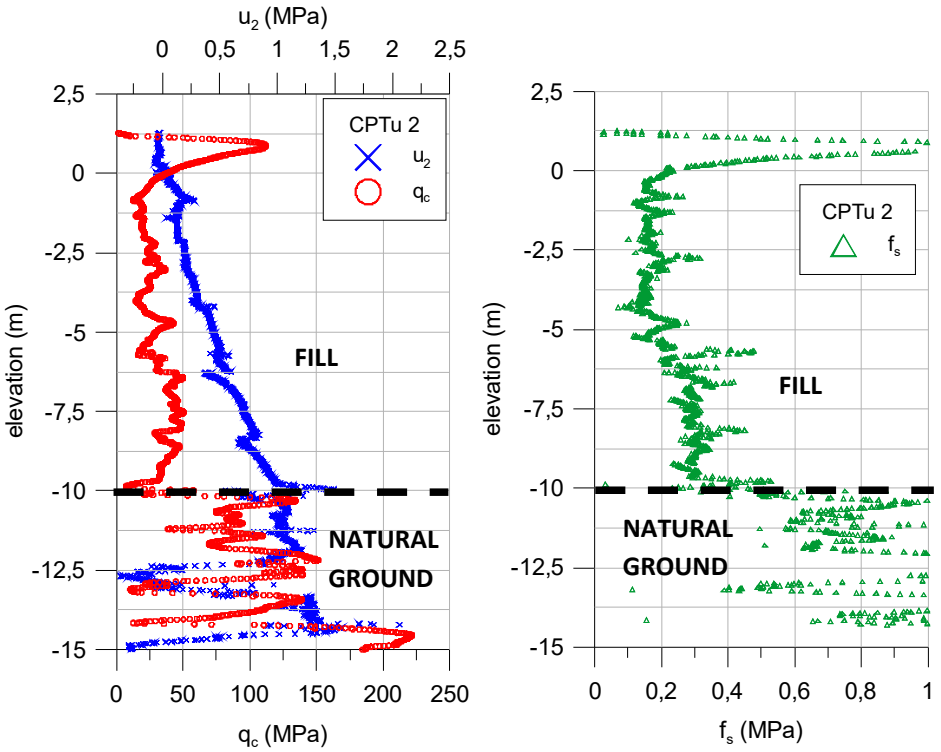

Figure 5.34. Representative CPTu in backfill of Stage 1 of Phase 1 reconstruction.

Derived undrained shear strength values from CPTu are generally much higher than $0.25 \cdot \sigma'_v$ apart from a few localised points, as it can be observed Figure 5.35.

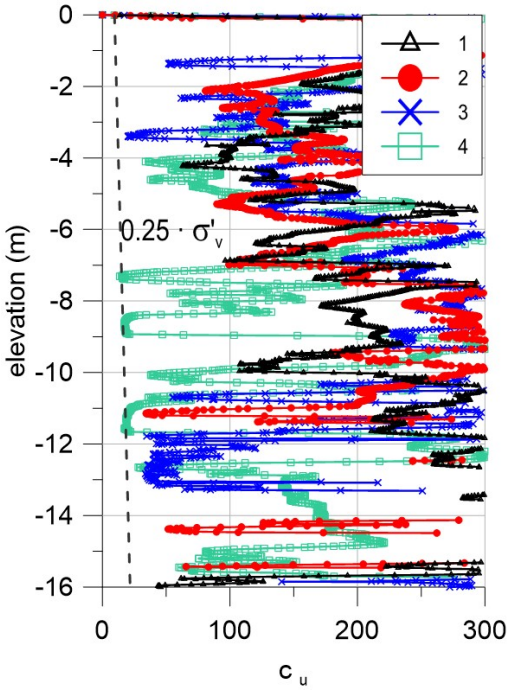

Figure 5.35. CPTu results for c_u from terrestrial fill of Stage 1 of Phase 1 reconstruction.

Figure 5.36 shows the CPTu results of the new fill plotted on Robertson (2016) F_r-Q_{tn} screening chart. It can be noted that points correspond to the region of dilative sand-like (SD) and transition soils (TD). Therefore, there is no flow liquefaction potential.

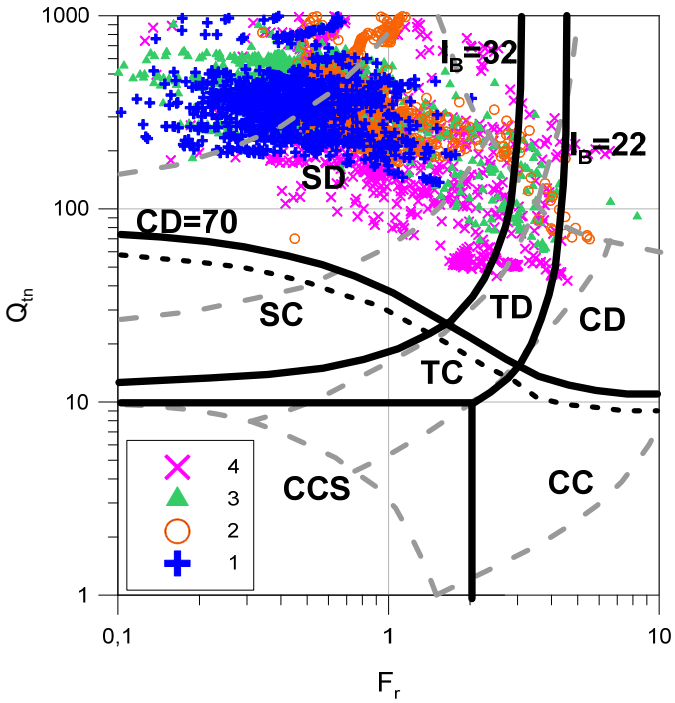

Figure 5.36. Location of the observations in four CPTu tests in Roberson (2016) F_r-Q_{tn} charts, backfill of Stage 1 of Phase 1 reconstruction.

Equivalent results are obtained from Plewes et al. and Mayne criteria. (Figure 5.37 to Figure 5.40). All state parameter values correspond to dilatant behaviour.

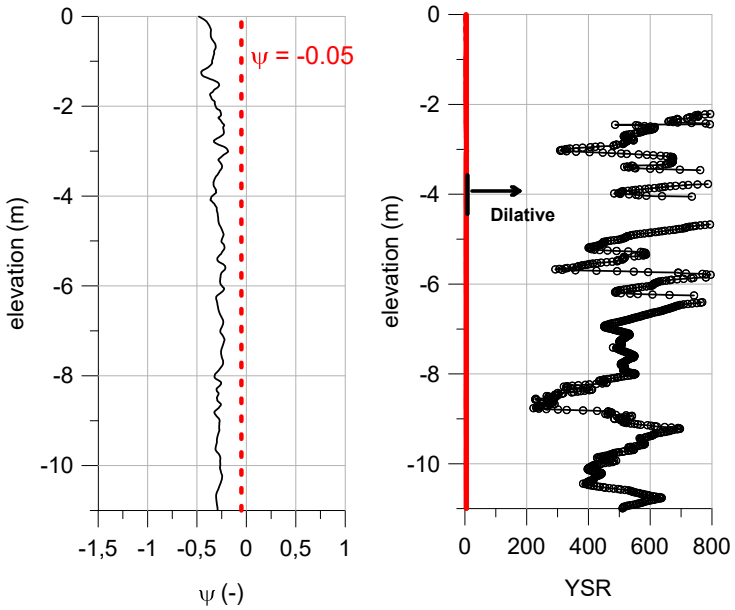

Figure 5.37. Results of Plewes et al. and Mayne criteria for CPTu 1, backfill of Stage 1 of Phase 1 reconstruction.

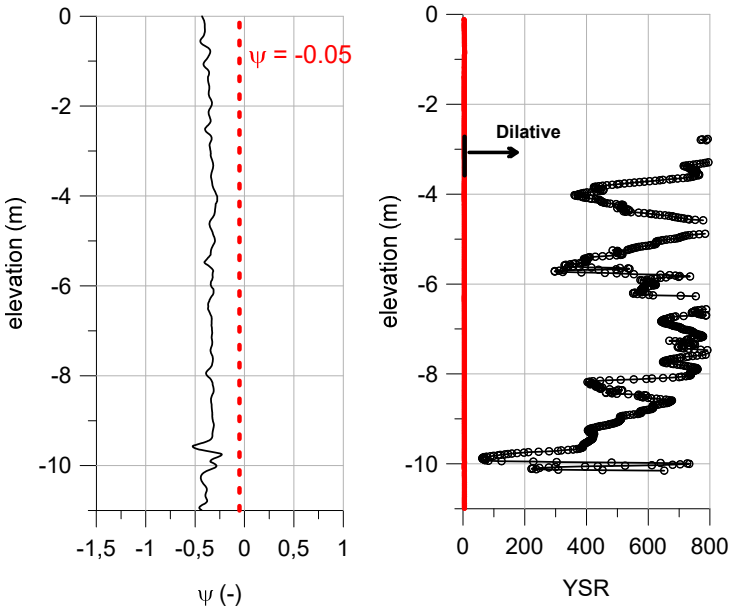

Figure 5.38. Results of Plewes et al. and Mayne criteria for CPTu 2, backfill of Stage 1 of Phase 1 reconstruction.

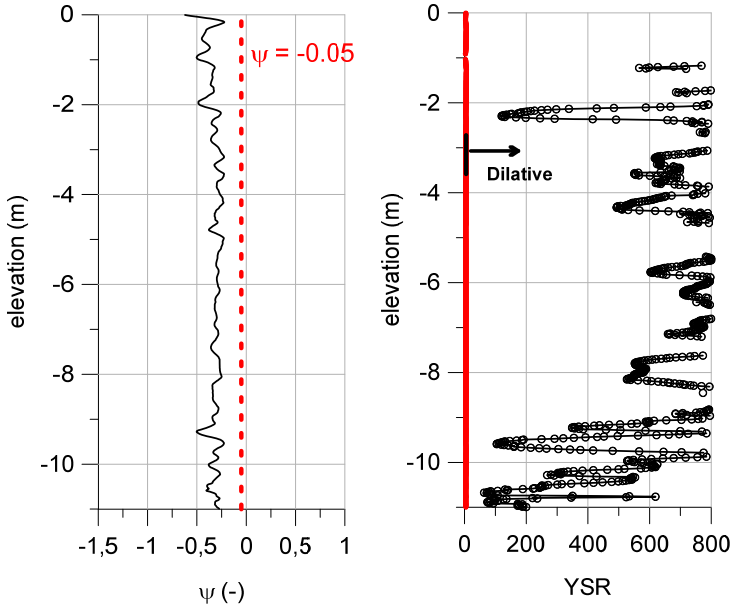

Figure 5.39. Results of Plewes et al. and Mayne criteria for CPTu 3, backfill of Stage 1 of Phase 1 reconstruction.

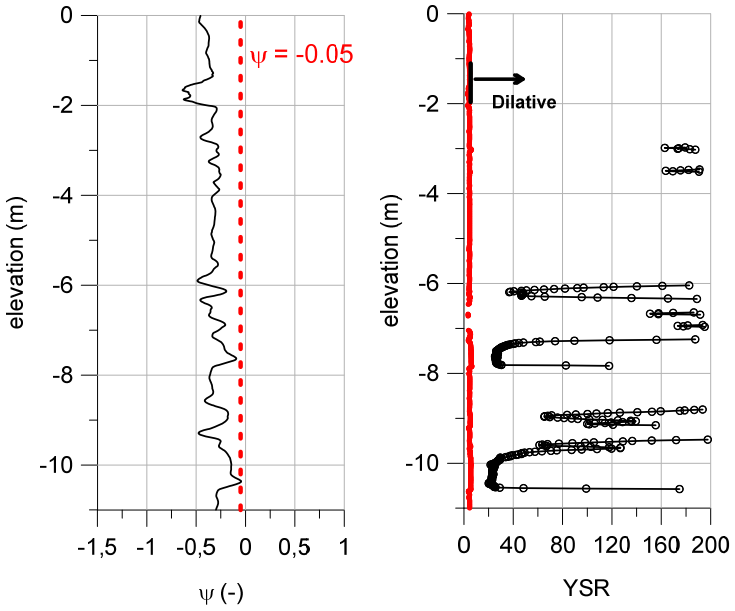

Figure 5.40. Results of Plewes et al. and Mayne criteria for CPTu 4, backfill of Stage 1 of Phase 1 reconstruction.

Two-dimensional numerical analysis using FEM were performed for the Stage 1 of Phase 1 reconstruction. In accordance with the previous liquefaction assessment, no flow liquefaction was assumed in this case. The geometry and materials distribution are shown in Figure 5.41.

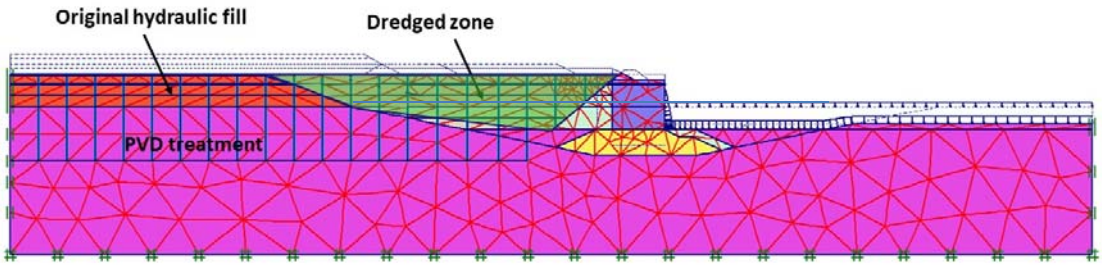

Figure 5.41. Geometry of Stage 1 of Phase 1 reconstruction.

Finally, Figure 5.42 presents the design of the Stage 2 of Phase 1 reconstruction that has many similarities to that of Stage 1. The designed was geared to avoiding any potential problem of soil liquefaction. The zone against the caisson was backfilled with a rock fill wedge and, subsequently, a larger region over 30 m wide was filled with coarse-grained placed by terrestrial means. After the reconstruction, only a small wedge of the initial hydraulic fill remained at the bottom of the quay fill. In addition, a surcharge preloading with prefabricated strip drains was applied as depicted in Figure 5.42. In any case, no evidences of flow liquefaction potential in the fill were identified from CPTu results even before the preloading. In fact, the main objective of the preloading was to reduce eventual settlements that could affect quay operations.

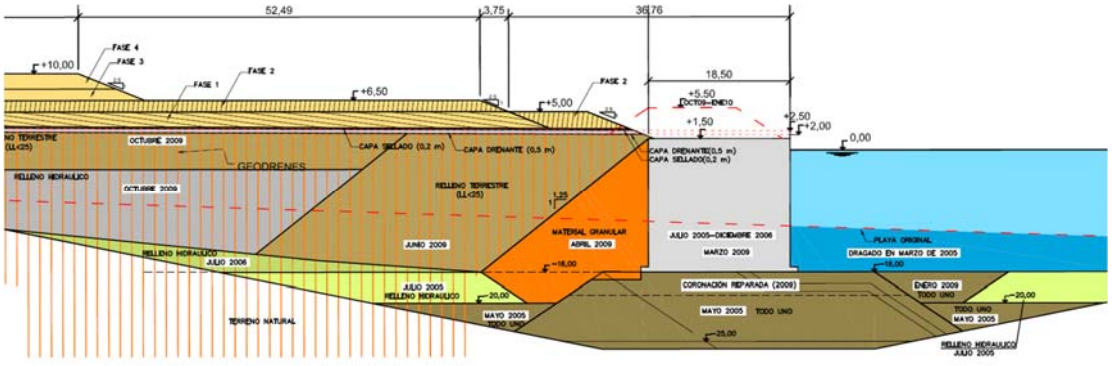

Figure 5.42. Cross section of Stage 2 of Phase 1 reconstruction, APB (2009).

As expected, the designs of both stated amply fulfilled the required stability conditions. No special difficulties arise during the Phase 1 quay reconstruction. The information collected from the monitoring system and the final round of CPTu tests are outside the scope of this PhD thesis.

5.8. *Proposed protocol to evaluate liquefaction potential for hydraulic fills*

Based on the experience gathered in the Prat quay case reported in this PhD thesis, a new protocol to improve the identification of hydraulic fill with liquefaction potential is proposed. Both flow and cyclic (Appendix E) liquefaction are considered.

The protocol encompasses different requirements for the three phases hydraulic fill deposition: before, during and after emplacement.

5.8.1. *Before hydraulic fill emplacement*

This phase is likely to be the most important because part of the final conditions can be evaluated. The main points to be studied are the following:

- General assessment of volumes.
- Type of dredge and placement system.
- Description of the soils to be dredged.
- Lab tests: soil identification with LL, LP, particle size determination (PSD), fine content % and mineral identification, X-ray diffraction.
- Settling columns.

These studies shall be used for performing preliminary assumptions of the hydraulic fill and to propose future soil improvement if required.

5.8.2. *During hydraulic fill placement*

At the beginning of this phase the quay wall is constructed and it can not be modified easily of difficulties arise. The proposal for tests to be performed is:

- Soil samples from the dredged soil.
- Settling columns.
- Lab tests: soil identification with LL, LP, particle size determination (PSD), fine content %, and mineral identification, X-ray diffraction.

The results should confirm the results obtained before fill placement and, in this way, confirm design assumptions.

5.8.3. After hydraulic fill emplacement

Once the hydraulic fill is emplaced, a certain amount of time is required for soil settling and formation. That time depends fundamentally on soil type, particle size, fine content and presence of flocculants minerals. It can be evaluated from the information gathered in the tests performed during emplacement. Once the material has settled, in-situ tests and lab tests should be performed.

- In-situ testing.

The CPTu and the seismic CPTu tests is likely to be the most appropriated due to the continuous and complete recording of soil parameters and suitability to liquefiable soils. Seismic CPTu is capable to provide the soil shear velocity, particularly useful for the evaluation of cyclic liquefaction potential. Currently, the offshore site investigation industry has developed new tools such as the T-Bar and Ball penetrometers to characterize very soft soils. They are collectively known as full-flow penetrometers. There are a number of advantages in the use of full-flow penetrometers with respect to CPTu tests as discussed in Einav and Randolph (2005), Yafrate et al. (2009) and DeJong et al. (2011):

- The larger probes require minimal correction for the overburden pressure (or ambient water pressure in offshore investigations) in order to provide a net resistance and higher accuracy in soft soils.
- Since the resistance is primarily due to flow around the probe, rather than insertion of additional volume (of cone shaft) into the ground, the resistance should be less affected by secondary soil characteristics such as the rigidity index or the in-situ stress ratio.
- A well-defined failure mechanism may be postulated -essentially plane strain for the T-bar and axisymmetric for the ball-, thus providing a more robust theoretical basis for deriving factors relating penetration resistance and shear strength.
- Improved accuracy in very soft soils since a larger volume of soil is engaged during penetration as compared to the CPTu.
- Corrections for overburden are minimized since the overburden stress is nearly equal above and below full-flow penetrometers.
- Penetration resistance is less affected by soil rigidity and stress anisotropy because the resistance measured is a result of soil flow around the probe rather than of complete soil displacement as is the case with the cone penetration test CPT.

Therefore, it is strongly recommended the use of full-flow penetrometers to evaluate strength and soil sensitivity for very soft soils.

Additionally, other in-situ tests as DMT, SDMT, shear velocity or SPT are also useful to perform cyclic liquefaction assessments. Field Vane tests (FVT) and SPT test may also provide useful information.

- Laboratory testing

Continuous undisturbed samples from boreholes should be extracted from boreholes although the operation may present difficulties for very soft materials and special sampling techniques may be required. Sampling and in-situ test should be performed in close proximity to facilitate comparison.

Soil identification tests involving the determination of LL, LP, particle size distribution (PSD), fine content %, mineral identification, X-ray diffraction as well as settling columns should be performed. Results should be compared with results from tests carried out before and during hydraulic fill emplacement.

It shall be suitable to evaluate soil liquefaction potential as soil index tests, oedometer tests, direct simple shear tests and triaxial CAU tests with monotonic and cyclic loading provide important information for the assessment of liquefaction potential, if suitable samples are available. The lab results shall be used for:

- Comparison between in-situ and lab tests to obtain a robust soil characterization.
- Application of liquefaction potential criteria.

Finally, flow and cyclic liquefaction criteria shall be applied depending on location conditions. Flow liquefaction potential will have to be performed in all hydraulic fills, thus state parameter and soil sensitivity should be precisely characterized. In addition, seismic conditions (a_{max} and M_w) must be known to assess the cyclic liquefaction of a particular site.

The proposed protocol for liquefaction potential evaluation for hydraulic fills is summarised in the flow chart shown in Figure 5.43.

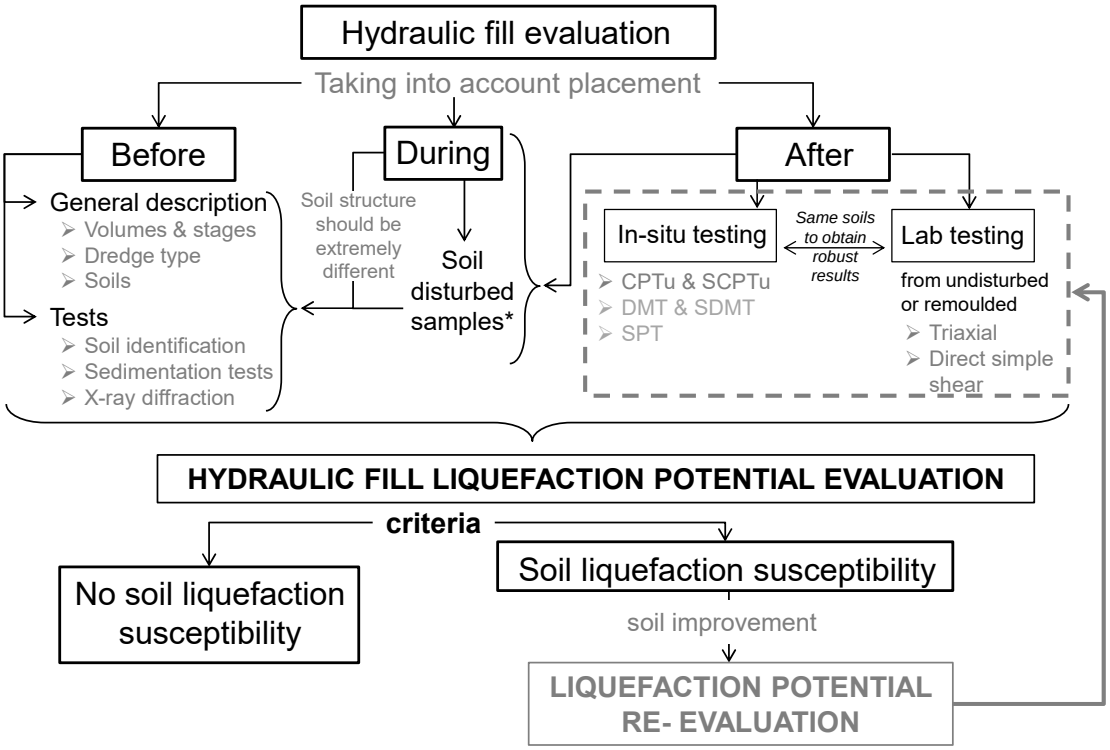

Figure 5.43. Protocol for the evaluation of hydraulic fill liquefaction potential.

5.9. Summary

The main points of this Chapter are summarised here:

Phase 2 quay construction was simulated assuming the possibility of a general liquefaction of the hydraulic fill that was represented by the CASM constitutive model. Under those conditions, the numerical analysis showed the stability of Phase 2 quay was marginal.

There is a wide range of remedial measures that can be applied to reduce liquefaction potential. The proposal of hydraulic fill improvement procedure for Phase 2 involved surcharge preloading with prefabricated strip drains and installation of stone columns in part of the section. The results of the hydraulic fill improvement procedure were checked by two extensive geotechnical investigations that included CPTu and laboratory tests, before and after soil improvement. The results of the site investigation after soil improvement showed a significant increase of the undrained shear strength of the hydraulic fill, and a condition of no flow liquefaction potential according to the Plewes et al. and the Mayne criteria. This is contrast to the results of the site investigation before preloading when significant flow liquefaction potential had been found.

It can thus be concluded that the performed soil improvement was effective to remove the flow liquefaction potential of the hydraulic fill. It can also be stated that the CPTu results have provided good and consistent information on liquefaction potential and its variation due to preloading, although a more comprehensive programme of laboratory tests on good quality samples would have been advisable.

Although it is not described in this Chapter, the cyclic liquefaction potential has been evaluated (Appendix E) according to the Spanish seismic regulations. It is concluded that no cyclic liquefaction can be triggered under those seismic conditions of the Barcelona area.

The new Phase 2 design and construction was analysed using finite elements. The numerical analysis was instrumental to define the construction stages in conjunction with monitoring data -observational method-, in order to obtain an adequate FoS. A good agreement of observations and numerical results increased the confidence of having a good understanding of the quay behaviour. When soil improvement was completed, the possibility of liquefaction was removed from the analysis.

For the reconstruction of Phase 1 quay, most of the hydraulic fill placed in Phase 1 was removed to exclude the possibility of fill liquefaction. This was confirmed from site investigations carried out after construction.

Finally, the lessons learned during the study of the Prat quay have led to the proposal of a protocol to evaluate the liquefaction potential for hydraulic fills. This protocol involves liquefaction evaluation before, during and after hydraulic fill emplacement. For each stage, specific tests to be performed to be applied are proposed.

5.10. References

Adalier, K., Elgamal, A., Meneses, J., and Baez, J. I. 2003. Stone column as liquefaction countermeasure in non-plastic silty soils. Soil. Dyn. Earthquake Eng., 237, 571–584.

Adalier, K., Elgamal, A. 2004. Mitigation of liquefaction and associated ground deformations by stone columns. Eng. Geol., 72(3–4), 275–291.

Almeida, M. S. S., Santa Maria, P. E. L., Martins, I. S. M., Spotti, A. P., Coelho, L. B. M. 2000. Consolidation of a very soft clay with vertical drains. Géotechnique 50, No. 6, 633–643; Discussion. 52, No. 2, 148–154.

Alonso, E.E., Gens, A., Lloret, A. 2000. Precompression design for secondary settlement reduction. Géotechnique, Vol. 50, No. 6, pp. 645-656.

Alonso, E.E., Madrid, R., Tarragó, D. 2008. Prueba de precarga piloto 2008 – Muelle Prat Fase 2. Proyecto de ampliacion del puerto de Barcelona. Confidential report UPC-CIMNE, Autoritat Portuaria de Barcelona.

Alonso, E.E., Gens, A., Madrid, R., Tarragó, D. 2010. Preloading design based on long term extensometer readings. A comparison of alternative methods. New soft soil tecniques Ed, M. Almeida, pp 23-38.

Andrus, R., Chung, R. 1995. Ground improvement techniques for liquefaction remediation near existing lifelines. Report, Building and Fire Research Laboratory. National Institute of Standards and Technology, U.S. Department of Commerce.

APB 2008. Project reports of Phase 2 completion of the construction. Confidential information. Autoritat Portuaria de Barcelona, Port de Barcelona.

APB 2009. Project reports of Phase 1 reconstruction. Confidential information. Autoritat Portuaria de Barcelona, Port de Barcelona.

Arulrajah, A., Nikraz, H., Bo, M.W. 2004. Factors affecting field instrumentation assessment of marine clay treated with prefabricated vertical drains. Geotext. Geomembranes 22, 415-437.

Arulrajah, A., Bo, M.W., Chu, J., Nikraz, H. 2008. Application of prefabricated vertical drains to the Changi land reclamation project, Singapore. Proceedings of the 4th Asian Regional Conf. On Geosynthetics, pp. 651-655. Shanghai.

Atkinson, M. S., Eldred, P. J. L. 1981. Consolidation of soil using vertical drains. Geotechnique, London, England, 31(1), 33-43.

Baez, J.I., Martin, G.R., 1995. Permeability and shear wave velocity of vibro-replacement stone columns. Soil Improvement for Earthquake Hazard Mitigation. ASCE Geotechnical Special Publication, vol. 49, pp. 66 – 81. New York, NY.

Bahadori, H., Manafi, S. 2015. Effect of tyre chips on dynamic properties of saturated sands. Int J Phys Model Geotech 2015;15(3):1–13.

Bahadori, H., Farzalizadeh, R. 2016. Dynamic properties of saturated sands mixed with tyre powders and tyre shreds. Int J Civil Eng 2016;16(4):395–408.

Bergado, D.T., Balasubramaniam, A.S., Fannin, R.J., Holtz, R.D. 2002. Prefabricated vertical drains (PVDs) in soft Bangkok clay: a case study of the new Bangkok International Airport project. Canadian Geotechnical Journal 39, 304–315.

Bishop, A.W., Vaughan, P. R. 1972. Consolidation of fine grained dredge material after hydraulic deposition. National Ports Council, Dept. of Civil Engineering, Imperial College of Science and Technology, London.

Boulanger, R., Idriss, I., Stewart, D., Hashash, Y., Schmidt, B. 1998. Drainage capacity of stone columns or gravel drains for mitigating liquefaction. Proc., Geotech. Earthquake Eng. and Soil Dynamics III. ASCE Geotech. Special Publ. No. 75, vol. 1, pp. 678– 690.

Bray, J. D., Sancio, R. B., Riemer, M. F., Durgunoglu, T. 2004. Liquefaction susceptibility of fine-grained soils. 11th Int. Conf. on Soil Dynamics and Earthquake Engineering and 3rd Int. Conf. on Earthquake Geotechnical Engineering, D. Doolin et al., eds., Stallion Press, pp 655-662.

Carrera, A., Coop, M.R., Lancellotta, R. 2011. The influence of grading on the mechanical behaviour of Stava tailings. Géotechnique 61, 935–946.

Castro, G. 1969. Liquefaction of sands. Harvard Soil Mechanics Series, No. 81. Cambridge, MA: Harvard University.

Da Silva, E.M., Justo, J.L., Durand, P., Justo, E., Vazquez-Boza, M. 2017. The effect of geotextile reinforcement and prefabricated vertical drains on the stability and settlement of embankments. Geotextiles and Geomembranes 45 (2017) 447-461.

Davis, J. A., Humpheson, C. 1981. A comparison between the performance of two types of vertical drain beneath a trial embankment in Belfast. Géotechnique, London, England, 31(1), 19-31.

DeJong, J.T., Yafrate, N.J., DeGroot, D.J. 2011. Evaluation of undrained shear strength using full-flow penetrometers. ASCE J. of Geot. and Geoenv. Enginnering, Vol 137, Nº 1, 14-26.

DeJong, J.T., Montoya, B.M., Boulanger, R.W. 2013. Dynamic response of liquefiable sand improved by microbial-induced calcite precipitation. Géotechnique 2013;63(4):302–12.

Drnevich, V.P., Bobet, A., Mohtar, C.S.E., Johnston, C.T., Santagata, M.C. 2014. Pore pressure generation in sand with bentonite: from small strains to liquefaction. Géotechnique 2014;64(2):108–17.

Einav, I., Randolph, M. F. 2005. Combining upper bound and strain path method for evaluating penetration resistance. Int. J. Numer. Methods Eng., 63(14), 1991–2016.

Fourie, A.B., Tshabalala, L. 2005. Initiation of static liquefaction and the role of K0 consolidation. Canadian Geotechnical Journal 42, 892–906.

Gens, A., Tarragó, D., Madrid, R. 2009a. Estabilidad del muelle Prat Fase 2 - Proyecto de ampliacion del puerto de Barcelona. Confidential report UPC-CIMNE, Autoritat Portuaria de Barcelona.

Gens, A., Alonso, E.E., Tarragó, D. 2009b. Prueba de Precarga Piloto 2008 - Muelle Prat Fase II - Adenda Proyecto de Ampliación del Puerto de Barcelona. Confidential report UPC-CIMNE, Autoritat Portuaria de Barcelona.

Hamderi, M., Gallagher, P.M. 2015. Pilot-scale modelling of colloidal silica delivery to liquefiable sands. Soils Found 2015;55(1):143–53.

Huang, Y., Wang, L. 2016. Laboratory investigation of liquefaction mitigation in silty sand using nanoparticles. Eng Geol 2016;204:23–32.

Hansbo, S. 1981. Consolidation of fine-grained soils by prefabricated drains. Proc., 10th ICSMFE, A. A. Balkema, Rotterdam, The Netherlands, Vol. 3, 677-682.

Hazarika, H., Hyodo, M., Yasuhara, K. 2010. Investigation of tire chips–sand mixtures as preventive measure against liquefaction. Geoshanghai International Conference. 207: 2010. p. 338–45.

He, J. Chu, J., Ivanov, V. 2013. Mitigation of liquefaction of saturated sand using biogas. Géotechnique 63, No. 4, 267–275.

Holtz, R. D. 1987. Preloading with prefabricated vertical strip drains. Geotextiles and Geomembranes, 6, 109–131.

Holtz, R. D., Jamiolkowski, M. B., Lancellotta, R., Pedroni, R. 1991. Prefabricated vertical drains: design and performance. Butterworth- Heinemann, Oxford, England.

Ibraim, E., Diambra, A., Wood, D.M., Russell, A.R. 2010. Static liquefaction of fibre reinforced sand under monotonic loading. Geotextiles Geomembr 2010;28(4):374–85.

Indraratna, B., Redana I. W. 2000. Numerical modeling of vertical drains with smear and well resistance installed in soft clay. Canadian Geotechnical Journal, 37, No. 1, 132–145.

Kamon, M., Pradhan, T. B. S., Suwa, S. 1992. Laboratory evaluation of the discharge capacity of prefabricated band-shaped drains." Soil improvement, T. Mise, K. Nishida, M. Kamon, and M. Mashima, eds., Current Japanese materials research, Vol. 9, Elsevier Science Publishing Co. Inc., New York, N.Y., 23-38.

Kaneko, T., Orense, R.P., Hyodo, M., Yoshimoto, N. 2013. Seismic response characteristics of saturated sand deposits mixed with tire chips. J Geotech Geoenviron Eng 2013;139(4):633–43.

Karakan, E., Eskişar, T., Altun, S. 2018. The liquefaction behavior of poorly graded sands reinforced with fibers. Adv Civil Eng 2018;4:1–14.

Ladd, C.C., Rixner, J.J., Gifford, D.C. 1972. Performance of embankments with sand drains on sensitive clay. Perform. Earth Earth Supported Struct. 1, 211e464. ASCE, N.Y.

Ladd, C.C. 1991. Stability evaluation during staged construction. Journal of Geotechnical Engineering, ASCE, 117(4): 540–615.

Leroueil, S., Tavenas, F., Lebihan, J. P. 1983. Proprietes caracteristiques des argiles de l'est du Canada," Canadian Geotech. Journal, Vol. 20(4), pp. 681-705.

Liu, J., Wang, G., Kamai, T., Zhang, F., Yang, J., Shi, B. 2011. Static liquefaction behavior of saturated fiber-reinforced sand in undrained ring-shear tests. Geotextiles Geomembr 2011;29(5):462–71.

Long, R. P., Hover, W. H. 1984. Performance of sand drains in a tidal marsh. Proc., lnt. Corif. on Case Histories in Geotech. Engrg., A. A. Balkema, The Netherlands, Vol. 3, 1235-1244.

Long, R. P., Fontaine, L. F. 1992. Performance of wick drains at Windsor, Connecticut. Advances in geotechnical engineering, Transp. Res. Ree. 1369, Transp. Res. Board, Washington, D.C., 1-7.

Long, R. P., Fontaine, L. F., Olmstead, B. 1994. Performance of wick drains installed by vibration. Vertical and horizontal deformations of foundations and embankments, A. T. Yeung and G. Y. Felio, eds., Geotech. Spee. Pub!. No. 40, ASCE, New York, N.Y., Vol. 2, 1193-1201.

Ma, L., Shen, S.L., Luo, ChY., Xu, Y.S. 2011. Field evaluation on the strength increase of marine clay under staged construction of embankment. Mar. Georesources Geotechnol. 29 (4), 317-332.

Mayne, P.W. 2019. Analytical CPTu model for sensitive clay at Tiller-Flotten site, Norway. Proceedings of the XVII ECSMGE-2019 Geotechnical Engineering foundation of the future ISBN 978-9935-9436-1-3 © The authors and IGS: All rights reserved, 2019 doi: 10.32075/17ECSMGE-2019-0153.

McGown, A., Hughes, F. H. 1981. Practical aspects of the design and installation of deep vertical drains. Géotechnique, London, England, 31(1), 3-17.

Mitchell, J. M., Jardine, F. M. 2002. A guide to ground treatment, CIRIA Report C573. London: Construction Industry Research and Information Association.

Mohtar, C.S.E., Clarke, J., Bobet, A., Santagata, M., Drnevich, V. 2008. Cyclic response of a sand with thixotropic pore fluid. Geotech Earthq Eng Soil Dyn Congr IV 2008;318:1–10.

Mohtar, C.S.E., Bobet, A., Santagata, M.C., Drnevich, V.P., Johnston, C.T. 2012. Liquefaction mitigation using bentonite suspensions. J Geotech Geoenviron Eng 2012;139(8):1369–80.

Nicholson, D. P., Jardine, R. J. 1981. Performance of vertical drains at Queenborough bypass. Géotechnique, 31, No. 1, 67–90.

Noorzad, R., Amini, P.F. 2014. Liquefaction resistance of Babolsar sand reinforced with randomly distributed fibers under cyclic loading. Soil Dyn Earthq Eng 2014;66:281–92.

Ochoa-Cornejo, F., Bobet, A., Johnston, C., Santagata, M., Sinfield, J.V. 2014. Liquefaction 50 years after Anshorage 1964; how nanoparticles could prevent it. Tenth U.S. National Conference on Earthquake Engineering Frontiers of Earthquake Engineering. Anchorage, Alaska; 21–25 July 2014.

Otsubo, M., Towhata, I., Hayashida, T., Liu, B., Goto, S. 2016. Shaking table tests on liquefaction mitigation of embedded lifelines by backfilling with recycled materials. Soils Found 2016;56(3):365–78.

Pantazopoulos, I.A., Atmatzidis, D.K. 2012. Dynamic properties of microfine cement grouted sands. Soil Dyn Earthq Eng 2012;42:17–31.

Pardo, G.S., Sarmah, A.K., Orense, R.P. 2019. Mechanism of improvement of biochar on shear strength and liquefaction resistance of sand. Géotechnique 69, No. 6, 471–480.

Peck, R. B. 1969. Advantages and limitations of the observational method in applied soil mechanics, Géotechnique, Vol. 19, No. 2, pp. 171–187.

Phear, A. G., Harris, S. J. 2008. Contributions to Géotechnique 1948-2008: Ground improvement. Géotechnique, 58(5), 399–404.

Plaxis 2010. Materials Models Manual.

Plewes, H.D., Davies, M.P., Jefferies, M.G. 1992. CPT based screening procedure for evaluating liquefaction susceptibility. In Proceedings of the 45th Canadian Geotechnical Conference, pp. 41-49.

Porcino, D., Marcianò, V., Granata, R. 2015. Cyclic liquefaction behaviour of a moderately cemented grouted sand under repeated loading. Soil Dyn. Earthq. Eng. 2015;79:36–46.

Priebe, H.J. 1989. The prevention of liquefaction by vibro-replacement. Proc., Earthquake Resistance Construction and Design, Berlin, Germany.

Priebe, H.J. 1991. Vibro-replacement—design criteria and quality control. In: Esrig, Bachus (Eds.), Deep Foundation Improvements: Design, Construction, and Testing, ASTM STP 1089, pp. 62–72. Philadelphia.

Robertson, P. K., Campanella, R. G., Brown, P. T., Robinson, K. E. 1988. Prediction of wick drain performance using piezometer cone data. Can. Geotech. J., 25(1), 56-61.

Robertson, P.K. 2016. Cone penetration test (CPT)-based soil behaviour type (SBT) classification system - an update. Canadian Geotechnical Journal 53, 1910-1927.

Rowe, R.K., Li, A.L. 2002. Behaviour of reinforced embankments on soft rate sensitive soils. Géotechnique 52 (1), 29–40.

Santagata, M., Clarke, J.P., Bobet, A., Drnevich, V.P., El Mohtar, C.S.E., Huang, P-T., Johnston, C.T. 2014. Rheology of concentrated bentonite dispersions treated with sodium pyrophosphate for application in mitigating earthquake-induced liquefaction. ApplClay Sci;99:24–34.

Seed, H.B., Booker, J.R. 1977. Stabilization of potentially liquefiable sand deposits using gravel drains. ASCE Journal of Geotechnical Engineering Division 103 (7), 757– 768.

Seed, R.B., Cetin, K.O., Moss, R.E.S., Kammerer, A., Wu, J., Pestana, J. and Riemer, M., Sancio, R.B., Bray, J.D., Kayen, R.E., Faris, A. 2003. Recent Advances in Soil Liquefaction Engineering: A Unified and Consistent Framework. Earthquake Engineering Research Center Report No. EERC 2003-06. http://eerc.berkeley.edu/reports/.

Simpson, L.A., Jang, S.T., Ronan, C.E., Splitter, L.M. 2008. Liquefaction potential mitigation using rapid impact compaction. Geotech Earthq Eng Soil Dyn IV 2008:1–10.

Tan, S.A., Tjahyono, S., Oo, K.K. 2008. Simplified plane-strain modeling of stone-column reinforced ground. J. Geotech. Geoenviron. 134 (2), 185–194.

Tarragó, D., Deu, A., Gens A., Alonso, E.E., Griell, R. 2012. Preload improvement and monitoring in a newly reclaimed area. International Conference on Ground Improvement and Ground Control, Wollongong (Australia).

Thevanayagam, S., Martin, G.R. 2002. Liquefaction in silty soils-screening and remediation issues. Soil Dynamics and Earthquake Engineering, 22(9-12): 1035-1042.

Tomlinson, M. J. 1956. Telford and soil mechanics. Géotechnique 6, No. 3, 99–105.

Yafrate, N. J., DeJong, J. T., DeGroot, D. J., Randolph, M. F. 2009. Evaluation of remolded shear strength and sensitivity of soft clay using full-flow penetrometers. J. Geotech. Geoenviron. Eng., 135(9), 1179–1189.

Yao, W., Pang, J., Liu, Y. 2018. An experimental study of Portland cement and superfine cement slurry grouting in loose sand and sandy soil. Infrastructures 2018;3(2):9.

Yamamuro, J. A., Lade, P. L. 1998. Steady-state concepts and static liquefaction of silty sands. J. Geotechmical Geoenvironmental Engineering ASCE 124, 868–877.

Yang, J. 2002. Non-uniqueness of flow liquefaction line for loose sand. Géotechnique 52, 757-760.

Yasuda, S., lida, T., Kita, H., Saimura, Y., Tanaka, H. 1996. Countermeasures by sheet piles with drain holes against the settlement of embankments due to liquefaction. Proc., Int. Symp. on Seismic and Envir. Aspects of Dam Des.: Earth, Concrete and Tailing Dams, I(Oct.), 489-496.

Yegian, M. K., Eseller-Bayat, E., Alshawabkeh, A., Ali, S. 2007. Induced-partial saturation for liquefaction mitigation: experimental investigation. J. Geotech. Geoenviron. Engng, ASCE 133, No. 4, 372–380.

Xiao, P., Liu, H., Xiao, Y., Stuedlein, A.W., Evans, T.M. 2018. Liquefaction resistance of biocemented calcareous sand. Soil Dyn. Earthq. Eng. 2018;107:9–19.

Chapter 6. Conclusions and future research

6.1. Conclusions

The Phase 1 of Prat quay failed catastrophically due to the flow liquefaction of the hydraulic fill. The failure involved large displacements of the quay wall caissons. The flow liquefaction potential of the hydraulic fill has been established from several sources: the characteristic features of the failure, field observations after the failure, test results from the subsequent site investigation and the application of existing liquefaction criteria, based mainly on CPTu test results.

A suitable modified state parameter elasto-plastic constitutive law has been selected to reproduce the undrained brittle behaviour of liquefiable hydraulic fills. It has been used in the simulation of the construction and failure of the Phase 1 quay. In the modelling, failure occurs with the hydraulic fill at the same elevation as in the real case. Two different triggering mechanisms are identified that equally explain the failure: spontaneous liquefaction, or liquefaction of a limited zone associated with the location of the embankment being built at the time of failure. The behaviour of the quay wall prior to the failure is also adequately reproduced. A parametric study has verified the robustness of the simulation and the dependence of stability on the brittleness of the hydraulic fill. It is important to note that liquefaction of the hydraulic fill was not triggered by a conventional sliding failure in the ground underlying the site or by a pore pressure increase. On this occasion, it was the fill liquefaction that initiated the horizontal sliding of the caissons.

After the failure, it was found that the Phase 2 of Prat quay had only a marginal degree of stability in case of hydraulic fill liquefaction, although, in this case, the critical failure mechanism was a deep sliding involving the natural ground. Therefore, remedial measures were adopted to reduce the flow liquefaction potential. Soil improvement consisted of surcharge preloading with prefabricated strip drains and the installation of stone columns in part of the cross-section. Additional site investigation performed after soil improvement provides valuable data for the assessment of the reduction of flow liquefaction potential achieved. The results clearly indicated an increase of undrained shear strength

and a condition of no flow liquefaction potential according to available flow liquefaction criteria, based on mainly in CPTu results. It can be therefore concluded that the flow liquefaction potential was removed due to the soil improvement operations performed. An additional evaluation of cyclic liquefaction using Spanish seismic standards (Appendix E) also indicated no cyclic liquefaction potential remaining after soil improvement. Although the CPTu results have provided good and consistent information on liquefaction potential and its variation due to preloading, a more comprehensive programme of laboratory tests on good quality samples would have been also advisable.

The completion of the construction of Phase 2 was based on the observational method whereby the sequence and duration of the different construction stages depended on the monitoring information while supported by the comparisons with the results of the numerical analysis. In the stability calculations, it was assumed that the hydraulic fill was potentially liquefiable until the full sequence of soil improvement operations was concluded. The Phase 1 quay wall was reconstructed with mainly terrestrial fill with no flow potential liquefaction, as confirmed by the corresponding CPTu tests.

Based on the experience gathered in the Prat quay case, it is possible to propose an operational scheme for the case of quays constructed with hydraulic fills potentially susceptible to flow liquefaction. The scheme includes:

(i) A protocol to evaluate liquefaction potential for hydraulic fills,
(ii) An appropriate numerical analysis in which soil liquefaction is adequately simulated,
(iii) Soil improvement procedures to reduce flow liquefaction potential of a hydraulic fill.
(iv) A monitoring system to control and check the behaviour of the quay during construction.

(i) A protocol to evaluate liquefaction potential for hydraulic fills has been proposed in Chapter 5 using information before, during and after fill emplacement. For each phase, specific tests to be performed are suggested. The same protocol can be used to assess liquefaction potential after soil improvement. No specific liquefaction criteria are prescribed because those criteria are still under intense development. However, criteria based on CPTu test appear to be the most robust and reliable.

(ii) The numerical analysis has to incorporate a constitutive model capable of reproducing the undrained brittle behaviour characteristic of materials capable of undergoing flow liquefaction. A modified CASM constitutive model, as described in this PhD thesis, has proved capable of simulating satisfactorily a failure caused by the flow liquefaction of a hydraulic fill.

(iii) A soil improvement procedures should be used to remove liquefaction potential. The preloading surcharge with PVD provides excellent results for fine grained soils (Chapter 5), but, other solutions

may be required for coarse grained soils. Preliminary trial of soil improvement procedures should be used to check its efficiency and to optimize design.

(iv) A monitoring system should be designed to provide suitable data for understanding the quay behaviour. The monitoring system is the key component of an observational approach aimed to ensure a sufficient margin of stability in all construction stages. Constant comparison with the numerical simulation results should be used to detect anomalous behaviour that may require a change in the design and/or the construction programme. Reliance on a monitoring system, however, should be tempered by the knowledge that, often, failures involving brittle material give scant warning. For this reason, the prior evaluation of flow liquefaction potential for hydraulic fills is always a matter of crucial importance.

6.2. Future work

The recommendation for future work is classified in three categories: (i) the improvement of the proposed protocol for liquefaction potential evaluation, (ii) additional developments of the constitutive law and (iii) the applicability for the proposed operational scheme.

Additional tests on hydraulic fill samples can be added to the protocol. Basically, four additional test sets can be defined:

i) Anisotropically consolidated triaxial tests with undrained shear under compression and extension (Trx-CAUc and Trx-CAUe) to obtain of $c_{u\ SS}$ and $c_{u\ peak}$.

ii) The definition of the CSL and the RCL position from: (i) Trx-CAUc and Trx-CAUe tests (ii) oedometer tests and (iii) anisotropically consolidated triaxial tests with drained shear under compression and extension (Trx-CADc and Trx-CADe).

iii) The characterization of the soil rate dependence from Trx-CAUc and Trx-CAUe tests using different shear strain rates.

iv) Hollow cylinder tests under different loading conditions to describe the anisotropic behaviour of hydraulic fills. Some tests were in fact carried out in the UPC Geotechnical Laboratory on Prat quay hydraulic fill. However, the enormous difficulties to obtain adequate specimens prevented the performance of more tests.

As a matter of fact, there is still material from the hydraulic fill of Prat quay in the UPC Geotechnical Laboratory. It could be interesting to perform further tests for a better understanding of the hydraulic fill behaviour. For that purpose, the slurry deposition technique in a settling column can be used to try to obtain good quality soil specimens for testing (following the procedure described in Appendix F).

New developments can improve the constitutive law to simulate flow liquefaction, as, for instance, the incorporation of rate effect recently implemented in CASM, Mánica (2020). Other potential advances are:

i) Soil anisotropy could be implemented in the CASM model. Although there are not yet conclusive experimental results, hydraulic fills are likely to exhibit an anisotropic behaviour due to the type of soil formation.

ii) Incorporate in the CASM model the possibility of considering the changes of fabric and undrained brittleness due to soil improvement operations.

iii) Automatic φ - c reduction method should be developed for CASM model.

iv) The implementation of a suitable model that simulates liquefaction due to cyclic loading.

The operational scheme presented above for dealing with hydraulic fill is quite general and it can be applied to a variety of problems other than quays. The following lines of work can be mentioned:

- Hydraulic fill, is used in a wide range of engineering projects. Thus, apart from quay walls, the scheme can be applied, for instance, to embankments and land reclamation projects. Currently a catastrophic failure involving a tailings dam is being studied using the same tools.

- Assessment and, if required, retrofitting of projects constructed using hydraulic fills in which liquefactions is possible. Priority should be given to structures that have the potential of causing the largest damage.

- In addition to those examined in the PhD thesis, there are other causes that may trigger flow liquefaction. A comprehensive list of potential causes could provide a useful guideline for good practice.

- Specific standards for potentially liquefiable hydraulic fills should be developed.

Publications

Alonso, E.E., Gens, A., Tarragó, D., Madrid. R. 2009. Liquefaction Potential of Hydraulic Fills. 17th International Conference on Soil Mechanics and Geotechnical Engineering, Alexandria (Egypt).

Alonso, E.E., Gens, A., Madrid, R., Tarragó, D. 2010. Preloading Design Based on Long Term Extensometer Readings. A Comparision of Alternative Models. Symposium on New Techniques for Design and Construction in Soft Clays, Sao Paulo (Brazil).

Tarragó, D., Gens, A., Alonso, E.E., Romero, E.E., Griell, R. 2010. The Sustainability of the Barcelona Port enlargement works. 6th International Congress on Environmental Geotechnics, New Delhi (India).

Tarragó, D., Deu, A., Gens, A., Alonso, E.E., Griell, R. 2012. Preload improvement and monitoring in a newly reclaimed area. International Conference on Ground Improvement and Ground Control, Wollongong (Australia).

Tarragó, D., Gens, A., Alonso, E.E. 2013. Liquefaction potential criteria applied to hydraulic fills. Young International conference on Soil Mechanics and Geotechnical Engineering, Paris.

Madrid, R., Gens, A., Alonso, E.E, Tarragó, D. 2013. A simplified procedure to assess the dynamic stability of a caisson breakwater. International conference on Soil Mechanics and Geotechnical Engineering, Paris.

Martínez, J. M. (Ponente) Fernández, R., Dávila, M., Grau, J.I., Rodríguez, I., Gómez, G., Lope, A., Ginard, A., Zatarain, J.L., Hernáez, M., Pérez, J.P., Burgos, M., García, C., Uzcanga, J., Pérez, J.D., Noya, F., Ruiz, A., González, J., Tarragó, D., Rodríguez, F., Burbano, G., Pita, M., Enamorado, C., Pita, E., Ametller, X., Samper, F. 2014. Rellenos Portuarios: Conclusiones del Grupo de Trabajo IP-03 Técnicas y metodologías para la evaluación, caracterización y mejora de rellenos portuarios: Propuesta de clasificación. Grupo de Trabajo IP-03 del Comité Técnico de Ingeniería Portuaria Infraestructuras, logística y sostenibilidad. IV Congreso Nacional de la Asociación Técnica de Puertos y Costas.

Tarragó, D., Gens, A. (2018). Gas effect on CPTu and dissipation test carried out on natural soft-soil of Barcelona Port. 4th International Symposium on Cone Penetration Testing, Delft, Nederland. Best poster award.

Appendix A. Factor of Safety

1. Introduction

Terzaghi (1929), Felleniius (1936), Taylor (1937) and Bishop (1955) developed stability analysis during the study of real cases histories of failures or construction processes. The stability assessment is generally quantified using Factor of Safety in which is roughly associated with the reliability of a particular design. Bishop (1955) gave a general definition of FoS in geotechnical engineering terms: "F (or FoS) is defined as the ratio of the available strength of the soil to that required to maintain equilibrium", and proposed the following expression:

$$s = \frac{1}{F} \cdot [c' + (\sigma_n - u) \cdot \tan(\varphi')] \quad [38]$$

Where: shear strength mobilized is s, *c'* denotes cohesion, *φ'* denotes friction angle, σ_n, denotes total normal stress, *u* denotes water pore pressure.

This concept has been widely implemented in numerical analysis due to the engineering requirements. In this PhD thesis, FoS is calculated to evaluate quay wall stability. However, the same methodology can be applied to other cases.

2. FoS in FEM analysis

FEM programs for geotechnical engineering usually have implemented the method of φ - c reduction proposed in Brinkgreve and Bakker (1991). This method resembles the system of calculating FoS as conventionally adopted in slip-circle analyses according to equation [39].

$$\sum M_{sf} = \frac{\tan \varphi_{input}}{\tan \varphi_{reduced}} = \frac{c_{input}}{c_{reduced}} = \frac{c_{u\ input}}{c_{u\ reduced}} \quad [39]$$

Lately, the safety factor total multiplier was renamed by partial material factor (γ_m). This term was discussed by Simpson (2000) and (2007), Bauduin et al. (2003), Cheung et al. (2010) and Potts &

Zdravkovic (2012) in order to know what was the influence of FoS analysis in advance numerical analysis.

In the last decade, some improvements of FoS have been performed because of the new Eurocode 7 (EC7) for geotechnical design. EC7 imposes two different ways to design according to FoS obtained from partial material factors on soil strength. These are DA1 and DA3 design approaches, Potts & Zdravkovic (2012).

3. Manual φ - c reduction method

The method of φ - c reduction is an automated calculation option in the commercial FEM programs. However, it cannot be used in analyses using CASM model because the strength of CASM model -described in Chapter 3-, does not depend on φ - c values. Therefore, although some of the defined materials in the analyses can be computed according to automatic φ - c reduction method, a set of materials with prescribed strength reduction have to be defined using [39].

The strength reduction of materials is performed for a specific stage of the analysis; at one point the strength reduction applied generates an instability. The obtained FoS is defined in accordance with the last converged step or the percentage of converged steps (M_{stage}) of the calculation. It is important to note that the upper boundary of the proposed FoS for CASM is 1.25 due to CASM limiting factors described below.

The materials to obtain different FoS for Prat quay analyses are Soft-Soil (Plaxis, 2010), CASM and Mohr-Coulomb constitutive models.

3.1. Soft soil φ – c reduction

The Soft Soil model is a modified Cam-Clay type model; nevertheless, the failure is controlled by Mohr-Coulomb yield. Therefore, $\varphi - c$ parameters control the soil strength, as it is represented in Figure A1.

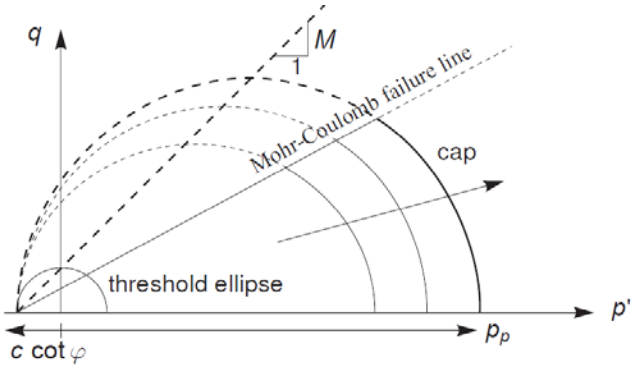

Figure A1. Yield surface of the Soft Soil model in p'-q plane, Plaxis 2010.

The manual φ – c reduction method in Soft Soil model should be used according some restrictions under undrained conditions in terms of undrained shear strength (c_u). Thus, some numerical analyses of triaxial CAU are simulated to define control the real reduction of c_u according to FEM program φ

– c reduction and obtained FoS. Triaxial test analyses have been performed with the same consolidation stress path of σ'_v=100 kPa and K_0=0.66. Soft soil model has been used to simulate natural ground therefore initial undrained shear strength has to yield the law $c_u = 0.25\ \sigma'_v$ (from laboratory tests results Chapter 2). The manual reduction of undrained shear strength for different FoS is presented in Table A1.

Table A1. Soft soil values of friction angle, strength ratio and FoS $_{cu}$ under triaxial conditions.

c_u/σ'_v	FS $c_{u\ T\text{-}CAU}$
0.25	1
0.23	1.08
0.22	1.13
0.21	1.18
0.20	1.24
0.19	1.33

3.2. CASM φ – c reduction

CASM model was previously described (Chapter 3), it is important to note that c_u cannot be directly modified.

To perform a reliable strength reduction, n -defined in Chapter 4-, is changed to maintain $c_{u\ peak}$. In addition, K_0 is modified by adjusting w and β to avoid stress path inconsistencies. Note that defined K_0 is reasonably close to failure. The adopted K_0 is 0.63 (η_{Ko}=0.49), which tolerates a 1.25 reduction on $c_{u\ peak}$, corresponding to a FoS=1.25.

A set of materials with different n are implemented to reach static liquefaction according different $c_{u\ peak}$, 0.25 σ'_v, 0.24 σ'_v, 0.23 σ'_v, 0.22 σ'_v, 0.21 σ'_v, 0.20 σ'_v, respectively, it is shown in Table A2.

Table A2. Additional CASM material parameters.

Material	r	n	β	w
Hyd. Fill $c_{u\ peak}$ =0.25 σ'_v	12	10	0.73	0.003
Hyd. Fill $c_{u\ peak}$ =0.24 σ'_v	12	8	0.69	0.012
Hyd. Fill $c_{u\ peak}$ =0.23 σ'_v	12	7	0.67	0.025
Hyd. Fill $c_{u\ peak}$ =0.22 σ'_v	12	6	0.64	0.050
Hyd. Fill $c_{u\ peak}$ =0.21 σ'_v	12	5	0.60	0.10
Hyd. Fill $c_{u\ peak}$ =0.20 σ'_v	12	4	0.56	0.20

The p'- q stress paths for undrained triaxial test with anisotropic consolidation (Trx-CAU) numerical simulations are presented in Figure A2. Additionally, vertical strains versus q are plotted in Figure A3. The defined materials satisfy the expected K_0 and undrained softening behaviour.

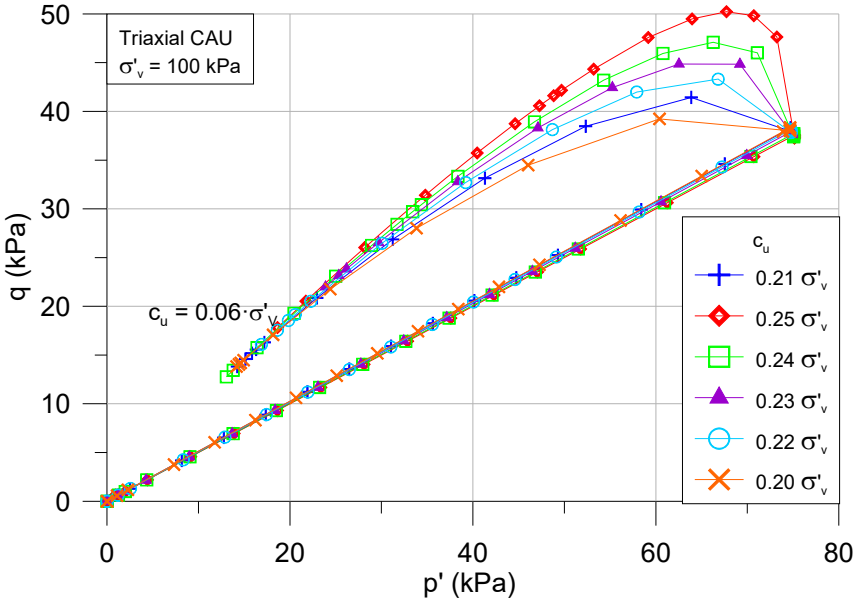

Figure A2. Effective stress paths for triaxial CAU simulations.

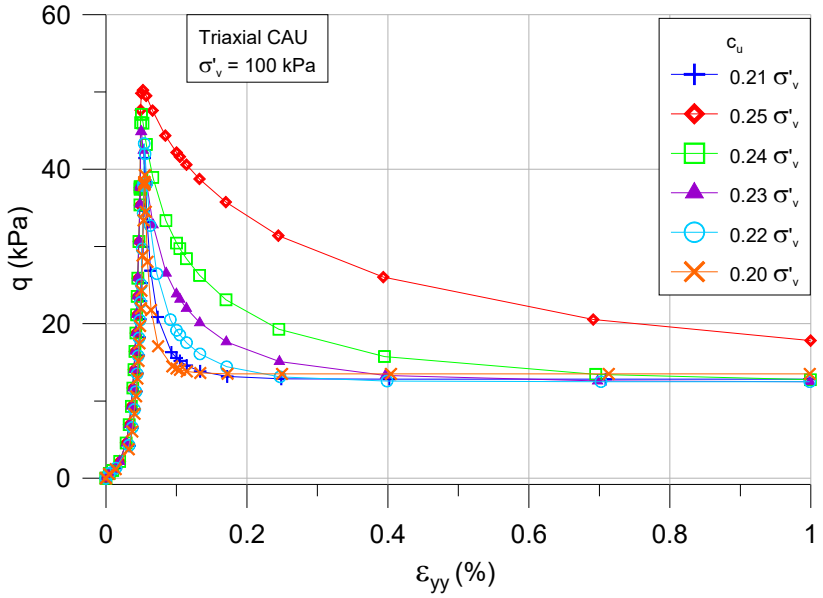

Figure A3. ε_1 vs. q curves during shear for triaxial CAU simulations.

Proposed materials for hydraulic fill reach the following FoS, see Table A3.

Table A3. FoS reached with the CASM materials.

Material	**FoS**
Hyd. Fill $c_u = 0.25\ \sigma'_v$	**1**
Hyd. Fill $c_u = 0.24\ \sigma'_v$	**1.04**
Hyd. Fill $c_u = 0.23\ \sigma'_v$	**1.09**
Hyd. Fill $c_u = 0.22\ \sigma'_v$	**1.14**
Hyd. Fill $c_u = 0.21\ \sigma'_v$	**1.19**
Hyd. Fill $c_u = 0.20\ \sigma'_v$	**1.25**

3.3. Mohr-Coulomb φ – c reduction

The manual Mohr-Coulomb *φ – c reduction* is presented in Table A4 for the strength parameters of the M-C materials.

Table A4. Reduction of Mohr-Coulomb materials.

FoS	Rubble mound, rock-fill and upper rock-fill	Dumping ground-fill	Improved soil with stone columns
	ϕ [°]	ϕ [°]	ϕ [°]
1	38	28	27
1.04	36.9	27.1	26.1
1.09	35.6	26.0	25.1
1.14	34.4	25.0	24.1
1.19	33.3	24.1	23.2
1.25	32.0	23.0	22.2
1.33	30.4	21.8	21.0

4. References

Bauduin, C., De Vas, M., Frank, R. 2003. ULS and SLS design of embedded walls according to Eurocode 7. Proc. 13th Eu. Conf. Soil Mech. Geotech. Engng, Prague 2, 41-46.

Bishop, A.W. 1955. The use of the Slip Circle in the Stability Analysis of Slopes. Géotechnique 01/1955; 5(1):7-17.

Brinkgreve, R.B.J., Bakker, H.L. 1991. Non-linear finite element analysis of safety factors Proc. 7th Int. Conf. Comp. Methods and Advances in Geomech, A.A. Balkema (1991), pp. 1117-1122.

Cheung, K., West, K., Yeow, H., Simpson, B. 2010. Do Eurocodes make a difference?. Geomech. Tunnelling 3, No. I, 35-47.

Fellenius, W. 1936. Calculation of the stability of earth dams. In Transactions of the 2nd Congress on Large Dams, Washington, D.C. Vol. 4, pp. 445–462.

Plaxis 2010. Materials Models Manual.

Potts, D. M., Zdravkovic, L. 2012. Accounting for partial material factors in numerical analysis. Geotechnique 62, No. 12, 1053-1065.

Simpson, B. 2000. Partial factors: where to apply them?. Proc. Int. Workshop on Limit State Design in Geotech. Engng, Melbourne, Australia (CD-ROM).

Simpson, B. 2007. Approaches to ULS design: the merits of Design Approach I in Eurocode 7". Proc. 1st Int. Symp. on Geotech. Safety and Risk, Shanghai, 527-538.

Taylor, D.W. 1937. Stability of earth slopes. Journal of Boston Society of Civil Engineers, 24 (3) (1937), pp. 197-246.

Terzaghi, K. 1929. The mechanics of shear failures on clay slopes and the creep of retaining walls. Public Roads 10 (10), 177–192.

Appendix B. Prat quay failure FEM analysis – Initial hypothesis

1. Introduction

Different assumptions of the failure causes were studied just after the failure. Hydraulic fill liquefaction assumption was identified as a major factor of the failure by the Technical expert's Committee that had been advising APB after the failure.

2. Hypothesis for hydraulic fill liquefaction

In order to perform a conservative modelling of soil liquefaction, an assumptions was implemented for the hydraulic fill. Specifically, a material was defined to simulate liquefied undrained shear strength ($c_{u\ LIQ}$). Thus, flow liquefaction is assumed for the hydraulic fill from the beginning. This type of analysis can be quite conservative, but at the same time, it is very robust.

3. FEM analysis

The analysis entailed the geometry and construction stages implemented in the analysis of Phase 1 that have been presented in Chapter 4. In this case, the Soft Soil model was established for simulating the hydraulic fill as well as the fine grained natural ground. In this sense, undrained shear strength obtained from model was adjusted to reach $c_u = 0.06 \cdot \sigma'_v$ for the hydraulic fill and $c_u = 0.25 \cdot \sigma'_v$ for the natural ground. Both adjusted models for hydraulic fill and natural ground -using parameters from Chapter 4-, reproduce correctly direct simple shear tests simulations performed in FEM analysis, see Figure B1.

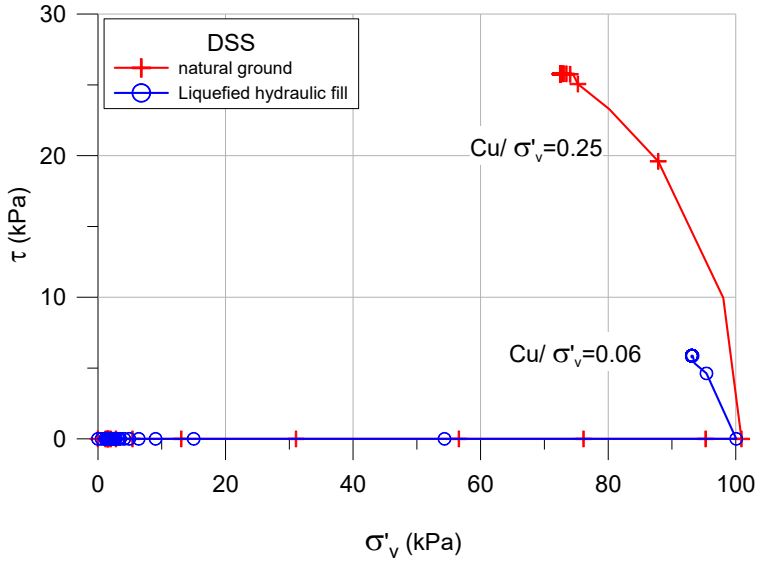

Figure B1. Undrained strength vs. effective vertical stress results for direct simple shear simulations.

The Soft Soil model parameters and properties for hydraulic fill are presented in Table B1. An interface element was provided between the caisson and the hydraulic fill with a friction angle of 9º.

Table B1. Parameters for liquefied hydraulic fill in Soft Soil constitutive model.

Properties	**Liquefied hydraulic fill**
Saturated unit weight [kN/m^3]	18 / 19
Poisson's ratio (ν)	0.3
Void ratio (e)	2
Compression index (c_c)	0.20
Swelling index (c_s)	0.02
Permeability [m/s]	10^{-8}
Undrained shear strength ratio (c_u /σ'$_v$)	0.06

The failure is reached for hydraulic fill up to +3m (stage 14), in this case at M_{stage}=0.07.

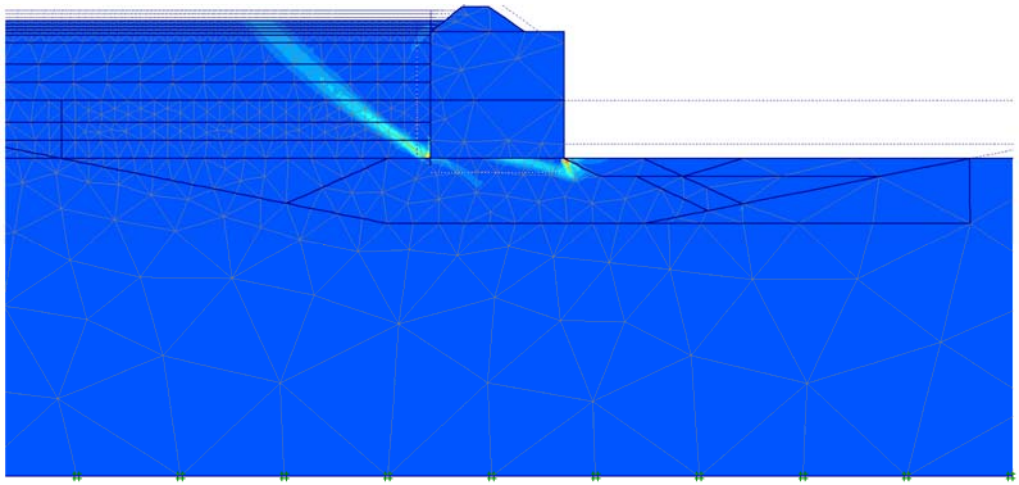

Figure B2. Incremental shear strains at failure, stage 14.

Additionally, Factors of Safety are computed for Stage 11 and 13 before the failure (Table B2). FoS are evaluated according to FoS methodology presented in Appendix A. Results point out that failure could occur during stage 14 because FoS in stage 13 was close to 1.

Table B2. FoS of preceding stages before the quay failure.

Stage	Identification	FoS Manual φ -c reduction
11	Hydraulic fill up to +0 m	>1.25
12	Hydraulic fill consolidation (+0 m)	-
13	Hydraulic fill up to +2 m	1.02
14	Failure - Hydraulic fill up to +3 m	< 1

Appendix C. Prat quay Phase 2 FEM analysis – Initial hypothesis

1. Introduction

The Prat quay Phase 2 stability is analysed using hydraulic fill simulation according to the liquefaction hypothesis proposed in Appendix B. Thus, only an adjustment to the soil model used for hydraulic fill is performed. The rest of the analysis has the same geometry and constructions stages that was described in Chapter 5. In the following sections, the stability analyses of Phase 2 quay are presented: (i) until the failure of Phase 1 and (ii) with soil improvement.

2. Prat quay Phase 2, until the failure of Phase 1

2.1. Stability evaluation

The analysis of the different construction stages from 0 to 11 (Chapter 5.2) has been calculated. Computed factor of safety for stage 11 is 1.08 according to manual φ – c reduction -as it was described in Appendix A-, are shown in Table C1.

Table C1. Factor of safety for stage 11 of the Prat quay Phase 2.

Description	Stage	FoS Manual φ – c reduction
Hydraulic fill up to +1.5m	10	1.08

FoS for the hydraulic fill level increase up to +1.5 m is consistent with the fact that Phase 2 of quay Prat had not developed instability. At this point, failure involves the hydraulic fill and natural ground, as it is presented in Figure C1. The failure passes below the rubble mound and the rock-fill.

If the quay wall construction would have continued, preloading improvement would have been carried out. Preloading stage generates the quay wall failure, in which an abrupt reduction in FoS (<1) is generated.

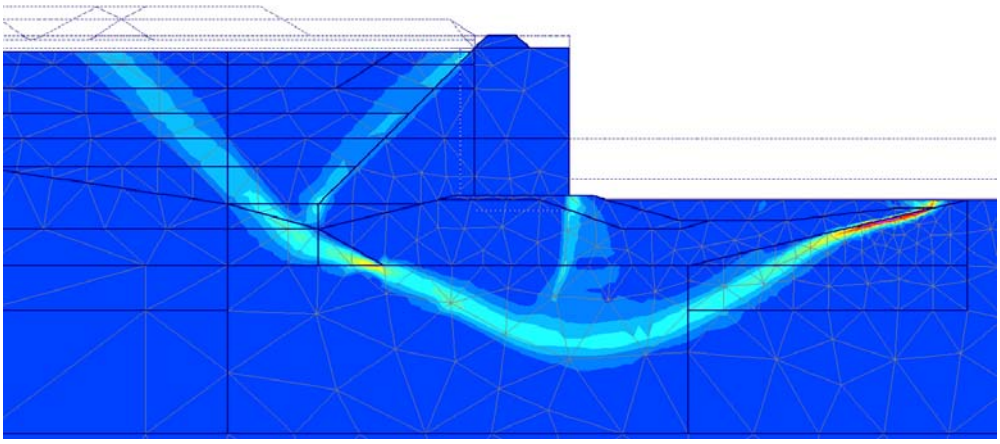

Figure C1. Contours of incremental shear strains at stage 10, FoS=1.08.

3. *Prat quay Phase 2, after soil improvement.*

The simulation after soil improvement for Phase 2 (Chapter 5.6) is performed. Although the entire stages of Phase 2 construction are simulated, only the stages after soil improvement are discussed.

3.1. Hypothesis for hydraulic fill

Fundamentally, hydraulic fill assumptions are related to liquefaction potential as presented in Appendix B. Thus, liquefied hydraulic fill are simulated according to c_u=0.06 σ'$_v$. Nevertheless, c_u=0.25 σ'$_v$ in hydraulic fill material is used once the preloading was unloaded, as presented in Chapter 5.6. Summarized strength assumptions of the hydraulic fill for each calculation stage are presented in Table C2.

Table C2. c_u ratio for the hydraulic fill during stages 12 to 34.

Description	Stage	Time (days)	Hydraulic fill strength
Removal of the earth bund over the caissons	12	80	0.06·σ'v
Granular Fill up to -0.5 m (placement by terrestrial means)	13	50	0.06·σ'v
Granular Fill up to +1 m (placement by terrestrial means)	14	30	0.06·σ'v
Drainage layer up to +1.5 m	15	50	0.06·σ'v
Vertical prefabricated strip drains installation (+1.5 m)	16	110	0.06·σ'v
Deposit zone preloading up to +6.5 m	17	20	0.06·σ'v
Deposit zone preloading consolidation	18	45	0.06·σ'v
Preloading up to +8.5 m, in part of the deposit zone. Caisson preloading with 6 layers of 0.5 m of soil	19	15	0.06·σ'v
Preloading up to +10 m, in part of the deposit zone. Caisson preloading with 6 layers of 0.5 m of soil	20	20	0.06·σ'v

Deposit zone and caissons preloading consolidation	21	45	0.06·σ'v
Deposit zone preloading consolidation. Caissons preloading with 7 layers of 0.5 m of soil	22	4	0.06·σ'v
Deposit zone and caissons preloading consolidation. Stone columns installation	23	55	0.06·σ'v
Deposit zone and caissons preloading consolidation.	24	85	0.06·σ'v
Deposit zone preloading consolidation. Unloading caissons preloading reduced to 3 layers of 0.5 m soil	25	10	0.06·σ'v
Deposit zone and caissons preloading consolidation.	26	50	0.06·σ'v
Deposit zone and caissons preloading consolidation. Manoeuvring zone preloading up to +5 m and +3 m.	27	10	0.06·σ'v
Deposit zone, manoeuvring zone and caissons preloading consolidation	28	15	0.06·σ'v
Deposit zone and caissons preloading consolidation. Manoeuvring zone preloading up to +6.5 m and +5 m.	29	20	0.06·σ'v
Manoeuvring zone and caissons preloading consolidation. Unloading deposit zone preloading	30	60	0.06·σ'v
Manoeuvring zone and caissons preloading consolidation	31	60	0.06·σ'v
Preloads unloading to final height, 3m	32	30	0.25·σ'v
Pavement, capping beam construction and dredge in the sea side to -16.5 m	33	360	0.25·σ'v
Service loads	34	90	0.25·σ'v

Soil parameters were defined in Chapters 4 and Chapter 5. However, Soft Soil constitutive model parameters that simulates liquefied hydraulic with PVD installation are listed in Table C3.

Table C3. Parameters for hydraulic fill with prefabricated vertical drains in Soft Soil constitutive model.

Properties	**Liquefied hydraulic fill improved using vertical drains**
Saturated unit weight (kN/m^3)	18 / 19
Poisson's ratio (ν)	0.3
Void ratio (e)	1
Compression index (c_c)	0.23
Swelling index (c_s)	0.07
Permeability (m/s)	$2 \cdot 10^{-7}$
Undrained shear strength ratio (c_u/σ'_v)	0.06

3.2. Stability evaluation

Stages during deposit zone preloading and manoeuvring zone preloading and service loads-, are calculated with both φ – c reduction methods described in Appendix A.

Computed factors of safety values for deposit zone preloading are presented in Table C4. These values are higher or equal than 1.25, enough to avoid any failure during this preload, taking into account the worst FoS obtained with manual *φ - c' reduction*.

Table C4. FoS of selected stages of Prat quay Phase 2.

Description	Stage	FoS Manual φ – c reduction
Deposit zone preloading up to +6.5 m	17	1.27
Preloading up to +10 m, in part of the deposit zone. Caisson preloading with 6 layers of 0.5 m of soil	20	1.27
Deposit zone preloading consolidation. Caissons preloading with 7 layers of 0.5 m of soil	22	1.26
Deposit zone preloading consolidation. Unloading caissons preloading reduced to 3 layers of 0.5 m soil	25	1.41
Deposit zone and caissons preloading consolidation. Manoeuvring zone preloading up to +5 m and +3 m.	27	1.34
Deposit zone and caissons preloading consolidation. Manoeuvring zone preloading up to +6.5 m and +5 m.	29	1.25
Service loads	34	1.28

The failure mechanism in stage 20 (Figure C2) is the most representative. This failure is fundamentally triggered by the caissons preloading. The failure surface crosses the stone columns treatment and it passes, as far as possible, thorough the natural ground just below the rubble mound.

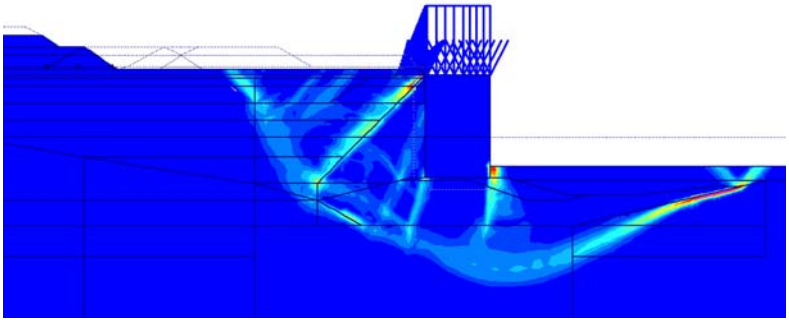

Figure C2. Contours of incremental shear strains at stage 20, FoS=1.38.

The lowest computed FoS is 1.25, it corresponds to the last preloading step of the manoeuvring zone, stage 29. The failure mechanism for stage 29 is presented in Figure C3. This failure is clearly generated by the emplacement of the preloading in the manoeuvring zone. The failure mechanism is a deep sliding that begins 40 m away from the quay wall.

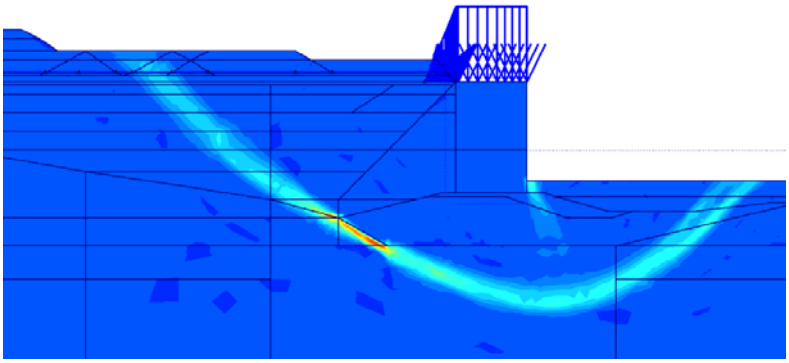

Figure C3. Contours of incremental shear strains at stage 29, FoS=1.25.

Appendix D. Barcelona seismic conditions

To evaluate the Barcelona Port liquefaction susceptibility due to cyclic liquefaction, it is necessary to bear in mind the range of maximum peak accelerations that an earthquake could generate in that area.

Seismic risk assessment studies in Barcelona have been common during last years. Authors, as Secanell (1999) and Cid et al. (2001) have implemented different methodologies to zone Barcelona city using a database of approximately 2000 earthquakes and other aspects as the soil type or the distance to the focus. Barcelona Port is placed inside Zone I according the zonation presented in Figure D.1.

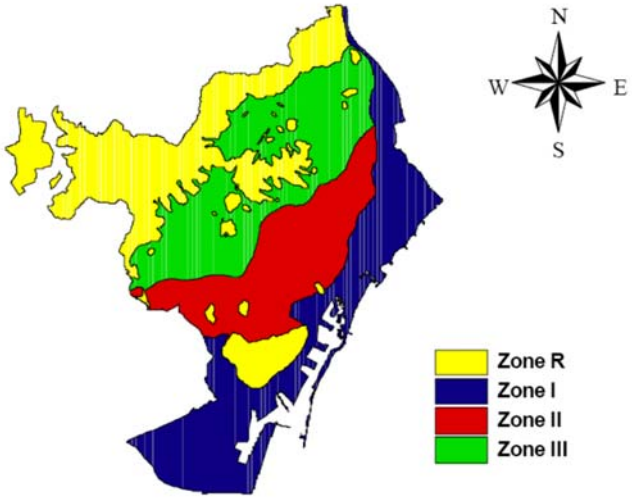

Figure D.1. Seismic zoning of Barcelona city according to local effects (Cid et al. 2001).

Irizarry (2004) calculated PGA (peak ground acceleration) for Barcelona zonation as it is shown in Figure D.2. Deterministic methodology and Probabilistic methodology had been performed to obtain PGA. Values of PGA for the Port of Barcelona are 0.14g for the Deterministic method and PGA=0.19g for the Probabilistic method.

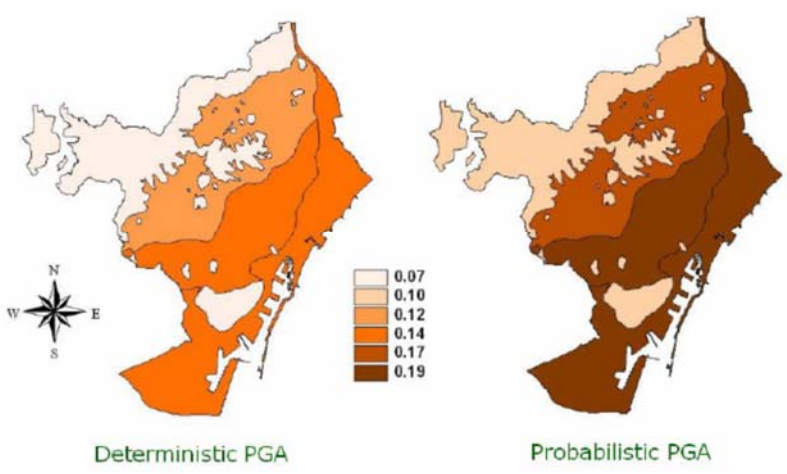

Figure D.2. The deterministic and probabilistic peak ground acceleration (g) according to soil effects in Barcelona city, Irizarry (2004).

Lantada et al. (2010) and Pujades et al. (2012) have used Irizarry (2004) assumption to perform seismic analysis in Barcelona buildings. However, Spanish seismic Standard NCSE-02 (2002) proposes other values of PGA or a_{max}. PGA values are performed using NCSE-02 procedure according to following equation:

$$PGA = \rho \cdot PGA_0 \cdot C \quad [40]$$

where: PGA_0 is peak ground acceleration for rigid material, C is the correction according to soil type and ρ is the magnification due to the construction importance, 1 or 1.3.

The NCSE-02 standard establishes the assumption of Barcelona city with PGA_0=0.04g. The C value depends on shear wave (V_s) propagation into the soil type. There are correlations of C between the zones and V_s, Cid et al. (2001) and NCSE-02 Standard presented in Table D.1.

Table D.1. Equivalence of NCSE-02 type soil and Barcelona soil zoning (Cid et al., 2001).

NCSE-02			Cid et al. (2001)	
NCSE-02 soil type	**C**	**$V_{S,30}$ (m/s)**	**Corresponding Barcelona soil zone**	**$V_{S,30}$ (m/s)**
I	1	V_S>750	R	800
II	1.286	750≥V_S>400	III	405
III	1.595	400≥V_S>200	II	384
III			I	225
IV	1.976	V_S≤200	-	-

Regarding NCSE-02 soil type and Barcelona soil zone, Barcelona Port is placed in zone III of NCSE-02 soil type.

PGA values calculations are performed with NCSE-02 Standard. These values obtained for NCSE-02 for soil type III and IV are 0.067g and 0.083g respectively, using magnification for high importance construction (ρ=1.3), see Table D.2.

Table D.2. Barcelona PGA values analysed according to soil type and ρ.

NCSE-02 soil type	*PGA* NCSE-02	*PGA** Deterministic	*PGA** Probabilistic
I	0.042g	0.07g	0.10g
II	0.054g	0.12g	0.17g
III	0.067g	*0.17g (average)*	*0.19g (average)*
III		0.14g	0.19g
IV	0.083g	-	-

* from Irizarry (2004)

Pujades (2012) -by means of a personal communication-, advised that PGA values from NCSE-02 could be used as a minimum; in contrast, PGA values of the Probabilistic method from Irizarry (2004) could be used as the maximum.

Although design earthquake magnitude in Barcelona is not specifically defined because of its complexity. A moment magnitude (M_w) equal to 5.25 is generally a good agreement (Pujades, 2012) and it is consistent regarding earthquake date base of Spain (IGME, 2014).

References

Cid, J., Susagna, T., Goula, X., Chavarria, L., Figueras, S., Fleta, J., Casas, A. & Roca, A. 2001. Seismic Zonation of Barcelona Based on Numerical Simulation of Site Effects. Pure Applied Geophysics 158: 2559-2577.

IGME 2014. Catálogo de los efectos geológicos de los terremotos en España. Grupo español de la escala macrosísmica ESI-07.

Irizarry, J. 2004. An Advanced Approach to Seismic Risk Assessment. Application to the Cultural Heritage and the Urban System Barcelona. PhD thesis. Dpto. Ingeniería del Terreno, Cartográfica y Geofísica. Universidad Politécnica de Cataluña, Barcelona. 290 pp.

NCSE-02 2002. Normativa de Construcción Sismorresistente Española. Comisión Permanente de Normas Sismorresistentes, Real Decreto 997/2002. Boletín Oficial del Estado No. 244 del 11 de octubre de 2002.

Pujades, L. G., Barbat, A. H., González-Drigo, R., Avila, J. and Lagomarsino, S. 2012. Seismic performance of a block of buildings representative of the typical construction in the Eixample district in Barcelona (Spain). Bull Earthquake Eng 10:331–349.

Pujades, L.G. 2012. Personal communication.

Secanell, R. 1999. Avaluació de la perillositat sísmica a Catalunya: anàlisi de sensibilitat per a diferents models d'ocurrència i paràmetres sísmics. PhD thesis. Universidad de Barcelona. Barcelona. 335 pp.

Appendix E. Cyclic Liquefaction potential evaluation for the hydraulic fill

1. Introduction

Cyclic loading could trigger cyclic liquefaction, cyclic mobility or flow liquefaction as it was described above in Chapter 3. The different criteria for cyclic liquefaction are described and evaluated in this Appendix.

2. Cyclic liquefaction criteria

Although different types of cyclic loading are able to produce liquefaction, the criteria have particularly focussed on earthquakes. The methodology was initially developed using disastrous earthquake events in Alaska and Japan, Seed & Idriss (1971). This methodology has been upgraded gradually since that time, by Seed and colleagues, Robertson and Campanella (1985), Robertson (1990), Jeffereis & Davies (1993), Stark and Olson (1995), Robertson and Wride (1998).

Youd and Idriss (2001) defined a landmark in terms of summary report on evaluation of liquefaction resistance of soils. At that point, the basic evaluation for:

(i) Cyclic stress ratio (CSR) for an earthquake was described

(ii) Cyclic resistance ratio (CRR) was evaluated from different in-situ tests (SPT, CPT or V_S).

(iii) Magnitude scaling factors (MSF) were recommended to evaluate cases for different earthquake magnitudes.

Afterwards, high progresses on CPTu liquefaction criteria have been performed in Zhang et al. (2002), Robertson (2004), (2009a) and (2009b), Jefferies and Been (2006) or Shuttle and Cunning (2007). In addition, for the same period, criteria for flat dilatometer Marchetti test (DMT) have been developed.

Later on, frequent developments from Seed and Idriss (1971) have been upgrading the initial methodology, Boulanger & Idriss (2006). This methodology is based on laboratory testing results and various theoretical assumptions, to obtain CRR for soils.

2.1. Cyclic stress ratio

Seed and Idriss (1971) presented stress calculation for a soil column. The cyclic stress ratio $(CSR)_{peak}$ is induced by shear stresses from an earthquake, normalized by effective vertical stress [41].

$$(CSR)_{peak} = \frac{\tau_{peak}}{\sigma'_v} \quad [41]$$

where: τ_{peak} is the peak horizontal shear stress.

CSR_{peak} has to be normalized by two factors r_e and r_d to obtain $(CSR)_M$ [42].

$$(CSR)_M = r_d \cdot r_e \cdot \frac{\tau_{peak}}{\sigma'_v} \quad [42]$$

where r_e is the necessary reduction to obtain a representative percentage of the earthquake shear stress, usually 65% of the τ_{peak} (r_e=0.65). r_d is the stress reduction factor which is dependent on depth.

Some approaches have been developed to calculate r_d, however the most commonly used is the approach of Liao and Withman (1986) [43], [44], [7] and [46] in which the r_d evaluation depends on the ground depth (z).

$$r_d = 1 - 0.00765\ z \qquad z \leq 9.15\ m \quad [43]$$

$$r_d = 1.174 - 0.0267\ z \qquad 9.15\ m < z \leq 23\ m \quad [44]$$

$$r_d = 0.744 - 0.008\ z \qquad 23\ m < z \leq 30\ m \quad [45]$$

$$r_d = 0.5 \qquad z > 30\ m \quad [46]$$

Even then, Idriss (1999) estimated stress reduction coefficient as [47], [48] and [49] depending on earthquake magnitude. It is compared to r_d values from Liao and Withman (1986) in Figure E.1. Afterwards, Youd et al. (2001) proposed these new equations to evaluate r_d.

$$r_d = \exp(\alpha(z) + \beta(z) \cdot M \quad [47]$$

$$\alpha(z) = -1.012 - 1.126 \cdot \sin\left(\frac{z}{11.73} + 5.133\right) \quad [48]$$

$$\beta(z) = 0.106 + 0.118 \cdot \sin\left(\frac{z}{11.28} + 5.142\right) \quad [49]$$

where: M, moment magnitude of the earthquake and z, depth in meters.

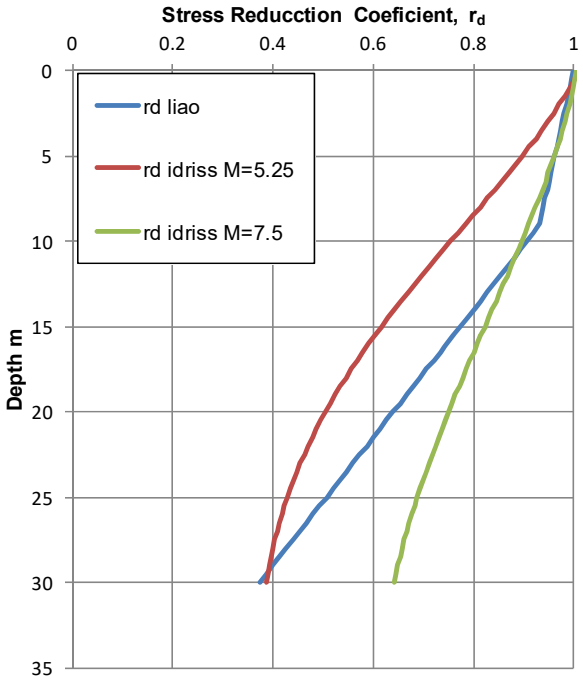

Figure E.1. Stress reduction coefficient according Liao and Withman (1986) and Idriss (1999).

The peak shear stress (τ_{peak}) is derived from vertical and horizontal forces of a soil column and the resulting equation is [50].

$$\tau_{peak} = \sigma_v \frac{a_{max}}{g} \quad [50]$$

where: σ_v is total vertical stress, a_{max} is the maximum possible acceleration of the study area due to an earthquake and g is the gravity acceleration.

Finally, the equation, which resumes the procedures, is the following, [51].

$$(CSR)_M = \frac{\tau_{av}}{\sigma'_v} = 0.65 \cdot \left(\frac{a_{max}}{g}\right) \cdot \left(\frac{\sigma_v}{\sigma'_v}\right) \cdot r_d \quad [51]$$

It is likely to depend on the maximum acceleration of M_w=7.5 earthquake.

2.2. Cyclic resistance ratio

Cyclic resistance ratio (*CRR*) is cyclic resistance normalized by vertical effective stresses of the soil. In the literature, some procedures were developed to obtain CRR according a specific CSR. The different criteria described below develop a methodology to derive CRR.

2.3. Magnitude Scaling Factors

To normalize the CRR or CSR for a particular earthquake magnitude (M_w), magnitude scaling factor (MSF) was defined Seed et al. (1975b).

$$MSF = \frac{CRR}{CRR_{M=7.5}} \quad [52]$$

Various MSF equations were presented in Arango (1996), Andrus and Stokoe (1997), Youd and Noble (1997) and Idriss (1999). The defined equations uniquely depend on earthquake magnitude (M_w). MSF resulting values are quite similar, although Youd et al. (2001) proposed a recommended range to use in practice, as it is shown in Figure E.2.

A boundary range was defined by Andrus and Stokoe (1997), [53]. Nevertheless, after, Youd et al. (2001) proposed [54].

$$MSF = (M_w/7.5)^{-2.56} \quad [53]$$

$$MSF = \frac{174}{M^{2.56}} \quad [54]$$

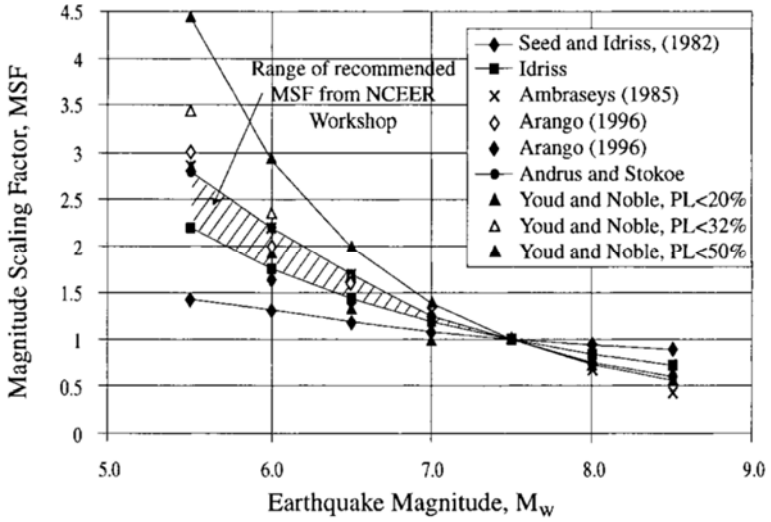

Figure E.2. MSF proposed by different authors, Youd and Noble (1997).

From a MSF revision presented in Idriss and Boulanger (2004), upgraded MSF was proposed for liquefaction analyses of sand-like soils that had been previously presented in Idriss (1999). Last proposal will be described below (Appendix E 2.5.1) because it has become fundamental part of a criterion for clay-like and sand-like soils, Boulanger and Idriss (2004).

In practice, engineers would like to know how far the soil is from liquefaction. Thus, MSF is likely to be used as function of factor of safety [55] (Youd et al., 2001).

$$FS = \frac{CRR_{M=7.5}}{CSR_{M=7.5}} = \frac{CRR_{M=7.5}}{CSR} \cdot MSF \quad [55]$$

2.4. In-situ tests criteria

In-situ testing holds an important role because of the extremely complex process to extract undisturbed soil samples.

First criterion for in-situ tests were defined for SPT results in Seed and Idriss (1971). Following upgrades extended the SPT results database, but also introduced newer and more complex in-situ tests -as CPT or CPTu, DMT, shear wave tests-, using the same framework.

However, although SPT criterion is supported by the largest database, testing conditions produce differences on results that the author do not believe precise enough to be used in the evaluation for the hydraulic fill of Prat quay.

Mentioned tests parameter were correlated with normalized CRR, from normalized cone resistance (q_c), friction resistance (f_s) and pore pressure (u) from CPTu, K_D from DTM and v_{S1} from shear wave tests.

2.4.1. Cone penetration test

Although the Robertson CPTu criterion described above in Chapter 3 and Chapter 5 could evaluate static liquefaction, this criterion was also recommended for cyclic liquefaction susceptibility in Robertson and Cabal (2012).

In this case, coarse grained soils ($I_c < 2.5$) and fine-grained soils ($I_c > 2.7$) regions have a specific behaviour against cyclic loading. Cyclic liquefaction could be reached depending on different conditions in four depicted regions:

- Dilative coarse-grained soils, level and duration of cyclic loading
- Contractive coarse-grained soils, loading and ground geometry
- Dilative fine-grained soils, level and duration of cyclic loading
- In contractive fine-grained soils, sensitivity, loading and ground geometry

Alternatively, CRR can be evaluated from CPTu profiles based on normalized cone resistance. Cyclic liquefaction potential criteria based on CPTu-based case-history liquefaction correlations, triggered by earthquakes have been developed by Roberston and Campanella (1985), Robertson & Wride (1998), Zhang et al., (2002) and (2004) and Robertson (2009b).

Criterion progresses from the original one presented in Robertson and Wride (1998) have been developed due to a number of contributions, Juang et al. (2003) and (2008), Idriss and Boulanger (2004), Moss et al. (2006) and Boulanger and Idriss (2006) proposal. Lately, this criterion was adapted in Robertson (2009b) by using the index I_c. Afterward, some changes were also performed in Robertson and Cabal (2012). It is in this last configuration of the criterion that three types of soil are defined:

(i) Fine-grained soils where I_c>2.7

(ii) Coarse-grained soils where $I_c \leq 2.5$

(iii) Transition zone that I_c lies on the range of 2.5 to 2.7.

Normalized cone resistance from Chapter 3 is used for evaluate this criterion. Also new parameters and assumptions were defined. Firstly, the factor regarding grain characteristics, K_c. was defined. This factor is related with I_c, as it is shown in equation [56] and [57].

$$\text{If } I_c \leq 1.64,\ K_c = 1.0 \quad [56]$$

$$\text{If } I_c > 1.64\ K_c = -0.403 \cdot I_c^4 + 5.581 \cdot I_c^3 - 21.63 \cdot I_c^2 + 33.75 \cdot I_c - 17.88 \quad [57]$$

Then, the equivalent clean sand normalized penetration resistance $(q_{c1N})_{cs}$ is generally calculated according equation [58]:

$$(q_{c1N})_{cs} = (Q_{tn})_{cs} = q_{c1N} \cdot K_c \quad [58]$$

Robertson (2009b) proposed different equations to achieve cyclic resistance ratio (CRR) for an earthquake of M=7.5 for fine-grained [59]. Different assumptions were implemented to evaluate $Q_{tn,cs}$ for coarse-grained soils [60], [23], [24], [25] and transition soils [26] and [27] to calculate $CRR_{7.5}$ according to [28] for a specific $Q_{tn,cs}$ range.

Fine-grained soils,

$$CRR_{7.5} = 0.053 \cdot Q_{tn} \cdot K_\alpha \quad [59]$$

Coarse-grained soils,

$$Q_{tn,cs} = K_c \cdot Q_{tn} \quad [60]$$

where:

$$K_c = 1, \text{ for } I_c \leq 1.64 \quad [61]$$

$$K_c = -0.403\ I_c^4 + 5.581\ I_c^3 - 21.63\ I_c^2 + 33.75\ I_c - 17.88, \text{ for } 1.64 < I_c \leq 2.5 \quad [62]$$

$$K_c = 1, \text{ for } 1.64 < I_c \leq 2.36 \text{ and } F_r < 0.5 \quad [63]$$

Transition soils,

$$Q_{tn,cs} = K_c \cdot Q_{tn} \quad [64]$$

$$\text{where: } K_c = 6 \cdot 10^{-7} \cdot (I_c)^{16.76} \quad [65]$$

$$CRR_{7.5} = 93 \cdot \left[\frac{Q_{tn,cs}}{1000}\right]^3 + 0.08 \quad [66]$$

(for sand-like and transition soil) where: $50 \leq Q_{tn,cs} \leq 160$.

$$CRR_{7.5} = 0.833 \cdot \left[\frac{Q_{tn,cs}}{1000}\right] + 0.05 \quad [67]$$

(for sand-like and transition soil) where: $Q_{tn,cs} < 50$.

It is important to note that it is important to test high quality samples with cyclic laboratory testing for high risk projects, Boulanger and Idriss (2007) and Robertson (2009b).

2.4.2. Flat Dilatometer test (DMT)

The K_D parameter -defined in Chapter 2-, is adequate to evaluate liquefaction because it is representative of stress state/history (σ_h, OCR), aging, prestraining, cementation and structure, all factors increasing liquefaction resistance (Monaco et al. 2005). Thus, evaluation of liquefaction

criterion for an M_w=7.5 earthquake in a clear sand was developed for CRR-K_D by Marchetti (1982), Robertson and Campanella (1986), Reyna and Chameau (1991).

Later on, Monaco et al. (2005) presented a new curve that bounds the liquefaction potential using *CRR-K_D*, from a translation of CRR-CPT and CRR-SPT correlations using D_R as an intermediate parameter. The correlation curve is represented by the following equation:

$$\text{where: } CRR = 0.0107\ K_D^3 - 0.0741\ K_D^2 + 0.2169\ K_D - 0.1306 \quad [68]$$

Different upgrades and last curves are presented in Figure E.3.

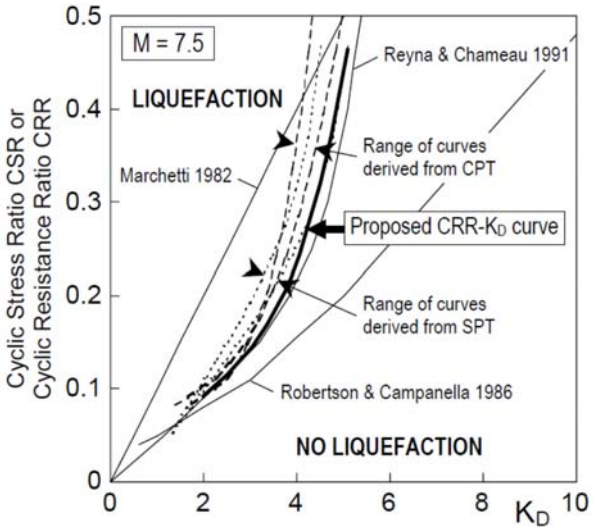

Figure E.3. K_D-CRR curves to evaluate cyclic liquefaction using DMT results, Monaco et al. (2005).

TC16 (2001) proposed a preliminary criterion of liquefaction for different seismic zones and K_D values. No liquefaction could occur if K_D values are higher than defined K_D according seismic zone, Table E.1.

Table E.1. Identification of the minimum K_D values which allow the clean sand liquefaction during an M=7.5 earthquake.

Seismic zone	K_D
No seismic	>1.7
Low (a_{max}/g=0.15)	>4.2
Middle (a_{max}/g=0.25)	>5.0
High (a_{max}/g=0.35)	>5.5

Liquefaction potential criteria for DMT allow discriminate clean sands, thus I_D values for sand-like soils, higher than 1.8.

2.4.3. Shear wave tests

The methodology to evaluate the liquefaction potential using shear wave velocity (V_S) values started with Andrus and Stokoe (1997). Various steps had to be followed. The first step, V_S values

should be corrected according to vertical effective stress [69] adapted from Sykora (1987). As a result of this correction V_{S1} is obtained.

Secondly, CSR should be set, as described above, using r_d and a_{max}. Finally, the definition of CRR in terms of V_{S1} derived according [70], Andrus and Stokoe (1997).

$$V_{S1} = V_S\,(100 / \sigma'_{v0})\cdot 0.25 \qquad [69]$$

$$CRR_{7.5} = a\,(V_{S1}/100)^2 + b\,[1/(V_{S1*} - V_{S1}) - 1/V_{S1*}] \qquad [70]$$

where: V_{S1}: overburden stress-corrected shear wave velocity, σ'_{v0}: effective vertical stress, a and b: curve fitting parameters and V_{S1*}: limiting upper value of V_{S1} for liquefaction occurrence.

A large number of case history information -liquefaction or no liquefaction-, is presented in Figure E.4. Those points were used for the adjustment of a and b values from [70]. Indeed, different curves were set for soils with ≥ 35 %, 20 % and ≤ 15 % fine content respectively. These curves are bounded the liquefaction potential condition for an M=7.5 earthquake, thus the V_S methodology results allow discriminating with reliability whether a soil liquefies or not. For uncemented soils, Holocene-age soils a and b values are 0.022 and 2.8 respectively.

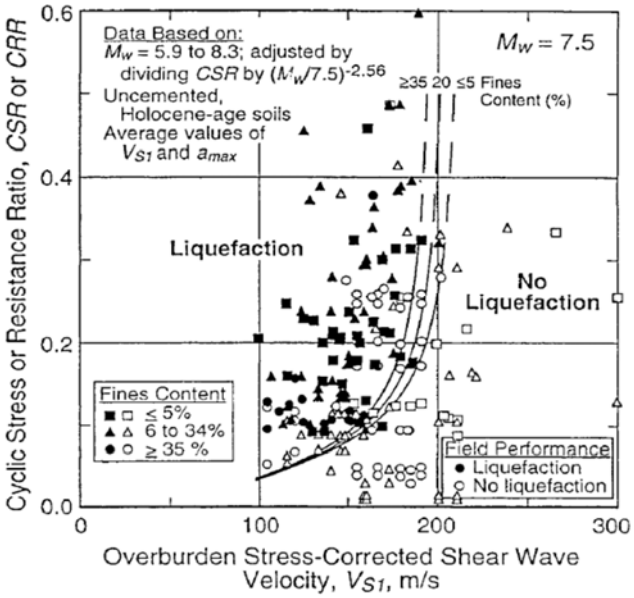

Figure E.4. Liquefaction potential evaluation according to V_{S1} from different uncemented soils during an earthquake of M_w=7.5, Andrus & Martin (2000).

The V_S tests can be performed differently, usually via borehole. In addition, there are some in-situ test -SCPTu and SDMT-, which incorporate V_S receptor. The criterion is included in the Guide for Shear-Wave-Based Liquefaction Potential Evaluation, Andrus et al. (2004).

2.5. Laboratory tests

Research during decades has created a large database of results from different soils. These results allowed the implementation of different criteria using tests that require undisturbed or disturbed samples.

These tests are separated in two types: (i) soil index tests, and (ii) cyclic and monotonic tests. The soil index tests are used in Bray et al. 2004 criterion that was presented in Chapter 3. Although these latest tests, are useful to evaluate the cyclic soil liquefaction. Tests results reliability depend fundamentally on sample quality. Notwithstanding the above, CRR can be obtained from laboratory test.

2.5.1. Semi-empirical criterion

Although first semi-empirical criterion based on relative density tests results was proposed in Seed and Idriss (1971) framework. A criterion for advanced cyclic tests on laboratory regarding this framework was not developed until Boulanger and Idriss (2004) because of low expectations on sample quality of coarse grained soils.

Meanwhile, laboratory apparatus -as cyclic simple shear test (DSS) or cyclic triaxial test (TrX)-, were progressively developed to obtain suitable results. Loading of cyclic tests can exactly impose CSR conditions with cyclic shear strength (τ_{cyc}), average shear strength (τ_{ave}) and number of uniform loading cycles (N_{eq}), see Figure E.5.

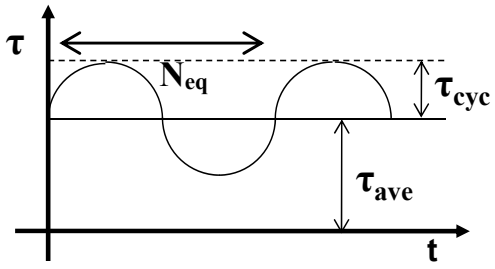

Figure E.5. Cyclic stresses applied in a conventional cyclic test.

Cyclic shear strength (τ_{cyc}) is defined in equation [71], average shear strength (τ_{ave}) in equation [72].

$$\tau_{cyc} = \frac{\tau_{max} - \tau_{min}}{2} \quad [71]$$

$$\tau_{ave} = \frac{\tau_{max} + \tau_{min}}{2} \quad [72]$$

The results interpretation of cyclic tests were stablished with interaction diagram, which represents the number of uniform cycles (N_{eq}) to trigger liquefaction because of cyclic shear ratio and average shear ratio during loading. It was initially used for Drammen clay in Andersen et al.

(1980) in which twelve cyclic direct simple shear tests were carried out, Figure E.6. It is important to note that constant N lines were interpolated from results (red points).

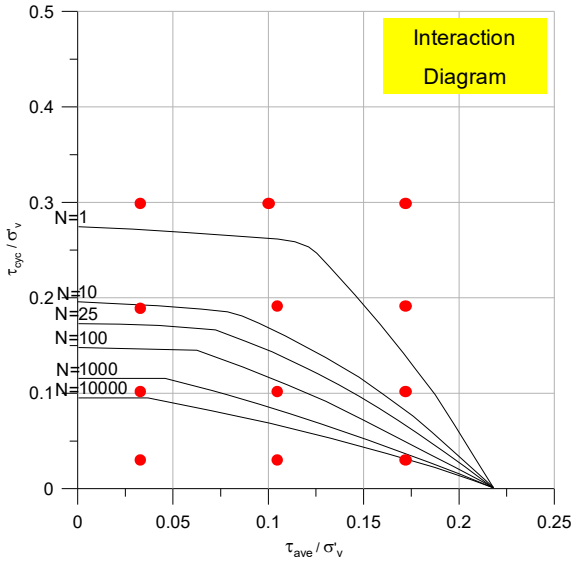

Figure E.6. Interaction diagram for Drammen clay cyclic DSS results, modified from Andersen et al. (1980).

If this interpretation is performed, the number of cycles could be used for calculating the liquefaction potential reached for an equivalent uniform cyclic loading of any soil. However, it was not directly linked with seismic loading -an irregular stress time series originated during an earthquake-. Thus, the method presented in Idriss (1999) and Boulanger and Idriss (2004) allowed to connect cyclic loading from laboratory tests for sand-like or clay-like specimens with seismic loading from earthquakes. At the same time, results from new cyclic testing provided feedback on data base to evolve the new method.

The Idriss and Boulanger method is based on a magnitude scaling factor. MSF provides a rough representation of the effects of shaking or equivalent number of stress cycle. The values of MSF are derived from: (i) correlations of the number of equivalent uniform cycles taking into account earthquake magnitude and (ii) laboratory based relations between cyclic stress ratio required to cause liquefaction and the number of uniform stress cycles, Idriss & Boulanger (2006).

To carry out the conversion of irregular cyclic stress time to an equivalent uniform cyclic time series, Seed et al. (1975) proposed equation [73]. It is defined to approximate CRR of sand-like and clay-like soils, and the number of uniform stress cycles.

$$CRR = a \cdot N^{-b} \qquad [73]$$

where: b is the slope of CRR – N and a is the CRR for N=1.

The CRR normalization was performed for N=15 because it is the number of cycles that generates liquefaction obtained for an M_w=7.5 earthquake and r_e=0.65 in clean sands (Idriss, 1999), see Figure E.7. From different tests results on clay-like and sand-like soils they obtained

representative b values. Clay-like b values were obtained after the normalization of cyclic DSS and Triaxial tests results, evaluating at 1 Hz loading and ± 3% shear strain to N=15. And Sand-like b values came from cyclic DSS for frozen samples. Representing b value for sand-like is 0.337 and b value for clay-like is 0.135, it is presented in Figure E.7.

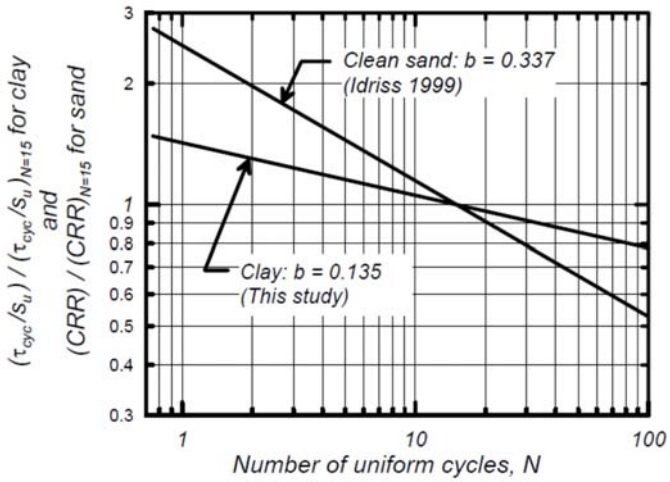

Figure E.7. Defined b values according to different normalized tests, Boulanger & Idriss (2004).

Additionally, they proposed [74] to allow the conversion an individual cycle at some stress level to an equivalent N at a different stress level by assuming equal N and equal fraction of N to failure.

$$\frac{N_A}{N_B} = \left(\frac{CRR_A}{CRR_B}\right)^{1/b} = \frac{1\ cycle}{X_A\ cycles} \qquad [74]$$

Then, sand-like soils with r_e=0.65, b=0.337, and the assumption of ¾ cycle provided equation [75], because it fits to MSF=1.8 for an M_w=5.25 earthquake. MSF_{max} is limited by equation [76] defined by Idriss (1999). The new MSF re-evaluated from Idriss (1999) was equation [77].

$$\mathrm{N_{min\ sand}} = \left(\frac{1}{0.65}\right)^{1/0.337} \cdot \left(\frac{3}{4}\ cycle\right) = 2.69 \qquad [75]$$

$$\mathrm{MSF_{max}}_{\ \ Mw \le 5.25} = \left(\frac{15}{2.69}\right)^{0.337} = 1.8 \qquad [76]$$

$$\mathrm{MSF} = 6.9 \cdot e^{\left(\frac{-M}{4}\right)} - 0.058 \qquad [77]$$

$$\mathrm{MSF} \le 1.8$$

Extensive study for 124 horizontal acceleration time series recorded at NEHRP class D soil sites in 13 different earthquakes -magnitudes in the range of 7 to 8- was performed to obtain the relationship of the number of equivalent uniform loading cycles. For sand-like and clay-like soil behaviour considering r_e=0.65 (Boulanger and Idriss, 2007).

The results confirms that sand usually presents N=15 for M=7.5 and r_e=0.65 (Seed et al. 1975), in contrast for clay, N=30 when r_e=0.65 (Boulanger and Idriss 2004), as shown in Figure E.8.

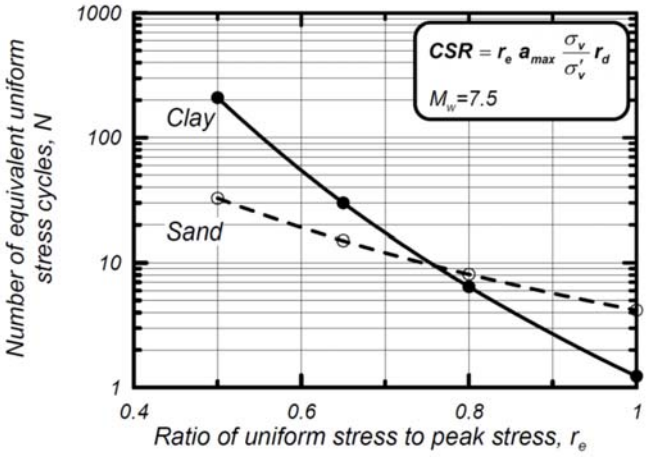

Figure E.8.N vs. r_e according to M_w=7.5 earthquakes for sand-like and clay-like soils, from Boulanger and Idriss (2004).

The MSF for clay-like soils is quite different. They proposed the same argumentation previously described because in this case N is 30. Moreover, it was suggested ½ cycle for equation [78] because of the lower value of b and clay-like soil representative N=30. Then, MSF_{max} was calculated from [79]. The resulting MSF for clay-like soils was [80], Boulanger & Idriss (2004).

$$N_{\text{min clay}} = \left(\frac{1}{0.65}\right)^{1/0.135} \cdot \left(\frac{1}{2}\ cycle\right) = 12.2 \qquad [78]$$

$$MSF_{max} \quad Mw \le 5.25 = \left(\frac{30}{12.2}\right)^{0.135} = 1.13 \qquad [79]$$

$$MSF = 1.12 \cdot e^{\left(\frac{-M_w}{4}\right)} + 0.828 \qquad [80]$$

$$MSF \le 1.13$$

Results of equations [77] and [80] are plotted in Figure E.9.

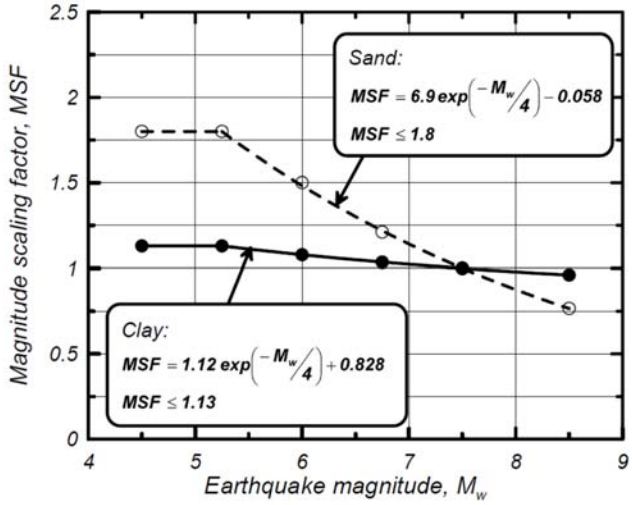

Figure E.9. Proposed MSF for clay-like and sand-like behaviour, Idriss (1999).

CRR proposal for fine grained soils can be estimated using equation [45] Boulanger and Idriss (2007).

$$CRR_M = C_{2D} \cdot \left(\frac{\tau_{cyc}}{c_u}\right)_{M=7.5} \cdot \frac{c_u}{\sigma'_v} \cdot MSF \cdot K_\alpha \quad [81]$$

where: C_{2D}: correction factor of cyclic loading, estimated around 0.96 (Boulanger and Idriss, 2004), $\left({}^{\tau_{cyc}}/_{c_u}\right)_{M=7.5}$: cyclic strength ratio for 30 cycles and M_w=7.5, $\frac{c_u}{\sigma'_v}$: undrained strength shear ratio for NC soil (OCR=1), and Kα: static shear stress ratio correction, which lies on the range of 0.4 to 1 for NC clay.

The criterion for clay-like soils proposed in Boulanger and Idriss (2007) can be performed to obtain MSF and $CRR_{Mw=5.25}$ using tests results of the hydraulic fill of Prat quay.

3. Application of cyclic liquefaction criteria

The four cyclic liquefaction criteria described above have been applied to results of in-situ tests and laboratory tests from Prat quay, Phase 1 and Phase 2. The Barcelona seismic conditions described previously in Appendix D are established for those criteria: a_{max} (0.083g, 0.14g and 0.19g) and M_w=5.25. The criteria are only performed for the hydraulic fill.

3.1. In-situ tests criteria

The results of CPTu, DMT and V_S criteria are described in following sections.

3.1.1. CPTu

The screening method proposed by Robertson and Cabal (2012) has been applied to representative CPTu tests (previously presented in Chapter 3). The results are presented according soil profile of (a) $CRR_{7.5}$ & $CSR_{5.25}$/MSF and (b) factor of safety (FoS) in Figure E.10, Figure E.11 and Figure E.12. In addition, clay-like, transition and sand-like soils are distinguished. It can be noted that large zones of hydraulic fill CRR values lower than CSR derived values for a_{max}=0.14g and are susceptible to cyclic liquefaction. Although there are different soils in the soil profiles, the results indicate that three soils can be classified as potentially liquefiable.

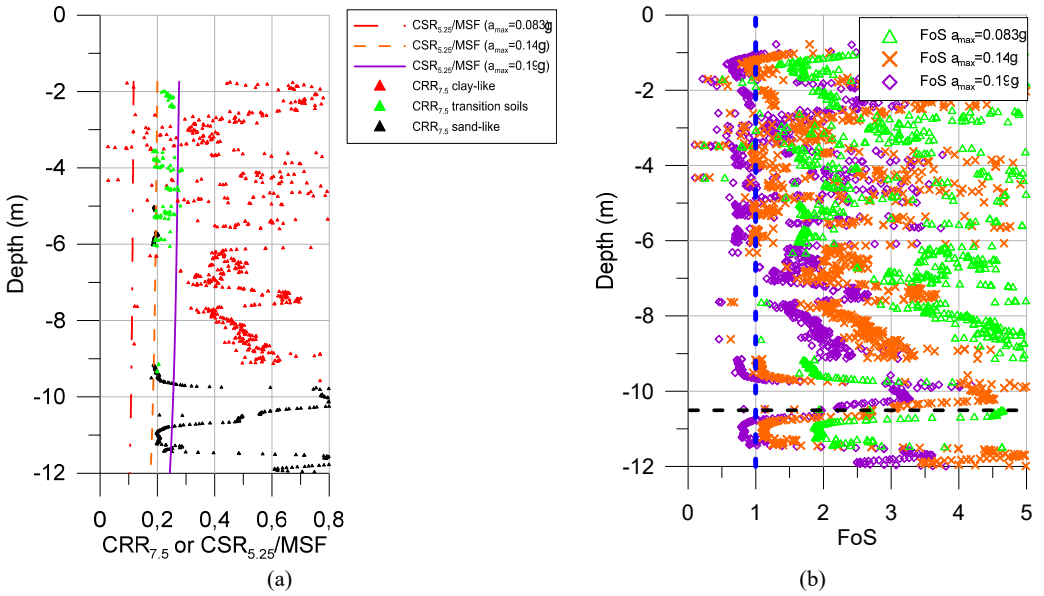

(a) (b)

Figure E.10. Robertson and Cabal (2012) criterion, (a) $CRR_{7.5}$ & $CSR_{5.25}$/MSF and (b) FoS for CPTu 6a12.

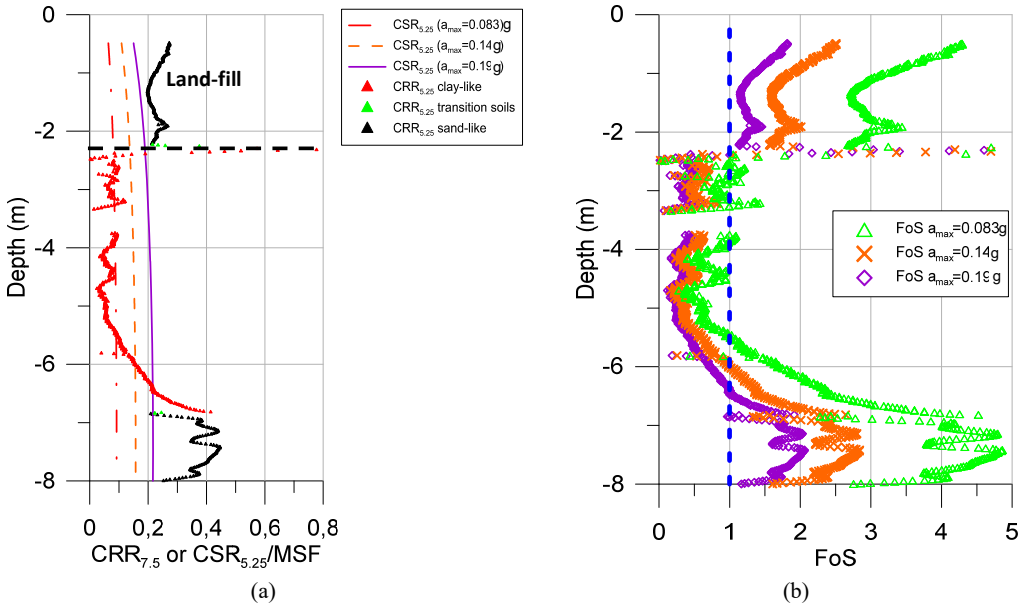

(a) (b)

Figure E.11. Robertson and Cabal (2012) criterion, (a) $CRR_{7.5}$ & $CSR_{5.25}$/MSF and (b) FoS for CPTu r5.

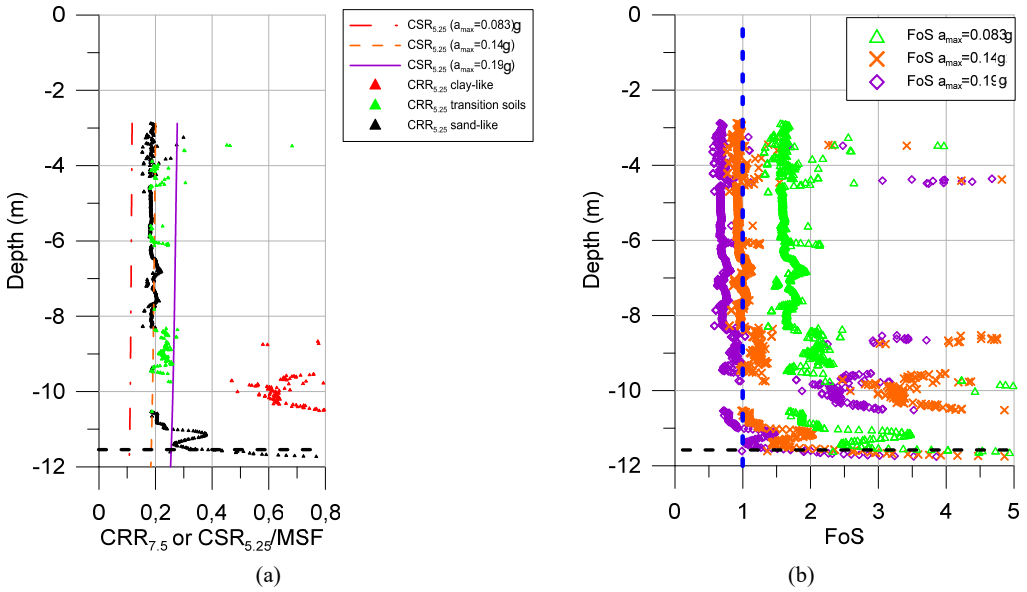

Figure E.12. Robertson and Cabal (2012) criterion, (a) $CRR_{7.5}$ & $CSR_{5.25}$/MSF and (b) FoS for CPTu 3b11.

3.1.2. SDMT

The seismic flat dilatometer (SDMT) provides cyclic liquefaction potential evaluation according to: (i) TC16 (2001) and Monaco et al. (2005) criteria for K_D values and (ii) Andrus et al. (2004) criterion for shear wave velocity (V_s) values.

It is important to note that K_D values are filtered according to I_D >1.8 to distinguish, as far as possible, sands from hydraulic fill for both K_D criteria.

The TC16 (2001) criterion results are presented in Figure E.13. Two seismic ranges could represent Barcelona seismic conditions a_{max} values (Appendix D): no seismic (a_{max}=0.083g) and low seismicity (a_{max}=0.14g and a_{max}=0.19g) zones. It should be noted that large part of hydraulic fill is susceptible to cyclic liquefaction for a low seismicity zone. Nevertheless, for no seismic zone only 30% of points are susceptible to liquefy (K_D < 1.7).

Alternatively, the performance of Monaco et al. (2005) criterion based on the K_D parameter is presented in Figure E.14. In this case, CSR lines are defined for M_w = 5.25 earthquake according to a_{max}=0.083g and a_{max} = 0.19 g assumptions.

The results indicate that there is an evident difference between Phase 1 and Phase 2 results. Phase 1 results present poor CRR values, meanwhile Phase 2 values are quite better. Therefore, hydraulic fill of Phase 1 can reach cyclic liquefaction for a_{max} = 0.083 g, whereas hydraulic fill of Phase 2 broadly needs a_{max} > 0.19 g to generate cyclic liquefaction.

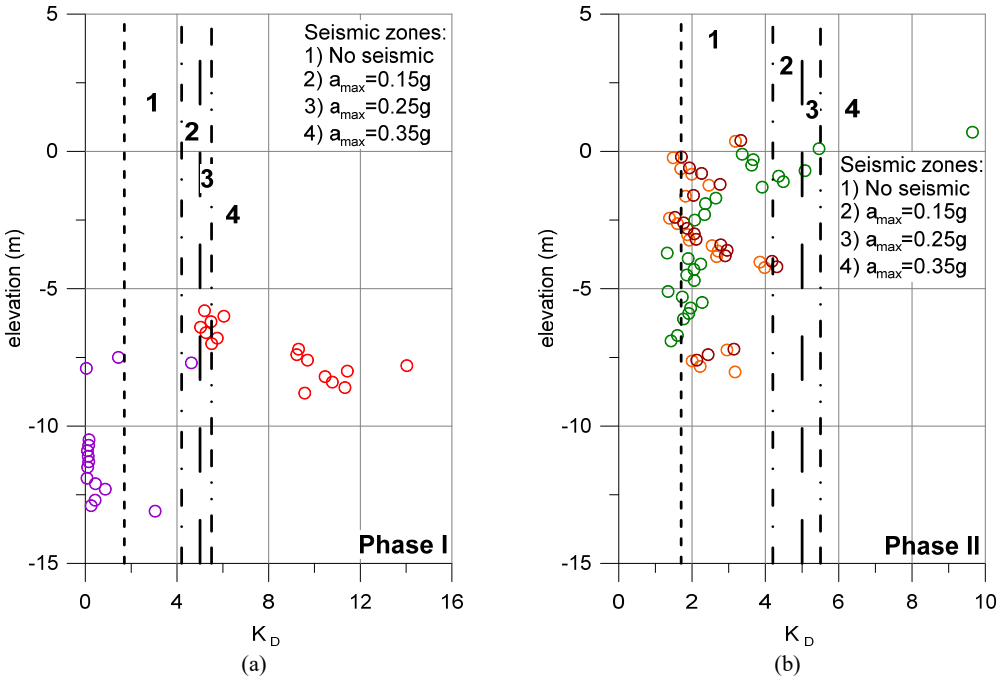

Figure E.13. TC16 (2001) criterion for (a) Phase 1 DMT and (b) Phase 2 DMT.

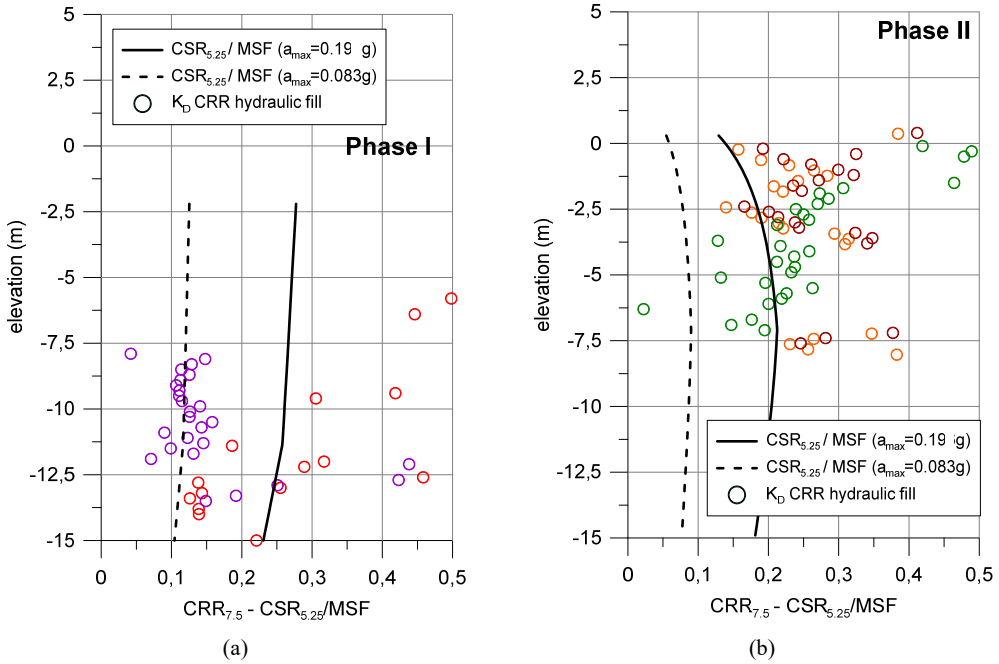

Figure E.14. Monaco et al. (2005) criterion for (a) Phase 1 DMT and (b) Phase 2 DMT.

Finally, Andrus et al. (2004) criterion is applied for V_{S1} values from Phase 1 (five tests) and Phase 2 (one test) according an M_w=5.25 earthquake with a_{max}=0.19 g and a_{max}=0.083g. It is important to note that criterion has been extended to V_{S1} values lower than 100 m/s.

The results are shown in Figure E.15a and Figure E.15b. The approach indicates susceptible soils to cyclic liquefaction for a number of points.

It is worth mentioning that zero values of V_{S1} were recorded in hydraulic fill possibly due to the 'liquefied state' of the soil during test, although the testing contractor considered that those values were invalid.

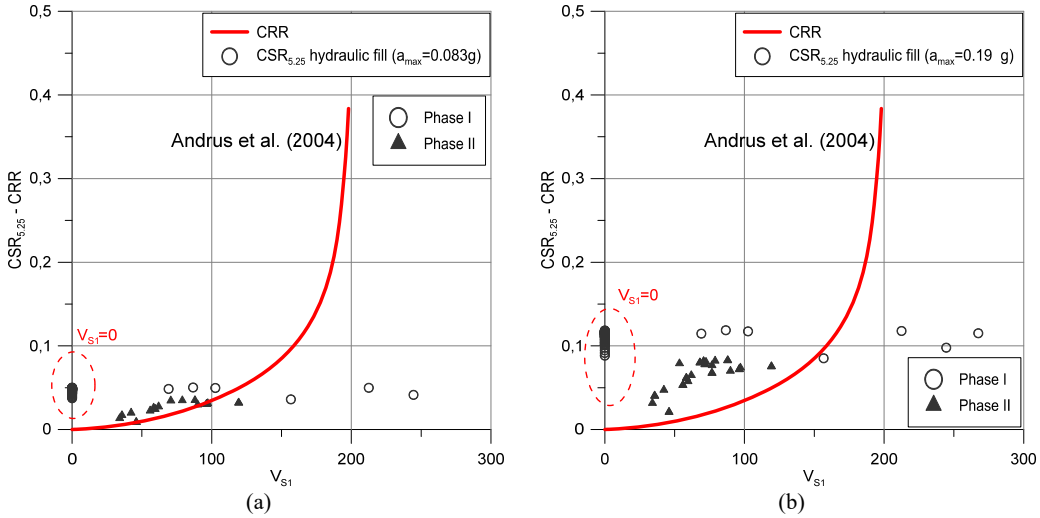

Figure E.15. Andrus et al. (2004) criterion for (a) a_{max}=0.19 g and (b) a_{max}=0.083g.

3.2. Idriss and Boulanger (2006) criterion

A set of 12 cyclic DSS tests were performed to specimens of remoulded hydraulic fill from Prat quay Phase 1 (NGI, 2008a), obtained from settling column presented in Appendix F. The interaction diagram for cyclic shear tests results is presented in Figure E.16. The agreement is quite good, although, there is a test (N=17) that does not fit as well as it should. This result could be related with some non-homogeneity detected in the hydraulic fill index properties.

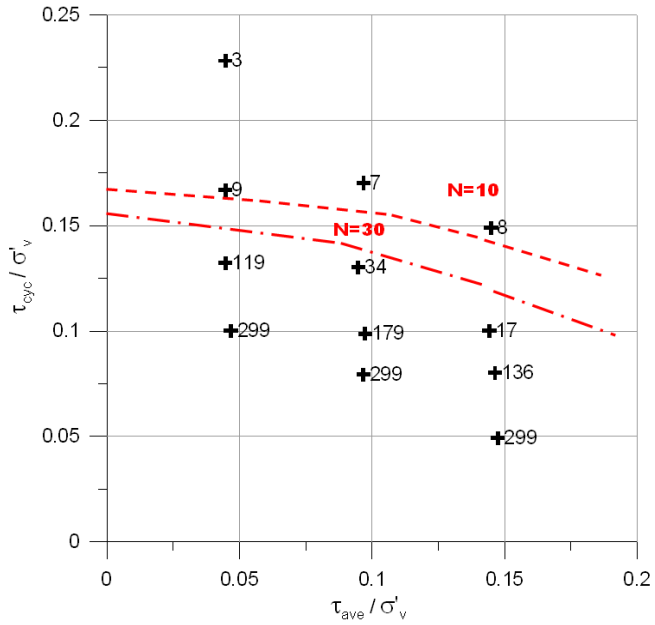

Figure E.16. Interaction diagram for hydraulic fill using results of cyclic shear tests.

The cyclic liquefaction criterion of Idriss and Boulanger (2006) has been applied to laboratory tests results. Therefore, the number of cycles (N) is normalized to 3% of strain and cyclic shear stress (τ_{cyc}) is increased 9% because of the period normalization.

To perform an objective normalization, some tests results are removed due to heterogeneities. The corresponding mean values of soil index are presented in Table E.2. All specimens satisfy the criterion assumptions as fine-grained soil (clay-like soil), PI ≥ 7 and FC% >20.

Table E.2. Soil index properties for hydraulic fill.

Sample	PI	LL	clay% <2µm	FC% <75µm
CSB	21.8	43.8	35	99
CSI	13.4	31.2	18.7	72
CSA	14.8	33.5	24.5	83

The normalized values and 'a' and 'b' adjustments [73] are shown in Figure E.17.

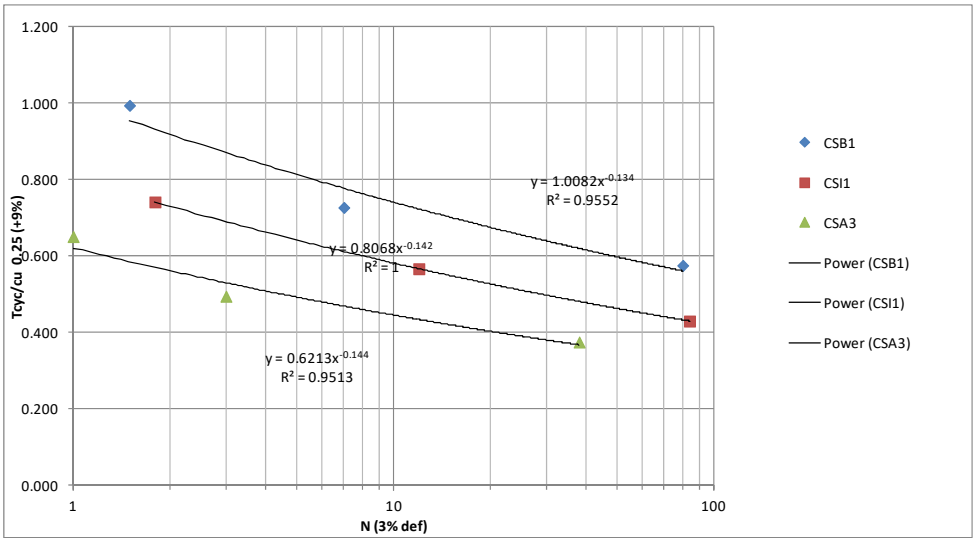

Figure E.17. Normalized τ_{cyc}/c_u vs. N values for hydraulic fill.

Last normalization is calculated according c_u / σ'_v ratio of 0.25 -from $c_{u\ peak}$ presented in Chapter 2 for the hydraulic fill-, and N=30. The corresponding values are presented in Table E.3.

Table E.3. Values of a, b, τ_{cyc}/c_u for hydraulic fill.

Sample	σ'_v test [kPa]	a	b	$(\tau_{cyc}/c_u)_{N=30}$
CSB	149,8	1	0,13	0,64
CSI	149,8	0,8	0,14	0,50
CSA	149,8	0,6	0,16	0,35

In Table E.4, results of MSF and CRR for an M=5.25 earthquake are shown. CRR values are analysed for: (i) non-explicit measurements to obtain K_α were performed, thus K_α=1 and K_α=0.6 are used, (ii) C_{2D} is 0.96 and (iii) undrained shear strength ratio, again 0.25.

Table E.4. Cyclic stress ratio, magnitude scale factor (MSF) and cyclic resistance ratio according Idris and Boulanger criterion for hydraulic fill.

Sample	MSF $_{M=5.25\ clay}$	CRR $_{M=5.25\ K\alpha=1}$	CRR $_{M=5.25\ K\alpha=0.6}$
CSB	1,05	0,15	0.09
CSI	1,09	0,12	0.07
CSA	1,17	0,08	0.05

The CSR values for Barcelona seismic conditions are calculated at two different elevations r_d=0.90 (z≈5 m) and r_d=0.62 (z≈15 m) and according to 3 different a_{max} assumptions: 0.083g from NCSE-02 (2002), 0.14g and 0.19g from Irizarry (2004). The CSR values are given in Table E.5.

Table E.5. Cyclic stress ratio for seismic conditions of Barcelona Port.

r_d	CSR M=5.25 amax=0.083g	CSR M=5.25 amax=0.14g	CSR M=5.25 amax=0.19g
0,90	0.07	0.12	0.16
0,62	0.05	0.08	0.11

Regarding the six values of CSR and the six values of CRR, the performed assumptions provide 36 values of FoS. The corresponding data is presented in Table E.6.

Table E.6. FoS for hydraulic fill.

Sample	r_d	K_α	FS a_{max}=0.083g	FS a_{max}=0.14g	FS a_{max}=0.19g
CSB	0,90	1	2.31	1.37	1.01
CSI	0,90	1	1.87	1.11	0.82
CSA	0,90	1	1.41	0.84	0.62
CSB	0,62	1	3.37	2.00	1.47
CSI	0,62	1	2.73	1.62	1.19
CSA	0,62	1	2.06	1.22	0.90
CSB	0,90	0.6	1.39	0.82	0.61
CSI	0,90	0.6	1.12	0.67	0.49
CSA	0,90	0.6	0.85	0.50	0.37
CSB	0,62	0.6	2.02	1.20	0.88
CSI	0,62	0.6	1.64	0.97	0.72
CSA	0,62	0.6	1.23	0.73	0.54

4. Application of cyclic liquefaction criteria after hydraulic fill improvement of Phase 2

The Robertson (2012) and Idriss and Boulanger (2006) criteria have been applied to results from site investigation Pray quay Phase 2 after soil improvement. The in-situ test results of the site investigation after soil improvement in Phase 2 -that were previously described in Chapter 5-, and additional laboratory tests performed during that site investigation are used. Unfortunately, DMT or shear velocity tests were not performed after soil improvement.

The aim of this chapter is to evaluate the effect of the preloading and prefabricated strip drains for cyclic liquefaction potential mitigation. The Barcelona seismic conditions described in Appendix D a_{max}: 0.083g, 0.14g and 0.19g and M_w=5.25 are assumed for those criteria.

4.1. Robertson and Cabal (2012) criterion

The criterion of Robertson and Cabal (2012) has been performed to CPTu test sounded at the same place that had been performed the previous CPTu (Appendix E.3.1.1). The corresponding results are shown in Figure E.18. Clay-like, transition and sand-like soils are distinguished to provide insight into interpretation.

The results indicate that cyclic liquefaction is possible for a_{max} >0.14 g seismic condition. It is important to note that there are sand-like and transition soils, clay-soils are not detected.

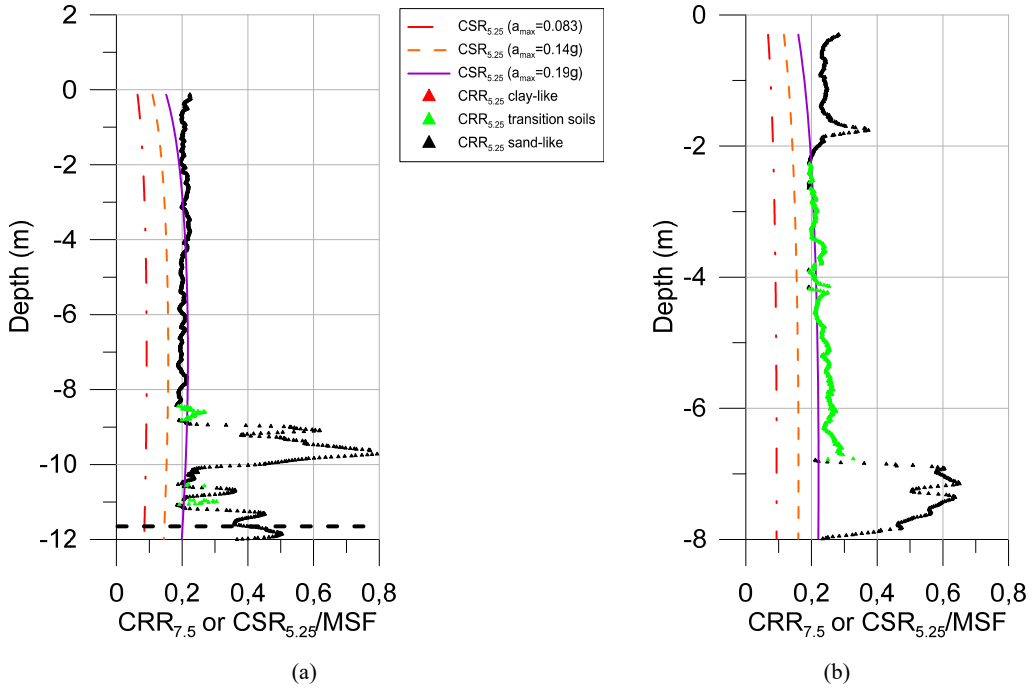

Figure E.18. Application of Robertson and Cabal (2012) criterion for hydraulic fills after soil improvement.

In Figure E.19, the FoS values for previous CSR and CRR results are presented. The derived FoS values in the soil profile are close to 1 for a_{max}=0.19 g.

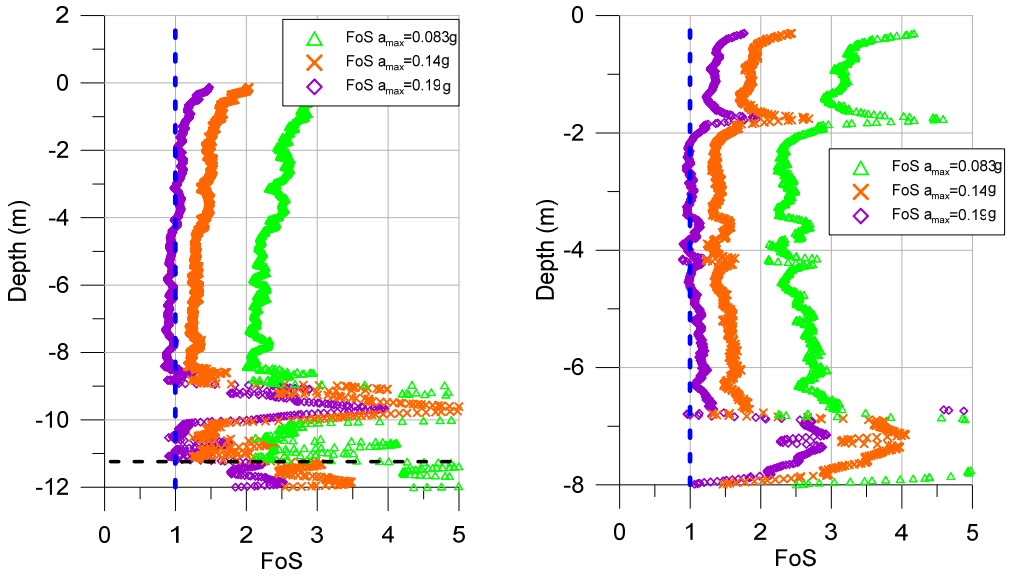

Figure E.19. Factor of safety for Robertson and Cabal (2012) criterion for hydraulic fills after soil improvement.

4.2. Idriss and Boulanger (2006) criterion

A set of 15 cyclic DSS tests were performed from specimens of hydraulic fill from Prat quay Phase 2 (NGI, 2008b). The interaction diagram for cyclic shear tests results is performed, see Figure E.20. The cyclic shear stress ratio value of 0.2 is mainly inside the zone enclosed by N=30.

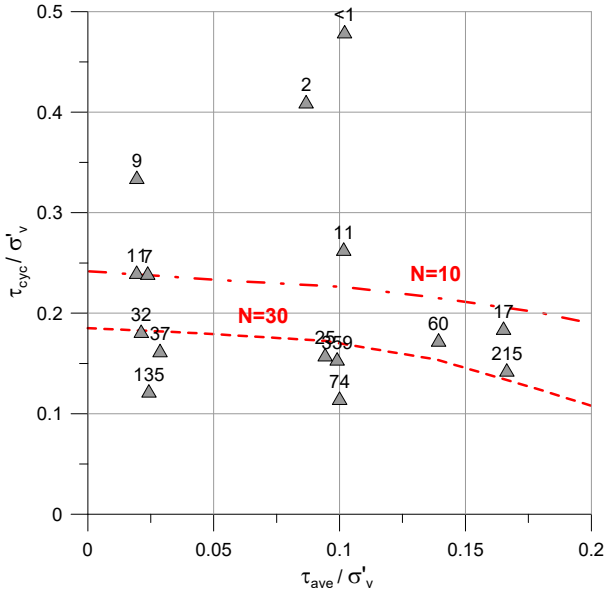

Figure E.20. Interaction diagram for hydraulic fill after soil improvement using results of cyclic shear tests.

The cyclic liquefaction criterion of Idriss and Boulanger (2006) (I&B) has applied to laboratory tests results. Therefore, the number of cycles (N) was normalized to 3% of strain and cyclic shear stress (τ_{cyc}) was increased 9% because of the period normalization.

To perform an objective normalization, some tests results are removed due to heterogeneities. The corresponding mean values of soil index are presented in Table E.7. All specimens satisfy the criterion assumptions as fine-grained soil (clay-like soil), PI ≥ 7 and FC% >20.

Table E.7. Soil index properties of improved hydraulic fill.

Sample	PI	LL	Clay % <2µm	FC% <75µm
s01MDG_SH1	9.6	27.2	15.4	77.0
s01MDG_SH3	15	33	20	90 - 58
s01MDG_SH4	9	25	12.5	52.5
s01MDG_SH5	10	28	16	49
s02_SH6	15.5	33.5	21.4	70
s02MDG_SH4_A_1	18	39	31	85

The normalized values and ‘a’ and ‘b’ adjustments [73] are shown in Figure E.21.

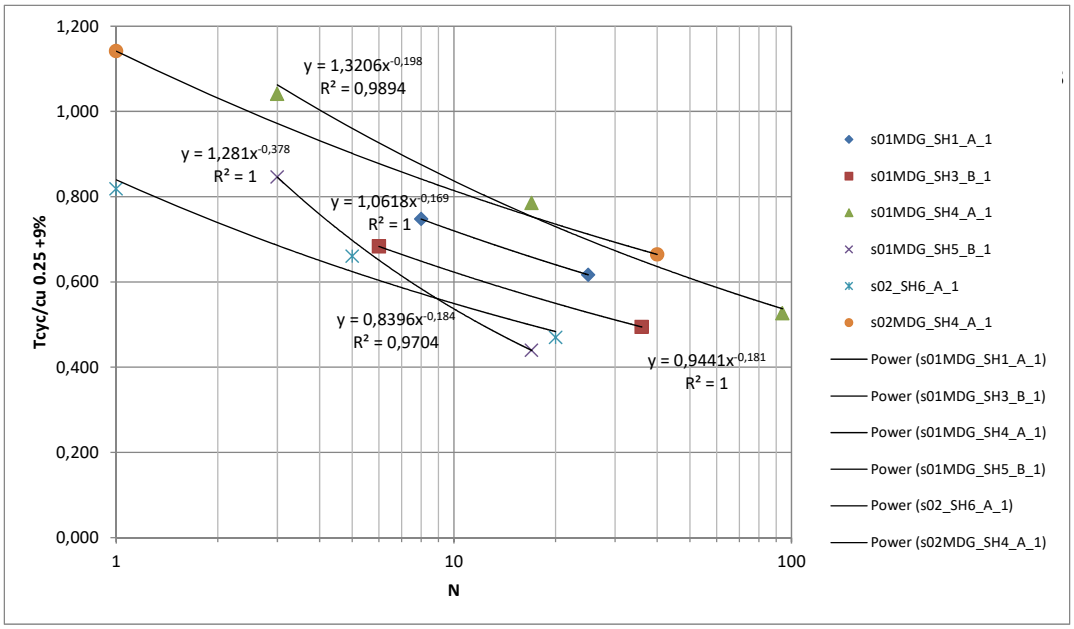

Figure E.21. Normalized τ_{cyc}/c_u vs. N values for hydraulic fill after soil improvements.

The final normalization is calculated according c_u / σ'_v ratio of 0.25 -from $c_{u\ peak}$ presented in Chapter 2 for the hydraulic fill-, and N=30. Results of s01MDG_SH3 are neglected. The corresponding values are presented in Table E.8.

Table E.8. Values of a, b, τ_{cyc}/c_u for improved hydraulic fill.

Sample	σ'_v test [kPa]	a	b	$(\tau_{cyc}/c_u)_{N=30}$
s01MDG_SH1	140	0,9	0,09	0,63
s01MDG_SH4	165	1,3	0,20	0,67
s01MDG_SH5	185	1,3	0,20	0,62
s02_SH6	185	0,8	0,18	0,45
s02MDG_SH4_A_1	194,9	1,1	0,15	0,69

The results of MSF and CRR for an M=5.25 earthquake are presented in Table E.9. CRR values are derived according: (i) non-explicit measurements to obtain K_α were performed, thus K_α=1 and K_α=0.6 are used, (ii) C_{2D} is 0.96 and (iii) undrained shear strength ratio is 0.25.

Table E.9. Cyclic stress ratio, Magnitude scale factor (MSF) and cyclic resistance ratio according I&B criterion for the improved hydraulic fill.

Sample	$MSF_{M=5.25\ clay}$	$CRR_{M=5.25\ K\alpha=1}$	$CRR_{M=5.25\ K\alpha=0.6}$
s01MDG_SH1	0.91	0.14	0.08
s01MDG_SH4	1.36	0.22	0.13
s01MDG_SH5	1.36	0.20	0.12
s02_SH6	1.26	0.14	0.08
s02MDG_SH4_A_1	1.13	0.19	0.11

The CSR values for Barcelona seismic conditions for elevation z≈5 m and z≈15 that were previously presented in Table E.5 are used. Afterwards, factors of safety are calculated, corresponding data are presented in Table E.10.

Table E.10. FoS performed for the improved hydraulic fill.

Sample	r_d	K_α	FS a_{max}=0.083g	FS a_{max}=0.14g	FS a_{max}=0.19g
s01MDG_SH1	0.89	1	1.99	1.18	0.87
s01MDG_SH4	0.89	1	1.06	0.63	0.46
s01MDG_SH5	0.89	1	3.17	1.88	1.39
s02_SH6	0.89	1	2.94	1.74	1.28
s02MDG_SH4_A_1	0.89	1	1.98	1.17	0.86
s01MDG_SH1	0.62	1	2.86	1.70	1.25
s01MDG_SH4	0.62	1	1.52	0.90	0.66
s01MDG_SH5	0.62	1	4.56	2.71	1.99
s02_SH6	0.62	1	4.22	2.50	1.84
s02MDG_SH4_A_1	0.62	1	2.85	1.69	1.24
s01MDG_SH1	0.89	0.6	1.19	0.71	0.52
s01MDG_SH4	0.89	0.6	0.63	0.38	0.28
s01MDG_SH5	0.89	0.6	1.90	1.13	0.83
s02_SH6	0.89	0.6	1.76	1.04	0.77
s02MDG_SH4_A_1	0.89	0.6	1.19	0.70	0.52
s01MDG_SH1	0.62	0.6	1.72	1.02	0.75
s01MDG_SH4	0.62	0.6	0.91	0.54	0.40
s01MDG_SH5	0.62	0.6	2.74	1.62	1.20
s02_SH6	0.62	0.6	2.53	1.50	1.11
s02MDG_SH4_A_1	0.62	0.6	1.71	1.01	0.75

Hydraulic fill results of Idriss and Boulanger criterion shows that cyclic liquefaction susceptibility exists for some cases according to a_{max}= 0.14g (38%) and 0.19g (75%). It is important to note that only two results (K_α=0.6 and r_d=0.89 and 0.62) indicate liquefaction susceptibility for a_{max}=0.083g assumption.

5. Results comparison before and after soil improvement in Phase 2

The comparison of criteria results for cyclic liquefaction is performed to evaluate the soil improvement.

5.1. Robertson and Cabal (2012) criterion

The criteria comparison indicates that different effects of the soil improvement are achieved, as shown in Figure E.22. Meanwhile, there are no evident changes in the soil profile of sand-like soil (Figure E.22a), for the fine grained soil profile (Figure E.22b) the CRR has increased significantly. Therefore, after soil improvement clay-like soil -that has changed to transition soil-, can cope with CSR loading higher than a_{max}=0.19 in the vast majority of results.

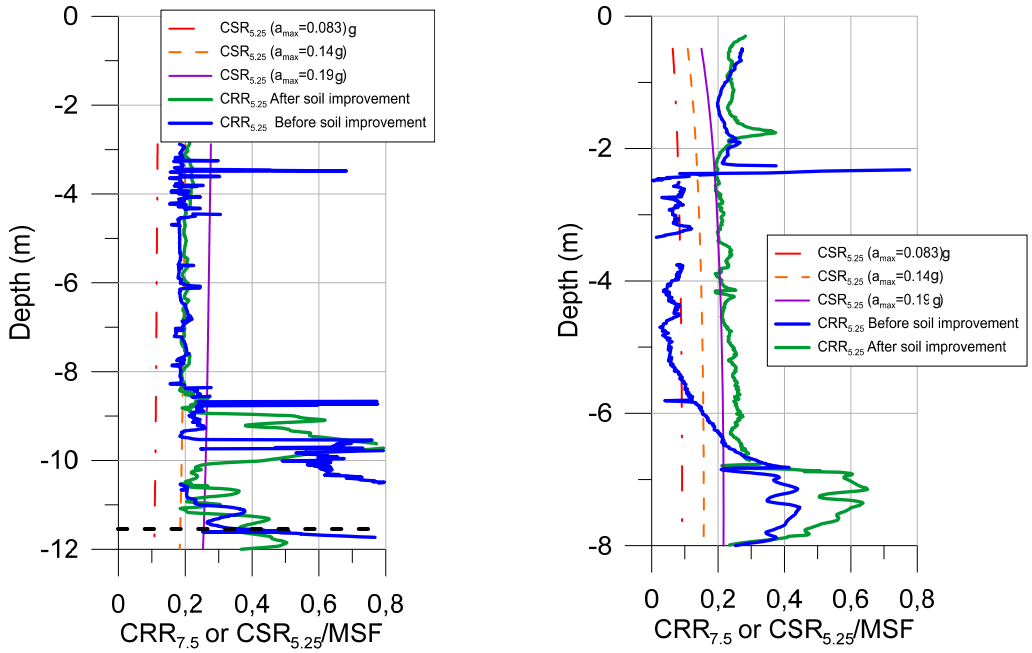

Figure E.22. Robertson and Cabal (2012) criterion comparison before and after soil improvement of Phase 2 (a) sand-like soil and (b) fine grained or transition soils.

5.2. Laboratory tests

The most notable parameters from tests are compared: τ_{cyc}/σ'_v – N, OCR - τ_{cyc}/σ'_v and N - $c_{u\ post\text{-}liq}/\sigma'_v$. The results of cyclic shear tests before and after soil improvement are presented in Figure E.23. A significant increase of τ_{cyc}/σ'_v is achieved for a constant N after the soil improvement of the hydraulic fill.

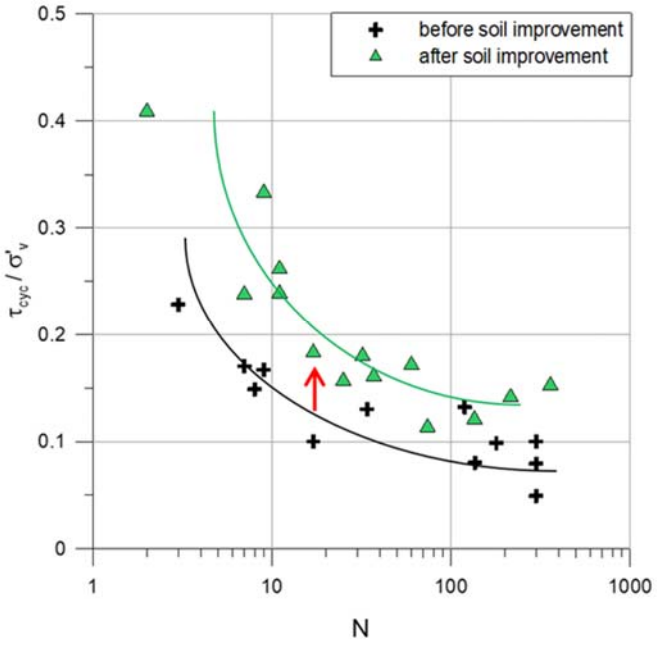

Figure E.23. Cyclic test results, τ_{cyc} / σ'_v vs. number of cycles, before and after soil improvement.

In this way, τ_{cyc} / σ'_v - OCR comparison is performed in Figure E.24. There is an increase of τ_{cyc} / σ'_v and evidently OCR due to the effect provided by the preloading surcharge.

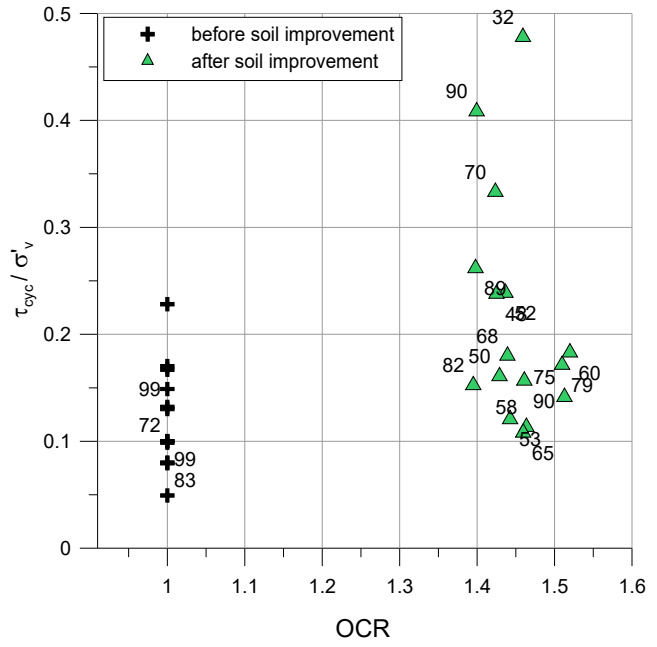

Figure E.24. τ_{cyc} / σ'_v vs. OCR due to soil improvement, labels indicate fines content %.

Finally, the comparison for post liquefaction undrained shear strength – N is presented in Figure E.25. The results indicate that higher $c_{u\ post\_liq}$ / σ'_v values are observed after the soil improvement. Thus, the soil improvement could lead to the reduction of soil sensitivity. Nevertheless, the tested specimens after improvement contained less fines content that could increase those resistances.

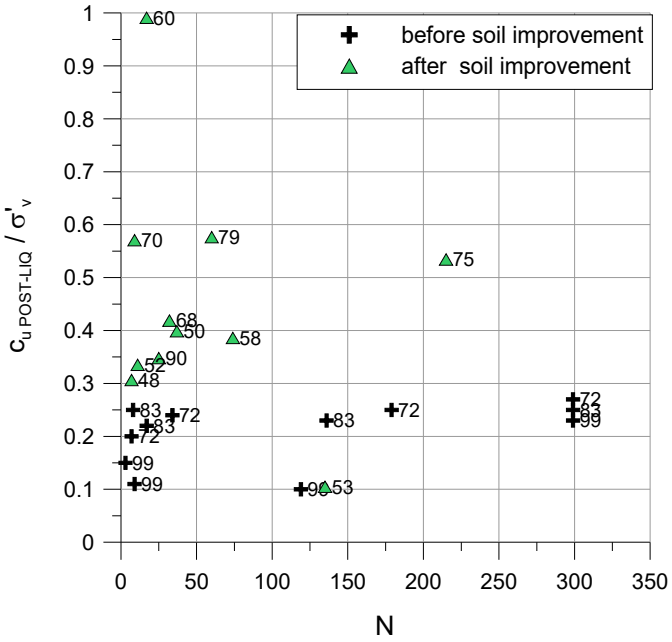

Figure E.25. $c_{u\ post\_liq}/\ \sigma'_v$ vs. N, labels indicate fines content %.

The interactions diagrams performed before and after soil improvement are shown in Figure E.26a and Figure E.26b respectively. It can be noted the improvement of soil due to the increase of cyclic shear for a constant number of cycles. However, this change is quite small for low values of τ_{ave}/σ'_v and N=30.

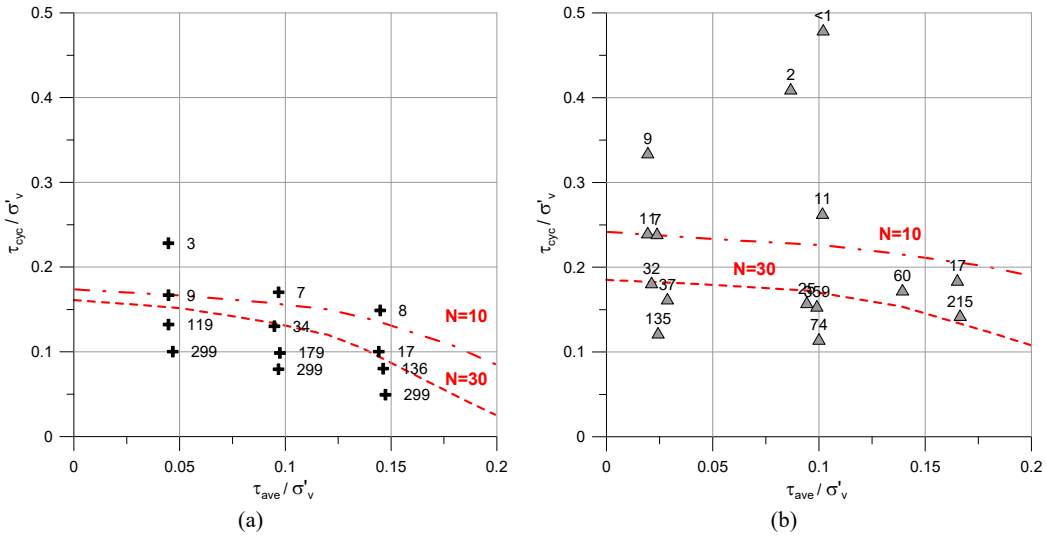

Figure E.26. Interaction diagrams for results of cyclic shear tests: (a) before and (b) after soil improvement.

The soil improvement can be observed by comparing previous Figures of laboratory tests results. Nevertheless, in order to quantify the mitigation of soil liquefaction, it is important to compare the cyclic liquefaction potential criteria results previously presented.

5.2.1. Idriss and Boulanger (2006) criterion

The results of the methodology proposed by Idriss and Boulanger (I&B) regarding R_d=0.90 and K_α=1 are compared in Table E.11. Although τ_{cyc}/σ'_v values were generally increased, FoS calculated do not significantly change because of the mentioned low improvement for N=30.

Table E.11. FoS performed for the hydraulic fill before and after soil improvement.

Sample	FS a_{max}=0.083g	FS a_{max}=0.14g	FS a_{max}=0.19g
BEFORE SOIL IMPROVEMENT			
CSB	2.31	1.37	1.01
CSI	1.87	1.11	0.82
CSA	1.41	0.84	0.62
AFTER SOIL IMPROVEMENT			
s01MDG_SH1	1.99	1.18	0.87
s01MDG_SH4	1.06	0.63	0.46
s01MDG_SH5	3.17	1.88	1.39
s02_SH6	2.94	1.74	1.28
s02MDG_SH4_A_1	1.98	1.17	0.86

6. Summary

The criteria of Robertson and Cabal, TC16, Monaco et al., and Andrus et al. and Idriss and Boulanger indicated that cyclic liquefaction of the hydraulic fill was possible before soil improvement. Although criteria were evaluated for different soil behaviour type, the results are consistent.

The results of the criteria evaluation after soil improvement showed a condition of no cyclic liquefaction potential -for Spanish seismic standards-, according to the Robertson & Cabal and Idriss & Boulanger criteria.

It can thus be concluded that the performed soil improvement was effective to reduce the cyclic liquefaction potential of the hydraulic fill according the NCSE-02 standard, especially for fine grained soils.

It can also be stated that the seismic loading is a point to investigate together with seismic experts and authorities, because a slightly variation of those assumptions changes sharply the soil response, as presented in Table E.12.

Table E.12. FoS for Robertson & Cabal (2012) and FoS for Idriss & Boulanger (2006) criteria, before and after soil improvement of Prat quay Phase 2.

Criterion	Assumption	a_{max}	FoS before	FoS after
Robertson (2009)	NCSE-02	0.083g	>0 to 1.7	≥2.2
	Deterministic*	0.14g	≤1	≥1.4
Idriss & Boulanger (2006)	NCSE-02	0.083g	1.04	1.48
	Deterministic*	0.14g	0.62	0.88

* from Irizarry (2004)

7. References

Andersen KH, Rosenbrand WF, Brown SF, Pool JH. 1980. Cyclic and static laboratory tests on Drammen clay. J Geotech Eng Div 1980;105(5):499–529.

Andrus, R. D., Stokoe, K. H., 1997. Liquefaction resistance based on shear wave velocity. Proc., NCEER Workshop on Evaluation of Liquefaction Resistance of Soils, Nat. Ctr. for Earthquake Engrg. Res., State Univ. of New York at Buffalo, 89–128.

Andrus, R.D., Stokoe, K.H. Juang, C. H. 2004. Guide for Shear-Wave-Based Liquefaction Potential Evaluation. Earthquake Spectra: May 2004, Vol. 20, No. 2, pp. 285-308.

Arango, I. 1996. Magnitude scaling factors for soil liquefaction evaluations. J. Geotech. Eng. 122(11), 929-936.

Boulanger, R. W. Idriss, I. M. 2004. Evaluating the potential for liquefaction or cyclic failure of silts and clays. Report nº UCD/CGM-04/01. Center for Geotechnical Modeling Department of Civil & Environmental Engineering.University of California Davis, California.

Boulanger, R. W. and Idriss, I. M. 2006. Liquefaction Susceptibility Criteria for Silts and Clays. Journal of Geotechnical and Geoenvironmental Engineering. ASCE November 2006, pp 1413-1426.

Boulanger, R. W. Idriss, I. M. 2007. Evaluation of cyclic softening in silts and clays. Journal of Geotechnical and Geoenvironmental Engineering. ASCE, 133: pp 641-652.

Idriss, I. M. 1999. An update to the Seed–Idriss simplified procedure for evaluating liquefaction potential. Proc., TRB Workshop on New Approaches to Liquefaction, Publication No. FHWA-RD-99-165, Federal Highway Administration.

Idriss, I.M., Boulanger, R. W. 2004. Semi-Empirical Procedures for Evaluating Liquefaction Potential During Earthquakes, Proceedings of the 11th ICSDEE & 3rd ICEGE, (Doolin et al. Eds.), Berkeley, CA, USA, 1, 32-56.
Jefferies, M. and Been, K. 2006. Soil Liquefaction. A critical state approach. Taylor & Francis Book.

Idriss, I. M., Boulanger, R. W. 2006. Semi-empirical procedures for evaluating liquefaction potential during earthquakes. Soil Dyn. Earthquake Eng., 26, 115–130.

Irizarry, J. 2004. An Advanced Approach to Seismic Risk Assessment. Application to the Cultural Heritage and the Urban System Barcelona. PhD thesis. Dpto. Ingeniería del Terreno, Cartográfica y Geofísica. Universidad Politécnica de Cataluña, Barcelona. 290 pp.

Juang, C. H., Yuan, H., Lee, D. H., Lin, P. S. 2003. Simplified cone penetration test-based method for evaluating liquefaction resistance of soils. J. Geotech. Geoenviron. Eng., 129(1), 66–80.

Juang, C. H., Liu, C., Chen, C., Hwang, J. and Lu, C. 2008. Calibration of liquefaction potential index: A re-visit focussing on a new CPTu model. Engineering Geology J., 102 (2008) pp 19-30.

Liao, S., and Whitman, R. V. 1986. Overburden correction factors for SPT in sand. J. Geotech. Engrg., ASCE, 112(3), 373–377.

Marchetti, S. 1980. In-situ tests by flat dilatometer. Journal of Geotechnical Engineering 107 (GT3), 832-837.

Marchetti, S., Monaco, P., Totani, G., Calabrese, M. 2001. The Flat Dilatometer Test (DMT) in soil investigations. A Report by the ISSMGE Committee TC16. Proceedings IN SITU 2001, Intnl. Conf. On In situ Measurement of Soil Properties, Bali, Indonesia.

Monaco, P., Marchetti, S., Totani, G., Calabrese, M. 2005. Sand liquefiability assessment by flat dilatometer test (DMT). In: Proceedings of the 16th international conference on soil mechanics and geotechnical engineering. Millpress Science Publishers/IOS Press, pp 2693–2697.

Moss, R.E.S, Seed, R.B., Kayen, R.E., Stewart, J.P., Der Kiureghian, A., Cetin, K.O. 2006. CPT-based probabilistic and deterministic assessment of in situ seismic soil liquefaction potential, Journal of Geotechnical and Geoenvironmental Engineering, 132(8): 1032-1051.

NCSE-02 2002. Normativa de Construcción Sismorresistente Española. Comisión Permanente de Normas Sismorresistentes, Real Decreto 997/2002. Boletín Oficial del Estado No. 244 del 11 de octubre de 2002.

NGI 2008a. Laboratory Testing Muelle Prat, 2008 Laboratory tests results on UPC sample, 20071315-3, Norwegian Geotechnical Institute.

NGI 2008b. Laboratory Testing Muelle Prat, 2008 Laboratory tests results, 20071315-2, Norwegian Geotechnical Institute.

Reyna, F. and Chameau, J. L., 1991. Dilatometer Based Liquefaction Potential of Sites in the Imperial Valley. Second International Conference on Recent Advances in Geotechnical Earthquake Engineering and Soil Dynamics, St. Louis, MO, Missouri University of Science and Technology, Rolla, MO, pp. 385–392

Robertson, P. K., Campanella, R. G. 1985. Liquefaction potential of sands using the CPT. J. Geotech. Eng., 111(3) pp 384–403.

Robertson, P.K. 1990. Soil classification using the cone penetration test. Canadian Geotechnical Journal, 27(1): pp 151-158.

Robertson, P.K., Wride, C.E., 1998. Evaluating cyclic liquefaction potential using the cone penetration test. Canadian Geotechnical Journal, Ottawa, 35(3): 442-459.

Robertson, P. K. 2004. Evaluating Soil Liquefaction and Post-earthquake deformations using the CPT. Proceedings of ISC2 on Geotechnical and Geophysical Site Characterization (2004) Pages: pp. 233-249.

Robertson, P. K. 2009a. Interpretation of cone penetration tests—A unified approach. Can. Geotech. J., 46, 1337–1355.

Robertson, P. K. 2009b. Performance based earthquake design using the CPT. Proc., IS Tokyo Conf., CRC Press/Balkema, Taylor & Francis Group, Tokyo.

Robertson, P. K. Cabal, K. L. 2012. Guide to Cone Penetration Testing for Geotechnical Engineering. Gregg 5th Edition.

Seed, H. B., and Idriss, I. M. 1971. Simplified procedure for evaluating soil liquefaction potential. J. Geotech. Engrg. Div., ASCE, 97(9), pp 1249–1273.

Seed, H. B., Idriss, I. M., Makdisi, F., Banerjee, N. 1975. Representation of Irregular Stress Time Histories by Equivalent Uniform Stress Series in Liquefaction Analyses. Report No. EERC 75-29, Earthquake Engineering Research Center, University of California, Berkeley, October.

Shuttle, D.A., Cunning, J. 2007. Liquefaction potential of silts from CPTu. Canadian Geotech. J. 44: 1-19.

Stark, T.D., Olson, S.M. 1995. Liquefaction resistance using CPT and field case histories. ASCE Journal of Geotechnical Engineering 121(12) 856–869.

Sykora, D. W. (1987). Creation of a data base of seismic shear wave velocities for correlation analysis. Geotech. Lab. Misc. Paper GL-87- 26, U.S. Army Engr. Waterways Experiment Station, Vicksburg, Miss.

TC16 - Marchetti, S., Monaco, P., Totani, G., Calabrese, M. 2001. The Flat Dilatometer Test (DMT) in Soil Investigations. A Report by the ISSMGE Committee TC16. May 2001, 41 pp.

Youd, T. L., Noble, S. K. 1997. Liquefaction criteria based statistical and probabilistic analysis. Proc., NCEER Workshop on Evaluation of Liquefaction Resistance of Soils, Tech. Rep. No. NCEER-97-0022. 1997, 201–216.

Youd, T.L. and Idriss, I.M. (ASCE-chairs) Andrus, Arango, Castro, Christian, Dobry, Finn, Harder, Hynes, Ishihara, Koester, Liao, Marcuson, Martin, Mitchell, Moriwaki, Power, Robertson, Seed, Stokoe. 2001. Liquefaction Resistance of Soils: 1996 NCEER and 1998 NCEER/NSF Workshops on Evaluation of liquefaction Resistance Soils. Journal of Geotechnical and Geoenvironmental Engineering, pp 817-833.

Zhang, G., Robertson, P. K., and Brachman, R. W. I. 2002. Estimating liquefaction induced ground settlements from CPT for level ground. Can. Geotech. J., 395, 1168–1180.

Zhang G, Robertson P.K., Brachman R.W.I. 2004. Estimating liquefaction-induced lateral displacements from CPT for level ground. J Geotech Geoenviron Eng August 2004:861–871.

Appendix F. Settling column

1. Introduction

Different authors -including Yamamuro and Wood (2004) and Jefferies and Been (2006)-, presented some techniques used in laboratories to remould non cohesive soils getting similar in-situ properties. Deposition techniques of sandy silts or silts are: dry deposition, water deposition, slurry deposition, mixed dry deposition and air pluviation. Nevertheless, Patrask and Puri (2003) concluded that the most adequate technique for silty soil is the slurry deposition (Figure F.1). This technique consists in mixing soil with water to make slurry. The slurry should be sufficiently liquid to deposit inside a sampler. After that, it has to drain and settle, after that it can be considered as soil.

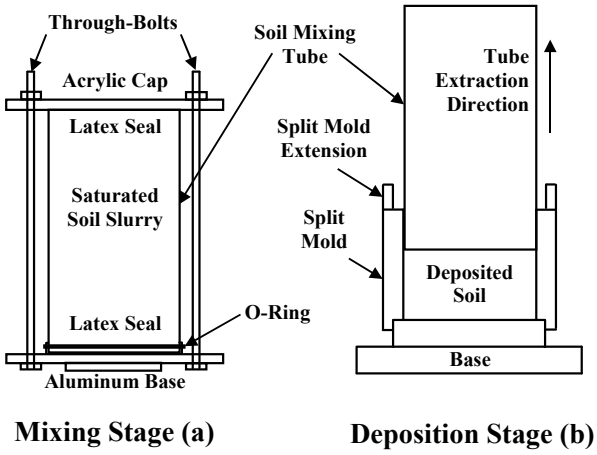

Figure F.1. Slurry deposition technique, Wood et al. (2008)

Although hydraulic fill of Prat quay is not strictly a silt, it can be accepted that the hydraulic fill of Prat quay is deposited in a loose state. Thus, the technique of slurry deposition should be suitable.
In this way, a guidance for project confined dredge materials were presented in US army Corps of Engineers (1987). It includes an extensive document of confined disposal of dredged material, in which the settling test is defined. It described the used apparatus and the process to evaluate the sedimentation (Figure F.2). Some ideas have been adopted to carry out the settling column tests for

the hydraulic fill of Prat quay including: (i) the slurry poured into a transparent (8” diameter) pipe. (ii) there was a porous stone at the bottom of the pipe, which allowed the soil consolidation.

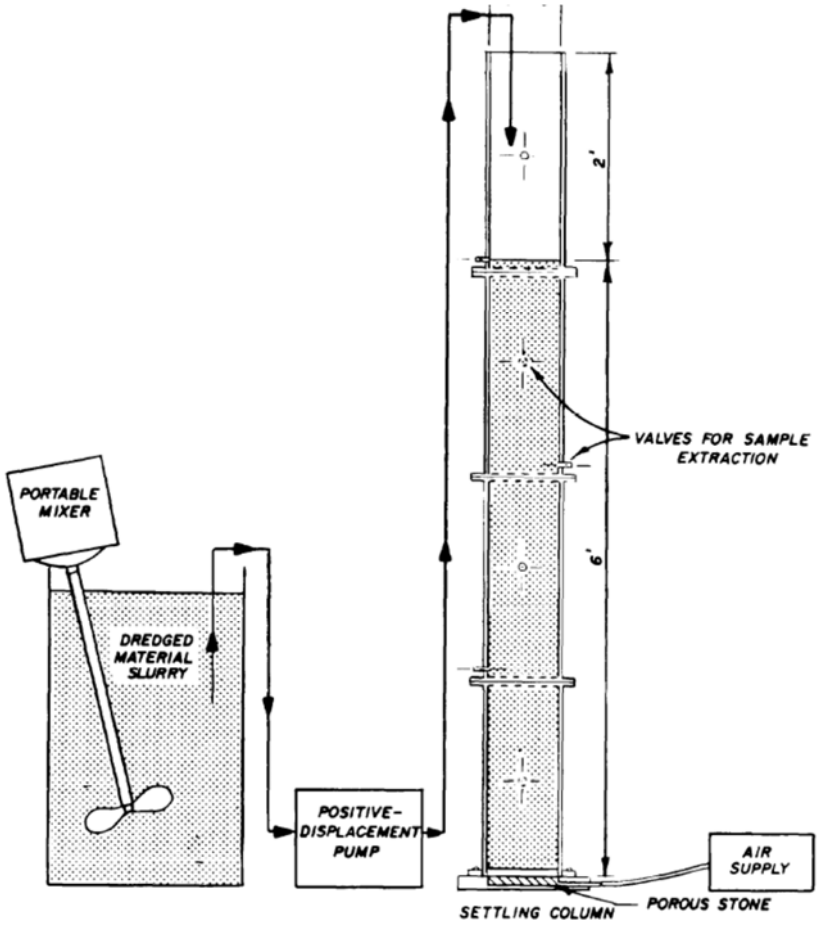

Figure F.2. Schematic of apparatus for settling tests. US Army Corps of Engineers (1987).

Different aspects that control the behaviour were also described: settling type, sedimentation governing factors and the salinity function during settling. There were four types of settling defined: discrete settling, flocculent settling, zone settling and compression settling. Flocculent settling and zone settling occur during the initial part of the test. If an interface is formed within one day of the test the slurry mass, it means that the zone settling is formed. In case that no interface is detected on the first day, the slurry mass reveals flocculent settling. If there are not changes in the particles during the settling process, it indicates that the discrete settling is developing. Finally, the compression settling is defined by the compression of the slurry-soil structure.

It is important to remark that the existence of certain types of clay minerals may produce a flocculent behaviour. This behaviour is generally produced as a natural reaction of the montmorillonite clay group. It produces a colloid with clays, forming a floc and the posterior sedimentation. This process reduces the sedimentation time and facilitates the consolidation of the new soil. However, high salinity of water frequently changes the flocculent behaviour. The use of X-ray diffraction (XRD)

has been established to characterize those mineral phases. In the hydraulic fill and the natural ground of Prat qua, as presented in Chapter 2, there are not flocculent minerals.

Although the settling test is capable to determine the settling types, the test uses a small cylinder. Therefore, the results are not acceptable for the use in design because wall effects affect the settling. Nevertheless, this test provides high quality soil samples to be tested afterwards in the laboratory.

2. *Hydraulic fill settling column*

A small-scale settling column using slurry deposition was developed to create soil specimens for hydraulic fill of Prat quay. However, this column was also focused on the natural density measurement during sedimentation.

The stages of the column is described in following points:

i) Hydraulic fill was mixed with seawater using a concrete mixer.

ii) The slurry was deposited inside a methacrylate tube. This tube had a diameter of 20 mm and 2 m long, with a porous stone at the bottom.

iii) During a period of 110 days the slurry consolidated.

iv) The height of the tube was reduced.

v) An increase of vertical stress (45 kPa, equivalent to 5 m depth) was applied on the top (Figure F.3). There was a porous stone between the slurry and the loading head.

vi) During a period of 92 days the slurry consolidated.

vii) The loading head and the base was removed.

viii) The tube was prepared to be sent to NGI.

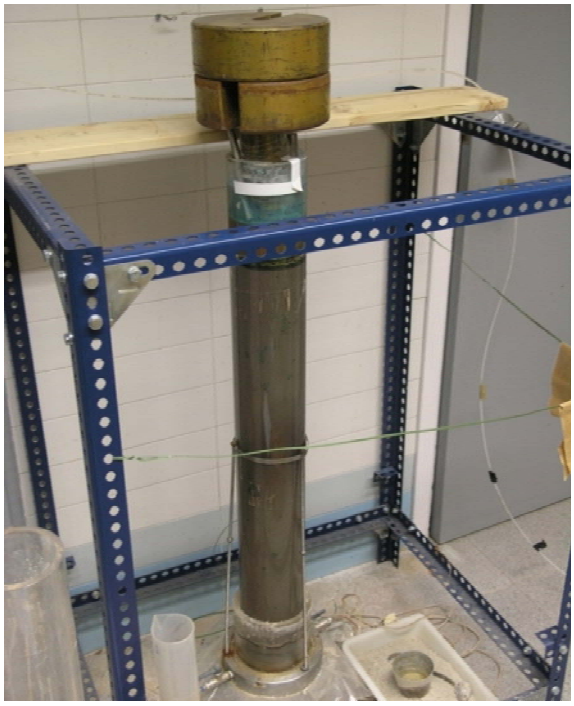

Figure F.3. Sedimentation test of hydraulic fill after the application of 45 kPa.

The results of the settling column in terms of density are presented in Figure F.4. Initially, the natural density was 1.35 Mg/m^3 when the slurry was placed in the tube. After 110 days, it increased up to 1.74 Mg/m^3. Once the top of the tube was loaded, density increased up to 1.83 Mg/m^3.

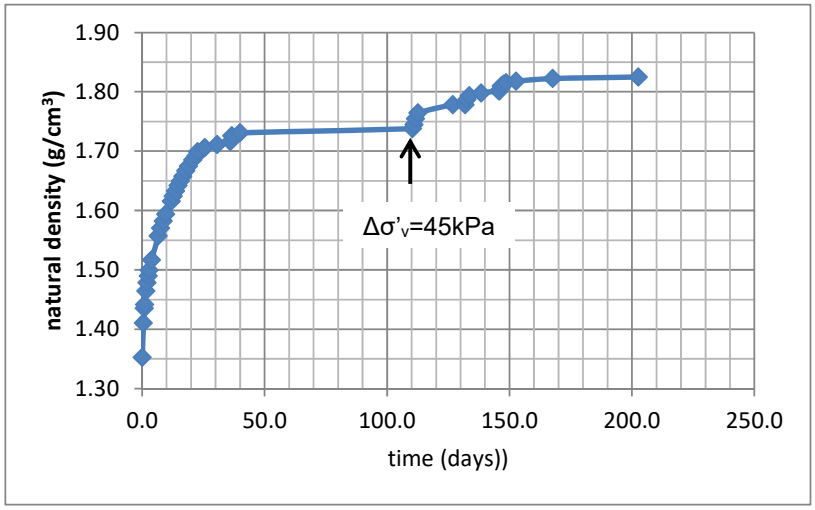

Figure F.4. Natural density evolution of the hydraulic fill in the settling column.

The results of this chapter were used in the interpretation of hydraulic fill weight. Furthermore, the obtained soil specimens were at NGI, results (NGI, 2008) are presented in Chapter 3, Chapter 5 and Appendix E.

It is important to note that, on the first day, an interface was observed. Therefore, no flocculent behaviour was revealed which was consistent with the XRD results. In this way, the inexistence of flocculants did not facilitate the consolidation of the hydraulic fill.

3. References

Jefferies, M., Been, K. 2006. Soil Liquefaction. A critical state approach. Taylor & Francis Book.

NGI 2008. Laboratory Testing Muelle Prat, 2008 Laboratory tests results on UPC sample, 20071315-3, Norwegian Geotechnical Institute.

Prakash, S., Puri V.K.U.S. 2003. Liquefaction of Silts and Silty –Clay mixtures. Taiwan Workshop on Soil Liquefaction 2003.

US army Corps of Engineers 1987. Confined Disposal of Dredged Material. Engineer Manual nº 1110-2-5027.

Wood, F. M., Yamamuro, J. A. and Lade, P. V. 2008. Effect of depositional method on the undrained response of silty sand. Can. Geotech. J. 45: pp 1525-1537.

Yamamuro, J.A. and Wood, F.M. 2004. Effect of depositional method on the undrained behavior and microstructure of sand with silt. Soil Dynamics and earthquake Engineering, 24 (2004), pp 751-760.